Russian Academy of Sciences

Kola Science Centre RAS

Geological Institute

F.F. Gorbatsevich

Acoustopolariscopy of rock forming minerals and crystalline rocks

Apatity

F.F. Gorbatsevich. Acoustopolariscopy of rock forming minerals and crystalline rocks.

Editor Prof. C. Gillen

The fundamentals of the acoustopolariscopy method, determination results for elastic and non-elastic properties of some rock forming minerals and crystalline rocks are outlined in the work. Previously unknown effects – linear acoustic anisotropic absorption and depolarization of shear waves have been revealed in the samples of naturally occurring minerals and rocks. The book is destined for specialists dealing with acoustics, geophysics, geology as well as theory and practice of determining solid body properties.

INTRODUCTION

Physical anisotropy is one of the most interesting forms of matter organization that has not received sufficient study yet. Its implications and peculiarities were most conspicuous in a mineral study. For this purpose since the beginning of the 19-th century a microscope has been used. In 1828 after William Nikol had introduced polarizers in a microscope, optical methods occupied an important place in the mineral study. Internal laws of their structure enabled Ye.S.Fyodorov and V.Goldschmidt to make a complete classification of 230 spatial point groups of symmetry related to anisotropy of optical, dielectrical, magnetic, elastic, thermal and other properties. Of these the study of anisotropy of elastic properties is most important since these properties are associated with the behaviour of a large number of diverse construction units, natural objects and materials under load. The theory of elastic anisotropy of media has been thoroughly elaborateed in the works of Rayleigh, A.E.H.Love, W.Voigt, Y.F.Nye, F.I.Fyodorov, S.G.Lekhnitsky, G.I.Petrashen et al. A much worse situation is in the field of experimental methods of its study. On the one hand, the use of optical polarization methods for this purpose is limited by the fact that the optical elasticity constants of medium are described by the tensor of not higher than the second rank, while the elasticity constants of a medium of lower symmetry – by the fourth-rank tensor. On the other hand, the study of many objects, in particular rocks, by optical methods is limited by their opacity.

The elaboration of a theory and methods for the study of elastic anisotropy of solid media and in particular minerals and rocks is in large demand – without them an adequate interpretation of geophysical, seismic and seismological data is impossible.

Considerable progress in these fields was provided by the works of L.Bergmann, L.M.Brekhovskikh, A.N.Guz', K.E.Ermilin, G.V.Farnell, H.Kolsky, F.M.Lyakhovitsky, V.E.Lyamov, W.P.Mason, H.J.McSkimin, F.D.Murnaghan, Zh.G.Nikiforenko, V.M. Prokhorov, N.N.Puzyryov, R.T.Smith, et al. To determine anisotropy paramaters the dynamic ultrasound method is used. The method was greatly improved in the works of K.S.Aleksandrov, B.P.Belikov, B.Chick, C.Elbaum, E.P.Papadakis, O.G.Shamina, N.N.Silaeva, S.Ya.Sokolov, R.Truel, I.N.Yermolov, et al.

This work outlines the theoretical grounds of propagation of elastic, mainly transverse (shear) waves in solid bodies, particular emphasis being placed upon practical measurements of anisotropic media properties. The fundamentals of acoustopolarisation measurements method are given. The physical essence of a linear anisotropic absorption effect (acoustic dichroism) is explained. Based on the analysis of laws of reflection in half-space and reflection-transmission on the media boundary, the ways of creating efficient transducers and receivers of purely shear linear-polarized waves are considered. The constructions of combined transducers for transition and reception of longitudinal and shear waves as well as transducers for determination of elastic constants of anisotropic media have been analyzed, developed and tested. Their advantages and disadvantages are shown on the basis of comparative tests results. Acoustopolariscopes of three modifications and the ways of conducting acoustopolarization measurements are described. The ways of processing the measurement results, identification of a symmetry type and elasticity constants of anisotropic media are set forth. The rules for constant calculation, for analyses of media with rhombic, tetragonal, pseudohexagonal, cubic and isotropic symmetry are given. At the same time it is shown that according to the number of the revealed

symmetry elements it is possible to analyze media with lower symmetry forms, for instance, trigonal et al.

The concluding sections are dedicated to the experimental study results for elastic anisotropy of rock forming minerals and rocks from some deposits (Voche-Lambina testing ground, Kola Peninsula, Kola and Ural superdeep boreholes). The possibility to determine the direction and comparative value of palaeo- and modern stresses is shown on the rocks from the Voche-Lambina testing ground and Ural Borehole SG-4.

The book is intended for the specialists working in the field of theory and practice of determining solid body properties. It may be useful to specialists in acoustics, geophysicists and geologists.

The author expresses his deep appreciation to M.Z.Abdrakhimov, O.S.Golovataya, V.P.Gusev, H.Kern (Germany), P.V.Krauklis, A.V.Zharikov, S.B.Imasheva, I.L.Il'chenko, R.V.Medvedev, F.P.Mitrofanov, L.L.Panasyan, I.A.Panina, G.I.Petrashen', G.T.Prodaivoda, Yu.P.Smirnov, V.I.Starostin, N.N.Tesovskaya, V.V.Filippov, N.V.Sharov, V.L.Shkuratnik, Yu.N.Yakovlev for support, benevolent treatment, valuable advises and assistance in the monograph preparation. Especially thanks I express to my editor prof. C.Gillen.

The author thanks George Soros, the founder of the International Sientific Fund, and the Russian Foundation for Basic Research. The publication of this monograph was supported financially by Soros's Fund through the emergency grant and the Russian Foundation for Basic Research through project grants 94-05-16034a, 97-05-64167 and 03-05-64169. Partly the work was fulfilled in the framework of IGCP-UNESCO Project № 408 and INTAS-01-0314.

1. PHYSICAL PRINCIPLES OF ACOUSTOPOLARISATION MEASUREMENTS METHOD

1.1. Propagation of elastic waves in transverse-isotropic medium

In general terms, the propagation of elastic waves in anisotropic media is described by Green-Christoffel equation [Dieulesaint et Royer, 1974]:

$$(\Gamma_{il} - \delta_{il}\rho V^2)U_i = 0, \tag{1.1}$$

where $\Gamma_{il} = n_j n_k C_{ikjl}$ is Christoffel's tensor, C_{ikjl} are the elasticity constants of an anisotropic solid body, n_j, n_k are the directional cosines, δ_{il} is Kronecher's symbol, ρ is the medium density, V is the wave propagation velocity, U_i is the displacement of medium particles in the wave.

For a relatively simple but practically common transverse-isotropic medium the components Γ_{il} will take the following values:

$$\Gamma_{11} = n_1^2 C_{11} + n_2^2 C_{66} + n_3^2 C_{44},$$

$$\Gamma_{22} = n_1^2 C_{66} + n_2^2 C_{11} + n_3^2 C_{44},$$

$$\Gamma_{33} = n_1^2 C_{44} + n_2^2 C_{44} + n_3^2 C_{33},$$

$$\Gamma_{12} = (C_{12} + C_{66}) n_1 n_2,$$

$$\Gamma_{13} = (C_{13} + C_{44}) n_1 n_3,$$

$$\Gamma_{23} = (C_{23} + C_{44}) n_1 n_3, \tag{1.2}$$

where C_{ij} are the elasticity constants of an anisotropic solid body, n_i are the directional cosines.

These values of Γ_{il} can be substituted in Eq. (1.1) and the complete Green-Christoffel equation for transverse-isotropic medium can be thereby obtained. Three independent solutions – three values of elastic wave propagation velocities in one direction will determine proper values of Christoffel's tensor. Consider two simple cases of elastic wave propagation in a transverse-isotropic medium.

1. An elastic wave propagates along the symmetry axis OX_3. In this case $n_1 = n_2 = 0$, $n_3 = 1$. From the Green-Christoffel's equation we shall get that

$$(C_{33} - \rho V^2)(C_{44} - \rho V^2)(C_{44} - \rho V^2) = 0.$$

Whence it follows that the values of elastic waves propagation velocity will be:

$$V_{p1} = \sqrt{C_{33}/\rho}, \quad V_{s1} = V_{s2} = \sqrt{C_{44}/\rho} \tag{1.3}$$

Thus, during the elastic waves propagation along the symmetry axis only two velocities will be observed V_{p1} and $V_{s1} = V_{s2}$ Measuring only these velocity parameters it is impossible to conclude whether this medium is anisotropic.

2. An elastic wave propagates along the axis OX_1 (the direction of its propagation is in the medium symmetry plane). Such a case is most interesting when analyzing anisotropic media. In this case $n_1 = 1$, $n_2 = n_3 = 0$. From general equation (1.1) we deduce that

$$(C_{11} - \rho V^2)\,(C_{66} - \rho V^2)\,(C_{44} - \rho V^2) = 0.$$

The last equation has three solutions:

$$V_{p2} = \sqrt{C_{11}/\rho}\,,\ V_{s1} = \sqrt{C_{44}/\rho}\,,\ V_{s2} = \sqrt{C_{66}/\rho}\,, \tag{1.4}$$

where V_{p2} is the longitudinal wave velocity along the symmetry plane; V_{s1} is the shear wave velocity with the polarization vector oriented along the normal to the symmetry plane; V_{s2} is the shear wave velocity with the polarization vector lying in the symmetry plane. Similarly, with $n_1 = 1$, $n_2 = n_3 = 0$ from Eq. (1.2) we obtain that $\Gamma_{11} = C_{11}$, $\Gamma_{22} = C_{66}$, $\Gamma_{33} = C_{44}$. Then the Green-Christofel's equation may be replaced by three motion equations:

$$\rho\frac{\partial^2 U_1}{\partial t^2} = C_{11}\frac{\partial^2 U_1}{\partial x^2},$$

$$\rho\frac{\partial^2 U_2}{\partial t^2} = C_{44}\frac{\partial^2 U_2}{\partial x^2},$$

$$\rho\frac{\partial^2 U_3}{\partial t^2} = C_{66}\frac{\partial^2 U_3}{\partial x^2}. \tag{1.5}$$

The simplest solutions of wave equations (without regard for absorption) for harmonic stationary waves are expressions:

$$A_{p2} = A_0 \sin(\omega t - \frac{2\pi f_0 x}{V_{p2}} + \varphi_0),$$

$$A_{s1} = A_0 \sin(\omega t - \frac{2\pi f_0 x}{V_{s1}} + \varphi_0),$$

$$A_{s2} = A_0 \sin(\omega t - \frac{2\pi f_0 x}{V_{s2}} + \varphi_0), \tag{1.6}$$

where $\omega = 2\pi f_0$ is the wave circular frequency, x is the distance and φ_0 is the initial phase shift.

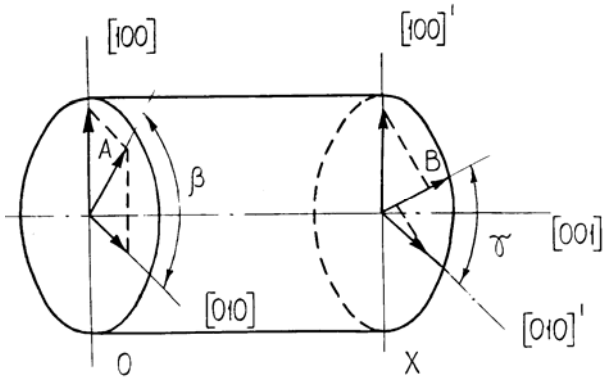

Fig. 1.1. Registration diagram of a quasi-shear wave propagating through a sample with transverse-isotropic symmetry at arbitrarily oriented polarization vectors (OPV) of transducer and receiver.

1.2. Phase difference and phase shift in the wave of shear vibrations

Let us consider a relatively simple but rather well known case where shear waves propagate in a medium with transverse-isotropic symmetry. The waves will be considered to transmit from a transducer of linear-polarized stationary harmonic shear waves to the sample made of transverse-isotropic medium in the direction coinciding with the elastic symmetry plane [010] (Fig 1.1).

In this case perturbations arising in the sample will be described by the superposition of amplitudes A_{s1} and A_{s2}. The polarization type of the total shear wave will depend on the position of the vector A with respect to the medium symmetry elements and the wave x propagation direction. If the vector A lies in the plane [010], then the wave harmonic phase along this direction will be described by the expression

$$\Psi_1 = \omega t - \frac{2\pi x}{\lambda_1} + \varphi_0 .$$

Along the direction [100] the harmonic phase is

$$\Psi_2 = \omega t - \frac{2\pi x}{\lambda_2} + \varphi_0 ,$$

where $\lambda_1 = V_{s1}/f_0$, $\lambda_2 = V_{s2}/f_0$. At a distance of x from the section [010]-[100] a phase difference appears

$$\delta = \Psi_1 - \Psi_2 = 2\pi x(1/\lambda_1 - 1/\lambda_2) \qquad (1.7)$$

At the increase of the phase difference δ along the propagation way, the change of polarization type and polarization vector orientation (PVO) of the total shear wave will be observed. If we give the vector A (Fig.1.1) an angle $\beta = 45°$ or $135°$, then, when the phase difference $0 < \delta < \pi/2$ (Fig. 1.2), the wave polarization will transform from linear to elliptic right-hand and the orientation of the ellipse's longer axis will coincide with the PVO when $\delta = 0$.

When the phase difference reaches the value of $\delta = \pi/2$ a circular right-hand polarization will be observed. When the phase difference $\pi/2 < \delta < \pi$ the polarization will again become elliptic. But now the ellipse's longer axis will be rotated through 90^o as compared with the PVO when $\delta = 0$. Furthermore, when $\delta = \pi$ the polarization will become linear, the PVO being 90^o in relation to the PVO when $\delta = 0$. Within the phase difference $\pi < \delta < 2\pi$ a counter-clockwise rotation of the polarization vector is observed. The type and parameters of polarization are the same for $\delta = 5\pi/4$ and $\delta = 3\pi/4$ (elliptic), for $\delta = 7\pi/4$ and $\delta = \pi/4$ (elliptic), for $\delta = 3\pi/2$ and $\delta = \pi/2$ (circular). As Fig 1.2 suggests, the type of polarization, the direction of rotation and orientation of polarization vectors fully coincide when the phase difference is equal to 2π. If the phase difference along the sample length is exactly equal to $\delta = 2\pi$, the type and parameters of polarization do not allow one to distinguish an anisotropic sample from an isotropic one.

Let us consider the propagation process of a quasi-shear wave in the sample, Fig. 1.1, when the polarization vector of the transducer A and receiver B is arbitrarily oriented. For instance, the polarization vector orientation of the transducer makes an

angle β with the symmetry plane [010] of the sample; its amplitude is equal to A_S. The polarization vector orientation of the receiver makes an angle γ with the same plane [010], its sensitivity is equal to A_R. Having done the decomposition of the polarization vector of the transducer A in terms of the symmetry elements [010] and [100] and at a distance of x composition of projections on the direction B, we shall obtain, with regard to Eq. (1.6), the summary amplitude of the waves A_P registered by the receiver:

$$A_P = A_S A_R [\cos\beta\cos\gamma \sin(\omega t - \frac{2\pi x}{\lambda_1} + \varphi_0) + \sin\beta\sin\gamma \sin(\omega t - \frac{2\pi x}{\lambda_2} + \varphi_0)]. \qquad (1.8)$$

Let us follow the variation of the amplitude A_P as the sample rotates around the direction [001].

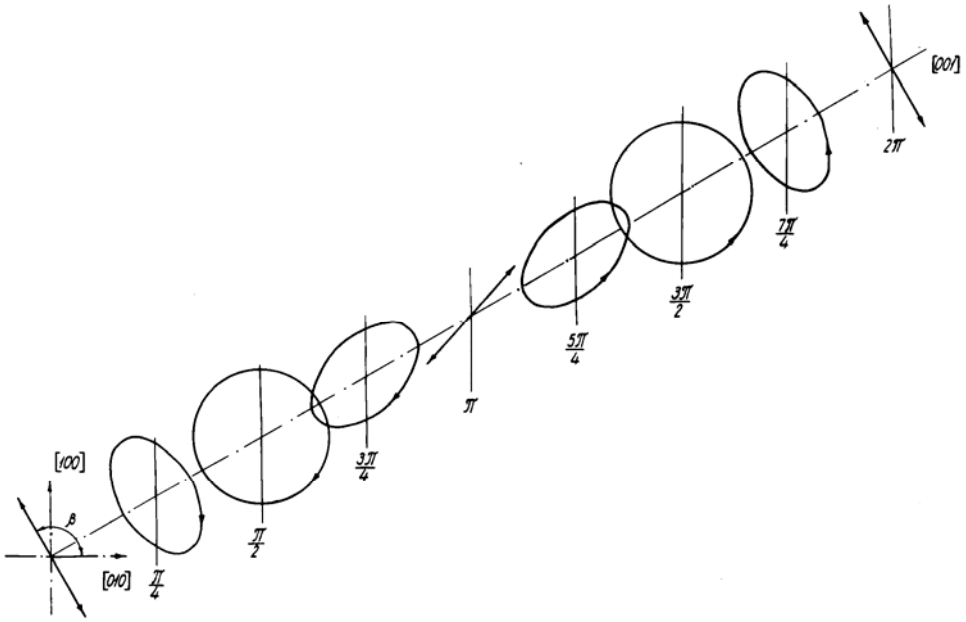

Fig. 1.2. The change of polarization type during shear wave propagation in an anisotropic sample.

If the orientations of the transducers' vectors A and B coincide, i.e. the polarization vectors of the source and receiver are parallel (VP position), then from (1.8) we obtain

$$A_{VP} = A_S A_R [\cos^2\beta \sin(\omega t - \frac{2\pi x}{\lambda_1} + \varphi_0) + \sin^2\beta \sin(\omega t - \frac{2\pi x}{\lambda_2} + \varphi_0)]. \qquad (1.9)$$

If the polarization vectors of the source and receiver are directed at a right angle, crossed (VC position), then from (1.8) we obtain

$$A_{VC} = \frac{1}{2} A_S A_R \sin 2\beta [\sin(\omega t - \frac{2\pi x}{\lambda_1} + \varphi_0) - \sin(\omega t - \frac{2\pi x}{\lambda_2} + \varphi_0)]. \qquad (1.10)$$

As follows from Eq. (1.9)-(1.10) the amplitudes A_{VP} and A_{VC} depend on the sample length x, rotation angle β relative to the plane [010] and current wave phase

ωt. In a general case when $\beta = 0$ the waves ωt get a phase shift. The value of the phase shift depends on the angle β and the value of the phase difference δ.

The solution of Eq. (1.9) and (1.10) when $A_{VP} = 0$ and $A_{VC} = 0$, allows one to find the values of this phase shift for the VP (ω_{n0}) and VC (ω_{c0})

$$A_{VP} = A_S A_R [\cos^2 \beta \sin \omega t + \sin^2 \beta \cos \delta \sin \omega t + \sin^2 \sin \delta \cos \omega t] = 0,$$

whence

$$\omega_{n0} = arctg \frac{-\sin \delta}{ctg^2 \beta + \cos \delta} \pm n\pi. \qquad (1.11)$$

Similarly for A_{VC} we obtain

$$A_{VC} = \frac{1}{2} A_S A_R \sin 2\beta [\sin \omega t - \sin \omega t \cos \delta - \cos \omega t \sin \delta] = 0,$$

whence

$$\omega_{c0} = arctg \frac{\sin \delta}{1 + \cos \delta} \pm n\pi, \qquad (1.12)$$

where the value of δ is defined by the expression (1.7), $n = 0, 1, 2, 3\ldots$.

In Fig 1.3 is shown the relation for the phase shear ωt_c (ω_{n0}), calculated by formula (1.11), that will be observed when the source and receiver vectors are parallel [Gorbatsevich, 1995].

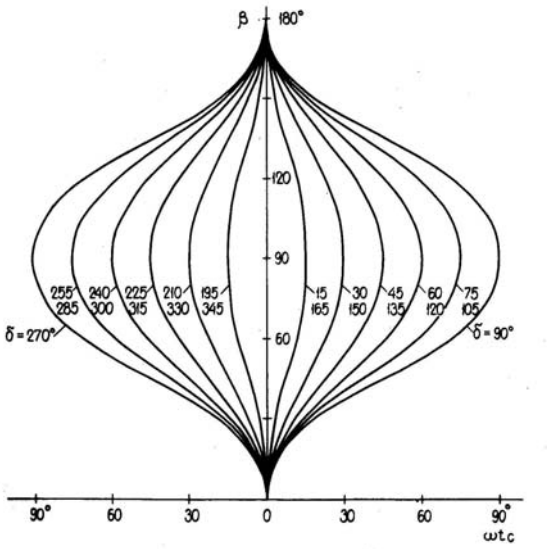

Fig. 1.3. Dependence of the phase shear value $\omega t_c = \omega_{no}$ vs angles β and δ in the VP position of the source and receiver.

As follows from this Figure, when $\delta = 0$, 180^o, $\omega_{n0} = 0$, at any β. The greatest changes in the shear phase value ω_{n0} are observed when $\beta \to 90^o$ (270^o) and $\delta \to 90^o$ (270^o). The shear phase value ω_{n0} is even with respect to the sign of angle β, but in accordance with the value δ it may take both positive and negative values. The shear value for the wave current phase ω_{c0} at the transducers VC position depends only on the phase difference δ. Similarly, when $\delta = 0$, 180^o, the angle $\omega_{c0} = 0$. From formula (1.12) it follows that by the value of ω_{c0} the phase difference δ can be calculated.

1.3. Variation of the envelope of stationary shear waves

Let us examine in greater detail Eq. (1.8). With Ferma theorem we shall determine the value of the circular frequency ω_{nm}, at which the amplitude A_{BM} takes the maximum value:

$$\frac{\partial}{\partial \omega t} A_S A_R [\cos^2 \beta \sin \omega t + \sin^2 \beta \cos \delta \sin \omega t + \sin^2 \beta \sin \delta \cos \omega t] = 0 .$$

From the above:

$$\cos^2 \beta \cos \omega_{mn} + \sin^2 \beta \cos \delta \cos \omega_{mn} - \sin^2 \beta \sin \delta \sin \omega_{mn} = 0,$$

whence

$$\omega_{nm} = arctg \frac{1}{\sin \delta} (ctg^2 \beta + \cos \delta) \pm n\pi . \qquad (1.13)$$

Then if we substitute the value of ωt in Eq. (1.9) for the obtained value of ω_{nm}, we will get the equation of the summary wave envelope at the receiving transducer input (position VP),

$$A_{VPM} = A_S A_R \sqrt{\cos^4 \beta + 2\cos^2 \beta \sin^2 \beta \cos \delta + \sin^4 \beta}. \qquad (1.14)$$

Similarly we shall analyze Eq. (1.10):

$$\frac{\partial A_{VC}}{\partial \omega t} = \frac{\partial}{\partial \omega t} \frac{1}{2} A_S A_R \sin 2\beta [\sin \omega t - \sin(\omega t + \delta)] = 0 .$$

From the above equation

$$\omega_{cm} = arctg \frac{\cos \delta - 1}{\sin \delta} \pm n\pi . \qquad (1.15)$$

If we substitute ωt in Eq.(1.10) for the obtained value of ω_{cm}, we will receive the equation of the harmonic waves envelope at the receiving transducer input (VC position),

$$A_{VCM} = A_S A_R \sin 2\beta (\delta/2). \qquad (1.16)$$

Equations (1.11)-(1.16) determine important properties of the amplitudes A_{VP} and A_{VC} and their envelopes that are observed with parallel and crossed polarization vectors. Equations (1.11) and (1.13) as well as (1.12) and (1.15) show that:

$\omega_{nm} = \omega_{n0} \pm 90^o$,

$\omega_{cm} = \omega_{c0} \pm 90^o$.

It means that the angles $\omega t = \omega_{n0}$ and $\omega t = \omega_{c0}$, at which the amplitudes A_{VP} and A_{VC} are equal to zero, are shifted with respect to the same amplitudes' maxima by 90^o.

1.4. Peculiarities of circle diagrams with parallel and crossed polarization vectors

In accordance with the physical meaning, Eq. (1.9) and (1.10) represent instantaneous values of harmonic wave amplitudes at the point in time t. The amplitudes A_{VP} and A_{VC} recording is possible, especially at great frequencies, only with equipment of high resolution both in time and wave quantity terms. If a signal is close to harmonic, it is more convenient to observe variations of the maximum amplitudes (envelopes) in the course of the sample rotation (Fig. 1.1) with parallel (A_{VPM}) and crossed (A_{VCM}) polarization vectors. The amplitudes A_{VPM} and A_{VCM} behavior is described by Eq. (1.14) and (1.16) accordingly.

By the equations the values of A_{VPM} and A_{VCM} depend only on the value of the sample β rotation angle and the phase difference δ. In Figure 1.4 are shown the configurations of the envelopes A_{VPM} (solid line) and A_{VCM} (dotted line) with the phase difference $\delta = \pi/4$ observed within the phase difference 0 - 2π [Gorbatsevich, 1982].

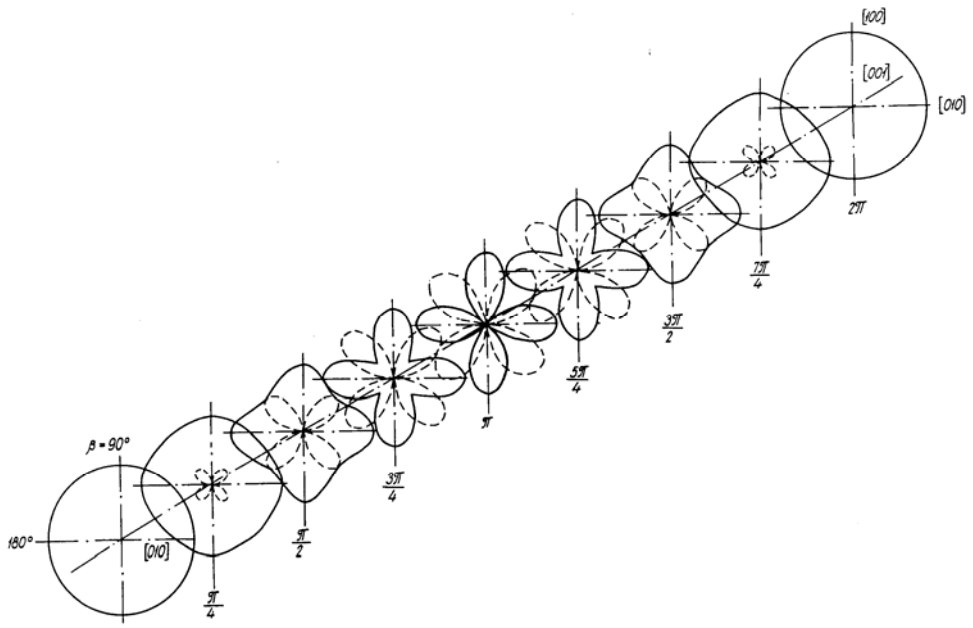

Fig. 1.4. Variation of maximum amplitudes (envelopes) recorded by the receiver with parallel (solid line) and crossed (dotted line) polarization vectors of the source and receiver of shear waves versus the sample rotation angle β and the phase difference δ.

As Fig 1.4 shows, beyond the dependence versus the rotation angle β of an isotropic sample ($\delta = 0$) in the VP position of linear-polarized transducers of shear waves, one and the same envelope amplitude equal to A_{VPM} recorded. The configurations of the envelopes A_{VPM} and A_{VCM}, obtained as anisotropic samples rotate, greatly depend on the value of the phase difference δ. For instance, in the VP position the A_{VPM} configuration gradually turns from the circle shape ($\delta = 0, 2\pi, 4\pi\ldots$) to a symmetric four-petal figure (($\delta = \pi, 3\pi, 5\pi\ldots$). Beyond the dependence versus the value of δ, the greatest amplitudes A_{VPM} are observed when the direction of symmetry elements [010] and [100] coincide with the orientation of polarization vectors of the source and receiver. With these orientations the value of A_{VPM} (without regard for attenuation) is independent of the phase difference δ. The amplitudes A_{VPM} minima

will be recorded when the rotation angle $\beta = 45^o \pm n\pi/2$. The value of $A_{VPM} = 0$ with the same rotation angles β and the phase difference $\delta = (2n - 1)\pi$.

The envelopes A_{VCM} configuration (Fig. 1.4) when an anisotropic sample is rotated between the transducers in the position VC is a symmetric four-petal figure independently of the phase difference $0 > \delta > 2\pi$. This figure is described by the function $A_{VCM} \sin 2\beta$. Depending on the value of δ only the maximum amplitude A_{VCM} that is observed at the rotation angles $\beta_м = 45^o + n\pi/2$, changes. The maximal A_{VCM} ($\beta = \beta_м$) will be registered by $\delta = \pi, 3\pi, 5\pi$ ....When $\delta = 0$ the achievable value of A_{VCM} is equal to A_{VPM}. By the value of A_{VCM} according to Eq. (1.16) one may calculate the phase difference δ,

$$\delta = \pm \arcsin \frac{A_{VCM}}{A_S A_R \sin 2\beta} + 2n\pi, \tag{1.17}$$

where $n = 0, 1, 2, 3\ldots$.

Independently of the value of δ minima A_{VCM} are observed when the orientation of symmetry elements [010] and [100] coincides with the orientation of the polarization vector of the source or receiver. Thus, strait lines drawn through the configuration A_{VCM} minima will always point to the spatial location of the axes or planes (their projections) of the symmetry of an anisotropic medium, of which the sample is made. On the basis of Fig 1.4 and Eq. (1.14) and (1.16) the following conclusions can be drawn:

1. The envelopes A_{VPM} and A_{VCM} configuration called acoustopolarigrams [Gorbatsevich, 1982] are repeated with a step of the phase difference $\delta = 2\pi$. The acoustopolarigrams with $\delta = (n+k)\pi$ are similar to those observed with $\delta = (n-k)\pi$, where $n = 0, 1, 2, 3\ldots$ and the quantity k may take any fractional values.
2. With the phase difference $\delta = 2\pi$ the acoustopolarigrams reflect the equalities $A_{VPM} = A_S A_R$ and $A_{VCM} = 0$ independently of the rotation angle β. With phase difference $\delta = (2n+1)\pi$ the acoustopolarigrams A_{VPM} and A_{VCM} are the same but shifted with respect to each other by 45^o. Opposite the maximum A_{VPM} is always the minimum A_{VCM}. The minima and maxima of the acoustopolarigrams are separated by 90^o.
3. When the values of the phase difference δ are small, relative A_{VCM} variations are considerably more distinct than those of A_{VPM}. Polarization measurements of amplitudes made in VC position allow one to determine the spatial orientation of symmetry axes and planes of an anisotropic sample much more precisely (over the measurements in VP position).
4. The greatest (lowest) velocities of quasi-shear waves propagation should be determined in the directions of the strait lines drawn through the symmetry centre of the VC acoustopolarigram and the value of A_{VCM} minima. The mentioned directions reflect a spatial orientation of the symmetry axes (planes) of an anisotropic medium. The dispersion of elastic waves propagation velocity is relatively low. Therefore, experimental observations of the acoustoplarigrams A_{VPM} and A_{VCM} can be taken over a wide range of frequencies, as well as with the use of acoustic impulses.
5. Due to the revealed shift of the current phase ωt (see Fig. 1.3), one should not measure the velocities of quasi-shear waves propagation in anisotropic media by observation of the wave phase or by the phase correlation method. The measurements by such methods are possible only in the cases when the orientation

of the wave shift vector coincides with the orientation of an elastic symmetry element (axis or plane) of an anisotropic medium.

1.5. Circle diagrams at time separation of shear pulses

The processes of harmonic stationary wave propagation in an anisotropic medium have been considered above. But in the course of practical measurements pulses with harmonic filling are used most often. This filling is formed through piezoelectric transducer (piezoelectric ceramic element) waves at natural frequency of a mechanical resonance [Skuchik, 1976; Tyulin, 1976; Glozman, 1972]. The pulse duration and the rate of the pulse rise depend on the form of the actuating electric signal and even more on the degree of the piezoelectric ceramic element damping [Ermolov, 1981].

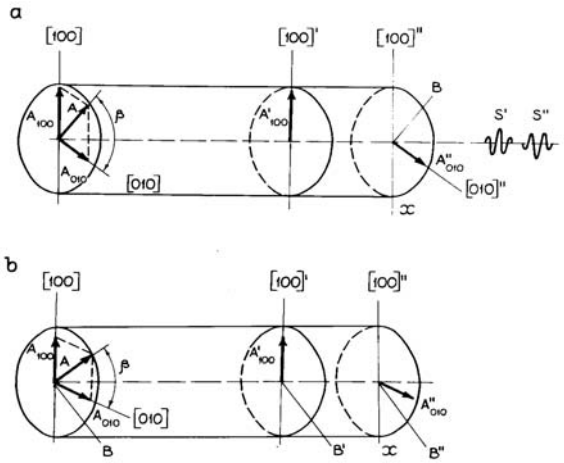

Fig. 1.5. Diagram of a quasi-shear wave propagation through an anisotropic sample with the spatially separated pulses S_1 and S_2.

The above Eq. (1.8-1.16) as well as a qualitative assessment by the envelopes (Fig. 1.4) can be also applied when in the course of measurements the pulses with harmonic filling are used. But in this case the pulses propagating for instance, along the directions [100] and [010] for the length of x (Fig. 1.1), should not separate spatially. Now let us consider the case when for the length of x the pulses separate spatially into $S'' = S_1$ and $S' = S_2$, Fig. 1.5.
Such a separation is observed when

$$T_i > (x/V_1) - (x/V_2), \qquad (1.18)$$

where T_i is the pulse duration.

As follows from the last mentioned expression, the separation into S_1 and S_2 can be realized with a sufficiently "short" pulse (T_i is small), a rather long propagation distance x and a large difference in the values of shear waves velocities along the medium symmetry elements [100] and [010]. If the source A polarization vector and the direction of the receiver B greatest sensitivity are parallel, Fig. 1.5a, then, by Eq. (1.8), the amplitude of the pulse S_1 that was the first to cover the distance x, will be equal to

$$A_{VP1} = A_S A_R \cos\beta \sin(\omega t - \frac{2\pi x}{\lambda_1} + \varphi_0) \qquad (1.19)$$

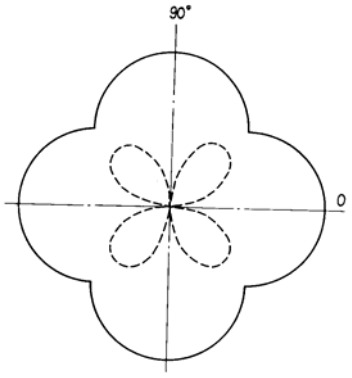

Fig. 1.6. Change of maximum amplitudes (envelopes) at the source and receiver parallel (solid line) and crossed (dotted line) polarization vectors, observed at the separated pulses S_1 and S_2'.

and the amplitude of the impulse S_2 will be

$$A_{VP2} = A_S A_R \sin\beta \sin(\omega t - \frac{2\pi x}{\lambda_2} + \varphi_0). \quad (1.20)$$

Accordingly, without regard for the attenuation the amplitude $A_{VP1} = A = A''_{010}$ when the vector A orientation coincides with the plane [010]. The amplitude $A_{VP2} = A = A'_{100}$ when the vector A orientation coincides with the axis [100]. It is also true that $A_{VP1} = 0$ when A is directed along the axis [100] and $A_{VP2} = 0$ when A is directed along the plane [010]. Thus, at the VP position of the source and receiver and separated pulses the location of the medium symmetry elements may be determined rather exactly by the moments of the pulses attenuation. For instance, the location of the moment [100] is determined by the moment of the pulse S_1 extinction and that of the element [010] – by the moment of the pulse S_2 extinction.

The values of $A_{VP1} = A_{VP2} = \sqrt{2}/2A_S A_R$ when $\beta = 45^o \pm n\pi/2$, where $n = 0, 1, 2,\ldots$. The shape of the envelope circle diagram (Fig. 1.6), observed at the separated pulses S_1'' and S_2', will not change with increasing sample length or frequency f_0. Such a change is possible only when other effects manifest themselves.

Now let us consider the case when the orientations of A and B are crossed. As the diagram (Fig. 1.5b) suggests, the reception of the waves takes place in the direction B that makes a right angle with the direction of the attenuation A. If the vector A makes an angle β with the direction [010], its projection will make $A_{010} = A\cos\beta$ and in the direction $A_{100} = A\sin\beta$. Reflecting the projections A_{010} and A_{100} to the direction B we obtain that

$$A_{B010} = A\cos\beta\cos(90^o - \beta) = A\cos\beta\sin\beta, \quad A_{B100} = A\sin\beta\cos\beta.$$

The total amplitude B will be equal to

$$B = A\cos\beta\sin\beta + A\sin\beta\cos\beta = A\sin 2\beta. \quad (1.21)$$

The expression (1.21), as a whole, coincides with the more general Eq. (1.10). As the waves propagate, after the time T_i has passed, a complete separation of pulses, generated by the components A_{010} and A_{100}, will take place. The faster pulse A_{010} will be in the cross-section [100]"-[010]", while as a slower one A_{100} – in the cross-section [100]'-[010]'. Accordingly, each of them will create in the receiving transducer, oriented in the direction B, the following signal amplitudes:

$$A_{VC1} = \frac{1}{2} A_S A_R \sin 2\beta \sin(\omega t - \frac{2\pi x}{\lambda_1} + \varphi_0), \quad (1.22)$$

$$A_{VC2} = \frac{1}{2} A_S A_R \sin 2\beta \sin(\omega t - \frac{2\pi x}{\lambda_2} + \varphi_0). \quad (1.23)$$

As follows from the last-mentioned expressions, $A_{VC1} = A_{VC2} = 0$ when $\beta = 0 \pm n\pi/2$, where $n = 0, 1, 2,\ldots$.

So, at the VC position of the source and receiver and separated pulses, the spatial location of the medium elements is at the moments of the pulses S_1 and S_2 simultaneous attenuation. The shape of the circle diagram VC, Fig. 1.6, will not change with increasing sample length or frequency f_0. But in the presence of linear

acoustic anisotropic absorption [Gorbatsevich, 1982] with increasing x qualitative changes of the circle diagrams may occur, Fig. 1.6.

As a whole, even with the separated pulses observations of the circle diagrams enable to determine the spatial location of the elastic symmetry elements of the medium under study with a high precision. In this case such a determination can be fulfilled both with crossed and parallel polarization vectors of the source and receiver of shear waves.

2. EFFECT OF LINEAR ACOUSTIC ANISOTROPIC ABSORPTION (LAAA)

2.1. Models of media exhibiting LAAA

Pleochroism or the phenomenon of linear anisotropic absorption is observed as the light passes through transparent media [Shurkliff, 1962]. It reflects an ability to absorb a beam of the polarized light in various ways when rotating its polarization vector with respect to the medium structural elements. In this case, as a rule, the greatest absorption of the polarized light is observed when the polarization vector is directed along the perpendicular to linearly stretched structural elements of the medium. The direction of the light greatest pass coincides with the orientation of linear elements. Because of this, the observed phenomenon got the second name – linear anisotropic absorption. Some natural minerals – tourmaline, kunzite, cordierite exhibit the effect of optical dichroism [Smith, 1972]. On the basis of polyvinyl and other compounds high-efficiency polarizers of ordinary light, using the effect of pleochroism, have been developed [Zhevandrov, 1978].

The effect of linear acoustic anisotropic absorption of elastic waves (LAAA) has been studied and used to a much lesser degree. Let us consider, for instance, a device that can serve as a passive analyzer to determine the orientation of the polarization vector of shear transverse waves emitted by ultrasonic transducers [Proctor, 1971]. The device represents a pack of glass plates glued together for example, by wax or epoxy resin. But the contact between them may be left dry. Working planes parallel to each other are ground to the normal of the faces of the pack of glass plates. Through these faces bundles of shear waves are sent into the device.

On testing of a similar passive analyzer it was revealed that if the polarization vector (the direction of the medium particles shift in a wave of shear vibrations) coincides with the orientation of the glass plates, then the wave amplitude is transmitted through the analyzer virtually without loss. If we turn the polarization vector perpendicularly to the glass plates surfaces, nearly complete attenuation of the shear waves in analyzer will happen. According to T.M. Proctor [1971], the amplitude variation of the shear waves propagating through the analyzer versus the polarization vector rotation angle relative to the plates orientation is close to the cosine function. The deviations from the regularity $A = A_S \cos j$ may be explained by inaccurate count of angles and amplitudes. The analyzer quality depends on the length of the wave propagation in it and on the wavelength to plates thickness ratio.

Such a passive analyzer may be considered to be a model of the medium in which the effect of linear acoustic anisotropic absorption (LAAA) of shear waves is realized. Among natural formations there are texturized, layered media and media with a linear texture, in which a regular alternation of one elements, stretched in a certain direction, with others is observed. Such a texture is inherent to many crystalline rocks. So the manifestation of LAAA should be expected in rocks. The degree of its display will depend on the level of the texture "organization" of a rock sample, heterogeneity presence, acoustic contrast and its structural elements [Gorbatsevich, 1990].

The effect of linear anisotropic absorption will, probably, be displayed in combination with the effect of elastic anisotropy. A joint analysis of these effects for low symmetry media is very complicated. Therefore below, using some particular cases as examples, we shall consider the LAAA display in isotropic media and its manifestation in combination with the effect of elastic anisotropy during the propagation of shear waves in the simplest transverse-isotropic medium. The results

of a theoretical analysis given below do not claim to be full and complete, since only phenomenological consequences of the phenomenon have been considered.

For LAAA observation of most interest is the analysis of circle diagrams obtained when the polarization vectors are parallel (VP position). But when the LAAA and elastic anisotropy effects are acting jointly, one should observe the changes in the circle diagrams obtained with the crossed polarization vectors of the source and receiver (VC position).

2.2. Isotropic medium

Let us imagine that the medium, of which the sample analyzed has been made, is isotropic and exhibits the LAAA effect ideally. Such a sample acts as a linear polarizer and fully absorbs shear waves when their polarization vector is orthogonal to the greatest transmission direction (GT). On the basis of LAAA cosine function [Proctor, 1971], for the received waves amplitude A_{VP}, measured at the parallel polarization vectors of the transducers (VP position), we obtain

$$A_{VP} = A_S A_R A_{RE} \cos j \sin(\omega t - \frac{2\pi x}{\lambda} + \varphi_0), \qquad (2.1)$$

where A_S is the amplitude of waves radiated by the source; A_R is the value of the receiver greatest sensitivity; A_{RE} is the factor of analyzer transmission in the GT direction; j is the angle between the direction of polarization vectors and the GT direction.; ω is the waves circle frequency; t is time; λ is the wavelength; x is the sample length; φ_0 is the initial phase shift. The circle diagram of the A_{VP} value within the angle $j = 2\pi$ is given in Fig. 2.1.

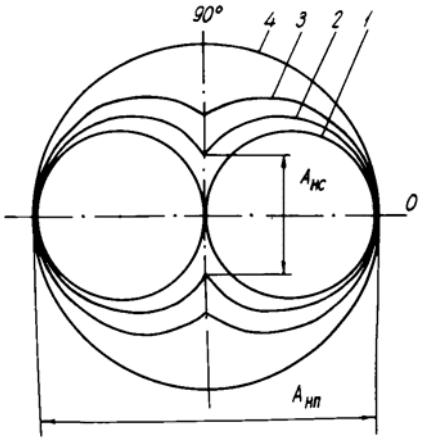

Fig. 2.1. Circle diagrams of the amplitude variation of shear waves that have passed an isotropic medium with different degrees of LAAA effect manifestation. 1 – D = 1.0; 2 – D = 0.5; 3 – D = 0.25; 4 – D = 0.

The medium, of which the sample has been made, may not manifest itself as an ideal linear polarizer. In this case in the direction perpendicular to GT the receiver should register some amplitude A_{RE} depending on the degree of LAAA manifestation. Taking the transmission factor in the direction perpendicular to GT to be equal to $A_{RR,}$ we obtain that in the direction of "the greatest transmission" the factor $A_{RE} = A_{RN} + A_{RR}$, where A_{RN} is an additional to A_{RR} transmission factor in the GT direction. Equation (2.1) for the case of non-ideal LAAA manifestation will be

$$A_{VP} = A_S A_R (A_{RN} \cos j + A_{RR}) \sin(\omega t - \frac{2\pi x}{\lambda} + \varphi_0). \qquad (2.2)$$

The degree of LAAA manifestation in a sample can be expressed by the following index [Acoustic polarization…, 1985]

$$D = \frac{A_{RE} - A_{RR}}{A_{RE} + A_{RR}}, \tag{2.3}$$

where the value of A_{RE} is determined when $j = 0$ and A_{RR} – when $j = 90^o$.

According to (2.3), the sample with a full effect of LAAA has a degree of $D = 1$, with the absence of LAAA $D = 0$. Figure 2.1 shows the circle diagrams of the amplitude A_{VP} variation (VP position) for media with different degrees of LAAA. If the polarization vectors of the transducers are crossed (VC position), then for an isotropic medium the amplitude $A_{VC} = 0$ with any degree D.

2.3. Transverse-isotropic medium

The amplitudes of the shear waves that have passed through the sample in the direction of the isotropy plane (VP position), are described by Eq. (1.9) and (1.10). When the effects of LAAA and elastic anisotropy act jointly, with the multiplier of the expression (2.2), Eq. (1.9) and (1.10) become:

$$A_{VP} = A_S A_R (A_{RN} \cos j + A_{RR})[\cos^2 \beta \sin(\omega t - \frac{2\pi x}{\lambda_1} + \varphi_0) + \sin^2 \beta \sin(\omega t - \frac{2\pi x}{\lambda_2} + \varphi_0)], \tag{2.4}$$

$$A_{VC} = \frac{1}{2} A_S A_R (A_{RN} \cos j + A_{RR}) \sin 2\beta [\sin(\omega t - \frac{2\pi x}{\lambda_1} + \varphi_0) - \sin(\omega t - \frac{2\pi x}{\lambda_2} + \varphi_0)]. \tag{2.5}$$

Equations (2.4) and (2.5) describe variation of harmonic amplitudes of shear waves that have passed the sample made of the medium exhibiting transverse-isotropic symmetry of elastic properties and LAAA effect when, in the former case, the polarization vectors are parallel and, in the latter one, when they are crossed at 90^o. In the presence of the effect the envelope amplitude registered by the receiver in the VP position, Eq. (1.14), with the multiplier (2.2) will be equal to:

$$A_{VPM} = A_S A_R (A_{RN} \cos j + A_{RR}) \sqrt{\cos^4 \beta + 2\cos^2 \beta \sin^2 \beta \cos \delta + \sin^4 \beta}. \tag{2.6}$$

In the VC position the envelope amplitude A_{VCM}, Eq. (1.16), will be supplemented by the multiplier,

$$A_{VCM} = A_S A_R (A_{RN} \cos j + A_{RR}) \sin 2\beta \sin \frac{\delta}{2}. \tag{2.7}$$

For practical analysis of the peculiarities of the joint display of LAAA and elastic anisotropy effects we shall follow the variation of amplitudes A_{VP} and A_{VC} (their envelopes) within the circle diagrams ($\beta = 0 \div 2\pi$) for some particular cases, that are characterized by certain phase ratios of waves, propagating along the axis and symmetry plane of the medium, and by the degree D.

1. The size of an anisotropic sample, expressed in the wavelengths, is equal to:

$$x = \frac{\lambda_1 \lambda_2}{4(\lambda_1 - \lambda_2)}.$$

With such a value of x the phase of the wave propagating with the polarization vector, oriented along the plane of elastic symmetry, is ahead of the wave phase with the vector oriented along the symmetry axis, by the angle $\delta = \pi/2$. Taking the GT direction to coincide with the medium symmetry plane (angle $j = \beta$), from (2.4), for the signal amplitude, detected in the VP position, we obtain ($D = 1$)

$$A_{VP} = A_S A_R A_{RE} \cos\beta[\cos^2\beta \sin(\omega t + \psi) + \sin^2\beta(\omega t + \psi)]. \quad (2.8)$$

For the signal amplitude, detected in the VC position, from (2.5) we obtain ($D = 1$)

$$A_{VC} = \frac{1}{2} A_S A_R A_{RE} \cos\beta \sin 2\beta[\sin(\omega t + \psi) - \cos(\omega t + \psi)]. \quad (2.9)$$

Similarly, from Eq. (2.6) and (2.7) the expressions for the envelopes A_{VP} and A_{VC} can be obtained. Figures 2.2.1–2.2.5 show the circle diagrams for variation of the envelopes of the harmonic amplitudes A_{VP} and A_{VC} ($\delta = 90°$) versus the rotation angle with respect to the plane of the medium elastic symmetry.

Circle diagrams for the VP position are given in a solid line, those for the VC position - in a dotted line. In Figure 2.2.1 the circle diagrams are given for the sample that does not exhibit LAAA ($D = 0$) [Acoustic polarization…, 1985], in Fig. 2.2.2 – for $D = 0.25$, in Fig. 2.2.3-2.2.5 – for $D = 0.5$ and $D = 0.75$, $D = 1$ accordingly.

2. The size of an anisotropic sample, expressed in the wavelengths is equal to

$$x = \frac{\lambda_1 \lambda_2}{2(\lambda_1 - \lambda_2)}.$$

In this case $\delta = \pi$. We shall maintain the condition $j = \delta$. Equation (2.4) with $\delta = \pi$ and $D = 1$ will be

$$A_{VP} = A_S A_R A_{RE} \cos\beta \cos 2\beta \sin(\omega t + \psi). \quad (2.10)$$

From (2.5) with $\delta = \pi$, $j = \delta$, $D = 1$ we shall obtain

$$A_{VC} = A_S A_R A_{RE} \cos\beta \sin 2\beta \sin(\omega t + \psi). \quad (2.11)$$

The circle diagrams for the case $\delta = \pi, j = \delta, D = 0$ and also for $\delta = \pi, j = \delta, D = 0.25$, $D = 0.5$, $D = 0.75$, $D = 1$ are given in Figs 2.2.6-2.2.10. A joint examination of the analysis results and Figs 2.1, 2.2 shows that for both isotropic and anisotropic media the circle diagrams can serve to determine the direction of the greatest and the least transmission as well as the degree of the LAAA manifestation. The LAAA effect is most conspicuous in variation of the circle diagrams envelopes, calculated for the transducers VP position. In the absence of the phase difference δ along the selected direction in the sample and with a full effect of LAAA the circle diagram in the VP position should be close to the function $A_{VP} = \cos j$. As the phase difference (from $\delta = 0$ to $\delta = \pi$) increases the circle diagram of an anisotropic sample in the VP position

becomes more stretched along the GT direction, additional minima appear on it. The presence of LAAA leads only to some envelope distortion of the circle diagrams, calculated for the VC position, to the area decrease and reduction in the petals size. As the medium index D increases the VP circle diagram stretches along the GT direction.

2.4. Observations of LAAA in model media

To check the above stated theoretical concepts we performed model experiments trying to determine the impact of linear heterogeneity on the amplitude and values of compression and shear waves velocities. The measurements were made by the acoustopolarization determination methods [Gorbatsevich, 1986]. A cylindrical sample made of polymethylmethacrylate (organic glass) was used as a model (Fig. 2.3.A).

Before every measurement cycle holes 2 mm in diameter parallel to each other and perpendicular to bundle of ultrasonic waves were formed. Measurements were made with unfilled, hollow and filled with thick mineral oil holes. To a certain extent, in the first case the model represented a porous medium with strongly oriented fractures filled with gas while in the second case it represented also oriented but filled with mineral oil or, otherwise, liquid hydrocarbons fractures. Altogether 15 individual measurements were made, first in a model without holes, then successively in the model with 1, 2, 3, 4, 5, 7 and 9 holes. For measurements standard ultrasonic apparatus was used [Acoustic polarization…, 1985] and transducers of purely shear, linear-polarized waves with natural frequency of f_0 = 0.47 MHz. The main measurement results are given in Table 2.1, the acoustopolarigram of the model without holes - in Fig. 2.3.B and acoustopolarigrams of the models with unfilled – in Fig. 2.3.1-2.3.3 and filled holes – in Fig. 2.3.4-2.3.6.

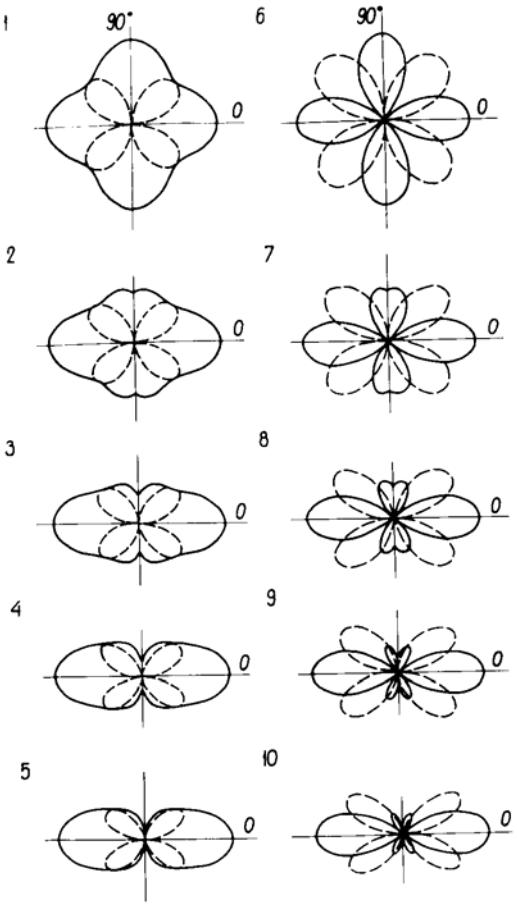

Fig. 2.2. Circle diagrams for variation of the amplitude of shear waves propagation in anisotropic medium with different degrees of LAAA effect. 1, 6 – D = 0; 2, 7 – D = 0.25; 3, 8 – D = 0.5; 4, 9 – D = 0.75; 5, 10 – D = 1.0. For patterns 1-5 the phase difference is equal to $\delta = \pi/2$, for 6-10 $\delta = \pi$. Solid lines are for VP, dotted lines - for VC.

The table gives the value of conditional porosity n calculated as the holes volume to the model volume ratio in relation to the holes quantity. The compression wave velocities V_p are presented in the table as well. The shear wave velocities measured with the polarization vector oriented along the holes V_{s1} and perpendicular to them (V_{s2}) are given in the table too. The value of V_{s2} was calculated

with regard to the phase difference δ, determined in the course of acoustopolarization measurements [Gorbatsevich, 1995]. In the table the ratio of the amplitude of the compression wave that has passed through a model with holes A_{pi}, to the amplitude A_{p0} measured in the sample without holes is given. Similarly, the ratio of the shear wave amplitudes A_{sim}/A_{s0} was obtained, A_{sim} being measured when the polarization vector of the transducers was in the plane passing through the holes axes.

Table 2.1.

Results of measuring elastic wave velocity and amplitude in models with different numbers of holes*).

Number of holes	Conditional porosity n, %	Holes filled with gas						Holes filled with oil					
		V_p, km/s	V_{s1}, km/s	V_{s2}, km/s	A_{pi}/A_{p0}	A_{sim}/A_{s0}	D	V_p. km/s	V_{s1}, km/s	V_{s2}, km/s	A_{pi}/A_{p0}	A_{sim}/A_{s0}	D
0	0	2.75	1.38	1.380	1.0	1.0	0.0	2.75	1.380	1.380	1.0	1	0.0
1	1.27	2.75	1.38	1.380	0.81	0.69	0.0	2.75	1.380	1.375	0.81	0.69	0.27
2	2.54	2.75	1.38	1.379	0.45	0.56	0.030	2.75	1.380	1.378	0.45	0.60	-
3	3.81	2.75	1.38	1.377	0.45	0.45	0.064	2.75	1.380	1.374	0.45	0.40	0.31
4	4.72	2.75	1.38	1.374	0.45	0.35	0.088	2.75	1.380	1.365	0.45	0.35	0.44
5	5.63	2.73	1.38	1.374	0.38	0.39	0.091	2.73	1.380	-	0.38	0.38	0.53
7	7.45	2.71	1.38	1.369	0.25	0.34	0.106	2.71	1.380	1.358	0.25	0.33	0.65
9	9.27	2.71	1.38	1.361	0.25	0.24	-	2.71	1.380	-	0.25	0.28	-

*) Measurements on the model have been made by PhD M.Z. Abdrakhimov and Eng. S.K. Belyaev.

Linear anisotropic absorption was measured by formula (2.3) that reflects various absorption of shear waves at different orientation of the polarization vector relative to the medium structure (in this case – the holes axes). Figure 2.4 shows the dependence of the value D in the model with unfilled and filled with oil holes as well as the amplitude ratio A_{sim}/A_{s0} on the holes number in the model.

As the test results (Fig. 2.3) suggest, the acoustopolarigram, obtained at the transducers' parallel polarization vectors, is a curve very close to a circle. This shows that the model initial material is elastic-isotropic [Gorbatsevich, 1986].

The model with holes filled with air exhibits a slight increase in elastic anisotropy as the number of holes or conditional porosity index n rises (Tab. 2.1, Fig. 2.4). Judging by the acoustopolarigrams VC distinct anisotropy is observed with 5-7 holes in the model. With such number of holes a slight decrease (0.8-1.5%) in the velocity of compression V_p and shear V_{s2}, waves is observed with the polarization vector oriented along the normal to the holes. As the number of holes increases in the path of the ray bundle, the amplitude of both compression A_{pi}/A_{p0} and shear A_{sim}/A_{s0} waves substantially decreases.

For instance, with 9 holes both compression and shear waves attenuate nearly 4 times. Moreover, the degree of this attenuation does not depend on the fact whether the holes are filled or not (Fig. 2.3.A). Quite another picture is observed when analysing the variation of the shear wave amplitude with the polarization vector oriented along the normal to the hole axis. It is best shown in Fig. 2.3.4–2.3.6. For example, the acoustopolarigram obtained for the model with five filled holes, Fig. 2.3.5, is similar to the theoretical circle diagram, Fig. 2.2.3, with $D = 0.5$, $\delta = \pi/2$.

When the number of the oil-filled holes in the model increases the acoustopolarigram VP flattens and the index D greatly increases (Fig. 2.4). Judging by the slope of the averaged straight lines the index D in the case with filled holes is 6 times higher than that in the model with unfilled holes. The reason is that as shear waves with the displacement vector oriented along the normal to the holes pass, most of the vibrational power does not reflect at the hole boundary, but passes in the liquid and dissipates there.

This conclusion is drawn from the fact that ultrasound velocity in mineral oil (V_p = 1.44 *km/s*) is close to the shear wave velocity in the model material (V_s = 1.38 *km/s*) with a slight difference in the density of oil (ρ = 0.87 *g/sm*^{3}) and polymethylmethacrylate (ρ = 1.18 *g/sm*^{3}). If the holes or pores are not filled then elastic energy does not overcome the medium-gas boundary and hence is not lost. In this case due to diffraction a shear wave rounds the holes.

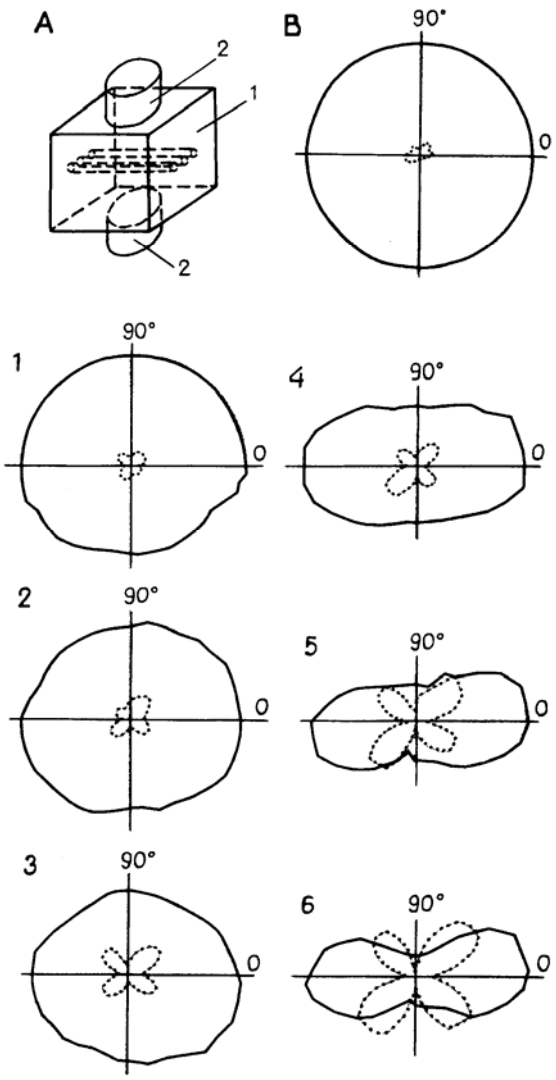

Fig. 2.3. Model and acoustopolarigrams of the model with oriented holes.
A – model, B - acoustopolarigrams of the model without holes. Acoustopolarigrams of the model with holes: (1), (2) and (3) – 3, 5 and 7 holes respectively, a filler is air; (4), (5) and (6) – 3, 5 and 7 holes respectively, a filler is mineral oil. VP, solid lines; VC, dotted lines.

On the basis of the above model experiments the following conclusion may be drawn. The effect of linear acoustic anisotropic absorption arises in media when linear polarized shear waves interact with heterogeneity oriented along the line or planes. Those may be both filled, for instance, with liquid and unfilled oriented fractures. The degree of LAAA greatly depends on the fact whether the holes are filled with liquid or they are dry. Filling the fractures, for instance, with liquid hydrocarbons may substantially rise the LAAA index D. The observation of LAAA in natural media allows one to register some forms of this phenomenon.

As a whole, the LAAA effect may be represented by two basic models. One of them is the above Proctor's model [Proctor, 1971] or model I. In rocks this model may be realized in the media that have oriented cracks or plane elements (minerals), such as mica, talc et al. On a sample of the medium representing model I the LAAA effect will be observed on the sides where the butt-ends of the plane elements are exposed, Fig. 2.5a. In this case the "greatest transmission" directions and, accordingly, the

largest diameters of the VP acoustopolarigrams on the neighbouring sides will be directed to each other and pinpoint the arrangement of the plane elements. On the side parallel to the plane elements VP acoustoplarigrams that are close to isometric will be detected. The observation results (Fig. 2.3) allow one to conclude that there is another, radically different from the first model - model II. It consists of linear elongated in one direction, isometric in the cross section elements (Fig. 2.5b).

As follows from the Figure, on the sample representing the medium of model II the LAAA effect will be most conspicuous on the sides parallel to linear elements. Unlike model I, the directions of "the greatest transmissions" and, accordingly, the largest diameters of the VP acoustopolarigrams will be directed to the side perpendicular to linear elements. On this side the VP acoustopolarigram close to isometric should be obtained. As follows from Fig. 2.5a and 2.5b, the difference between the medium of model I and that of model II may be established only on the basis of spatial measurements system.

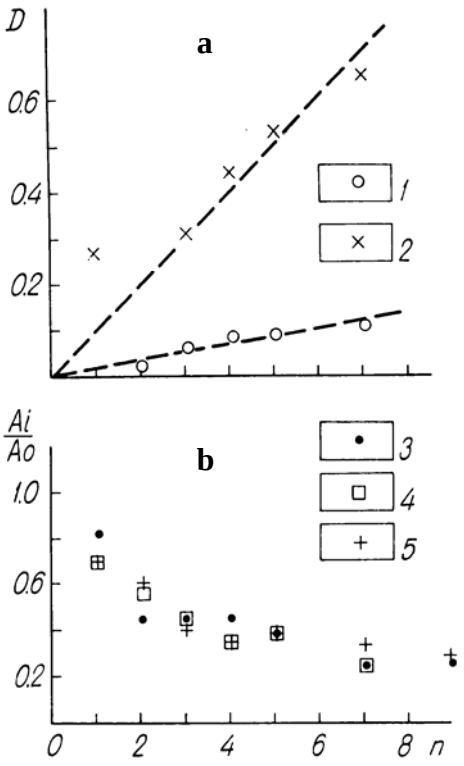

Fig. 2.4. (a) LAA index *D* measured on the model with unfilled (1) and filled (2) holes. (b) Ratio A_{pi}/A_{po} (3), ratio A_{sim}/A_{so} in the model with unfilled (4) and filled (5) holes in relation to the holes number in the model.

2.5. LAAA observations on a model with an angular unconformity with elastic symmetry elements

An arrangement of symmetry elements of elastic anisotropy and linear acoustic anisotropic absorption in solid bodies may not coincide since those phenomena are of different physical nature. With an angular unconformity between the symmetry elements of LAAA and elastic anisotropy formulae (2.6) and (2.7) take the following form:

$$A_{VPM} = A_S A_R (A_{RN} \cos(j+\tau) + A_{RR}) \sqrt{\cos^4\beta + \cos^2\beta \sin^2\beta \cos\delta + \sin^4\beta}\,, \quad (2.12)$$

$$A_{VCM} = A_S A_R (A_{RN} \cos(j+\tau) + A_{RR}) \sin 2\beta \sin\frac{\delta}{2}, \quad (2.13)$$

where τ is an angle between an elastic symmetry element of the media and a symmetry element of the LAAA spatial figure of the solid body.

By formulae (2.12) and (2.13) we have calculated circle diagrams of A_{VPM} and A_{VCM} amplitudes with two values of the phase difference $\delta = \pi/2$, $\delta = \pi$ and different unconformity angles τ. The calculation results are given in Fig. 2.6.

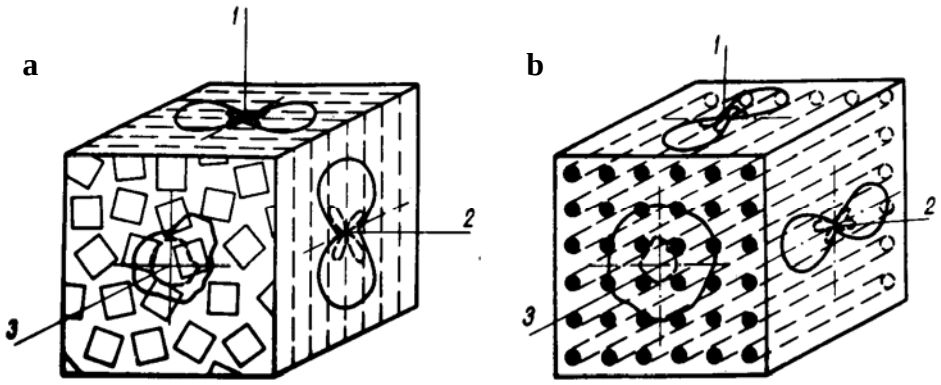

Fig. 2.5. Plane (a) and linear (b) models of LAA display. VP, solid lines; VS, dotted lines.

As follows from the diagrams, with the angular unconformity $0<\tau<45^o$ A_{VPM} diagrams become asymmetric both with $\delta = \pi/2$ and $\delta = \pi$. These diagrams become symmetric with $\tau = 0, 45^o + n\pi/4$, where $n = 0, 1, 2, 3\ldots$. Such a peculiarity of the VP diagrams may serve as a diagnostic sign for the presence of the angular unconformity between the elastic symmetry element of the media and the symmetry element of the LAAA spatial figure of the solid body. With this unconformity the variations in the A_{VCM} diagrams obtained at crossed polarization vectors are all the more conspicuous. The petals of these diagrams become unequal in size and area and with $\tau = 45^o$ a four-petal figure becomes two-petal. With the phase difference $\delta = \pi$ and $65^o > \tau > 25^o$ an intriguing phenomenon is observed - in a certain angle range the amplitude with the crossed polarization vectors becomes larger than that with the parallel ones ($A_{VCM} > A_{VPM}$). These signs are determining at the angular unconformity diagnosis.

Besides the calculations, we have taken model measurements of the mutual influence the mentioned effects exert on the acoustopolarigram shape [Gorbatsevich & Il'chenko, 1997]. The model prepared for measurements was made of two plates (Fig. 2.7). One of the plates was made of piezoelectric ceramics of PZT type. The material of this plate is an anisotropic medium of transverse-isotropic symmetry type. The plate was sawn in such a way that its surfaces were parallel to the elastic symmetry axis of the ceramics. It was 4.25 *mm* thick. The second plate was made of wood with regular foliation, since it has a strong LAAA effect [Gorbatsevich, 1999]. The wooden plate of 2.25 *mm* thickness was sawn in such a way that the direction of its fibres coincides with the symmetry axis along elongation. Acoustopolarigrams for the ceramic and wooden plates are presented in Fig. 2.7. The measurements were taken at the basic frequency f_0 = 1.12 MHz. The phase shift along the axis and the symmetry plane in the ceramic plate is 88^o and in the wooden plate - 56^o.

Before the measurements on the model the position of the plates relative to each other was rigidly fixed with a special clamp. Then the fastened plates were placed on the rotating platform of the acoustopolariscope [Gorbatsevich, 1995]. The acoustic contact between the plates was performed with a high-viscous solution of non-crystallized polysaccharides [Acoustic polarization….1985]. In the sequence of measurements the pulse amplitude of the passing waves in the rotation angle range of $0\text{-}360^o$ with a step of 10^o was fixed. The amplitude measurements were conducted

both at crossed (VC) and parallel (VP) polarization vectors. In a sequence of measurements the mutual orientation of the model plates was successively changed. At first the angle between the plates was 0^o. Then the angle between the plate axes was changed to 15^o. After that the mutual angle was increased by further 15^o. Thus, a set of acoustopolarization measurements was performed with the angles between the model symmetry elements of 0, 15, 30, 45, 60, 75 and 90^o.

By the VP acoustopolarigram we determined the degree of LAAA manifestation D and by the VP and VC acoustopolarigrams - angles α_1, α_2 and α_3. The angle α was determined between the reference axis 0^o and a strait line passing through the model rotation axis and opposing amplitude maxima of the VP acoustopolarigram (petal tops of a larger pair). The angles α_2 and α_3 were determined between the reference axis 0^o and strait lines passing through the opposite minima of the VC acoustopolarigram. At every measurement stage the change in the size and shape of the acoustopolarigram petals was detected. The measurement results are given in Fig. 2.7 and Table 2.2.

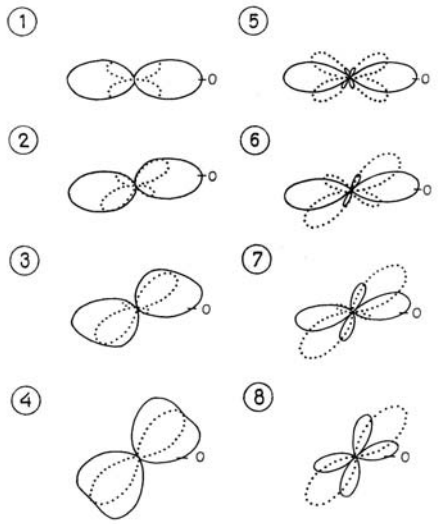

Fig. 2.6. Circle diagrams of A_{VPM} amplitudes for two values of the phase difference $\delta = \pi/2$ (1-4), $\delta = \pi$ (5-8) and different discordance angles $\tau = 0^o$ (1, 5), 15^o (2, 6), 30^0 (3, 7), 45^o (4, 8). The angle count is performed from the elastic symmetry element of the media, the LAAA symmetry element is displaced by an angle τ. VP - solid lines; VC - dotted lines.

When the angle τ between the elastic symmetry elements is 0^o, Fig. 2.7.a, the summary acoustopolarigram presents a combination of acoustopolarigrams, Fig. 2.7.2 and 2.7.3, and the model presents a transverse-isotropic medium with a high LAAA manifestation. An estimation of its degree by formula (2.3) gives $D = 0.53$, angles $\alpha_1 = 0^o$, $\alpha_2 = 0^o$, $\alpha_3 = 90^o$, Table 2.2.

When the plates rotate relative each other through $\tau = 15^o$ the LAAA degree increases to $D = 0.58$ (Fig. 2.7b). The VC acoustopolarigrams petals become asymmetric. For instance, the petals located in quarters I-III of the circle became twice larger and wider and those from quarters II-IV became slightly longer, by some 10%. Judging by the angle α_1 the VP acoustopolarigram has rotated relative to the reference axis by about 10^o. The angles marking the position of the elastic symmetry elements are $\alpha_2 = 0^o$, $\alpha_3 = 114^o$.

When rotated through $\tau = 30^o$ the LAAA index changed to the value of $D = 0.37$ (Fig. 2.7c). The rotation angles of the acoustopolarigrams symmetry elements were $\alpha_1 = 15^o$, $\alpha_2 = 0^o$, $\alpha_3 = 130^o$. When rotated through $\tau = 45^o$ the LAAA degree increased to $D = 0.52$ (Fig. 2.7d). The VP and VC acoustopolarigrams took near-two-petal shape. In this case it was possible to measure only two angles - $\alpha_1 = 0^o$ and $\alpha_2 = 0^o$. A great increase in the amplitude of the waves detected at the VC position is observed. This amplitude markedly exceeds the amplitude of the waves detected in the VP position.

The observations performed at $\tau > 45^o$ show that the resultant acoustopolarigrams are mirror images of the previous ones. The discrepancy between the acoustopolarigrams obtained at $\tau = 15^o$ and $\tau = 75^o$, $\tau = 30^o$ and $\tau = 60^o$, are likely to be caused by inaccurate setting of the angle between the model plates and unstable

contact conditions. If the values of D, α_1, α_2 and α_3 are similar, the acoustopolarigrams at $\tau = 90^o$, on the whole, are close to the acoustopolarigrams outlines at $\tau = 0^o$.

Analysing the data from Fig. 2.7 and Table 2.2 it should be noted that increasing the angle between the model plates, a slight rotation of the acoustopolarigram symmetry axis (its largest diameter) at the VP position occurs. From $\tau = 0$ to $\tau = 45^o$ this rotation takes place in the same direction as the rotation of one of the model plates. But at $\tau > 45^o$ this rotation occurs in the opposite direction.

When the angle τ is changed the LAAA degree does not vary greatly. Judging by the constant value of the angle $\alpha_2 = 0^o$, the elastic symmetry element singled out on the VC acoustopolarigrams and corresponding to the symmetry element of the wooden plate remains unchanged. It can be easily explained by the fact that in a sequence of measurements the ceramic plate changed its position, while the wooden plate remained in place regarding the acoustopolariscopy reference scale.

The elastic symmetry second element corresponding to the symmetry element of the ceramic plate is adequately reflected on the VC acoustopolarigrams only at low rotation angles τ. At $\tau \sim 20^o$ and higher the real position of the symmetry elements of the ceramic plate cannot be determined by the VC diagrams minima. This aspect should be taken into consideration in the presence of an angular unconformity between the symmetry elements of LAAA and elastic anisotropy.

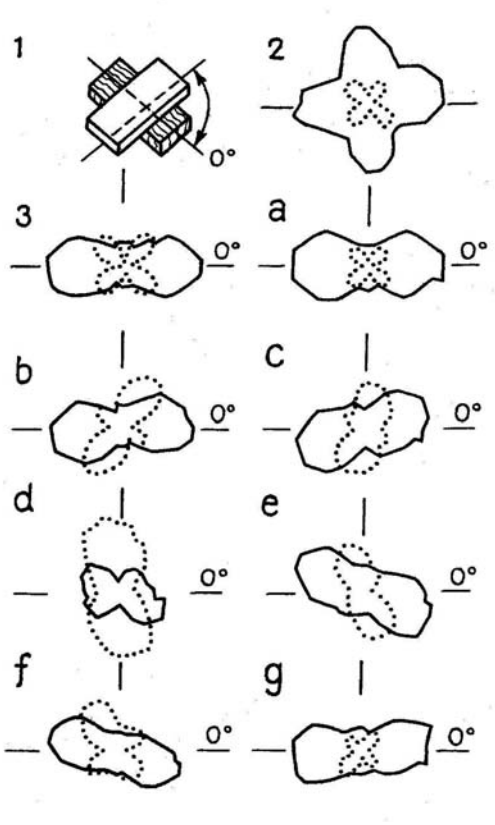

Fig. 2.7. Sketch model and acousto-polarigrams obtained at different angles between the symmetry elements of the ceramic and wooden plates.
1 - sketch model, - the upper plate is ceramic, the lower – wooden. 2 - acoustopolarigrams for the ceramic plate. 3 - acoustopolarigrams for the wooden plate. Acoustopolarigrams for the model with angles τ between the symmetry elements of the plates, accordingly: a – 0^o, b – 15^o, c – 30^o, d – 45^o, e – 60^o, f – 75^o, g – 90^o. The angle count is performed from the LAAA symmetry element of the wooden plate, the elastic symmetry element is displaced by the angle τ. VP - solid line; VC - dotted line.

Thus, both theoretical calculations and model tests revealed that the most characteristic sign for the presence of an angular discrepancy between the symmetry elements of LAAA and elastic anisotropy is inequality of the petals size and area in the VC acoustopolarigram. In this case the largest diameter of the VC acoustopolarigram may be greater than that of the VP acoustopolarigram.

A theoretical analysis and observations on the joint display of elastic anisotropy and the LAA effect on model media allow one to draw the following conclusions:

1. The acoustopolarigrams for the samples of the media exhibiting the linear acoustic anisotropic absorption (LAAA) effect enable determining the direction of the greatest and least "transmission" of shear waves and the LAAA manifestation

degree.

Table 2.2.

Angles measured on the acoustopolarigrams of the model made of ceramic and wooden plates[**)].

Angles between the symmetry elements of the model plates τ, grad		0	15	30	45	60	75	90
Rotation angles of the acoustopolarigrams symmetry elements	α_1, grad	0	10	15	0	160	165	0
	α_2, grad	90	114	130	0	65	78	90
LAAA degree D		0.53	0.58	0.37	0.52	0.49	0.53	0.49

Notes: angle $\alpha_2 = 0$ for all the values of angles α_1 and α_3.
[**)]The measurements have been made by PhD V.L. Ilchenko

2. The influence of the LAAA effect is most conspicuous in the change of the shape of the acoustopolarigrams obtained in the VP position of the source and receiver. As the phase difference increases in the range of 0-π the VP acoustopolarigram of anisotropic type becomes more elongated, additional minima appear on it.
3. The LAAA effect brings only a slight distortion of the shape of the acoustopolarigrams obtained in the VC position.
4. Two main types of the LAAA display have been identified - plane and linear. With plane type of LAAA the acoustopolarigrams largest diameters are oriented to the opposite sides of the cubic sample. With the linear type of LAAA the acoustopolarigrams largest diameters are oriented to the same side.
5. The spatial orientations of elastic symmetry elements and structural elements that cause the LAAA effect do not always coincide. When they coincide the shape and size of petals of the acoustopolarigrams obtained at crossed polarization vectors are identical.
6. The most characteristic feature of the angular divergence between the symmetry elements of LAAA and elastic anisotropy is inequality of the petals size and area of the VC acoustopolarigram. The largest diameter (maximum amplitude) of the VC acoustopolarigram may be larger than that of the VP acoustopolarigram.

3. DEPOLARIZATION OF SHEAR WAVES IN ANISOTROPIC HETEROGENEOUS MEDIA

As indicated above, the effect of linear acoustic anisotropic absorption (LAAA) manifests itself in the media containing plane or linear elements. Another effect observed in propagating seismic waves through geological media is associated with a change in the degree of polarization of shear oscillation trains. Such a change is accompanied by a buildup in the ellipticity of shear oscillations or by their depolarization. Following Aleksandrov [1997], the polarization phenomenon is accounted for by the scattering of shear waves from small- and large-scale inhomogeneities. His conclusions were corroborated by Crampin's experiments on inhomogeneous cracked media [Crampin, 1985]. A different interpretation of the polarization phenomenon was proposed by Obolentseva [1992]. According to her theory, depolarization occurs in some solids due to their gyrotropic or acoustical activity. When a shear wave propagates in such media, its polarization vector rotates through an angle proportional to the distance travelled.

To our opinion, the polarization effect is also appreciably manifested as shear waves propagate in a medium consisting, for example, of differently oriented elastic anisotropic layers. This paper describes some theoretical aspects of the shear wave depolarization (SWD) effect, modeling results, and determinations of the effect in crystalline rock samples. The obtained results show that the SWD effect is rather frequently observed in anisotropic crystalline rocks composed of grains whose elastic symmetry is sufficiently maintained, for example, in two directions.

3.1. Theoretical aspects of SWD

We consider the problem on the propagation and detection of shear waves in a transversely isotropic medium composed of two parts (I and II), whose lengths in the wave direction are x_I and x_2 respectively (Fig. 3.1). In part I, the medium symmetry axis is oriented in the direction [100], and the symmetry plane in the direction [010]-[010']. In part II, the symmetry axis runs along the direction [100"] and the symmetry plane passes through the direction [010"]-[010'"]. The symmetry axis and plane of part II form an angle α to the symmetry axis and plane of part I. These parts make contact with each other (maintaining the acoustical contact) along planes [l00']-[0l0'] and [l00']-[0l0"]. A linearly polarized harmonic shear oscillation $A_S = A\sin(\omega t + \varphi_0)$ is applied in plane [100]-[010] of part I, in the direction *OK*, at an angle β to direction [010]. The vector A_S has the component $B = A\sin\beta\sin(\omega t + \varphi_0)$ in direction [100] and the component $C = A\cos\beta\sin(\omega t + \varphi_0)$ in direction [010]. Once the shear oscillations in part I have run distance x_1 the component B in direction [100'] becomes equal to [Gorbatsevich, 1982]

$$B' = A\sin\beta\sin\left(\omega t - 2\pi x_1 / \lambda_{11} + \varphi_0\right), \tag{3.1}$$

and in direction [010']

$$C' = A\cos\beta\sin\left(\omega t - 2\pi x_1 / \lambda_{12} + \varphi_0\right), \tag{3.2}$$

where λ_{11}, λ_{12} are the wavelengths with the polarization vectors oriented along the symmetry axis and symmetry plane, respectively.

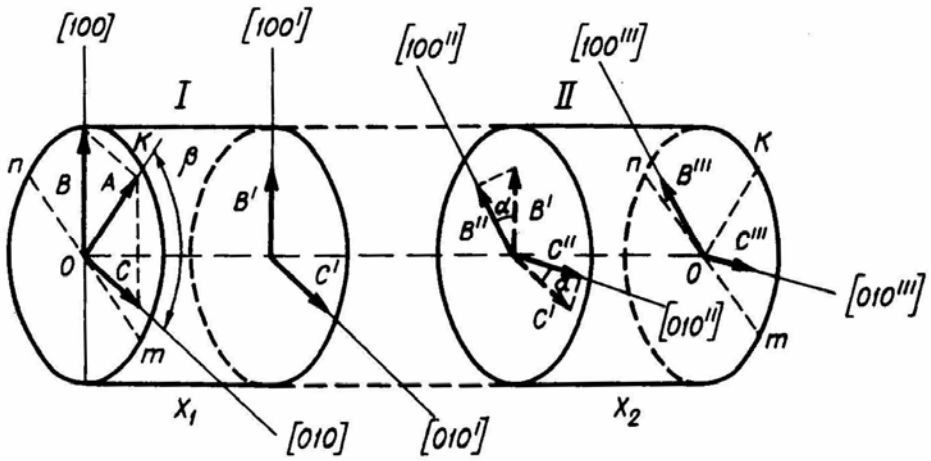

Fig. 3.1. Sketch of detecting the amplitude of a shear wave passing through parts *I* and *II* of the sample. The elastic symmetry elements form an angle α to each other.

In the acoustical contact of parts I and II, vectors B' and C' produce the displacements along direction [100"]

$$B'' = A \cdot (Z_{BB} \cos\alpha \sin\beta \sin r_{11} - Z_{CB} \sin\alpha \cos\beta \sin r_{12}), \tag{3.3}$$

and along direction [010"]

$$C'' = A \cdot (Z_{BC} \sin\alpha \sin\beta \sin r_{11} + Z_{CC} \cos\alpha \cos\beta \sin r_{12}), \tag{3.4}$$

where Z_{BB}, Z_{CB}, Z_{BC} and Z_{CC} are the coefficients of shear wave passage, depending on the ratio between the velocities of waves in the contact along directions B', C', B'' and C'' and on the densities of the parts of medium ρ_1 and ρ_2; $r_{11} = \omega t - 2\pi x_1 / \lambda_{11} + \varphi_0$, $r_{12} = \omega t - 2\pi x_1 / \lambda_{12} + \varphi_0$.

When the oscillations have propagated over distance x_2 in part II, components B'' and C'' take new values. The component of displacement along axis [100"'] is

$$\begin{aligned} B''' = A \cdot [&Z_{BB} \cos\alpha \sin\beta \sin(\omega t - 2\pi x_1 / \lambda_{11} - 2\pi x_2 / \lambda_{21} + \varphi_0) - \\ &- Z_{BC} \sin\alpha \cos\beta \sin(\omega t - 2\pi x_1 / \lambda_{12} - 2\pi x_2 / \lambda_{22} + \varphi_0)] \end{aligned}, \tag{3.5}$$

and along axis [010"']

$$\begin{aligned} C''' = A \cdot [&Z_{BC} \sin\alpha \sin\beta \sin(\omega t - 2\pi x_1 / \lambda_{11} - 2\pi x_2 / \lambda_{21} + \varphi_0) + \\ &+ Z_{CC} \cos\alpha \cos\beta \sin(\omega t - 2\pi x_1 / \lambda_{12} - 2\pi x_2 / \lambda_{22} + \varphi_0)] \end{aligned}, \tag{3.6}$$

where λ_{21}, λ_{22} are the lengths of the waves whose polarization vectors are oriented in the direction of the symmetry axis [100"]-[100"'] and symmetry plane [010"]-[010"'], respectively.

Assume that the receiver of oscillations is in contact with plane [100"']-[010"'] and possesses the highest sensitivity A_n in the direction parallel to line *OK,* i.e., to the displacement vector of the medium in the source plane — the position when the vectors are parallel (VP).

In this case, considering equations (3.1)-(3.6), the amplitude produced in the receiver is

$$A_{VP} = AA_n[\sin(\beta-\alpha)(Z_{BB}\cos\alpha\sin\beta\sin r_{1121} - Z_{CB}\sin\alpha\cos\beta\sin r_{1222}) + \\ +\cos(\beta-\alpha)(Z_{BC}\sin\alpha\sin\beta\sin r_{1121} + Z_{CC}\cos\alpha\cos\beta\sin r_{1222})] \quad . \quad (3.7)$$

For the case when the maximum sensitivity of the receiver is in the direction *n-m* coinciding with the normal to line *OK* — the position when the vectors are crossed (VC) we have

$$A_{VC} = AA_n[\cos(\beta-\alpha)(Z_{BB}\cos\alpha\sin\beta\sin r_{1121} - Z_{CB}\sin\alpha\cos\beta\sin r_{1222}) - \\ -\sin(\beta-\alpha)(Z_{BC}\sin\alpha\sin\beta\sin r_{1121} + Z_{CC}\cos\alpha\cos\beta\sin r_{1222})] \quad , \quad (3.8)$$

where

$r_{1121} = \omega t - 2\pi x_1 / \lambda_{11} - 2\pi x_2 / \lambda_{21} + \varphi_0$, $r_{1222} = \omega t - 2\pi x_1 / \lambda_{12} - 2\pi x_2 / \lambda_{22} + \varphi_0$.

Both amplitudes A_{VP} and A_{VC} depend on the ratios between the wavelengths λ_{11}, λ_{12}, λ_{21}, λ_{22} in each part of the medium, as well as on the distances x_1 and x_2, the densities ρ_1 and ρ_2, the indicatrix of wave velocity, the oscillation frequency, and the angles α and β.

In view of a large number of variables, formulas (3.7) and (3.8) are fairly complicated for a direct analysis. Therefore, we consider the case when a composite sample (Fig. 3.1) consists of two equal-length parts made of the same material. The arrangement of their symmetry elements is shown in Fig. 3.1. Thus, for the composite sample, we have $x_1 = x_2 = x$; $\lambda_{11} = \lambda_{21} = \lambda_1$; $\lambda_{12} = \lambda_{22} = \lambda_2$; and $\rho_1 = \rho_2 = \rho$. Assuming that the anisotropy of shear waves is weak and setting $\rho_1 = \rho_2$, the transmission coefficients are approximately equal to one, $Z_{BB} \approx Z_{CB} \approx Z_{BC} \approx Z_{CC} \approx 1$. Then, for the amplitudes A_{VP} and A_{VC} we obtain the expressions

$$A_{VP} = AA_n[\sin(\beta-\alpha)(\cos\alpha\sin\beta\sin r_{1111} - \sin\alpha\cos\beta\sin r_{2222}) + \\ +\cos(\beta-\alpha)(\sin\alpha\sin\beta\sin r_{1111} + \cos\alpha\cos\beta\sin r_{2222})] \quad , \quad (3.9)$$

$$A_{VC} = AA_n[\cos(\beta-\alpha)(\cos\alpha\sin\beta\sin r_{1111} - \sin\alpha\cos\beta\sin r_{2222}) - \\ -\sin(\beta-\alpha)(\sin\alpha\sin\beta\sin r_{1111} + \cos\alpha\cos\beta\sin r_{2222})] \quad , \quad (3.10)$$

where $r_{1111} = \omega t - 4\pi x / \lambda_1 + \varphi_0$, $r_{2222} = \omega t - 4\pi x / \lambda_2 + \varphi_0$.

Formulas (3.9) and (3.10) help to explain the features of shear waves propagating in a medium that consists, for example, of layers with the same thickness and properties, in which, however, the elastic symmetry elements are oriented in an arbitrary way. The specific case of such analysis, described below, uses the measured amplitude of shear waves in a model composed of two identical anisotropic plates.

3.2. Modeling of shear wave propagation in anisotropic plates

The acoustical polarization method was used to measure the amplitude of shear waves passing through two anisotropic plates [Acoustic polarization…, 1985]. The model prepared for measuring consisted of two anisotropic plates of uniform thickness, composed of the same elastically anisotropic ceramic material (PZT-19). The elastic symmetry plane is perpendicular to the plane of the plates with a thickness of 4.2 *mm*. The longitudinal wave velocity is V_p = 3.51 *km/s*, and the shear wave velocities are V_{s1} = 1.72 *km/s* and V_{s2} == 1.89 *km/s* for the polarization vectors perpendicular and parallel to the symmetry plane, respectively. The measurement frequency is f_0 = 1.12 MHz and the wavelengths are λ_1 == 1.54 *mm* and λ_2 = 1.69 *mm*. The difference in phase between the shear oscillations propagating normally and parallel to the symmetry plane, over a distance equal to the thickness of one plate, is δ = 88.4°.

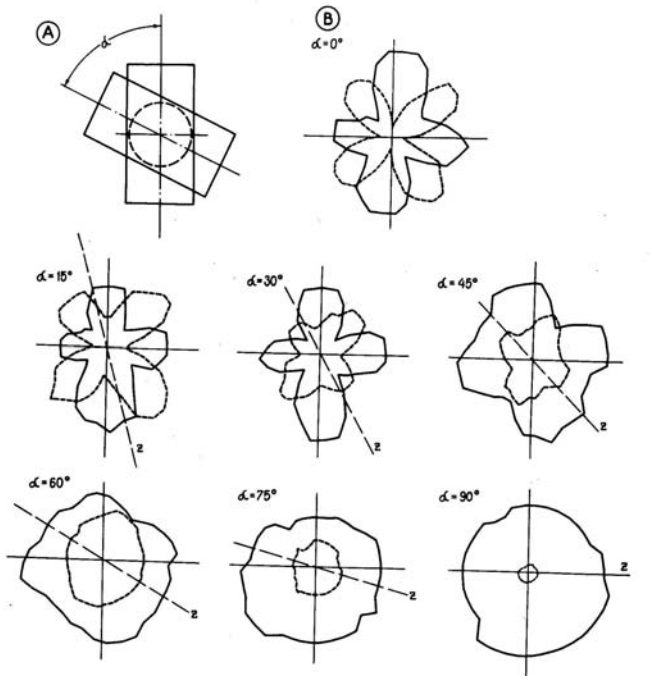

Fig. 3.2. (A) Arrangement of the plates on the acoustical polariscope platform and (B) acoustical polarization diagrams obtained for different angles α between the elastic symmetry elements of the plates. Solid and dashed lines are for the parallel and crossed polarization vectors, respectively.

In the course of measuring, the plates were superimposed on one another and placed on the platform of the acoustical polariscope [Patent No. 1281993], between the source and receiver of linearly polarized, purely shear ultrasonic oscillations, in a way that the cylindrical beam of rays passed through both of them. The relative position of the symmetry elements of the plates was fixed by a clamp (Fig. 3.2A). The first measurement of A_{VP} and A_{VS} was made for an angle of $\alpha = 0^o$ between the plate symmetry elements. The obtained VP and VC polarization diagrams are shown in Fig. 3.2B ($\alpha = 0^o$).

Then, similar diagrams were obtained for α = 15°, 30°, 45°, 60°, 75°, and 90° (Fig. 3.2B). The VP diagrams show a gradual change-over from a four-petal pattern to a figure more and more resembling a circle, as the angle α increases. The diagram for α = 90° almost coincides with that of an isotropic medium (Fig. 1.4). While increasing α the VC diagrams exhibit a pronounced feature. Specifically, the minimum amplitudes A_{VCMIN} at the points through which the elastic symmetry elements pass (α = 0°) are most likely caused by an imperfection of the shear wave converters, i.e., by the energy fraction that is detected in the so-called "dark field". At these points, A_{VCMIN} amounts to 0.126-0.141 of the maximum amplitude. However, as

α increases, A_{VCMIN} grows reaching the maximum at α = 45-60°. The further increase in $\alpha > 60^o$ results in a decrease of A_{VCMIN} which, for α = 90°, reaches the values of 0.1-0.126, which are close to those observed for $\alpha = 0^o$.

Figure 3.3 presents the measured dependence of A_{VCMIN} versus α; the averaged results of measurements are shown by the dashed line.

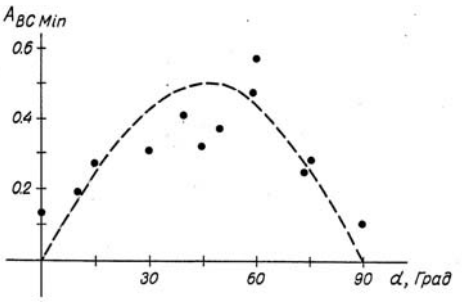

Fig. 3.3. Measured amplitudes A_{VCMIN} VERSUS the angle α. Dashes show the averaged variation in VC_{MIN}'

Thus, the shape and relative sizes of acoustical polarization diagrams, particularly of the A_{VCMIN} diagram, obtained for the crossed polarization vectors, may indicate, for example, the degree of disorientation of elastic symmetry elements in the crystalline grains of both polycrystalline and polymineral rocks.

It is necessary to note that the SWD effect manifests itself on the background of the usual change in the degree of ellipticity of shear waves while propagating in anisotropic media [Lyamov, 1983]. Consequently, the method used to detect the effect must not be sensitive to such a change. One such method is provided by the acoustical polariscopy. The SWD effect will manifest itself in the following conditions.

1. If the elastic symmetry elements in layers or grains composing the anisotropic medium are relatively disoriented within an angle range of 10-80°, the propagation of linearly polarized shear waves in the directions close to the normal to the disorientation plane is accompanied by their depolarization, i.e., by their greater ellipticity. This phenomenon, called the effect of shear wave depolarization (SWD), is mostly manifested in the case when the elastic disorientation angle in grains (layers) is close to 45°.
2. The SWD effect can be found in acoustical polarization diagrams for multicomponent media in the case when the polarization vectors are crossed and the minimum amplitudes A_{VC} are appreciably higher than those detected by the acoustical polariscope without a sample, at the same points of the polarization diagram. The SWD effect allows us to estimate the elastic disorientation angle in grains (layers) of mono- and polymineral rocks.
3. Unlike a similar phenomenon observed in inhomogeneous media transmitting shear waves, the SWD effect is detected only in one or two directions in anisotropic media whose structure is characterized by different-oriented elastic symmetry elements.
4. Based on the analysis of the data on shear wave propagation, obtained, for example, by using the acoustical polariscopy technique, an anisotropic heterogeneous medium actually consisting of mutually orthogonal elastic layers (grains) can, in contrast, be identified as an isotropic one.

4. EQUIPMENT FOR ACOUSTOPOLARIZATION MEASUREMENTS

4.1. Peculiarities of measuring elastic wave velocities in anisotropic media

When choosing a method and devices for measuring elastic wave velocities in the samples of greatly absorbing anisotropic media of great importance are geometrical, wave and energy conditions of wave propagation. First of all let us briefly consider geometrical conditions of energy transfer from transducer-source to a medium. Generally vibratory energy can be transferred by a point, linear and flat source radiating along a surface (in a particular case – along a plane). As follows from [Brekhovskikh, 1973; Skuchik, 1976], a wave amplitude from the point source decreases with distance due to geometric divergence of the power on the wave-front (generally – spherical, ellipse-shaped or a more complicated surface), as well as due to absorption and diffusion.

With the spherical front, due to the geometric divergence, the amplitude of the wave A_x increases inversely with the distance [Skuchik, 1976]

$$A_x = \frac{A_0}{x} e^{-\alpha_s x}, \tag{4.1}$$

where A_0 is the initial amplitude, x is distance to the source, α_s is the factor of absorption and diffusion in the spherical wave.

An idealized linear source of an infinite length excites a wave with a cylinder-shaped front. A the distance x increases the wave amplitude decreases proportionally to $1/\sqrt{x}$:

$$A_x = \frac{A_0}{\sqrt{x}} e^{-\alpha_c x}, \tag{4.2}$$

where α_c is the factor of absorption and diffusion in the cylindrical wave.

If the source is flat (or, to be more exact, local-flat, according to G.I. Petrashen, [1980]), then as the distance increases there are no losses due to divergence. Thus, the flat source, unlike the point and linear ones, decreases the losses of the wave energy as the front propagates in an elastic medium. Such a source is the most suitable for measuring parameters of greatly absorbing heterogeneous media. Such media are, for instance, rocks.

But besides the mechanisms of divergence, diffusion and absorption elastic anisotropy of the sample media greatly influences the wave propagation. As practice shows, anisotropy of elastic properties is typical of minerals, it is also registered in volcanic, metamorphic and sedimentary rocks [Nevsky, 1974; Chesnokov, 1977]. Determination of elastic wave velocities in anisotropic rocks has its own peculiarities.

Solving this problem requires examination of specific distinctions between phase V_i and radial (group) v_i velocities, as well as particular conditions of exciting and reception of waves [Petrashen', 1980]. The distinctions between V_i and v_i are most conspicuous on the diagrams (Fig. 4.1a, b).

The radial velocity v_i of disturbance is calculated according to the ray, for instance, OM_1 – for quasi-longitudinal qPV (i = 1), OM_2 for quasi-shear qSV (i = 2)

and OM_3 for the wave *qSH* (i = 3). The rays OM_1, OM_2 and OM_3 are the directions of wave energy propagation. The phase velocity V_i (i=1, 2, 3) characterizes the travel velocity of extended sections of the wave fronts in the normals direction to them. It is precisely the phase velocity V_i value that enters into the known Green-Christoffel equation (1.1) that allows one to calculate all the elasticity constants of an anisotropic medium.

In isotropic media one can observe an equality of the radial and phase velocities in any direction. In anisotropic media such an equality is observed only in some particular directions coinciding with the direction of elastic symmetry elements. In an isotropic medium the curves for radial velocities v_i (i = 1, 2, 3), Fig. 4.1a and 4.1b, are regular circles, the circles i =2 and i =3 being superimposed.

In anisotropic media the relationship between V_i and v_i is always observed [Dieulesaint et Royer, 1974]

$$\frac{1}{V_i}(\vec{n}v_i) = 1. \qquad (4.3)$$

This relationship means that the phase velocity V_i of the front (its element) is the projection of the radial velocity on the normal direction to the front $\vec{n}$.

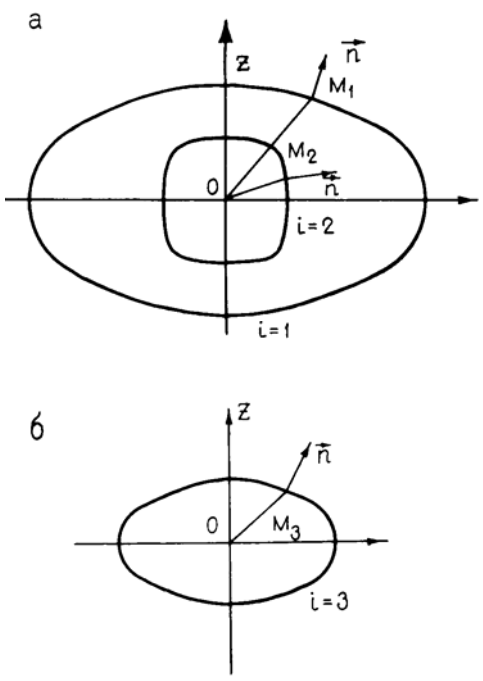

Fig. 4.1. Typical curves of the radial velocities $V_i\vec{n}$ front for waves i = 1, i = 2 (a), for the wave i = 3 (b), propagating in transverse-isotropic medium.

Let us consider in greater detail propagation of waves in an arbitrary weakly anisotropic medium, Fig. 4.2.

From the point source O at the time point t along the ray $OM'M''$ the waves will reach the point M'. At the time point $t + \Delta t$ the waves will reach the point M''. The ray $OM'M''$ is directed to the symmetry element OZ of the medium at ϕ angle. It is not difficult to show that in a homogeneous medium the spatial direction of the normal $\vec{n}$ to the wave front at the points M' and M'' at the time points t and $t + \Delta t$ will be the same. The angle between the normal $\vec{n}$ and symmetry element OZ is equal to θ. From point M' to point M'' along the ray $OM'M''$ the waves pass the distance of $v_i\Delta t$ during Δt time with the radial velocity v_i. During the same time the wave front will pass the distance $V_i\Delta t$ with the phase velocity V_i.

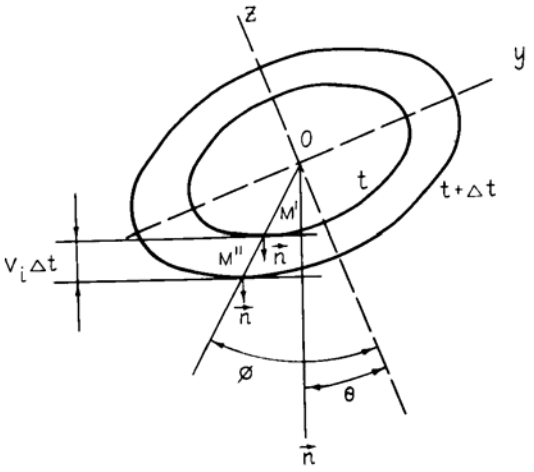

Fig. 4.2. Propagation of elastic waves in a homogeneous weakly anisotropic medium of an arbitrary symmetry type.

Judging by the relative displacement of the points M' and M'' (Fig. 4.2) with the point source of waves in an anisotropic medium, as the waves propagate, in a general case, a lateral displacement of points occurs. Accordingly, as the distance $V_i\Delta t$ increases, the point, at which the maximum amplitude (maximum energy) will be registered, moves farther and farther from the normal $\vec{n}$, passing through the point O. Thus, when using point sources and receivers for measuring the phase velocity values of the wave front, one should observe at the points M', M'' etc. But the distance covered by the waves should be counted from the normal $\vec{n}$ making an angle θ with the axis of the medium symmetry OZ. Practical performing of such operations is rather labour-intensive.

Now let us consider the propagation peculiarities of radial and phase fronts from plane sources. A plane (locally plane) source of waves may be imagined as a set of point sources arranged in the plane and oscillating synchronously, Fig. 4.3.

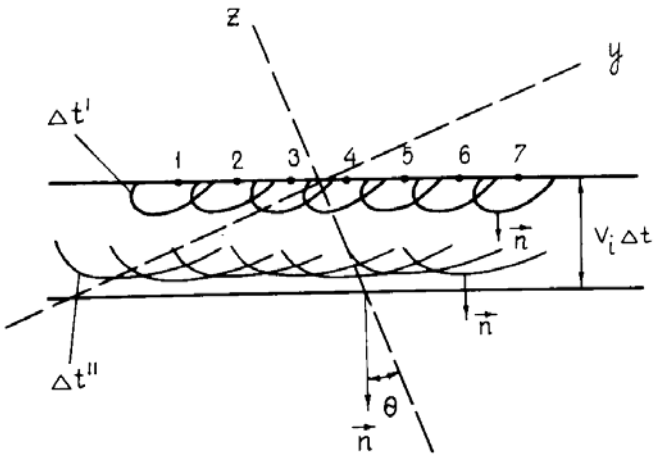

Fig. 4.3. Family of envelopes that, according to the Huygens principle, are a front of waves from point sources lying in one plane.

According to the Huygens principle, a wave front is a family of envelopes, in which the normal to extreme points is the normal to the plane, where the sources are placed. As follows from Fig. 4.3 the position of the normal to the front is preserved at the moments Δt, $\Delta t'$, $\Delta t''$ and any others. As in Fig 4.2 with the point source, Fig. 4.3 shows that the normal $\vec{n}$ in relation to the symmetry element OZ preserves the angle θ, which does not change its value as a wave front propagates.

If point sources are located in one plane close to each other (a plane source), then, excluding edge areas, the emitted front will be plane. The element ds of such a front moves along the vector $\vec{v}_i$, remaining parallel to itself, Fig. 4.4.

From this Figure it follows that over the time Δt the front element ds passes along the vector $\vec{v}_i$ from the source to the receiver with the radial velocity v_i and at the same time along the ort $\vec{n}$ with the phase velocity V_i. The considered peculiarities of elastic wave propagation from point and plain sources can be observed during propagation of both

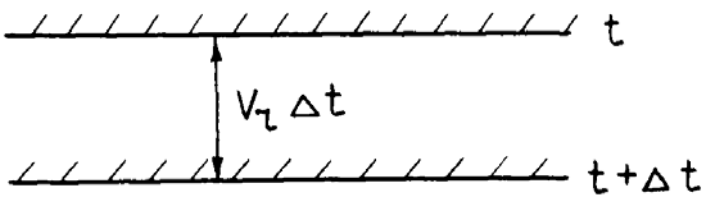

Fig. 4.4. Propagation of the reference element ds of the expanded plane front in an anisotropic medium.

quasi-compressional and quasi-shear waves at any direction of their polarization vectors.

Figures 4.3 and 4.4 and the relation (4.3) allow one to draw conclusions that are necessary for proper practical measurements:

1. The time of wave propagation corresponding to the value of phase velocity V_i is measured independently of the element and symmetry type of an anisotropic medium in samples bounded by plane-parallel surfaces with the help of plane (local-plane) sources and receivers of waves.
2. If we define the orientation of a medium symmetry elements, for instance, with the acoustopolarization method [Gorbatsevich, 1995], then the angle θ will be equal to the angle between the normal to the plane-parallel surfaces bounding the sample and orientation of a symmetry element.

Besides these condition it is necessary to provide even distribution of amplitudes (pressures) in the cross-section of the bundle of rays (within the local-plane front) passing from the source to the sample [Skuchik, 1976]. For example, in the near zone (Fresnel zone) the amplitude of waves from a plane source (made in the form of a disk) in the cross section (in relation to the axis of the radiated bundle) varies in a complicated manner. Within this zone a great variation of the registered wave amplitude is observed. The far zone (Fraunhofer zone) begins at a certain distance of the front from the source. At this point the amplitude distribution along the radiating surface becomes monotonous. A transition from the near to far zone occurs when the following condition is met [Tyulin, 1976],

$$\frac{x}{R} > \frac{R}{\lambda} - \frac{\lambda}{4}, \tag{4.4}$$

where x is a distance from the plane source, R is a radius of its radiating surface, λ is a wave length.

Thus, to provide even distribution of the amplitude within the cross section of the bundle of radiated waves it is necessary to use buffer rods (acoustic lines) whose length should be determined by the condition (4.4). Long acoustic lines also promote increasing the area of the local plane front. They are often used for increasing the accuracy of measurements [MacSkimin, 1950].

In conclusion we shall point out one more important and evident requirement: when measuring elastic characteristics of such heterogeneous and anisotropic media as rocks, the propagation ways of the ray bundles of compression and shear waves should coincide. Herewith it is very important to provide coincidence of contact conditions as well [Gorbatsevich, 1995].

The above analysis allows one to formulate general requirements for measurement equipment. Meeting these requirements ensures correct and exact measurement of phase velocities of compression and shear waves:

1. Ultrasound sources and receivers (transducers) should be plane (locally plane).
2. A radiating transducer should form a non-divergent or weakly divergent beam of ultrasonic waves.
3. To increase accuracy in the measurements it is necessary to use buffer rods (acoustic lines) which size is larger than Fresnel zone.
4. Oscillations in the ultrasonic wave impulses should be monofrequency ones, their frequency should be the same for compression and shear waves.

5. The propagation way of the ray bundle of compression and shear waves should be the same. Contact conditions on the sample-transducer boundary should be identical, too.

4.2. Requirements for devices and materials

To conduct acoustopolarization determinations and measurements of compression wave velocities in anisotropic samples one may use impulse ultrasonic devices (defectoscopes) for example of Krauthkramer type etc. with oscillographical – on the electron-beam tube (EBT) and digital indication of results. The repetition frequency of outgoing pulses should be higher than 25 Hz, while the amplification factor – no less than $1 \cdot 10^5$. A step control of the input signal in 1 dB within 0–60 dB is also necessary. The device band pass may vary within 0.4–10.0 MHz. The determination accuracy of the travel time of an ultrasonic pulse should be no less than $1 \cdot 10^{-7}$–$1 \cdot 10^{-8}$ *s* and the scanning time - within $(10\text{-}200) \cdot 10^{-6}$ *s*.

The mentioned accuracy of the time determination can be attained by the circuit, in which a frequency meter, used in the regime of time interval counting, is connected to an ultrasonic defectoscope. In this case the pulse from the pulse generator is applied to the frequency meter input and starts time counting, while the pulse from the ultrasound waves receiver, amplified by the device amplifier (or strobe pulse), is used to stop the frequency meter counting.

For acoustopolarization determinations and velocity measurements transducers radiating intensive linear-polarized pure shear waves are needed [Bergman, 1954]. The transducers whose design is given in [Gorbatsevich, 1995] meet these requirements. The most efficient is the transducer, which acoustic line consists of two parts (Fig. 4.5).

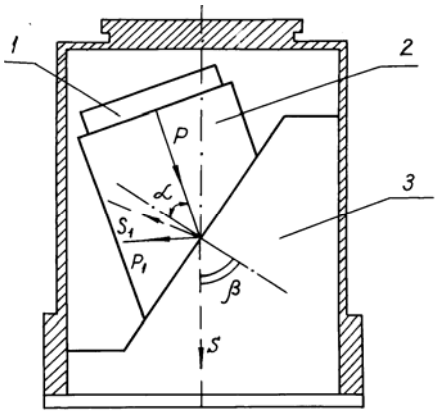

Fig. 4.5. Transducer of shear waves with the converter of compessional waves into shear waves [Patent No. 785737, USSR].
1 – piezoplate; 2 - acoustic line first part; 3 – acoustic line second part.
P, S – rays of compression and shear waves, accordingly.

The basic frequency of transducer waves is determined by the piezoplate natural frequency and may make up f_0 = 0.4-10.0 MHz. For determinations it is necessary to have two pairs of shear wave transducers, one, for instance, with natural frequency of 0.7 MHz, the other – 1.1 MHz. On the transducer case the direction mark of polarization vector (PV) should be.

The shear wave transducers prepared for measurements should be subjected to check-up. For this purpose two similarly designed transducers rated at one and the same natural frequency are connected together at their working surfaces by a special contact medium. The PV mark of the source is made coincident with the PV mark of the receiver. The shear wave pulse originated on the EBT screen should consist of 6-10 individual periods (Fig. 4.6).

The waves in the pulse should be monofrequency ones, close to harmonic; they should not be distorted by bends. The check is performed in the following order:

1. One measures the amplitude A_{PM} of the pulse located along the sweep trace in front of the shear wave pulse and the factor A_{VPM1} (Fig. 4.6). The pulse ratio should follow the inequality $A_{PM}/A_{VPM} \leq 0.1$.

2. One of the transducers is turned by an angle of +90° from the PV position of the other transducer and the signal A_{VCM1} minimum is fixed. Then the same transducer is turned by an angle of -90° from the PV position of the other one and the pulse A_{VCM2} amplitude is fixed. The measured values should be in the ratio $A_{VCM1}/A_{VPM} \leq 0.15$, $A_{VCM2}/A_{VPM} \leq 0{,}15$ and differ from one another by no more than 10%.

3. One of the transducers is turned by an angle of 180° from the PV position of the other one. The measured amplitude A_{VPM2} of the pulse envelope should differ from the A_{VPM} by no more than 10%.

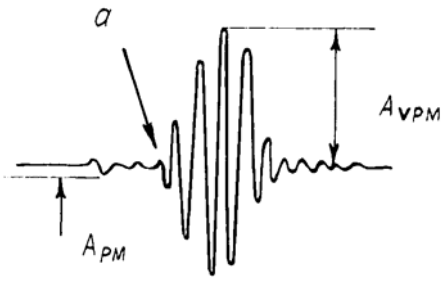

Fig. 4.6. Shear wave pulse on the ultrasonic device screen.
a is the moment of its first entrance.

Even more qualitative check of the transducers pair may be performed if we plot the indicatrix of their polarization vectors (Fig. 4.7). If the transducers radiate linear-polarized purely shear waves, then the indicatrix points should lie on the regular circle line [Volkova, 1974].

As is known, for efficient transmission of compression waves from transducers to a sample water, mineral oils and glycerine are suitable. If it is necessary to make measurements on a large number of samples, vacuum rubber plates 1-3 *mm* thick are glued on to the transducers' contact pads. These plates are a contact medium. A similar contact medium may be polyurethane. But a transmission of shear waves through contacts presents some difficulties.

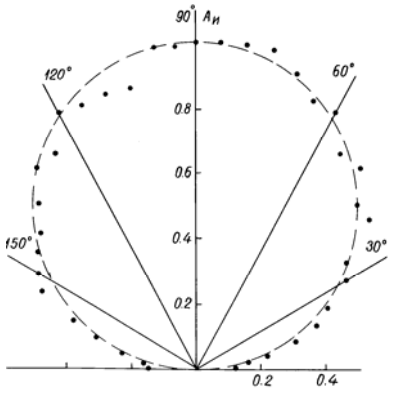

Fig. 4.7. Polarization vector indicatrix of the shear wave transducers.

Physically, liquids, i.e. media acquiring the shape of the vessel they are placed in, do not possess shear elasticity and cannot transmit shear waves. Gluing transducers to a sample with hardening glues is very labour intensive [Merkulov, 1968]. Numerous attempts have been made to use water, transformer oil [Volkov & Grebennik, 1988], the solution of rosin in alcohol, glycerine, unhardened epoxy resins [Alyoshin et al., 1968] to transmit shear waves from transducers to a sample. Following Alyoshin [1968], an application of liquids with high viscosity has the greatest effect – the higher the viscosity, the fewer the losses. A number of experiments helped us to establish that liquids with polymer properties having low shear elasticity at low frequencies and high shear elasticity at ultrasonic frequencies are more suitable. For instance, unhardened epoxy resins pertain to media with required properties. But epoxy resins are toxic; they are difficult to remove from the sample with corrosive liquids, such as acetone.

For a long time we have been using a high-viscous solution of non-crystallizing polysaccharides as a contact medium [Gorbatsevich, 1982]. Such a solution may be prepared, for instance, from artificial honey. By evaporating the solution is brought to high viscosity. The solution viscosity is checked up at high temperature. The solution

taken on a rod should not flow down from it. The contact medium prepared in such a way transmits shear waves efficiently at frequencies from 0.3 MHz and higher, allows transducers' rotation relative to the sample at a speed of about 1 *rev/min* and is easy to remove with water.

4.3. Design of acoustopolariscope with rotating platform

Recently several designs of acoustopolariscopes [Gorbatsevich, 1995] have been developed. They are of two main types – with rotating handle and rotating platform. The most frequently used by us is the acoustopolariscope with rotating platform [Patent No. 1281993, USSR]. When using the acoustopolariscope with rotating platform the sample fixed on the rotating platform in the course of measurements rotates relative to immobile ultrasonic transducers (Fig. 4.8).

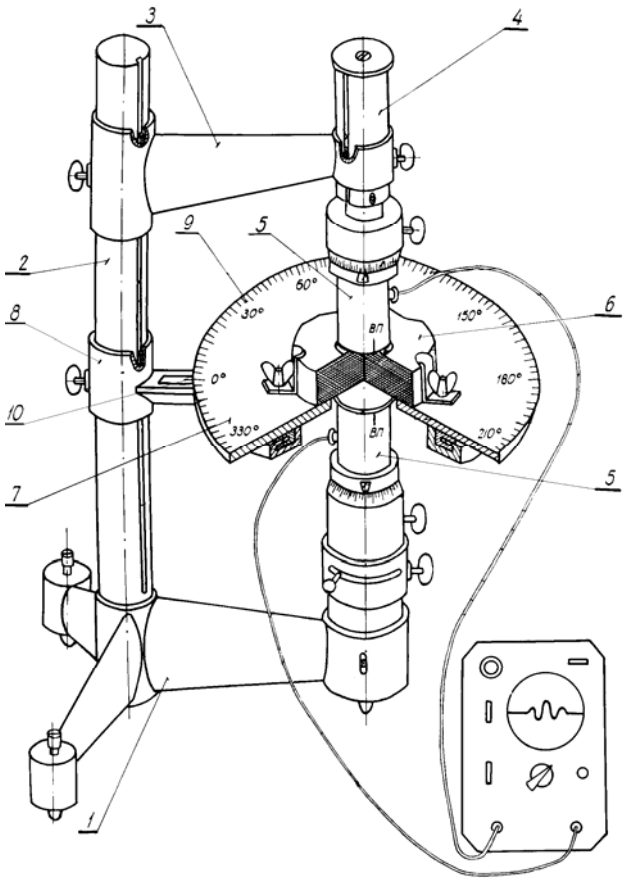

Fig. 4.8. Design of acoustopolariscope with rotating platform.
(1) base; (2) pole; (3) bracket; (4) travelling rod; (5) transducers; (6) sample; (7) rotating platform; (8) additional bracket; (9) angle scale; (10) pointer.

The apparatus comprises a base (1), a pole (2) fastened in it and a bracket (3) placed on the pole. A travelling rod (4) passes through the bracket bush. At the rod lower end and in the base there are sockets, in which upper and lower transducers (5) are located. They are meant for radiating and reception of pure shear linear-polarized waves. A sample (6) is fastened on the rotating platform (7) with holders. The rotating platform itself is set on the additional bracket (8). On the rotating platform there is a scale (9) for calculating a rotation angle of the sample in relation to the polarization

vectors (PV) of the transducers. The calculation of this angle is made with respect to the mark (10) on the additional bracket.

Along the pole (2) and rod (4) grooves have been made and in the bracket bushes keys and stoppers have been fastened to key the brackets and rods position. The upper and lower sockets design allows for the rotation of the transducers fastened in them. To calculate the angles of the transducers mutual rotation angular scales have been placed on the sockets.

The socket base of the upper transducer fits into the rod cavity where a spring is located. In the rod opening there is a pin fastened in the socket base. The pin and opening ensure the spring initial compression and transducer elastic motion in its axis direction. The socket base of the lower transducer fits into the cavity of the base (1) cowling. In the same cavity is the spring ensuring, as the corresponding pin and opening, elastic travel of the transducer (without its rotation) in the direction of its axis.

Additionally in the lower socket there is an external and internal cups. In the external cup there is a circular groove, the internal cup is connected with the handle going from the groove outside. The cups, circular groove and handle allow one to rotate the lower transducer exactly through 90°. In the external cup there is a fixing rod that enables to fix the handle in its extreme positions. The transducers (5) conductor cables are connected to an ultrasonic device. As the device design of Fig. 4.8 suggests, the rotating platform with the hole in the centre, the angle scale and sample holder allows one to make measurements within the sample complete rotation relative to transducers polarization vectors. Spring-loading of the transducers sockets enables to eliminate the gaps between the contact surfaces of the transducers and sample. Figure 4.9 presents the device photo.

Fig. 4.9. General view of acoustopolariscope with rotating platform (Patent N 1281993, USSR). One pole type.

A more perfect type of acoustopolariscope with rotating platform and three poles (Fig. 4.10) has Hooke's joint connected with the upper transducer cup. The total load on the contact surfaces of the

transducers and sample is realized through a spring. Hooke's joint substantially decreases the measurement errors even if the sample faces are not quite parallel.

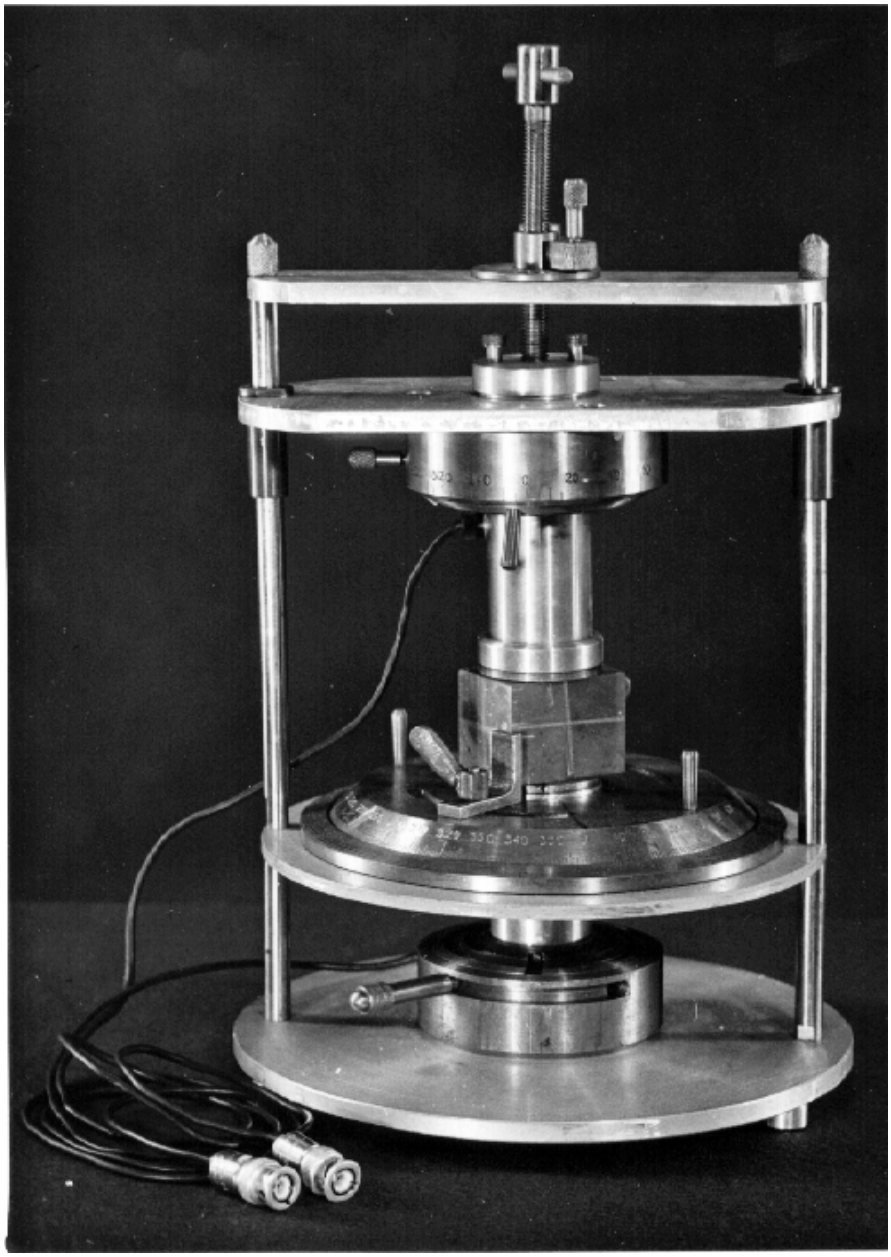

Fig. 4.10. General view of acoustopolariscope with rotating platform. Three pole type.

The last design has a mechanical drive of the rotating platform (Fig. 4.11). The rotating platform through the worm-wheel, placed on its rim, is set in motion by an electric motor. The indicating instrument is interfaced with a personal computer by a special controller. The registered envelope amplitudes of the signal that has passed through a sample are digitized and processed. The computer plots and issues on the printer finished VP and VC acoustopolarigrams.

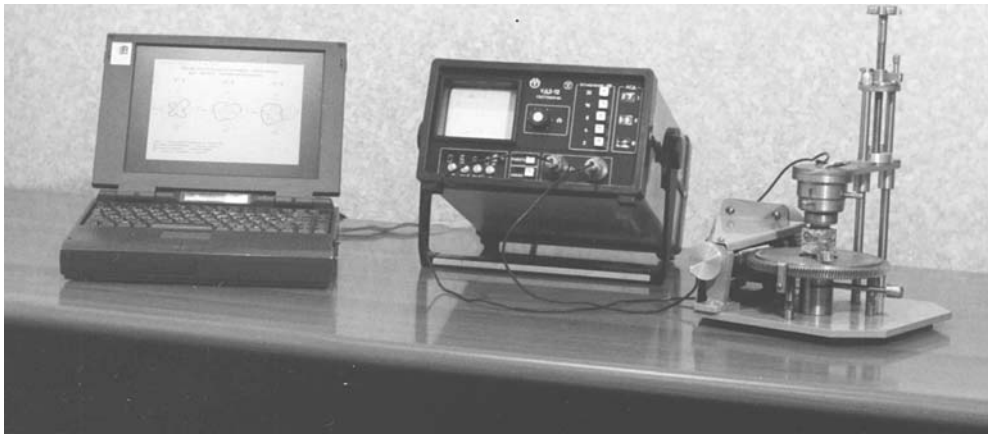

Fig. 4.11. General view of the automated acoustopolariscope with ultrasonic device and computer (The authors of this construction are Golovataya O.S, Gorbatsevich F.F.)

The mentioned types of acoustopolariscope design (Fig. 4.9-4.11) enable to make acoustopolariscope measurements over a wide range of ultrasonic frequencies (0.4-3.0 MHz) and sample sizes (10-100 *mm*).

4.4. Combined transducers for radiating and reception of compression and shear waves

Using the processes of reflection and transformation on the media interface we have elaborated combined (integrated) transducers of compression and shear waves [Gorbatsevich, 1995]. The design of one of these transducers is given in Fig. 4.12. In the transducer's container housing (1) there are compression waves piezoplates (2) glued to the acoustic line made up of two parts – a contact (3) and face (4) ones. On the contact part there are ribs to weaken the waves transmitted along the acoustic line surface. The acoustic line contact part is made of electrolytic copper (V_p = 4.75 *km*/*s*, V_s = 2.26 *km*/*s*), while the face part is made of lead (V_p = 2.16 *km*/*s*).

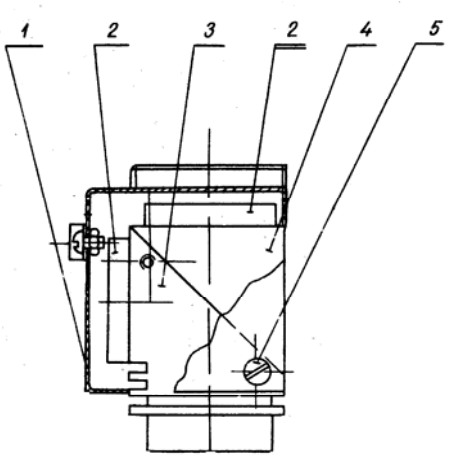

Figure 4.12. Design of combined transducer on copper-lead media.
1 – container housing; 2 – piezoelements; 3 – acoustic line contact part; 4 – acoustic line face part; 5 – fastening of container housing to the acoustic line.

When an electric pulse is applied to the piezoplate located on the acoustic line face part, a compression wave pulse is excited, which on the plane dividing the contact and face parts is transformed into a shear wave pulse. The latter gets into a sample through the contact plane. The compression wave pulse arisen during the electric pulse application to the piezoplate will reflect from the dividing plane. Then at an angle of reflection equal to the angle of incidence, it will get into a sample also through the contact plane without transformation into a shear wave pulse. On the basis of the combined transducer of such a type an elastic waves velocity combined meter (Fig. 4.13) has been developed.

The meter comprises a pair of combined transducers of ultrasonic waves (1), a stand (2), a switch of the work type (3), an ultrasonic device (4), connected to a digital

frequency meter (5), that is used for measuring short intervals of time. Figure 4.14 gives an external appearance of the device. The principle of operation follows from the design (Fig. 4.13). Depending on what piezoelements of the combined transducers are connected to the device with the switch (3), either compression or shear waves are radiated into a sample.

The special switch has a peculiar design. It consists of two individual units that are completely shielded from each other – a generator unit and a reception one. The piezoplates switching for radiating and reception of either compression or shear waves is performed by switches with a common handle. To fasten the combined transducers and to keep their contact surfaces plane-parallel during mutual travel a special stand has been designed.

The advantage of the meter is in reduction of the time required for measuring the elasticity constants of solid media, since measuring of V_p and V_s is performed at one application of the transducers to the sample. In this case the accuracy of determining the elasticity constants increases due to sheer coincidence of contact conditions, frequency and the ways of propagation of compression and shear wave rays.

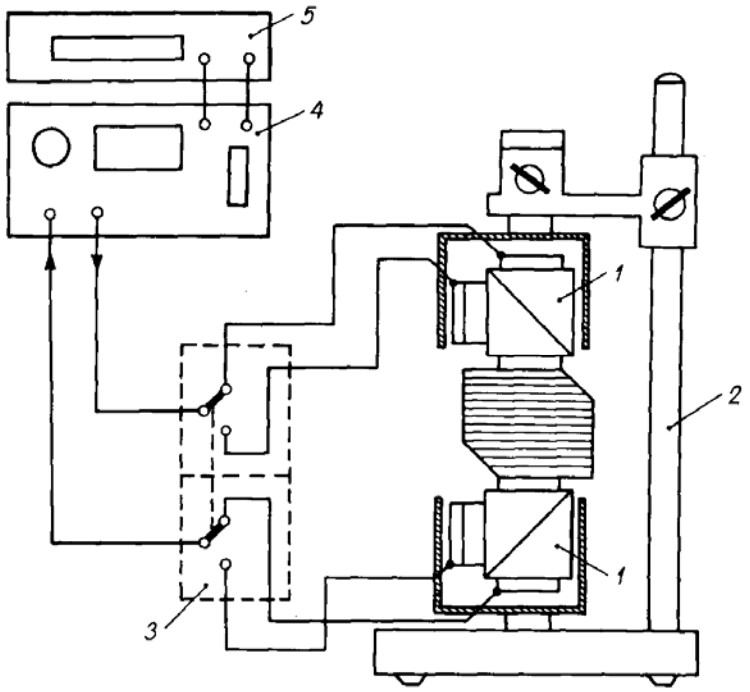

Figure 4.13. Design of elastic wave velocity combined meter. 1 – transducers; 2 –stand; 3 –switch of the work types; 4 – ultrasonic device; 5 – digital frequency meter.

The above measurement principles should be guided by in experimental investigations of elastic properties of anisotropic solid media. They allow one to conclude that to obtain the correct evidence it is necessary first to determine the orientation of symmetry elements by the acoustopolariscopy method. Then one should measure the density and velocity of compression and shear waves in the directions coordinated with the revealed symmetry elements.

It should be noted that the time of wave propagation corresponding to the phase velocity is measured independently of the element orientation and symmetry type of the anisotropic medium in samples limited by plane-parallel surfaces with the help of the plane (locally plane) source an receiver (see Fig. 4.3). The acoustopolariscope and velocity meter compensate for the lack of equipment required for determination of all parameters of elastic and non-elastic properties of an anisotropic heterogeneous solid body.

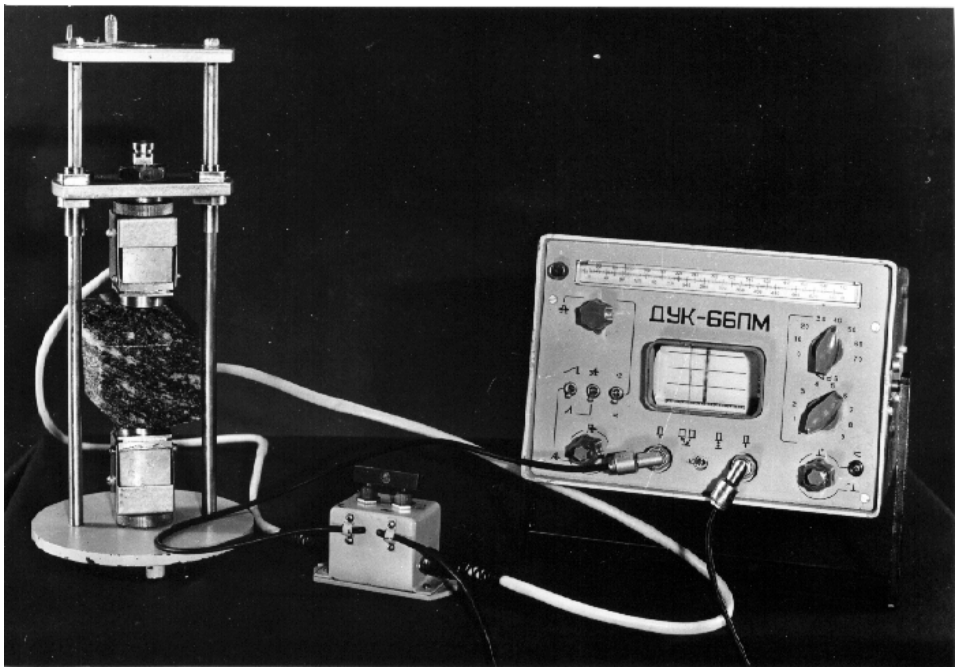

Fig. 4.14. External appearance of elastic wave velocity combined meter (without digital frequency meter device).

5. ACOUSTOPOLARISCOPY PROCEDURE

5.1. General requirements for measurements

Investigation of anisotropic media elastic properties covers preparation of a sample for tests, obtaining acoustopolarization diagrams, construction of spatial arrangement of elastic symmetry elements, determining elastic waves (compression and shear) velocities along the revealed elements and at certain angles to them. The last stage includes determination of a symmetry type and calculation of the sample elasticity constants.

As is well known, the sample acoustopolariscopy along a particular direction allows one to obtain only one projection of the elastic symmetry element (axis or plane). Besides, the measurements of elasticity characteristics made along the symmetry axis of transversely isotropic medium do not allow one to discriminate between this symmetry type and an isotropic one [Fyodorov, 1965; Shaskol'skaya, 1976]. The diagnostics of such media is possible only when the data are obtained in two non-equivalent projections. The spatial arrangement construction of a symmetry element of any medium is possible on the basis of no less than two projections. That is why the preferable form of the sample for tests is a cube or parallelepiped. The measurements made on two pairs of a cubic sample faces, as a rule, enable to determine the projections of two symmetry elements. The measurements made on the third pair of faces allow one to confirm the correctness of determinations performed for the other two pairs. This control measurement enables to increase the determination accuracy.

The final result of the measurements is determination of a mutual spatial arrangement of elastic symmetry elements of the medium, its symmetry type, degree of anisotropy and the values of constants of elasticity or rigidity [Nye, 1964].

Sampling for the subsequent manufacturing of samples should meet certain requirements [Acoustopolarimetry…, 1990]. For instance, when processing a rock sample one of the faces should be sawn to coincide with the foliation plane while the edge should be oriented along the linearity in the foliation plane. The linearity may be identified, for instance, by the elongated form of mineral grains (amphibole, biotite etc.). If plane and linear elements are not seen in the rock, the orientation of the sample faces may be of any kind. It may also be related to mining and technological parameters, for instance, to the borehole or mining working axis direction. The face direction of mineral samples should be determined by the orientation of the symmetry crystallographic elements.

The minimum length of a cube edge l is determined from the relation [GOST 21153.0-75]

$$l \geq V_p \frac{dt}{\delta_v}, \tag{5.1}$$

where V_p is the compression wave velocity; dt is the absolute error in time reckoning equal to half the scale marking of the measuring instrument, δ_v is the given relative error in the velocity measuring. The minimum size l should be also subject to the condition

$$l \geq 3V_p/f_0 \,. \qquad (5.2)$$

Sample sizes meeting the above conditions are indicated in standards including foreign ones [GOST 21153.0-75, D2845-83]. The sample faces are processed and reground in such a way that the results can be reproduced. The sample prepared for measurements and its indexing diagram are given in Fig. 5.1.

5.2. Acoustopolariscope adjustment

Before the acoustopolariscopy performance the acoustopolariscope should be adjusted. The purpose of the adjusting first stage is determining the mutual arrangement of the polarization vectors (PV) of the upper and lower transducers. At the second stage the transducers are set so that the lower transducer PV is oriented to 0^o on the rotating platform angle scale (Fig. 4.8). At the "vectors parallel" position the PV orientations of the upper and lower transducers should coincide.

To conduct the adjustment second stage an anisotropic material with the known orientation of symmetry elements is required. A long bar should be produced of this material in such a way that its long side was parallel to a symmetry element. The length of this trial bar should be equal to the diameter of the rotating platform angle scale. Its width should be no less than the diameter of the transducers contact surface. A segment of a wooden ruler with a well-defined structure may be used as such a medium. For better orientation a cutting line should be drawn along the structure lines through the ruler centre.

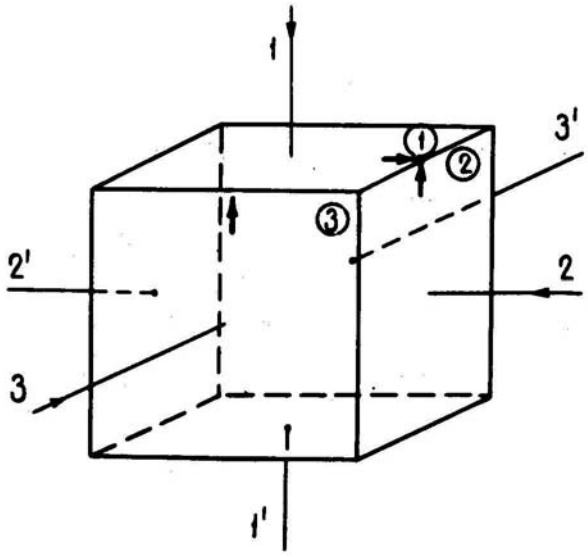

Fig. 5.1. Sample indexing diagram.
1, 2 and 3; (1), (2) and (3) are indexing of the sample directions and faces, respectively.

The acoustopolariscope adjustment covers the following operations.

1. To set the transducers in the acoustopolariscopy sockets and fastened by lock screws.
2. To apply a contact medium to the centres of the transducers working surfaces.
3. To move the device handle leftwards against stop to the position "vectors crossed" (VC) and fasten it.
4. To combine the transducers working surfaces, to free the turn stopper of the upper fixture and looking at the device screen find the position VC. At this position the signal amplitude on the screen will be minimum. To fasten the turn stopper of the upper fixture.
5. To apply a drop of the contact medium to each of the two sides of the test bar and place it between the transducers.

6. Turning the bar around the axis that passes through the transducers centres, to find its position at which the signal minimum is observed on the screen.
7. To superpose "zero" on the rotating platform scale with the rotation angle pointer, to count angle α_1 between the rotation angle pointer and the cutting line on the bar. To move apart the transducers working surfaces, to take the bar out of the gap between them.
8. To free a stop screw, to turn the lower transducer by an angle α_1 to the side opposite to the direction of counting the angle α_1 from the rotation angle pointer. After that to fasten the lower transducer in the socket by the stop screw again.
9. To apply the contact medium to the centres of the transducers working surfaces, to superpose the transducers working surfaces. To free the turn stopper of the upper fixture and watching the signal on the screen to find the position VC again (see point 4). Then to fasten the turn stopper of the upper fixture.
10. To perform operations according to points 5 and 6. If the cutting line on the bar coincides exactly with the rotation angle pointer (and at the zero on the scale of the rotating platform combined with the pointer the line passes through 0^o and 180^o of the scale) the adjustment may be considered to be completed. However, if between the texture line and the mark of the rotation angle pointer there is some angle α_2, the operations according points 5-9 should be repeated.

After all adjustment operations the handle is moved rightwards against stop to the position "vectors parallel" (VP) and is fastened in this position. In this case the transducers polarization vectors are on the line passing through the rotation angle pointer and centres of the contact pad.

5.3. Acoustopolariscopy performance

Polarization measurements of the test media samples are aimed at determination of the elastic anisotropy degree, effect of the linear acoustic anisotropic absorption (LAAA) and spatial orientation of elastic symmetry elements. The measurement procedure is comparatively fully set forth in the works [Lucas, 1961; Acoustic polarization…, 1985]. The measurements are performed by acoustoplariscopes, which designs are given in Figures 4.9-4.11. Before the measurements the transducers of shear waves are connected to an ultrasonic device so that the upper transducer is a radiator. Then the travelling platform is set at the angle scale zero mark opposite the mark on the additional bracket. The marks of the transducers polarisation vectors are aligned.

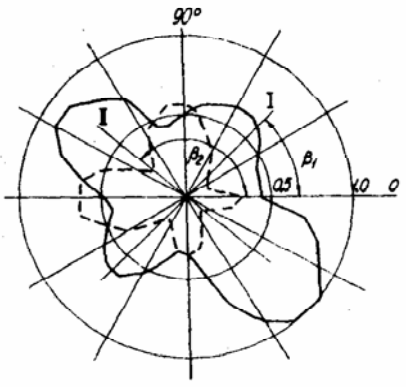

Fig. 5.2. Acoustopolarigram of metadiabase. Solid and dashed lines are for parallel and crossed polarization vectors, respectively. I, II are projections of symmetry elements; β_1, β_2 are angles between the directions of symmetry elements projections and a sample face.

The transducers contact surfaces and sample working faces are lubricated by a contact medium. In this case one must be careful that the contact medium coats the contact surfaces of the transducer and sample evenly without breaks and bubbles. After the sample has been set on the contact surface of the lower transducer and fastened on the rotating platform the rod with the

upper transducer is delivered downwards until there is an acoustic contact between the transducers and sample. Herewith compressing the spring at the rod base and fixing it in the compressed state, a uniform pressure of the transducers contact pads on the sample faces is ensured. Some time is required for the contact medium to form a thin even layer in the clearance between the transducer and sample. As a rule, on completion of this time the amplitude of the shear pulse (Fig. 4.6) on the device screen ceases to increase.

The measurements consist in moving the rotating platform with a step of 1^o, 5^o or 10^o and fixing the amplitude A_{VPM} of the shear waves passing through the sample (Fig. 5.2). The measurements at the VP position are concluded when the angle count pointer is set at 360^o. In the course of measurements to exclude the impact of non-linearity of the internal circuits of the ultrasonic device and its amplifier, it is recommended to maintain the same signal on the electron-beam tube (EBT) screen by the attenuator's handles. In this case the attenuation degree in decibels will reflect relative changes in the signal level in the course of measurements.

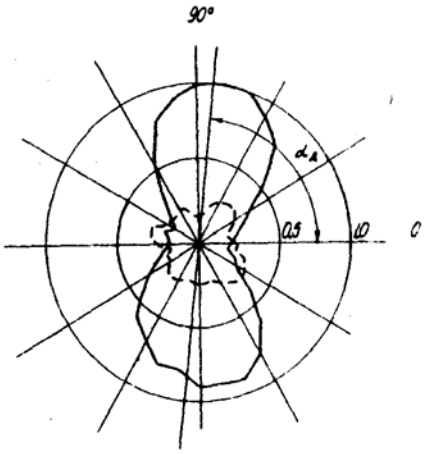

Fig. 5.3. Acoustopolarigram of amphibolite with LAAA manifestation, α_D is the angle between the axis of the greatest "transmission" and a normal to sample face.

On completion of the measurements at the VP position, the fixing rod is freed and the lower transducer is turned by 90^o with the handle and fixed in this position. Thus the transducers polarization vectors appear to be at the crossed position (VC). A set of amplitude A_{VCM} measurements (at VC position) are made with the same step within a full angle 2π of the platform rotation.

If within the rotation angle 0-360° alterations of the relative amplitudes at both VC and VP positions are not registered, the measurements should be repeated. To this effect the transducers with a natural frequency that is not a multiple to the initial one are installed in the acoustopolariscope sockets.

To increase precision the measurements can be duplicated at the reverse motion of the rotating handle or platform. Such a measure will allow one to assess the alteration of the contact medium thickness under the spring and to exclude the impact of this alteration when processing the data.

After observations of the amplitudes A_{VPM}, and A_{VCM} variations acoustopolarigrams are drawn in the following order:

1) the values of A_{VPM} (in decibels) within the angles of $0\text{-}360^o$ are examined and the maximum one (A_{MAX}) is found;
2) every A_{VPM} is extracted from A_{MAX}; $B_{VP} = A_{MAX} - A_{VPM}$, *dB*;
3) A_{VCM} is extracted from A_{MAX}; $B_{VC} = A_{MAX} - A_{VCM}$, *dB*;
4) using the table of conversion of decibels to relative amplitudes, by the values of B_{VP} and B_{VC} corresponding relative

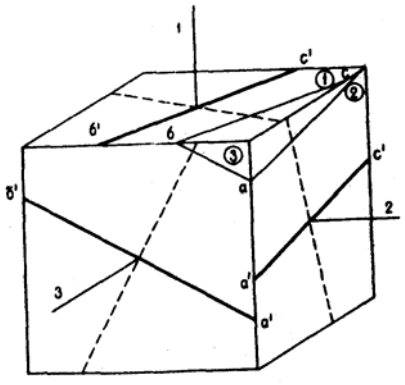

Fig. 5.4. Symmetry elements projections marked on the sample faces by acousto-polarization measurements.

amplitudes A_{VPM} and A_{VCM} are found. They are initial for drawing acoustopolarigrams. As a rule, the acoustopolarigrams are plotted in polar co-ordinates.

The points A_{VPM} are connected with solid lines and the points A_{VCM} with dotted ones. The figure outlined by the solid line is the VP acoustopolarigram and that outlined by the dotted line – the VC acoustopolarigram (see Fig. 1.4, 5.2). A computer programme for data input and drawing acoustopolarigrams is available (see Attachment 1).

By the VP acoustopolarigram the degree of LAAA effect for the medium D and the angle α_D of the greatest transmission (GT) axis are determined, Fig. 5.3. The angle α_D is determined between the axis O and the strait line drawn through the polar axis and opposed maxima A_{VPM1} and A_{VPM2}. The LAAA degree is calculated by formula (2.3).

On the VC acoustopolarigram strait lines are drawn through the polar axis and the opposed minima of the envelope A_{VCM} (Fig. 5.2). These lines are the projections of the symmetry axes and planes of the sample medium. The angles β_1 and β_2 between the co-ordinate axis and the strait lines drawn allow one to fix the location of the symmetry elements projections relative to the sample sides.

At the final stage the symmetry elements projections are transferred to the sample sides (Fig. 5.4). They characterize the peculiarities of the medium elastic anisotropy in three mutually perpendicular directions. The parameters of the spatial orientation of the elastic symmetry elements can be determined with Wolf's stereographic projection [Acoustopolarimetry…, 1990]. In the event that the revealed symmetry elements are not parallel to the sample sides, to perform further measurements one should cut in the sample the planes oriented along the revealed elements.

As an example, in Fig. 5.4 the line *abc* shows the plane formed by the elements *a'c'*, *a'b'* and *b'c'*. Cutting the planes parallel to *abc* as well as perpendicular to them is performed in such a way that a new cubic sample or parallelepiped is produced.

5.4. Elastic wave velocity determination

The necessary measurements are made on the sample whose sides are parallel and perpendicular to the revealed symmetry elements (Fig. 5.5). The combined meter of compression and shear wave velocities (Fig. 4.14) enables to make measurements most exactly and efficiently.

Before the measurements the sample is placed between the transducers so that its centre coincides with the centre of the contact pads. When measuring V_s, the transducer polarization vectors (PV) are superposed with the symmetry element projection of the media marked off on the sides. In the course of measurements the travel time of compression t_p and shear t_{s1} and t_{s2} waves in the sample is determined. To increase determination reliability of the first entry point of shear waves, one should turn the upper transducer by an angle from the position where its PV coincides with PV of the lower transducer. All half-periods belonging to the pulse to be found change their amplitude

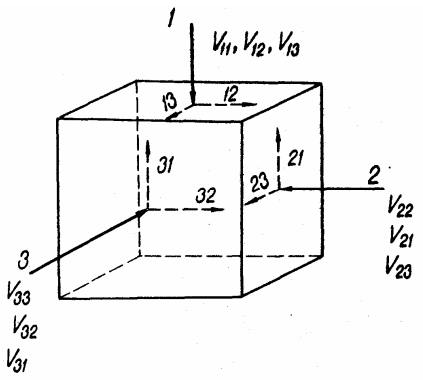

Fig. 5.5. Indexing of shear wave velocities in a cubic sample.

synchronously with the turn and at the point of the first entry a sudden change in the wave phase is observed. If the difference between t_{s1} and t_{s2} is so small that it can be compared with the scale factor of the measuring instrument, then only t_{s1} is determined.

Compression and shear waves velocities $V_{p,s}$ are determined by an ordinary formula

$$V_{p,s} = l/(t_{p,s} - t_d), \tag{5.3}$$

where l is the distance between the transducers along the sonic test line, mm; $t_{p,s}$ is the time of the wave pulse propagation from the source to the receiver, *msec*; t_d is the time of the pulse delay in the instrument and transducers circuits.

If due to a small difference between t_{s1} and t_{s2} only t_{s1} и V_{s1} have been determined, then the calculation of V_{s2}. is done by the following formula derived from (1.7):

$$V_{s2} = (360 f_0 l V_{s1})/(360 f_0 l + \delta V_{s1}), \tag{5.4}$$

where f_0 is the frequency of the transducers natural oscillations, Hz; l is the sample length, *m*; V_{s1}, *msec*; δ, *grades*, is the phase difference, calculated by formula (1.17).

In this case one should keep in mind that formula (1.17) provides a number of angle values: δ, 2π-δ, 4π-δ etc. With manifestation of LAAA formula (1.17) gives decreased values of δ. To calculate δ, the values of A_{VPM} relative units, at the points making an angle $n\pi/4$ with the orientation of the medium symmetry elements are usually taken.

After completing the measurement of all the velocity values for compression and shear waves for all the cubic sample sides, the following indexing order of the values under measurement is convenient to use:

$$V_{ij} = \begin{matrix} V_{11} & V_{12} & V_{13} \\ V_{21} & V_{22} & V_{23} \\ V_{31} & V_{32} & V_{33} \end{matrix}, \tag{5.5}$$

where V_{11} is the compression wave velocity measured in the direction 1-1'; V_{22} is the same velocity in the direction 2-2'; V_{33} is the same velocity in the direction 3-3', V_{12} is the shear wave velocity measured in the direction 1-1' with PV orientation in the direction 2-2'; V_{13} is the same velocity in the direction 1-1' with PV in the direction 3-3'. Similarly V_{21}, V_{23}, V_{31}, V_{32} are marked. The measured values of V_{ij} are presented as a rectangle table (quasimatrix). As will be shown later, the form (5.5) of presenting the results is convenient for analysing the type of the medium elastic symmetry.

Thus, the above measurement procedure allows to reveal the following.

1. The number of symmetry elements in any desired section of the sample, their arrangement and anisotropy presence.
2. Spatial location of the medium symmetry elements including their azimuth and angle of incidence in the sample oriented to cardinal-points.
3. The presence of linear acoustic anisotropic absorption and other effects.

The presented procedure enables to determine compression and shear waves velocities in the directions coinciding with the orientation of the symmetry elastic elements as well as in other directions that are necessary for calculation of the whole set of elasticity constants. The procedure allows to present the measurement results in the form that is suitable to analyse anisotropy in a sample.

To our mind, the acoustopolariscopy method as the radial-beam method for the sonic test of a subject of inquiry can be applied not only to samples. The method of seismic prospecting of a geological object [Patent No. 1434377] creates prerequisites for transference of the above acoustopolariscopy principles to comparatively stretched massifs. This method will allow to reduce expenditures on carrying out large-scale determinations of anisotropy parameters in the massifs within the upper crust and mantle by substituting the proposed method for the azimuthal one [Raitt, et al., 1969; Markov, 1977]. We think that the acoustopolariscopy method may be useful when solving some problems in crystal physics, in particular, when studying and developing new composite, metal-ceramic and other future materials.

6. DETERMINATION OF THE SYMMETRY TYPE AND ELASTICITY CONSTANTS IN ANISOTROPIC MEDIA

6.1. Ways for determining the medium symmetry type and elasticity constants

As is known, the medium symmetry type is determined by the number of symmetry elements, their appearance (axis, plane) and mutual arrangement [Berry et al., 1983]. There are several ways [Tillman & Bennet, 1973; Prodaivoda, 1978; Harder, 1988], that allow to perform the analysis of the elastic symmetry elements from the measurements of the elastic wave phase velocity in several mutually non-equivalent directions.

As mentioned in the introduction, anisotropic media can be described by triclinic, monoclinic, rhombic, tetragonal, trigonal, hexagonal and cubic systems of elastic symmetry. When calculating mineral elasticity constants, as a rule, to determine the number and orientation of elastic symmetry elements, optical, X-ray-structural, neutron transillumination and other methods are used [Belikov et al., 1970; Adamesku et al., 1985; Aleksandrov & Prodaivoda, 2000]. The constant calculation is carried out by using elastic wave velocities in crystal certain orientations [Voigt, 1910]. In some cases crystal deformability indices were used for calculations [Belikov et al., 1970]. For instance, to determine elastic and piezoelectric constants of rhombic crystals by the acoustic method, 4 samples are needed. The samples should be sawn at different angles to crystallographic axes [Bogdanov, 1997]. Experimental determination of all elastic constants of a low syngony mineral is a long and labour-intensive process including different methods and inquiring a few samples of different shape. The most complete enumeration of mineral elasticity constants is in the works [Belikov et al., 1970; Alexandrov & Prodaivoda, 2000]. But a full set of elasticity constants has not been determined for a large number of minerals so far.

For determination of the rocks elastic properties other approaches have been developed. As has been shown before rocks are polycrystalline and most often polymineral formations, whose elastic properties result from virtually indeterminable number of grains [Voigt, 1910; Hill, 1952]. Every one of those grains has its own elastic symmetry type and, accordingly, its own set of elasticity constants. Besides, most often every grain is bounded by a surface of a very complicated shape. At this surface one grain makes contact with another. But these contacts are seldom continuous. In crystalline rocks grain-to-grain contacts alternate with microcracks that arise as effusive rocks cool under metamorphic transformations, deformations etc. Due to a great number of factors, that in fact have not been defined but they influence the crystalline rock elasticity, the calculation of the rock elasticity constants can be made only averagedly [Voigt, 1910; Hill, 1952; Belikov et al., 1970]. For these reasons, on the whole, the system of elastic symmetry of polycrystalline formations is higher than that of minerals composing the [Adamesku et al., 1985; Archean…, 1991].

If, for instance, a rock consists of mineral grains of triclinic and monoclinic syngonies whose axes orientation is, on the average, determined, then this suggests the presence of elastic anisotropy. But the orientation of such axes, as a rule, is characterized by some statistical dispersion. In this case the rock symmetry system will be higher than the mineral symmetry system. Therefore the majority of crystalline rocks will be characterized by rhombic, tetragonal, hexagonal, cubic and isotropic symmetry type. This is corroborated by the known experimental data [Nevsky, 1974; Prodaivoda, 1980, Egorkina & Bezgodkov, 1987; Hess, 1964; Tien-

When Lo et al., 1986; Chandra & Kenneth, 1988], as well as by the indirect assessment results, obtained by microstructural analysis [Dobrzhinetskaya, 1978; Kozhevnikov, 1982].

In conclusion we can say that elastic properties of crystalline rocks have both determined and statistical components [Prodaivoda, 1991]. Their ratio should be determined for every specific rock taken at every specific site. We believe that for the most part the elastic symmetry type of crystalline rocks can be no lower than orthorhombic. This consideration is based on the fact that the most frequent factor forming the rock elastic anisotropy is the strain tensor, especially if those strains act in the Earth crust during a long period of (geological) time.

The particular merit of the acoustopolariscopy method is that it allows to determine the symmetry type of an anisotropy body before the stage of elastic wave velocity measurement. The velocity measurements performed at the second stage are made in the directions conformable with the orientation of the elastic symmetry elements revealed with acoustopolariscopy.

Determined velocities put down in the form of quasimatrix V_{ij} (5.5) allow to obtain additional information about the symmetry type of a solid body. At first the symmetry type is determined by the number and mutual angles of projections of elastic symmetry elements in every of mutually perpendicular directions in the sample. An additional distinguishing feature of the transverse-isotopic symmetry type is obtaining the VP acoustopolarigram in the circle form on one of the sample faces. The analysis of velocity values by their ratios in the V_{ij} quasimatrix enables [see Acoustopolarimetry…, 1990] to check up the conclusion concerning the symmetry type being determined.

6.2. Analysis of location of symmetry elements in rhombic symmetry media

Let us consider a model of a rhombic symmetry media consisting of two systems of thin parallel layers. The layer systems are perpendicular to each other, as Fig. 6.1 shows. Assume that the layers lying in the plane through which the directions 1 and 2 pass are more high-velocity ones while as those lying in the plane passing through the directions 1 and 3 are low-velocity ones. Accordingly, the plane 1 and 2 will be called the plane with higher anisotropy and the plane 1 and 3 - with weaker one.

From Fig. 6.1 one can easily conclude that the compression wave velocities will obey the inequality system $V_{11} > V_{22} > V_{33}$. For instance, if we orient a beam of shear waves in the direction 1 with the polarization vector oriented along the direction 2, we should register the greatest shear velocity $V_{12} = V_{21}$. The intermediate by value will be the velocity $V_{13} = V_{31}$. The least shear velocity $V_{23} = V_{32}$ will be registered along the direction 2 and 3 with the polarization vector oriented accordingly along the direction 3 and 2. On the whole for the medium (Fig. 6.1) the following inequality series can be formulated:

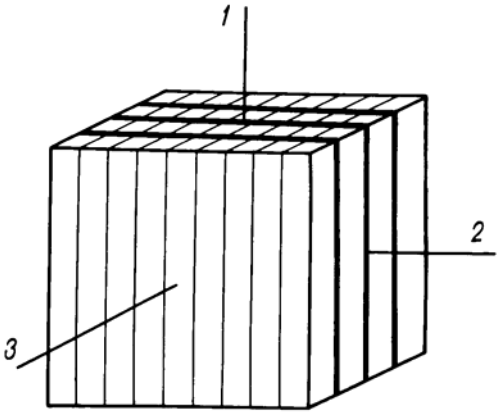

Fig. 6.1. Model of thin-layered medium consisting of mutually perpendicular systems of homogeneous isotropic layers with different elastic characteristics.

$V_{11} > V_{22} > V_{33}$, $V_{12} = V_{21} > V_{13} = V_{31} > V_{23} = V_{32}$. (6.1)

The ratios (6.1) represent only one version of element orientation for the rhombic medium elastic symmetry. If the measurements result in revelation of other inequalities between the values of V_{ij} then the spatial location of the planes with higher and weaker anisotropy will be different [Gorbatsevich, 1995].

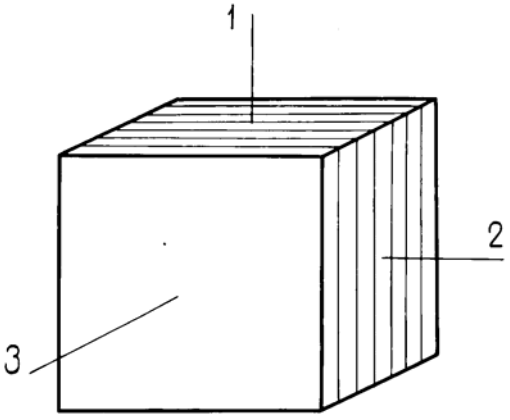

Fig. 6.2. Model of thin-layered medium composed of homogeneous isotropic parallel layers with different elastic characteristics

From the ratios (6.1) the inequality systems for velocities in transverse-isotropic media can be easily deduced. For the medium consisting of plane-parallel layers (Fig. 6.2) the symmetry axis will coincide with the direction 3. As is known, in such a medium the least compression wave velocity will be observed in the symmetry axis direction. On the whole, the velocity values will obey the following ratios:

$$V_{11} = V_{22} > V_{33}, \quad V_{12} = V_{21} = V_{13} = V_{31} > V_{23} = V_{32}, \tag{6.2}$$

It should be borne in mind that another type of a transverse-isotropic medium may occur. It is represented by a system of isometric parallel to each other rods penetrating homogeneous material (Fig. 6.3).

In this case the greatest compression wave velocity will be observed in the direction coinciding with the rods' axes. In the same direction the medium symmetry axis will run. For such a medium the inequality system will appear the following way:

$V_{11} = V_{22} < V_{33}$, $V_{12} = V_{21} < V_{13} = V_{31} = V_{23} = V_{32}$. (6.3)

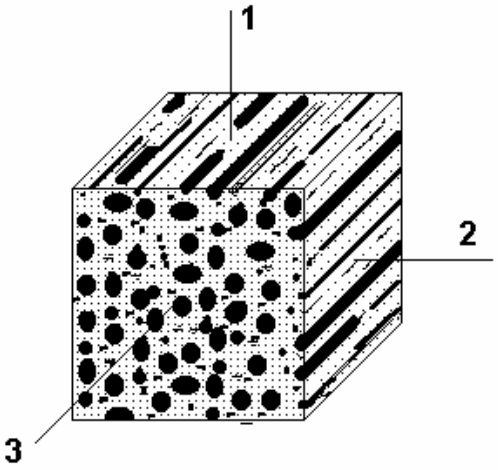

Fig. 6.3. Model of the medium composed of a system of quasi-isometric parallel to each other rods penetrating homogeneous material.

This type of transverse-isotropic symmetry occurred in amphibole-bearing rocks of the Kola Superdeep Borehole in the 6.6-7.7 km depth range [Gorbatsevich, 1995]. This type of symmetry is likely to result from metasomatic processes.

By the measurement results the ratios (6.1)-(6.3) allow one to determine the elements spatial location of orthorhombic and transverse-isotropic media. The acoustopolariscopy results should show the presence of elastic anisotropy for all the three pairs of faces in the sample of orthorhombic symmetry and for the two pairs of

faces in the sample of transverse-isotropic symmetry. It is worth noting that the ratios (6.2, 6.3) for transverse-isotropic symmetry media and (6.1) for the rhombic symmetry media should be strictly met for homogeneous fine-grained rock varieties. For substantially heterogeneous or coarse-grained rocks the ratios between the elastic wave velocities will reflect the natural scatter of their characteristics.

As follows from the above, determination of the medium symmetry type by the presented method is carried out by two independent ways: with acoustopolarigrams analysis and by velocity ratios in quasimatrix V_{ij} (5.5).

After determination of the symmetry elements number and type, their location and corresponding reorientation, three additional pads parallel to each other may be formed on the sample. Through those pads the values of V_{102}, V_{103},, V_{203}, are measured (Fig. 6.4). These values along with the values constituting the V_{ij} quasimatrix and the rock density value of ρ are necessary and sufficient for determining a full set of elasticity constants for orthorhombic media and media of higher symmetry types.

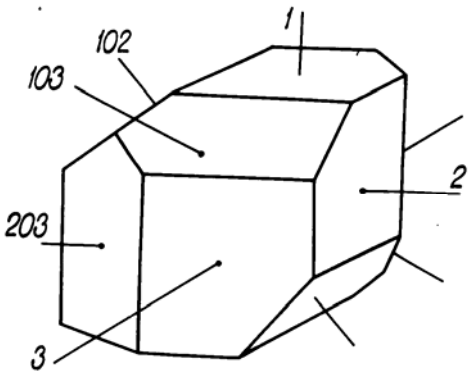

Fig. 6.4. Sample for determining elasticity constants of orthotropic media (irregular dodecahedron).

6.3. Calculation of elasticity constants for orthorhombic media and media of higher symmetry type

Let us consider a medium of orthorhombic symmetry as an initial one since from the equation system for calculation of elasticity constants of this symmetry medium, with the presence of some equalities, one can determine the constants of tetragonal, hexagonal and other symmetry types. A set of 9 independent constants meet an orthorhombic system of elastic symmetry [Belikov et al., 1970]

$$C_{\alpha\beta} = \begin{matrix} C_{11} & C_{12} & C_{13} & 0 & 0 & 0 \\ C_{21} & C_{22} & C_{23} & 0 & 0 & 0 \\ C_{31} & C_{32} & C_{33} & 0 & 0 & 0 \\ 0 & 0 & 0 & C_{44} & 0 & 0 \\ 0 & 0 & 0 & 0 & C_{55} & 0 \\ 0 & 0 & 0 & 0 & 0 & C_{66} \end{matrix} . \qquad (6.4)$$

In this matrix $C_{12} = C_{21}$, $C_{13} = C_{31}$, $C_{23} = C_{32}$.

After all 9 elastic rigidity constants $C_{\alpha\beta}$ of a rhombic symmetry medium have been determined one can calculate elastic compliance values $S_{\alpha\beta}$ or technical moduli using the known ratios [Belikov et al., 1970; Gorbatsevich, 1995]. The constants $C_{\alpha\beta}$ calculation for a rhombic symmetry medium can be performed with the following equations [Urupov & Lapin, 1972; Nevsky, 1974]:

$$C_{11} = \rho(V_{11})^2, \quad C_{22} = \rho(V_{22})^2, \quad C_{33} = \rho(V_{33})^2,$$

$$C_{44}= \rho(V_{23})^2, \quad C_{55}= \rho(V_{13})^2, \quad C_{66}= \rho(V_{12})^2. \tag{6.5}$$

In this case among the V_{ij} values the inequality $V_{11} > V_{22} > V_{33}$ should be met. The constant C_{12} can be calculated from the expression [Urupov & Lapin, 1972];

$$C_{12} = \frac{1}{\sin 2\theta_1}\sqrt{F_1^2 - F_2^2} - C_{66}, \tag{6.6}$$

where $F_1 = 2\rho V_{102}^2 - (C_{22} + C_{66}) - (C_{11} - C_{22})\sin^2\theta_1$,

$F_2 = C_{22} - C_{66} - \sin^2\theta_1(C_{11} + C_{22} - 2C_{66})$.

In the last-mentioned expressions θ_1 is the angle between the normal to the equal phase front and the plane of the weaker anisotropy of the orthotropic medium. The calculation of the angle θ_1 is performed from the direction in which V_{22} has been measured along the plane of stronger anisotropy passing through the directions in which the values of V_{11} and V_{22} have been measured. If the angle θ_1 is equal to 45^o then the equation (6.6) appears more compact:

$$C_{12} = \sqrt{[2\rho V_{102}^2 - \frac{1}{2}(C_{11} + C_{22}) - C_{66}]^2 - \frac{1}{4}(C_{11} - C_{22})^2} - C_{66}. \tag{6.7}$$

To determine C_{13} one can use the formula [Urupov & Lapin, 1972]:

$$C_{13} = \frac{1}{\sin 2\theta_2}\sqrt{F_1^2 - F_2^2} - C_{55}, \tag{6.8}$$

where $F_1 = 2\rho V_{103}^2 - (C_{33} + C_{55}) - (C_{11} - C_{33})\sin^2\theta_2$,

$F_2 = C_{33} - C_{55} - \sin^2\theta_2(C_{11} + C_{33} - 2C_{55})$.

The angle θ_2 is calculated from the direction in which the V_{33} value has been measured in the weaker anisotropy plane passing through the directions in which V_{11} and V_{33} have been measured. With $\theta_1 = 45^o$ the equation will take the form:

$$C_{13} = \sqrt{[2\rho V_{103}^2 - \frac{1}{2}(C_{11} + C_{33}) - C_{55}]^2 - \frac{1}{4}(C_{11} - C_{33})^2} - C_{55}, \tag{6.9}$$

To determine the constant C_{23} one can use the formula [Urupov & Lapin, 1972]:

$$C_{23} = \frac{1}{\sin 2\theta_3}\sqrt{F_1^2 - F_2^2} - C_{44}, \tag{6.10}$$

where $F_1 = 2\rho V_{203}^2 - (C_{33} + C_{44}) - (C_{22} - C_{33})\sin^2\theta_3$,

$F_2 = C_{33} - C_{44} - \sin^2\theta_3(C_{22} + C_{33} - 2C_{44})$.

The angle θ_3 is calculated from the direction, in which V_{33} has been measured in the weaker anisotropy plane passing through the directions, in which V_{22} and V_{33} have been measured.

As follows from the formulae (6.4-6.10), to calculate all 9 constants of a rhombic symmetry medium, in addition to the values of V_{ij}, given in the matrix form (5.5), it is necessary to determine the values of compression wave phase velocity V_{102}, V_{103} and V_{203} in the directions forming the angles θ_1, θ_2 and θ_3 to the weak and strong symmetry planes. The values of V_{102}, V_{103}, V_{203} can be determined if we form three additional pads parallel to each other in such a way that the normals to them are directions (102), (103) and (203) as Fig. 6.4 shows. The calculations of C_{12}, C_{13}, C_{23} are greatly simplified if directions (102), (103) and (203) form the angles $\theta_1 = \theta_2 = \theta_3 = 45°$ to the medium symmetry elements.

The measurements of V_{102}, V_{103}, V_{203} should be performed considering the requirements set forth in chapters 4 and 6, i.e. the phase velocity of the wave front propagation should be measured. One should also take into account that it is not known in advance how elastic symmetry elements and, in particular, weaker and stronger symmetry planes are arranged in the sample. But, as has been mentioned above, to calculate the constants $C_{\alpha\beta}$ one should know the arrangement of the medium elastic symmetry elements relative to the faces or directions in the sample. Therefore to define the type of elastic symmetry elements it is necessary to use the analysing procedure for acoustopolarigrams and matrices V_{ij} (5.5). The purpose of this analysis is to divide media of rhombic, tetragonal, hexagonal and cubic symmetry [Gorbatsevich, 1995].

The medium being analysed belongs to the orthorhombic system only when all the 9 constants are represented by substantial values that are not equal to zero and to each other. But the calculation results may reveal an equality or a relationship between individual constants.

A particular view of such inequalities or relationships allows to diagnose other simpler (higher) systems of elastic symmetry.

If the constants $C_{11} = C_{22}$, $C_{44} = C_{55}$, $C_{13} = C_{23}$, but C_{33}, C_{12} and C_{66} are not equal to each other, then the medium has tetragonal symmetry (symmetry classes 422, 4*mm*, 4/*mmm*, $4\bar{2}m$). A total number of independent constants is equal to 6.

If the constants $C_{11} = C_{22}$, $C_{13} = C_{23}$, $C_{44} = C_{55}$, $C_{12} = C_{11} - 2C_{66}$ are not equal to each other, the medium is transverse-isotropic. The number of independent constants is equal to 5.

If $C_{11} = C_{22} = C_{33}$, $C_{44} = C_{55} = C_{66}$, $C_{12} = C_{13} = C_{23}$, the medium is a cubic symmetry. The number of constants is equal to 3.

If $C_{11} = C_{22} = C_{33}$, $C_{44} = C_{55} = C_{66} = (C_{11} - C_{12})/2$, $C_{12} = C_{13} = C_{23}$, the medium is isotropic. The number of independent constants is equal to 2.

Elastic symmetry of crystalline rocks, probably, is not exhausted by the above systems. More complicated (low symmetry) than orthorhombic media are described by the number of the constants more than 9. The way of their determination has not been determined yet due to complex relations between elastic wave velocities and elasticity constants. A rock may be assigned to complex systems (trigonal, monoclinal or tetragonal) if more than two symmetry elements, their non-orthogonality, have been revealed by acoustopolariscopy in a medium section. An identification of the elastic symmetry class of such media may be performed by the search of a similarity with the corresponding class of the crystal symmetry. The example showing this possibility is given in Fig. 6.5.

One should take into account that elastic wave velocities in heterogeneous polycrystalline rocks absorbing elastic waves, as a rule, experimentally, cannot be precisely defined even with sophisticated measuring equipment. The obstacle for this is, first of all, heterogeneity - variations in composition and structure of such a medium. Moreover, the lower is the medium symmetry class, the higher is the uncertainty when calculating its constants. Therefore, the determined constants and class of elastic symmetry of some geological singularity should be corroborated by parallel measurements on other samples. First, we should consider the peculiarities of the media of pseudohexagonal and rhombic symmetries that are complicated ones.

6.4. Criteria for identification of weakly anisotropic media

A large number of observations performed on the samples [Belikov et.al., 1970; Reference book, 1975; Physical…, 1988; Petrophysics, 1992], as well as by the seismic methods in extended geological bodies [Chesnokov, 1977; Hess, 1964; Raitt et al., 1969] showed that weakly anisotropic rocks prevail. The paper [Thomsen, 1986] dedicated to weak anisotropy presents evidence that weakly anisotropic and transverse-isotropic media occur most frequently among sedimentary rocks. The paper shows that the angle dependence of V_p, V_{s1} and V_{s2} cannot be described by a function representing a comparatively simple figure, for instance, ellipse. M.V.Nevsky [1974] has considered a special criterion that enables to divide media into weakly and highly anisotropic. When elastic waves propagate through thin-layered media one can observe loops (lacunas) on the circle indicatrix of the shear wave velocity V_{sv} (with the polarization vector in the plane passing through the symmetry axis), if the maximum value of V_{svmax} at some point of the indicatrix exceeds 1.13-1.14 times the value of V_{sv} measured in the layers direction. The presence of loops means that in one and the same direction four various shear wave velocities can be detected. Note that only for one of them the polarization vector lies in the medium symmetry plane. M.Musgrave and M.Markham observed such splitting of a shear wave pulse in zinc crystals [Musgrave & Markham, 1961]. The absence of loops on the circle indicatrixes of the velocity may be one of the main signs of a weakly anisotropic medium.

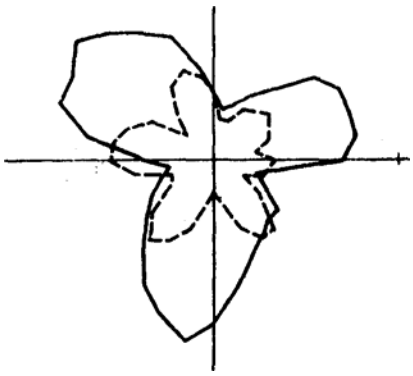

Fig. 6.5. Acoustopolarigram of quartz monocrystal (trigonal syngony), obtained in the section perpendicular to the third order axis.
Solid line - parallel vectors, dotted line - crossed vectors.

If the conditions, defining the medium belonging to transverse-isotropic or weakly anisotropic ones, have been met, the indicatrixes of the wave velocity may be calculated with the simplified equations suggested by L.Thomsen [1986]. According to this work, a medium is weakly anisotropic if the factors

$$\varepsilon = (V_{11} - V_{33})/V_{33} \le 0.2,\ \ \gamma = (V_{23} - V_{12})/V_{12} \le 0.2,\ \ \kappa = (V_{s102} - V_{12})/V_{12} \le 0.12. \quad (6.11)$$

In the last-mentioned inequalities the indexing given in the matrix V_{ij} has been used (5.5). The value of V_{s102} is determined in direction 102 (Fig. 6.4) so that the polarization vector of shear waves is oriented in the plane passing through the medium symmetry axis.

Following V.S. Seleznyov et al. [1986], a simplified way for calculation of the transverse-isotropic medium constants is suggested. The criteria that allow to assign a medium to weakly isotropic are inequalities similar to the above: $\varepsilon \le 0.13$, $\gamma \le 0.20$, $\kappa \le 0.13$. As test examples showed, the application of the simplified calculation with these inequalities being observed may result in an error not exceeding 3-4% [Seleznyov, 1986; Thomsen, 1986].

Thus, the review of the known works allows one to consider the following criteria of weakly to average anisotropic media to be close to universally recognized:

$$\varepsilon = (V_{11} - V_{33})/V_{33} \le 0.15, \quad \gamma = (V_{23} - V_{12})/V_{12} \le 0.2, \quad \kappa = (V_{s102} - V_{12})/V_{12} \le 0.13. \quad (6.12)$$

Similar criteria can be applied to an anisotropy assessment of more complicated media than transverse-isotropic. For instance, for an orthorhombic medium the number of such criteria rises to 9. Except for the assessment of the weak anisotropy degree by the indexes ε, γ and κ, the necessity of determining the anisotropy medium factor arises. The factor characterizes the anisotropy degree of a medium as a whole.

6.5. Integral assessment of elastic anisotropy in crystalline rocks

The recording of elastic wave velocities in quasimatrix V_{ij} form suggested by us (5.5) covers 9 values. The quasimatrix diagonal terms V_{11}, V_{22} and V_{33} are compression wave velocity values and the terms V_{12}, V_{13} are shear wave velocity values measured on the sample's first side, V_{21} and V_{23} - on the second and V_{31} and V_{32} - on the third side. If the indicated values have been determined along the sample elastic symmetry elements they take, accordingly, the greatest and the least, i.e. extreme values. Naturally, the comparison of, for instance, V_{11} and V_{22}, or V_{11} and V_{33} for determining the anisotropy index of the rock as a whole is not sufficient. A general index of the rock elastic anisotropy for compression waves should take into account the distinction of all the V_{11}, V_{22} and V_{33} values from one another. Respectively, the anisotropy generalized index for the shear waves measured values should take into account the V_{12}, V_{13}, V_{21}, V_{23}, V_{31} and V_{32} values.

First, we shall consider a possibility of presenting the anisotropy generalized index for compression waves through the quasimatrix diagonal terms (5.5), i.e. through V_{11}, V_{22} and V_{33}. In crystalline metamorphosed rocks the difference between the V_{ii} terms is most often caused by palaeostresses long influence resulting in rearrangement of their mineral composition and structure [Brace, 1960; Kozhevnikov, 1982]. From the elasticity theory [Bezukhov, 1968] it is known that the sum of $\sigma_{max} = \sigma_{11}$, $\sigma_{av} = \sigma_{22}$, $\sigma_{min} = \sigma_{33}$ values or, to put it otherwise, the sum of $\sigma_{11} + \sigma_{22} + \sigma_{33}$ is an invariant, i.e. it does not change when three mutually perpendicular directions, along which the values are determined, rotate in space. In accordance with the accepted conditions relating to proportionality of the measured velocities to the palaeostress values (2) and (3), the sum of $V_{11} + V_{22} + V_{33}$ with some assumptions, may be considered to be invariant in regard to mutually perpendicular directions along which they have been determined. Such determinations can be performed, for instance on a cubic sample.

By the expression

$$V_{av} = (V_{11} + V_{22} + V_{33})/3 \quad (6.13)$$

we calculate an average velocity of compression waves in an anisotropic sample. The value of V_{av} may be considered to be equivalent to the quasimatrix spherical tensor (5.5). Using this value one may introduce a characteristic that reflects the anisotropy degree of the sample as a whole. Such a characteristic (let us call it intensity or anisotropy generalized factor for compression waves) can be determined as the sum of standard deviations of individual V_{ii} values from V_{av}:

$$A_p = \frac{1}{V_{av}} \sqrt{(V_{11} - V_{av})^2 + (V_{22} - V_{av})^2 + (V_{33} - V_{av})^2} \ . \tag{6.14}$$

The assessment made by formula (6.14) is also important because it coincides in shape with the deviator expression for the stress tensor in a solid body and may be invariant relative to the variation in the co-ordinates direction [Bezukhov, 1968]. If the anisotropy generalized factor in respect to the elasticity constants is supposed to be applied then it should be transformed into:

$$A_c = \frac{1}{V_{av}^2} \sqrt{(V_{11}^2 - V_{av}^2)^2 + (V_{22}^2 - V_{av}^2)^2 + (V_{33}^2 - V_{av}^2)^2} \ . \tag{6.15}$$

In this expression of the anisotropy factor A_c it is taken into account that when calculating the elasticity constants the velocity values are squared (see (6.5)-(6.10). K.S.Alexandrov & G.T.Prodaivoda [2000] have suggested anisotropy factors reflecting the distinction of the medium of a certain symmetry type from an isotropic body.

Now let us consider the quasimatrix terms (5.5) composed of shear wave velocities. Previously it was conventional to evaluate the anisotropy degree for every side of a cubic sample through the birefringence factor [Clark et al., 1983; Gorbatsevich, 1995]. For instance, the shear wave birefringence factor determined for the first side is equal to

$$B_1 = \frac{2(V_{12} - V_{13})}{(V_{12} + V_{13})} \ . \tag{6.16}$$

Similarly the factors for the second and third sides of the sample are determined:

$$B_2 = \frac{2(V_{21} - V_{23})}{(V_{21} + V_{23})}, \tag{6.17}$$

$$B_3 = \frac{2(V_{31} - V_{32})}{(V_{31} + V_{32})}. \tag{6.18}$$

Let us determine the generalized factor for shear waves:

$$B_S = \sqrt{B_1^2 + B_2^2 + B_3^2} \ . \tag{6.19}$$

It should be noted that for a large number of rocks the anisotropy factors will most likely be evaluating ones, since anisotropic crystalline rocks, as a rule, are

heterogeneous in their elastic properties. It is impossible to evaluate their heterogeneity degree a priori in every specific case. On the other hand, a strict approach requires that the directions along which the values of V_{ij} are measured be close to the directions along which the elastic symmetry elements pass. To use the expressions (6.13-6.19) correctly it is necessary that the symmetry of the medium being evaluated is not lower than an orthorhombic one.

7. ACOUSTOPOLARISCOPY OF SOME ROCK FORMING MINERALS

7.1. Peculiarities of elastic properties of rock forming minerals

As is known, mineralogists have at their disposal a splendid reference book (in terms of data completeness) on mineral optic properties by W.E. Tröger [1959]. As to mineral elastic properties, such a reference book has not been created yet. To our mind, the reason for that is insufficient development of experimental equipment. Elastic properties of the lowest symmetry minerals are described by a tensor of the fourth order. This arises considerable complexity when analysing results of experimental observations. It is also known that mineral optic properties are described by a tensor of not higher than the second order. At the same time, elastic properties of ore forming minerals have great influence on some natural processes. With the advent of a new investigation method - acoustopolariscopy [Gorbatsevich, 1995] an actual possibility of creating a reference book similar to that by W.E. Tröger has appeared. The reference book might have included the data on fine peculiarities of elastic properties of rock-forming minerals.

The study of formation regularities of elastic-anisotropic properties and non-elastic effects of minerals and mineral formations is a basic scientific problem. This problem is related to the problem of thermodynamic balance of a mineral grain in a paragenetic ensemble of other grains in a crystalline rock during metamorphic transformations [Saxena, 1973]. For instance, the existing method of dynamic analysis of orientation of palaeostress field components during metamorphic processes is based on the study of oriented arrangement of crystallographic and more often optic axes in minerals. That is the essence of the microstructural method. Recently on the basis of this and other methods it has been established that elastic-anisotropic properties of mineral grains make the greatest impact on the orientation of the grains' crystallographic axes [Brace, 1960; Kozhevnikov, 1982; Kazakov, 1987]. Their orientation is also subject to the principle of free energy minimum, which is a consequence of the theorem of the change in thermodynamic potential of an anisotropic body in the field of mechanical stresses. As applied to mineral grains of a polymineral rock it is formulated in the following way: in greatly deformed rocks the direction, in which the constant value of mineral compliance is maximum, turns out to be in the direction of the greatest component of the palaeostress field [Delitsyn, 1985].

There are some minerals (biotite, phlogopite, muskovite etc.) in which the orientation of crystallographic and elastic symmetry axes is very close or coincides. In other minerals (quartz, calcite, diopside, amphibole, plagioclase etc.) the orientation of crystallographic axes may diverge from the orientation of elastic symmetry axes and respectively from the spatial location of the elasticity modulus greatest (least) value [Brace, 1960; Kazakov, 1987; Alexandrov & Prodaivoda, 2000].

What is more, the angles between peculiar orientations and crystallographic axes depend on the mineral modification and its composition. Peculiar orientations are those where $S_{\alpha\beta}$, ($C_{\alpha\beta}$) values are extreme. For instance, for quartz of different modifications (α, β) these angles vary in the range of ~30° to ~70° [Brace, 1960; Sobolev et al., 1964]. The same angles for amphiboles and plagioclases as well as elasticity characteristics $S_{\alpha\beta}$, $C_{\alpha\beta}$, depend on their composition [Kazakov, 1987].

At present information on orientation of elasticity axes and spatial location of the greatest (least) values of elasticity modulus for a large number of rock forming minerals are scarce. So we have carried out acoustopolariscopy of some widespread

rock forming minerals. Below some initial results of this investigation are presented. Certainly, this study has not approached solving the problem to the extent it has been solved in W.E.Tröger's book in relation to minerals optical properties. Our study is the initial stage on this way.

7.2. Minerals of higher and medium syngony

As is known, mineral syngonies are subdivided into three categories: higher, medium and lower [Geological dictionary, 1973]. The cubic syngony belongs to the higher category that has the greatest number of elastic symmetry elements among other homogeneous ordered anisotropic media. Hexagonal, tetragonal and triclinic symmetry types pertain to anisotropic media of the medium category [Berry et al., 1983].

As to cubic symmetry media we have performed acoustopolariscopy of minerals analcite, garnet halite and pyrite (Fig. 7.1, Table 7.1). The same determinations have been done for the group of minerals of medium syngony: apatite (hex.), nepheline (hex.), tourmaline (trig.) and quartz (trig.) - see Table 7.2.

First we have taken mineral samples of the suitable size (no less than 10x10x10 mm^3) and quality (the lack of fractures, high homogeneity). The samples were made in the form of a cube so that the main crystallographic axis of the crystal passed in 1-1' direction, Fig. 5.1.

At the first stage acoustopolariscopy of the samples was conducted at parallel polarization vectors (VP position). At the second stage the transducers' polarization vectors were set at the right angle (VC position). For some mineral samples acoustopolariscopy was performed at different frequencies. Accordingly, we have used the acoustopolariscopes in which the transducers having natural frequencies of 0.78, 1.26 and 2.67 MHz were set. The measurements were made on all the three pairs of the cubic sample sides. On each of the three pairs we have measured the values of mutual angles between the projections of symmetry elements (Table 7.1). Then we have determined the LAAA index *D* (Table 7.2).

The acoustopolarigrams of mineral samples of cubic syngony, Fig. 7.1, show that the shape of VP diagrams is rather strongly influenced by the crystal internal defects.

The VC diagrams for pyrite

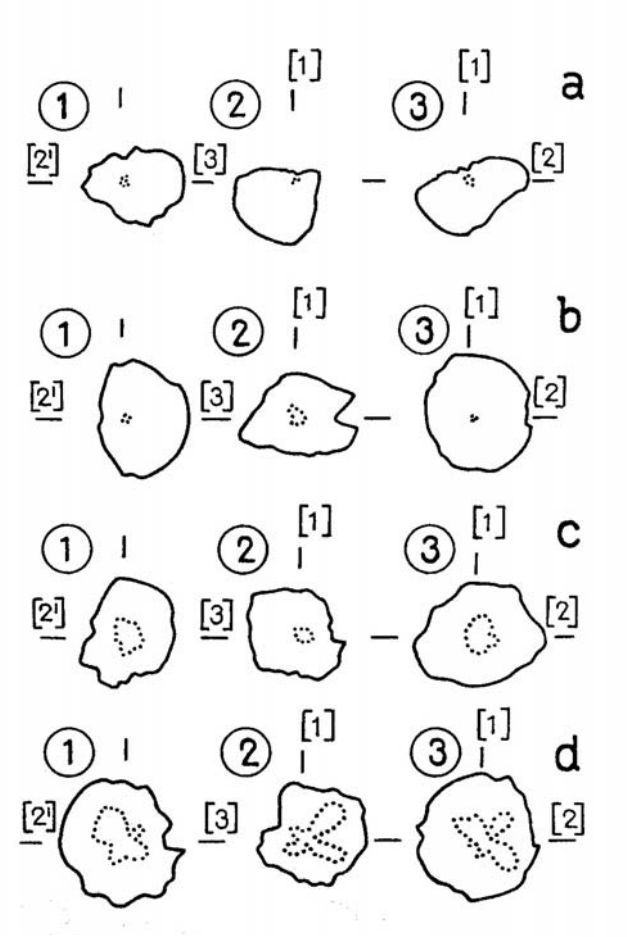

Fig. 7.1. Acoustopolarigrams of the mineral samples analcite (a), halite (b), garnet (c) and pyrite (d).

(Fig. 7.1d) allow one to distinguish the orientations of the symmetry elements projections on all three sample sides. As for other mineral samples, distinguishing these orientations presents a challenge due to the VC diagrams small size. But this can be done if this determination is made by the so-called reverse acoustopolarigrams (Fig. 7.2). The reverse acoustopolarigrams can be obtained if in the process of acoustopolarization measurements all amplitudes are normalized by the minimum amplitude received at the crossed polarization vectors of the source and receiver of shear waves. On sides 1 and 2 of the analcite sample the orientations of the symmetry elements projections passing through the maxima of the reverse diagrams amplitudes can be distinguished rather easily (Fig. 7.2a).

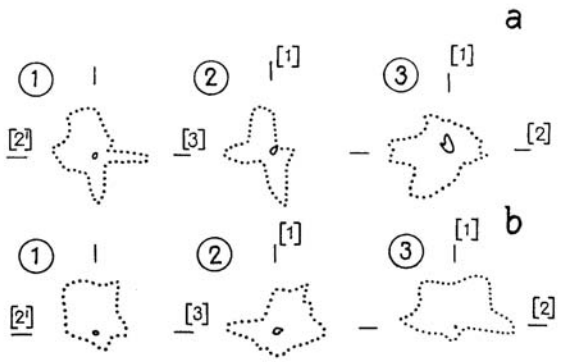

Fig.7.2. Reverse acoustopolarigrams for analcite (a) and halite (b).

The measurements of the angles between the symmetry elements projections, presented in Table 7.1, have been performed by the reverse acoustopolarigrams. These angles, for instance, for analcite at the frequencies f_0 = 1.67 and 2.67 MHz are the averages of two measurements. The angles for pyrite presented in Table 7.1 are the averages of three measurements. The absence of the data in some cells of Table 7.1 or their insufficient accuracy can be explained by heterogeneities and foreign inclusions in the structure of natural mineral samples.

Table 7.1

Mutual angles between the projections of elastic symmetry elements in the samples of some rock forming minerals of higher syngonies.

№ №	Mineral	Sample	Syn-gony	Expe-ri-ment №	f_0, MHz	Side 1		Side 2		Side 3	
						α_1	α_2	α_1	α_2.	α_1.	α_2.
1	Anal-cite	An-98-1	Cub.	1, 2	1.26	80	100	115	~65	85	95
2	Anal-cite	An-98-1	Cub.	1, 2	2.67	~107	~73	100	~80	~93	~87
3	Halite	Ga-1-5	Cub.	1	2.67	~95	~85	~73	107	104	76
4	Garnet		Cub.	1	1.26	-	-	~90	~90	-	-
5	Pyrite	P-001	Cub	1	0.78	79	101	99	81	-	-
6	Pyrite	P-001	Cub.	1-3	2.67	82	98	92	88	86	94

Notes: α_1, α_2 are represented in degrees.

For all the samples of cubic syngony presented in Table 7.2 manifestations of the LAAA effect are comparatively weak. The index D in analcite increases, on the average, with the rise in the impact frequency.

At f_0 = 2.67 MHz frequency a plane type of LAAA is detected in the sample (see point 2.4). Pyrite exhibits weak LAAA which can most likely be explained by an imperfect crystal structure.

The results of the determinations on the minerals of medium syngony - crystals of apatite, nepheline, quartz and tourmaline are presented in Fig. 7.3-7.6 and Tables 7.3 and 7.4.

Table 7.2.

Linear acoustic anisotropic absorption indexes in the samples of some rock forming minerals of cubic symmetry.

№ №	Mineral	Sample	Syn-gony	Expe-ri-ment №	f_0, MHz	D_1	D_2	D_3	Notes
1	Analcite	An-98-1	Cub.	1, 2	1.26	0.10	0.055	0.074	
2	Analcite	An-98-1	Cub.	1, 2	2.67	0.06	0.022	0.30	P2-3
3	Halite	Ga-1-5	Cub.	1	2.67	0.21	0.18	0.070	
4	Garnet	G-1	Cub.	1	1.26	0.13	0.11	0.13	
5	Pyrite	P-001	Cub.	1	0.78	0.14	0.076	0.048	
6	Pyrite	P-001	Cub.	1, 2	2.67	0.06	0.043	0.030	
Notes: P2-3 – LAAA plane of structural elements passes through the directions 2-2’ and 3-3’, see Fig. 5.1									

The apatite crystal has been selected from the skarns of the Dashkesansky iron ore deposit. It was a well cut crystal, formed by the combination of two hexagonal prisms, hexagonal pyramids and a pinacoid. In the directions parallel to the sides (0001) and (1010) weak hair-like microcracks of imperfect cleavage have been detected in the crystal. The sample prepared for acoustopolariscopy was cut from the crystal central part in the shape of a rectangle prism with a 12x12 *mm* base and 15 *mm* edge oriented parallel to the crystallographic axis L6 in apatite.

Acoustopolariscopy of apatite samples was performed several times and at various frequencies, see Tables 7.3 and 7.4, Fig. 7.3 and 7.4. The sample A-1 diagram for the first side was obtained in the axis direction [0001], Fig. 7.3a. As follows from the reverse diagrams, Fig. 7.4, the projections of the elastic symmetry elements are at a right angle. They are virtually normal to the sample sides. In the direction 3-3', on the diagram obtained at the frequency 1.26 MHz (Fig. 7.4a), the projections of the elastic symmetry elements are not practically conspicuous. But for the sample A-1-3, whose diagrams were obtained at 2.67 MHz frequency (Fig. 7.3b), revealing the orientation of the projections of elastic symmetry elements presents no problems.

A comparison of Fig. 7.3a and 7.3b enables one to notice that the VC diagrams, especially side 3 at a higher frequency, allow easier distinguishing of symmetry elements orientation. At 2.67 MHz frequency the apatite sample exhibits an orthorhombic symmetry type. An analysis of the data from Table 7.3 permits noticing that the values of angles between the projections of elastic symmetry elements range from 81^o to 99^o when their orientation is revealed with confidence. No frequency dependence of these angles has been noticed.

In the apatite samples (Table 7.4) an essential manifestation of the LAAA effect has not been detected. The maximum values of D do not exceed 0.14. At f_0 = 1.26 MHz in the sample A-1 a linear type of LAAA (L2) is detected as well as at f_0 = 2.67 MHz in the sample A-1-3 (L1). The nepheline sample (He-005, f_0 = 2.67 MHz), whose acoustopolarigrams are presented in Fig. 7.3c, is virtually a transverse-isotropic medium. Its symmetry axis passes along the normal to side 2. The reverse acoustopolarigram allows clear-cut detecting of elastic symmetry elements projections

on sides 1 and 3 (Fig. 7.4b). The mutual angles between the elastic symmetry elements in the nepheline samples are in the range of 85-95^o (Table 7.3).

In the nepheline samples (Table 7.4) at low frequencies (f_0 = 0.78-1.26 MHz) the LAAA index may reach medium and high values. For instance, the maximum values of D are 0.25-0.62. In nepheline a linear type of LAAA has been registered at f_0 = 0.78 MHz frequency (samples He-005, He-008) and a plane type at f_0 = 1.26 MHz frequency (sample He-008), the plane passing through sides 1 and 3.

In the acoustopolarigrams of the tourmaline sample P-011 (Fig. 7.3d, 7.4c) a simultaneous manifestation of two effects - LAAA and depolarization of shear waves (DSW) has been registered. The LAAA effect is mainly registered on sides 1 and 3. At f_0 = 1.26 MHz the sample shows a linear (L2) type of LAAA (Table 7.4).

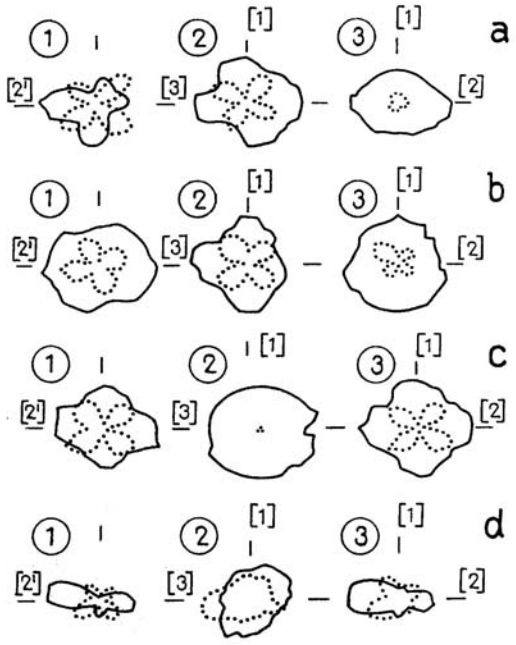

Fig. 7.3. Acoustopolarigrams for: apatite at 1.26 MHz (a), apatite at 2.67 MHz (b), nepheline (c) and tourmaline (d).

At f_0 = 2.67 MHz a combination of linear and plane types is exhibited where elongated elements of the media are oriented along side 2 and the plane passes through sides 1 and 2. The DSW effect is most conspicuous on side 2. It means that in the planes parallel to side 2 a fan pattern of the medium structural elements arrangement is observed in the tourmaline sample (see points 3.1 and 3.2).

Table 7.3.

Mutual angles between the projections of elastic symmetry elements in the samples of some rock forming minerals of medium syngonies.

№№	Mineral	Sample	Syngony	Experiment №	Frequency, MHz	Side 1		Side 2		Side 3	
						α_1	α_2	α_1	α_2	α_1	α_2
1	Apatite	A-1	Hex.	1, 2	1.26	85	95	90	90	91	89
2	Apatite	A-1	Hex.	1	2.67	96	84	91	89	103	~77
3	Apatite	A-1-3	Hex	1	0.78	94	86	81	99	~76	104
4	Apatite	A-1-3	Hex.	1, 2	2.67	93	87	90	90	90	90
5	Apatite	A-006	Hex.	1	2.67	97	83	93	87	~94	~86
6	Nepheline	He-3	Hex.	1, 2	2.67	90	90	-	-	85	95
7	Nepheline	He-005	Hex.	1	0.78	89	91	99	81	100	~80
8	Nepheline	He-005	Hex.	1	2.67	89	91	-	-	93	87
9	Nepheline	He-008	Hex.	1	0.78	90	90	86	94	90	90
10	Nepheline	He-008	Hex.	1, 2	1.26	103	~77	95	85	89	91
11	Tourmaline	P-011	Trig.	1, 2	2.67	86	94	-	-	98	82

Notes: α_1, α_2 are represented in degrees.

It is worth noting that tourmaline exhibits strong pleochroism in optics as well. The symmetry elements in the tourmaline sample are detected only on sides 1 and 3. Their mutual angles are in the range of 82-98° (Table 7.3).

The acoustopolariscopy of a quartz synthetic sample (sample Qu-11) was performed most thoroughly, the procedure and defining the arrangement of elastic symmetry elements with respect to the sample crystallographic axis [0001] being performed 4 times. The quartz sample prepared for measurements had the shape of a cube with a 4 *cm* edge. It has been cut so that its crystallographic axis [0001] is perpendicular to side 1 and, accordingly, parallel to the direction 1-1' with a precision of ±1° (Fig. 7.5a).

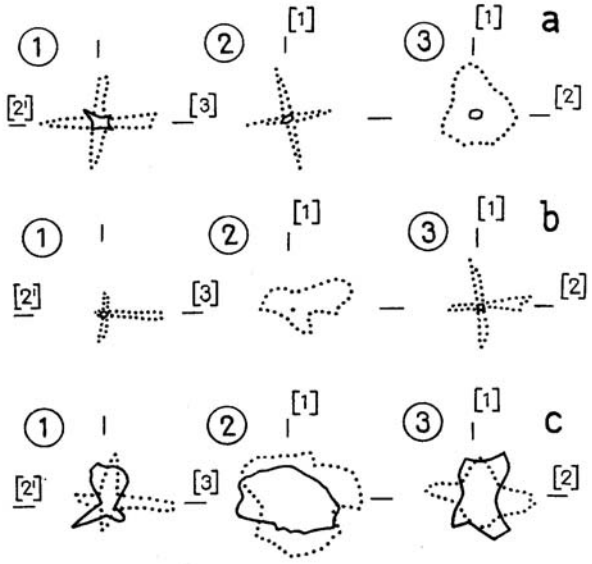

Fig.7.4. Reverse acoustopolarigrams for apatite (a), nepheline (b) and tourmaline (c).

Table 7.4.

Indexes of linear acoustic anisotropic absorption in the samples of some rock forming minerals of medium syngonies.

№№	Mineral	Sample	Syngony	Experiment №	Frequency, MHz	D_1	D_2	D_3	Notes
1	Apatite	A-1	Hex..	1, 2	1.26	0.045	0.01	0.08	L2
2	Apatite	A-1-3	Hex.	1	0.78	0.020	0.029	0.10	
3	Apatite	A-1-3	Hex.	1, 2	2.67	0.032	0.09	0.033	L1
4	Apatite	A-006	Hex.	1	2.67	0.04	0.14	0.10	
5	Nepheline	He-3	Hex.	1	2.67	0.021	0.00	0.00	
6	Nepheline	He-005	Hex.	1	0.78	0.038	0.25	0.32	L1
7	Nepheline	He-005	Hex.	1	2.67	0.048	0.00	0.022	
8	Nepheline	He-008	Hex.	1	0.78	0.10	0.072	0.14	L2
9	Nepheline	He-008	Hex.	1, 2	1.26	0.072	0.18	0.62	P1-3
10	Quartz	Qu-11	Trig.	3, 4	0.6	0.00	0.14	0.06	
11	Quartz	Qu-11	Trig.	1, 2	1.2	0.00	0.04	0.36	
12	Tourmaline	P-011	Trig.	1, 2	1.26	0.23	0.06	0.59	L2
13	Tourmaline	P-011	Trig.	1, 2	2.67	0.52	0.14	0.54	L2, P1-2
Note: L - linear, P - plane type of LAAA manifestation; directions 1-1', 2-2', 3-3' along which the effect is exhibited, see Fig. 5.1									

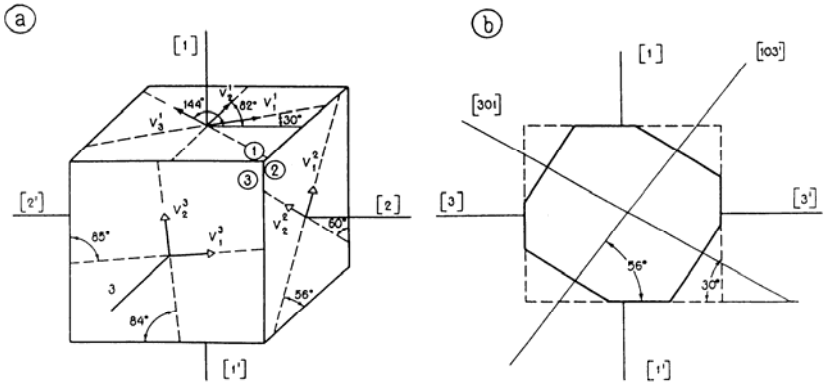

Fig. 7.5. Orientation of elastic symmetry elements in the synthetic quartz sample according to the acoustopolariscopy data (a) and schematic formation of complementary sides along the normal to directions 301 and 103 (b).

Figure 7.6 shows the acoustopolarigrams of four successive determinations obtained in the cube's three mutually perpendicular directions 1-1', 2-2', 3-3'. The acoustopolarigrams (Fig. 7.6a, 7.6b, Table 7.5, measurement numbers 1 and 2) were obtained with the recording device UD-2-12, whose amplifier has a resonance frequency of 1.2 MHz and device DUK-66 PM, with a frequency of 0.6 MHz (Fig. 7.6c, 7.6d, Table 7.5, measurement numbers 3 and 4).

In the direction 1-1' with parallel polarization vectors (VP position) three petal acoustopolarigrams were obtained. The maximum amplitude in each petal was registered in the directions coinciding with the position of the elastic symmetry planes passing through the axis [0001]. With the crossed polarization vectors (VC position) the diagrams with 6 petals were obtained.

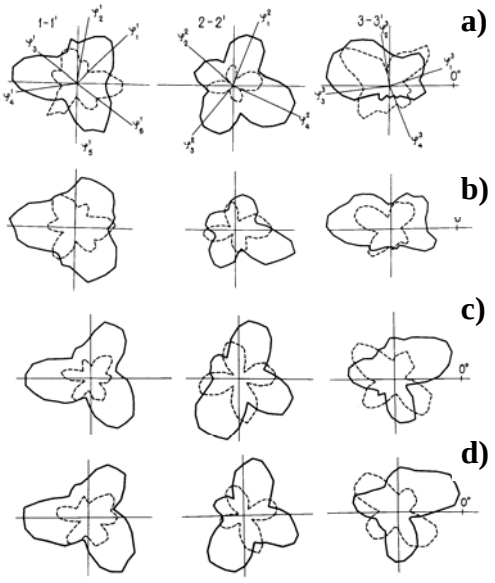

Fig.7.6. Acoustopolarigrams of the synthetic quartz cubic sample obtained at f_0 =1.2 MHz (a, b) and f_0 =0.6 MHz (c, d) frequencies.

The results of the measurements of the VC minima angular locations regarding the orientation of the sample sides are presented in Fig. 7.5. In the direction 2-2' VP acoustopolarigrams represent a four-petal figure that is typical of media with two crossing symmetry elements. The VC diagrams testify that.

The position of minima in the VC diagrams shows that the crystallographic axis (direction 1-1') and elastic symmetry elements form a certain angle (Table 7.5). The VP acoustopolarigram obtained in the direction 3-3' indicates a rather complicated nature of propagation of polarized shear waves in the elastic-anisotropic medium of the sample. However, by the VC diagram minima one may single out a spatial orientation of elastic symmetry two elements which arrangement is close to the orientation of the crystallographic axis (direction 1-1') and the axis perpendicular to the crystallographic one (Table 7.5).

The data from Table 7.5 also show that the arrangement of the symmetry individual elements vary from measurement to measurement by two and more degrees with regard to successive removing and a new setting the sample on the acoustopolariscopy tables. In this case the operation of the device with another resonance frequency of the amplifier affects the outlines of the VC and VP acoustopolarigrams. However, the position of the VC minima in relation to the directions 1-1', 2-2' and 3-3', as a whole, remains stable. Judging by the medium values from the set of measurements $\varphi_1^1 - \varphi_6^1$ on acoustopolarigrams, one of the quartz planes of the elastic symmetry along the direction 1-1' forms an angle $\varphi_1^1 = 30^o$, the other - $\varphi_3^1 = 144^o$ and the third $\varphi_5^1 = 266^o$ with the direction 2-2'. Their mutual angles are $\theta_1 = \varphi_3^1 - \varphi_1^1 = 144^o$; $\theta_2 = \varphi_5^1 - \varphi_3^1 = 122^o$; $\theta_3 = \varphi_1^1 - \varphi_5^1 = 124^o$.

On side 2 the average inclination angle of a symmetry element is $\varphi_{1-3}^2 = 56^0$ and $\varphi_{2-4}^2 = 150^0$ with the direction 3-3'. Respectively, the discrepancy with the crystallographic axis [0001] orientation of these elements is $\psi_{1-3}^2 = 34^0$ and $\psi_{2-4}^2 = 60^0$. From the measurements on side 3 we obtain the angles $\varphi_{1-3}^3 = 5^0$ and $\varphi_{2-4}^3 = 96^0$. The discrepancy with the axis [001] orientation is, accordingly, $\psi_{1-3}^3 = 85^0$ and $\psi_{2-4}^3 = 6^0$. In Fig.7.5a the elastic symmetry elements are removed on the sample sides. The Figure shows the spatial discrepancy between the axis [001] orientation and elastic symmetry elements.

At the next stage we measured phase velocities V_p and V_s along the directions 1-1', 2-2', 3-3' according to the diagram in Fig.7.5a. For this purpose additional parallel to each other and perpendicular to the directions [301] and [103'] sides were formed as shown in Fig.7.5b. The measured V_p and V_s are given in Table 7.5. Using these data, in the plane of side 2 V_p, V_s, and $V_{s\perp}$ indicatrixes (Fig.7.7) were built with the polarization vector parallel and perpendicular to plane 2 accordingly.

According to Table 7.5 and Fig. 7.5b the direction [301], in which the value $V_{pmax} = 7.07$ *km/s* has been measured, makes an angle of 60^o with the axis [0001]. It is well known that the elasticity modulus (constant) [Bezukhov, 1968]

$$C_\varphi = \rho f(V^2_{p\varphi}), \tag{7.1}$$

where ρ is density, $V^2_{p\varphi}$ is phase velocity.

Thus, the modulus (constant) of longitudinal elasticity in the direction [301] takes the maximum value. The direction [301] does not coincide with the crystallographic axis [0001] orientation. That is the reason for an angular divergence between the palaeostress orientation and the axis [0001] in the quartz grains of a metamorphosed rock [Kozhevnikov, 1982; Gorbatsevich & Basalayev, 1993].

We should note that the direction 3-3' in which the minimum value $V_{pmin} = 5.78$ *km/s* was detected is not perpendicular to the direction [301]. The maximum value $V_{s\perp} = 4.89$ *km/s* is in the direction [103'] and the minimum value $V_{s\perp} = 3.26$ *km/s* is in the direction [301]. The values V_{so} contrast in different directions is not great, it is in the range of $V_{so} = V_{21} = 4.33$ *km/s* (direction 1-1') to $V_{so} = V_{103} = 3.23$ *km/s*.

Table 7.5.

Determined arrangement of symmetry elements in the sample of synthetic quartz.

Measurement №	Side 1, angle						Side 2, angle				Side 3, angle			
	φ_1^1	φ_2^1	φ_3^1	φ_4^1	φ_5^1	φ_6^1	φ_1^2	φ_2^2	φ_3^2	φ_4^2	φ_1^3	φ_2^3	φ_3^3	φ_4^3
1	39	79	149	209	269	319	54	144	244	324	3	103	183	283
2	43	83	153	203	273	323	58	148	238	318	5	105	195	265
3	17	87	137	207	262	327	50	150	230	330	5	90	190	275
4	21	81	136	201	261	331	60	160	235	330	7	87	177	263
Average	30	82	144	205	266	325	56	150	237	326	5	96	186	271
K_{vr}, %	7.1	1.6	4.7	2.0	3.2	2.9	2.5	4.0	3.2	3.2	1.0	5.0	4.4	5.2
V_s,	4.33	4.30	4.33	4.31	4.33	4.30	4.89	3.26	4.81	3.25	3.64	4.00	3.64	4.09
Note: V_p: V_{11} = 6.32, V_{301} = 7.07, V_{22} = 5.77, V_{103} = 6.26, V_{33} = 5.78 *km/s* V_s: V_{12} = 4.32, V_{13} = 4.30, V_{21} = 4.33, V_{23} = 3.64, V_{31} = 4.00, V_{32} = 3.64 *km/s*														

The obtained indicatrix (Fig. 7.7) on the whole, is similar to the sections of the phase V_p surface by the plane (Table 7.5). Like data have been published before [Silayeva & Delitsyn, 1970; Farnell, 1961].

Thus, the acoustopolariscopy of synthetic quartz in the direction of the triple crystallographic axis fixes the projections of the three symmetry planes (VC diagram) that are turned relative to each other by an angle of 60°. The arrangement of these planes can be determined with a comparatively high precision, as follows from Fig. 7.6a.

The data presented in Fig. 7.6 and Table 7.5 show that the acoustopolariscopy method allows determining the spatial orientation of elastic symmetry elements in a mineral without measuring V_p and V_s. The obtained V_{ij} values, as a whole, agree with the recounted data from the reference books [Belikov et al., 1970; Aleksandrov and Prodaivoda, 2000]. But the constant values of quartz elasticity in the reference books have been measured along the crystallographic axes and do not reflect the greatest and least elasticity values for this mineral. The quartz sample (Fig. 7.5), judging by the D values, exhibits a comparatively low degree of LAAA. The LAAA degree depends on the sounding vibration frequency. As indicated above, the nepheline index D is also frequency dependent.

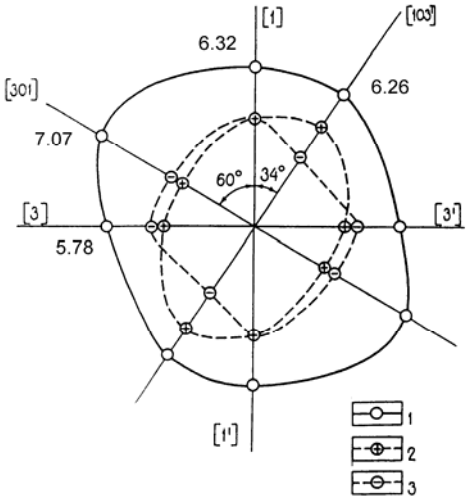

Fig. 7.7. Indicatrix of V_s in the quartz plane 2-2': 1 - V_p, 2 - $V_{s\perp}$ with the polarization vector along the normal to the plane 2-2'; 3 - V_{so} with the polarization vector in the plane 2-2'.

7.3. Minerals of lower syngonies

The lower syngony category comprises media of orthorhombic, monoclinic and triclinic symmetry systems. Figure 7.8 gives acoustopolarigrams for aragonite (rhomb.), staurolite (rhomb.), diopside (mon.) and amphibole (mon.). The aragonite crystal prepared for tests (sample X2-7, f_0 = 0.78 MHz) has a hair-like structure and perfect cleavage. The acoustopolarigrams point, as a rule, to the LAAA presence and heterogeneous structure of the samples at our disposal. In the sample X2-7 a great manifestation of the LAAA effect was detected on sides 2 and 3, Fig. 7.8a. The reverse acoustopolarigrams of the same sample (Fig. 7.9) enable one to determine the symmetry elements arrangement on sides 2 and 3 rather precisely. The mutual angles between those elements, according to a number of determinations, are in the range of 82-98° (Table 7.6). Unlike the sample X2-7, the LAAA degree in the sample X2-11 is much lower (Table 7.7). The data from Table 7.7 indicate that aragonite exhibits both linear and plane types of LAAA.

The staurolite (sample St-1-1), whose acoustopolarigrams were obtained at f_0 = 1.26 MHz (Fig. 7.8b) has a rather homogeneous structure. The orientation of symmetry elements is clearly seen in its all three reverse acoustopolarigrams (Fig. 7.9b). The mutual angles between the elements on side 1 are 85° and 95°, on other sides they do not virtually differ from a right angle (Table 7.6).

The sample St-1-1 exhibits a relatively low degree of LAAA of a plane type (Table 7.7). The plane along which the least absorption is observed passes through directions 2 and 3. As is well known, staurolite is characterized by a total absence of cleavage (Tröger, 1959) and this is the reason for a low degree of LAAA manifestation in it.

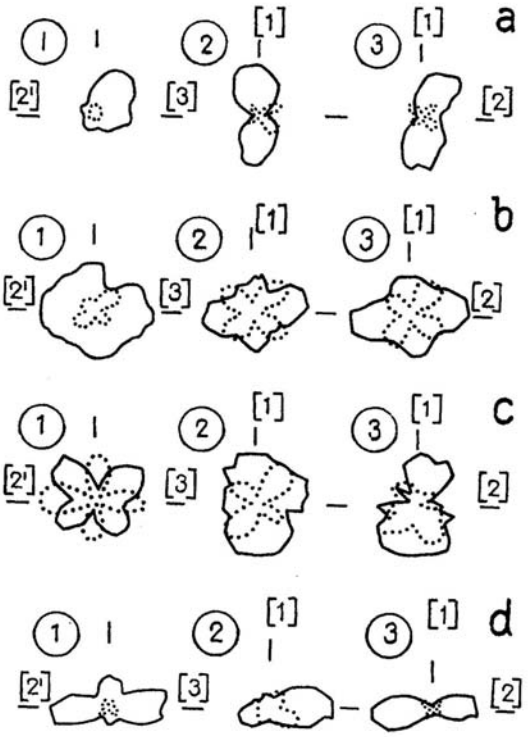

Fig. 7.8. Acoustopolarigrams of aragonite (a), staurolite (b), diopside (c) and amphibole (d).

The acoustopolariscopy of a diopside crystal (sample D-009, f_0 = 2.67 MHz) shows a much more intricate type of elastic anisotropy (Fig. 7.8c). If the first two directions (along the normal to sides 1 and 2) point to the presence of two symmetry elements forming virtually a right angle, the third side in the VC diagram shows three projections of the elements that form mutual angles of 83, 56 and 41° (Table 7.6). The symmetry elements orientation on the third side was determined at f_0 = 2.67 MHz. At f_0 = 1.26 MHz we failed to do that. The mutual angles between the symmetry elements on the first side may not differ from a right angle, but on the second side their values are 64-80° and 100-116°.

Diopside showed dependence of the LAAA effect on the vibration frequency (Table 7.7). At f_0 = 1.26 MHz the LAAA index measured on sides 2 and 3 is more than twice higher than that at f_0 =2.67 MHz. As the frequency increases the plane LAAA of the P2-3 type goes over into linear L1.

The acoustopolariscopy results (sample A-030) for amphibole (arfvedsonite) are given in Fig. 7.8d and Tables 7.6 and 7.7. The acoustopolarigrams were obtained at f_0 = 0.78, 1.26 and 2.67 MHz. The tests at all those frequencies showed a rather high manifestation of the LAAA effect. The index D at f_0 = 1.26, 2.67 MHz at least at one side reaches 0.8-0.9. As a rule, both linear and plane LAAA manifest themselves at the same time. Thus, it may be concluded that the elements of the mineral chain structure are not isometric in the cross section.

The mutual angles of the symmetry elements in an amphibole crystal vary from 85 to 95°. No dependence of these angles on the vibration frequency has been detected.

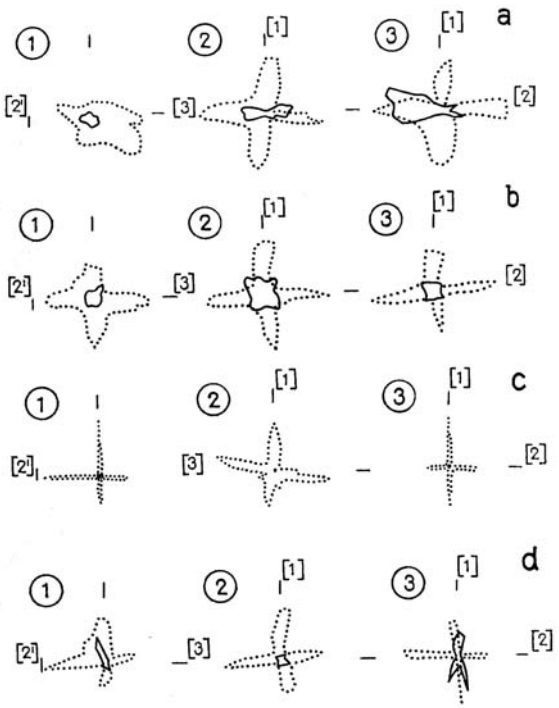

Fig. 7.9. Reverse acoustopolarigrams of aragonite (a), staurolite (b), nephrite (c) and microcline (d).

The nephrite sample Nefr-033 prepared for the measurements was rather homogeneous, it had no foreign inclusions. Respectively, the acoustopolarigrams shape of this sample is rather close to the theoretically predicted ones, Fig. 7.10a (see point 1.4). The remarkable homogeneity of the sample Nefr-033 is confirmed by the reverse acoustopolarigrams shape (Fig. 7.9c). The mutual angles between the symmetry elements on side 2 greatly differ from a right one and are 79-101° (Table 7.6). This nephrite sample is characterized by the LAAA low degree (Table 7.7) and combination of the linear and plane types of its manifestation (f_0 = 0.78 MHz). The sample Ne-3 has almost the same characteristics as Nefr-033. Despite a high homogeneity of the samples Ne-3 and Nefr-033 they are most likely monomineral and not monocrystalline formations.

Acoustopolarization measurements of orthoclase were performed on two samples, at some frequencies being repeated 2 and 3 times (Tables 7.6 and 7.7). The mutual angles between the symmetry elements in the sample O-15b at f_0 = 2.67 MHz on all the three sides do not virtually differ from a right one. But at f_0 = 0.78 MHz on side 1 of the same sample 78-102° angles have been detected. In the sample O-19b the same angles have been registered on side 1 (f_0 = 0.78 MHz) and side 3 (f_0 = 0.78 MHz).

Orthoclase as well as amphibole exhibits the LAAA effect of a high grade, especially at f_0 = 1.26 and 2.67 MHz (Fig. 7.10b, Table 7.7). A comparatively identical degree of this effect is registered on both samples - O-015b and O-019b.

As a rule on these samples a combination of the LAAA plane and linear types is observed. On the sample O-019b as the frequency increases a transition of directions (in which the LAAA linear and plane types are registered) is observed. For instance, at f_0 = 0.78 MHz the mineral linear structures that are oriented along the normal to the first side have been revealed (Table 7.7). At f_0 = 1.26 MHz the mineral linear structures oriented to the first side preserve their influence, but in this case the plane

passing through directions 1-3 manifests itself. At f_0 = 2.67 MHz the linear structures in direction 2 and the plane passing through directions 2 and 3 reveal themselves.

Table 7.6.

Mutual angles between the projections of elastic symmetry elements in rock forming minerals of lower syngonies.

Experiment №	Mineral	Sample	Syngony	Frequency, MHz	Side 1		Side 2		Side 3	
					α_1	α_2	α_1	α_2	α_1	α_2
1-3	Aragonite	X2-7	Rhombic	0.78	~91	~89	92	88	83	97
1,2		X2-11		0.78	86	94	91	89	97	83
1	Staurolite	St-1-1		1.26	95	85	91	89	90	90
1	Amphibole	A-030	Mon.	0.78	-	-	96	84	93	87
1, 2		A-030	.	1.26	95	85	~84	~96	~84	~96
1-3		A-030		2.67	91	89	~96	~84	93	87
1	Diopside	D-009		1.26	96	84	116	~64	-	-
1, 2		D-009		2.67	90	90	100	80	83, 56, 41	-
1	Nephrite	Ne-3	.	1.26	99	81	83	97	-	-
1		Nefr-033		0.78	93	87	95	85	92	88
1		Nefr-033		2.67	91	89	101	79	91	89
1	Orthoclase	O-015b		0.78	78	102	86	94	-	-
1-3		O-015b		2.67	90	90	91	89	89	91
1		O-019b		0.78	90	90	95	85	101	79
1, 2		O-019b	.	1.26	79	101	-	-	89	91
1	Spodumen	SP-1-1	.		90	90	91	89	-	-
1-3	Microcline	XIX-1-b	Tricl.	0.78	-	-	91	89	86	94
1		M-1		0.78	87	93	87	93	86	94
1		M-1		1.26	-	-	86	94	97	83
1		M-1		2.67	92	88	-	-	95	85
1		M-2		0.78	97	83	88	92	86	94
1		M-2		1.26	~83	~97	~84	~96	97	83
1, 2		M-2		2.67	89	91	90	90	87	93

Notes: α_1, α_2 are represented in degrees.

The mineral structural elements and cleavages are likely to respond to the frequency increase. For instance, as the frequency whose wave length will be comparable with a structural element or cleavage approaches the vibration, absorption will be maximum. T.M. Proctor [1971] observed this phenomenon on artificial media.

Microcline samples XIX-1-b, M-1 and M-2 were made so that the crystallographic axis [001] coincided with the normal direction 1-1' to a cube side and the axis [010] - with the direction 2-2'. The acoustopolarigrams obtained at the crossed polarization vectors show that the orientation of the elastic symmetry element projections is virtually perpendicular to the sample sides (Fig. 7.10c, 7.9d, Table 7.6). The projections of the elastic symmetry elements are observed in all the three mutually perpendicular directions.

Table 7.7.

Indexes of linear acoustic anisotropic absorption in the samples of some rock forming minerals of the syngony lower category.

Experiment №	Mineral	Sample	Syngony	Frequency, MHz	D_1	D_2	D_3	Notes
1, 2	Aragonite	X2-7	Rhom-bic	0.78	0.22	0.72	0.66	L1, P1-3
1, 2		X2-11		0.78	0.10	0.14	0.16	L3, P2-3
1	Staurolite	St-1-1		1.26	0.022	0.13	0.18	P2-3
1	Amphibole	A-030	Mon.	0.78	0.55	0.14	0.29	L1, P1-2
1, 2		A-030		1.26	0.34	0.64	0.89	L1, P1-3
1-3		A-030	.	2.67	0.43	0.57	0.88	L2, P2-3
1, 2	Diopside	D-009		1.26	0.013	0.56	0.66	P2-3
1, 2		D-009		2.67	0.012	0.20	0.18	L1
1	Nephrite	Ne-3		1.26	0.062	0.034	0.17	
1		Nefr-033		0.78	0.21	0.12	0.22	L1, P1-3
1, 2		Nefr-033		2.67	0.013	0.083	0.05	
1	Orthoclase	O-015b		0.78	0.44	0.24	0.14	L2, P1-3
1, 2		O-015b		2.67	0.64	0.67	0.45	L3, P1-3
1		O-019b		0.78	0.054	0.22	0.29	L1
1, 2		O-019b		1.26	0.33	0.41	0.50	L1, P1-3,
1-3		O-019b		2.67	0.53	0.61	0.74	L2, P2-3
1	Spodumen	SP-1-1		1.26	0.25	0.11	0.024	P1-3
1	Microcline	XIX-1-b	Tricl.	0.78	0.84	0.87	0.64	P2-3, L3
1		M-1		0.78	0.27	0.26	0.24	P2-3, L2
1		M-1		1.26	0.33	0.065	0.72	L2
1		M-1		2.67	0.42	0.022	0.40	P1-2
1		M-2		0.78	0.045	0.49	0.47	P2-3
1		M-2		1.26	0.78	0.11	0.87	L2
1		M-2		2.67	0.67	0.022	0.44	P1-3

This suggests that microcline has an elastic symmetry of the type not higher than orthorhombic. At the same time the mutual angles between the elastic symmetry elements just slightly differ from a right one. An overview of the data from Table 7.6 shows that at all frequencies and on every sample those differences do not exceed 5^o.

The results presented in Table 7.7 testify to a considerable range of the LAAA manifestation in microcline. For instance, in the samples M-1 and M-2, (Fig. 7.10c, 7.10d), whose acoustopolarigrams were obtained at $f_0 = 1.26$ MHz the LAAA effect is most conspicuous. For the first, second and third pairs of the sample M-2 sides they are $D_1 = 0.78$, $D_2 = 0.11$ and $D_3 = 0.87$ respectively. On sides 1 and 3 of the samples at parallel polarization vectors we have detected acoustopolarigrams which diameter along direction 2 is considerable and along directions 1 and 3 - small. Judging from the direction of the largest diameters of the VP acoustopolarigrams obtained on sides 1-1' and 3-3', a linear type of this effect L2 has been registered in the samples M-1 and M-2.

The most likely explanation for the observed LAAA phenomenon as well as its linear type is the following. In the crystallographic axis direction [010] in microcline crystals a perfect cleavage is observed, but its plane is parallel to the plane (001). In the direction 2-2' the planes of these two cleavage systems and the angle close to a right one intersect. For this reason we observe a great manifestation of the LAAA

effect in the direction 1-1' from one cleavage and in the direction 3-3' - from the other. In the direction 2-2' the signal attenuates to the same extent from both cleavages. That is why the degree of LAAA manifestation detected on side 2 is low.

However, at other vibration frequencies, as with orthoclase samples, changing of the LAAA manifestation type and the directions related to this effect occurs (Table 7.7). For instance, at f_0 = 0.78 MHz in the sample XIX-1-b both the plane P2-3 and linear L3 types are registered. At f_0 = 2.67 MHz in the microcline samples M-1 and M-2 the plane type of LAAA is observed - P1-2 and P1-3 respectively. Thus, in microcline, as well as in orthoclase, at one frequency the greatest absorption occurs on the structural elements of one cleavage, at the other frequency - on the elements of another cleavage. A comparatively identical absorption on both elements takes place at f_0 = 1.26 MHz.

For the first time the LAAA effect was found in the rocks from the lower section of the Kola Superdeep Borehole [Gorbatsevich, 1982]. This effect has been detected in 90% of the rock samples extracted from the 4.5-12.06 depth range [Gorbatsevich & Il'chenko, 1997]. A high degree of LAAA in microcline allows one to conclude that the presence of this effect in crystalline rocks may be caused by this mineral contained in the rocks as well as by some minerals of the feldspar series (oligoclase, orthoclase et al.).

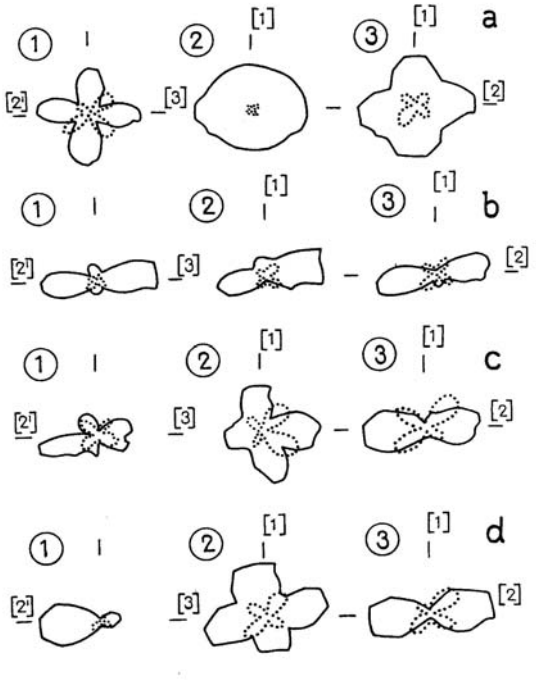

Fig. 7.10. Acoustopolarigrams of nephrite (a), orthoclase (b), microcline, sample M-1 (c) and microcline, sample M-2 (d).

In scientific literature we have not met any information on the LAAA and DSW manifestation in minerals. Most likely, the manifestation of LAAA and pleochroism in minerals are not interrelated. For instance, microcline does not virtually exhibit pleochroism [Tröger, 1959]. The results presented in this work show possibilities of the acoustopolariscopy method in relation to investigation of mineral physical properties. On the other hand, these data indicate that on the whole a lot of work is to be done for all mineral types.

The main results of investigation for mineral samples of higher and medium syngonies may be stated as follows:

1. The acoustopolariscopy method permits determining an arrangement and mutual angles between the elastic symmetry elements in a mineral with high precision. Such determinations are possible for media of cubic syngony as well.
2. As a rule, the mutual angles between the elastic symmetry elements in the samples of measured minerals are close to a right one. The exception is quartz. In one of the sections of this mineral three elements of elastic symmetry forming mutual angles other than a right one have been observed.
3. Classes of mineral elastic symmetry may differ from the symmetry classes defined by their optical properties. It is indicated by, for instance, determination

of elasticity parameters for quartz, which support the difference in element orientation for crystallographic and elastic symmetry.

4. In minerals of medium and lower syngonies the LAAA effect is conspicuous. The LAAA effect is rather weak in minerals of higher syngony which, most probably, is related to the crystal structure defects. In silicate minerals of lower syngonies this effect is observed virtually on all samples. In this case LAAA may be observed along with pleochroism (tourmaline) or independent of it (orthoclase, microcline). In such minerals as amphibole, orthoclase and microcline its manifestation is related to cleavage in natural samples.
5. On some minerals a clear dependence of LAAA and its type on the vibration frequency is observed. For instance, in microcline as well as in orthoclase at one frequency the greatest absorption occurs on structural elements of one cleavage, at another frequency - on the elements of another cleavage. A comparatively the same absorption on both elements takes place at $f_0 = 1.26$ MHz. Accordingly, as the frequency changes, the LAAA type changes, too. For instance, when the absorption on the structural elements of one system prevails, the plane type will be observed. When two orthogonal systems of cleavage act, the LAAA linear type will be detected.
6. In one of the sections of the tourmaline sample the acoustopolarigram with the clear manifestation of the DSW effect has been registered.

8. ACOUSTOPOLARISCOPY OF MONO- AND POLYMINERAL ROCKS

8.1. Manifestation types of the linear acoustic anisotropic absorption effect in crystalline rocks

In a sequence of acoustopolariscopy of mono- and polymineral rocks [Gorbatsevich, 1995] quite a lot of acoustopolarigrams have been obtained whose shapes cannot be explained only by the elastic anisotropy manifestation, Fig. 1.4. Some acoustopolarigrams' dissimilarity from theoretical ones can be explained by rock heterogeneity. Peculiar shapes of acoustopolarigrams are observed when the linear acoustic anisotropic absorption (LAAA) and depolarisation of shear waves (DSW) effects are displayed. Our observations confirm that the LAAA effect may be presented by two main models - plane and linear, Fig. 2.5. The plane model (I) is exhibited in crystalline rocks containing oriented cracks or plane elements (minerals), such as mica, talc et al. Other than the first the linear model (II) manifests itself in rocks containing linear elongated in one direction, isometric in the cross section mineral grains. As follows from the diagrams, Fig. 2.5, the difference of the model I medium from that of model II can be established only on the basis of the spatial measurements system.

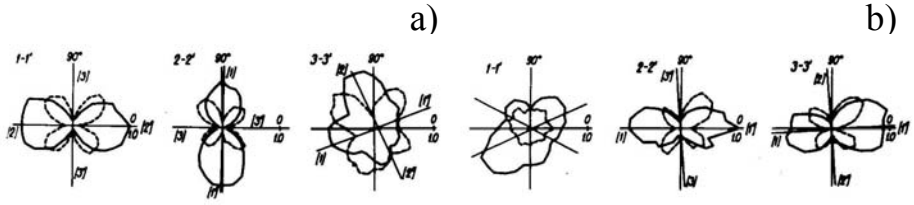

Fig. 8.1. Acoustopolarigrams: a - talc-phlogopite-tremolite schist (sample 26715); b - clinopyroxene amphibolite (sample 24788). Solid line - parallel vectors, dotted line - crossed vectors.

The LAAA display by the model I type was detected on cubic sample 26715 of talc-phlogopite-tremolite schist. Clearly expressed by phlogopite and talc schistosity enabled exact orientation of the sample sides during its preparation. The acoustopolarigrams for the three pairs of sides, accordingly in the directions 1-1', 2-2', 3-3', are given in Fig. 8.1a. In the directions 1-1' (D = 0.83) and 2-2' (D = 0.86) the media exhibits a high degree of LAAA. In the direction 3-3' (D = 0.13) the VP acoustopolarigram is more isometric. The direction of the greatest transmission on side I is oriented to side 2 and on side 2 - to side I.

The LAAA manifestation by the type of model II was observed on cubic sample 24788 of clinopyroxene amphibolite. The structure of clinopyroxene amphibolite is characterized by clearly visible greatly elongated grains of hornblende. The sample sides are formed in such a way that the direction 1-1' coincides with the axes of elongated grains. The VP acoustopolarigram obtained in the direction 1-1', Fig. 8.1b, showed, accordingly, a low grade of LAAA (D = 0.17). In the directions 2-2' (D = 0.79) and 3-3'(D = 0.73) the LAAA manifestation is much greater. Both directions of the greatest transmission are oriented to side I. Sample 24788 also pertains to highly anisotropic media.

In samples 26715 and 24788 the LAAA manifestation by model I and II types is most conspicuous. However, there are some media in which the LAAA manifestation is caused by elements of both linear and plane types [Gorbatsevich, 1995].

As follows from the observations, the LAAA effect arises in crystalline rocks

when linearly polarized shear waves interact with oriented linear, plane or some other heterogeneities. But these may be oriented holes or cracks both filled with, for instance, liquid and gas (Fig. 2.3). This effect is exhibited in minerals, rocks, wood and plastics [Gorbatsevich, 1999]. To our mind, it may be displayed in metals, concrete, ceramics, construction, building and composite materials.

8.2. Cross effect of elastic anisotropy and linear acoustic anisotropic absorption with an angular disagreement between their symmetry elements

In rocks elastic anisotropy and the LAAA effect most often manifest themselves together [Gorbatsevich & Il'chenko, 1997]. By the results of our observations the spatial arrangement of the symmetry elements of elastic anisotropy and linear acoustic anisotropic absorption in crystalline rocks do not always coincide. Consider the acoustopolarigrams of some rocks, Fig. 8.2.

Sample 30020 is biotite-plagioclase gneiss. It has been produced from the Kola superdeep borehole (SD-3) core extracted from a depth of 7959.1 m. According to acoustopolariscopy of one of its cross-sections, Fig. 8.2a. sample 30020 is an anisotropic medium with strong LAAA. The shape of this cross-section acoustopolarigram may be compared with the acoustopolarigram of the wooden plate (Fig. 2.7, 3).

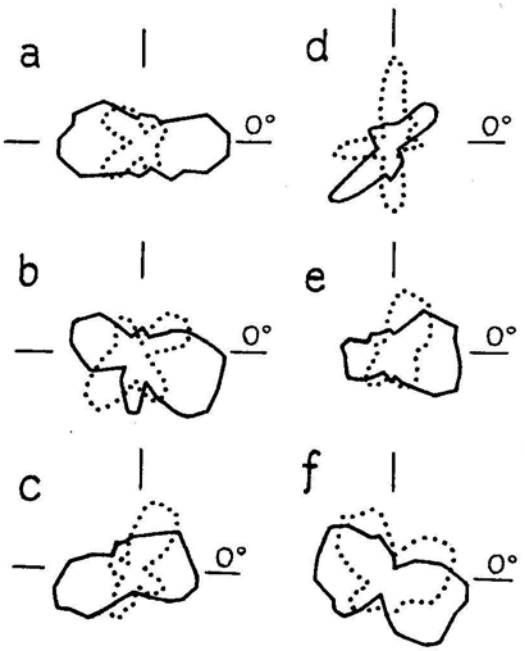

Fig. 8.2. Acoustopolarigrams of one of the cross-sections of crystalline rock samples.
a - biotite -plagioclase gneiss (30020); b - epidote-biotite-amphibole-plagioclase schist (27227Ш); c - cummingtonite amphibolite (27026Ш); d - sandstone (1753); e - fine-psephitic-psammitic andesite-basaltic tuff (1161); f - epidote-biotite-plagioclase gneiss (28184). Vectors parallel - solid line, vectors crossed - dotted line.

Sample 27227III of epidote-biotite-amphibole-plagioclase crystalloschist has been produced from the SD-3 core recovered from a depth of 8017.0 m. The shape of the VC acoustopolarigram from one of the sample cross-sections, Fig. 8.2.b, shows signs of the angular divergence between the orientation of elements of elastic symmetry and LAAA - the VC diagram petals are not equal in size and area. By the VC and VP diagrams shapes one may judge that this angular divergence is close to the value obtained by calculation (Fig. 2.6) and on the model (Fig. 2.7) with the angle of directions disagreement between the plates $\tau = 15^{o}$.

Sample 27026III of cummingtonite amphibolite has been cut from the SD-3 core. The acoustopolarigram (Fig. 8.2c) of one of its cross-sections shows a strong display of the LAAA effect. As in the previous case, the VC diagram petals differ in size and area. The shape of the VC diagram is close to that of the diagram obtained on the

model with the angle τ higher than 15°, but lower than 30° (Fig. 2.7c). The angular disagreement between the symmetry elements of elastic anisotropy and LAAA of the sample is reflected in great asymmetry of the petal sizes in the VC acoustopolarigram.

The acoustopolarigram (Fig. 8.2d) of the sandstone (sample 1753) from the borehole 30p1 at the Yarigskoye deposit (Komineft') is characterized by a very large amplitude obtained at crossed polarization vectors. It exceeds the amplitude detected at the VP position. A similar correlation was obtained for the model acoustopolarigram (Fig. 2.7d) at $\tau = 45°$.

Sample 1161 has been produced from the Ural Superdeep Borehole (SD-4) core. Its VC diagram is very elongated (Fig. 8.2e). The lateral petals located along the normal to the figure's largest diameter are very small. The shapes of the VC and VP diagrams are very close to the calculated ones (Fig. 2.6) and to the shapes obtained on the model (Fig. 2.7) at $\tau = 30°$.

Sample 28184III has been produced from the SD-3 core. Its acoustopolarigrams are given in Fig. 8.2f. Judging by their shapes the disagreement between the symmetry elements of elasticity and LAAA in this sample reaches 75° or 15°, Fig. 2.7.

Thus, the acoustopolarigrams, Fig. 8.2, show that in natural media a spatial orientation disagreement between the symmetry elements of elastic anisotropy and LAAA is observed. An indication of this disagreement is asymmetry in the petal sizes of the acoustopolarigrams obtained at crossed polarization vectors. Another sign is an amplitude enlargement of these petals, sometimes to the sizes exceeding the petal size of the acoustopolarigrams obtained at the VP position. As the diagrams, Fig. 8.2, analysis shows, by the shapes of the acoustopolarigrams obtained for natural media one can judge about the disagreement angles between the symmetry elements of elastic anisotropy and LAAA. The presence of such disagreement up to an angle τ = 30-75° allows one to think that physical grounds of elastic anisotropy and the LAAA effect are radically different. The LAAA effect is not only subordinate to the elastic anisotropy display in solid bodies.

This conclusion is also confirmed by the results from the SD-3 samples [Gorbatsevich et al., 1992]. During the tests on every side of the cubic sample the value of D and the factor of acoustic birefringence B_S (6.19) were determined. On every side the factor B_S and index D express the degree of elastic anisotropy and linear anisotropic absorption of the medium, accordingly.

Figure 8.3 presents the determined index D and the factor of acoustic birefringence for some 50 samples produced from the SD-3 core The shape of the point scattering in Fig. 8.3 indicates that there is virtually no correlation between the values of B_S and D.

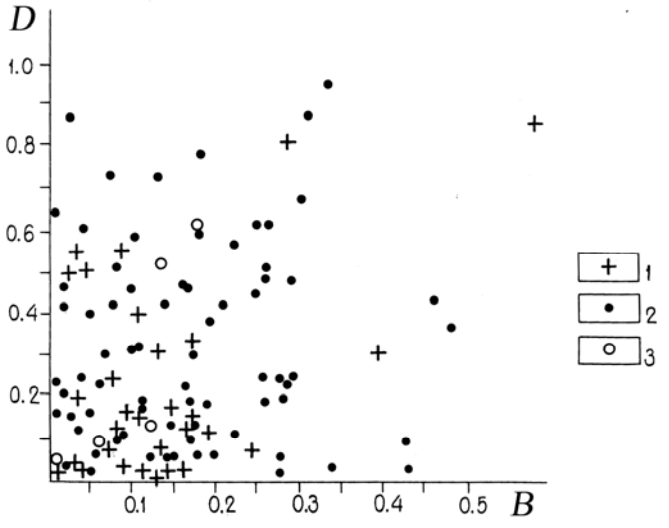

Fig. 8.3. Distribution of unit values D - LAAA index and birefringence factor B for rocks from the SD-3 section. 1 - schist, 2 - amphibolite, 3 - biotite gneiss (granite).

It should be believed that the cross effect of the elements of elastic

symmetry and linear anisotropic absorption will be observed as shear waves propagate not only in rocks but in layered plastics, composite materials, metal alloys and other media with a complicated structure.

The signs of disagreement between the symmetry elements of elastic anisotropy and LAAA can provide additional information on the structure, composition and peculiarities of a medium. As we showed above, such signs are the presence of asymmetry in the petal sizes in the acoustopolarigrams obtained at the crossed polarization vectors and an anomalous enlargement of their amplitude. The disagreement signs for the orientation of the symmetry elements of elastic anisotropy and LAAA detected in rocks as well as the absence of correlation between the anisotropy parameter B_S and the index D allow one to conclude that these effects can display themselves independently of one another.

The spatial function of LAAA, as well as the optical analogue of dichroism [Goncharenko et al., 1979], is likely to be described by the tensor of no less than the second order. The calculation of the parameters defining an interaction of the two tensors - elasticity and absorption - with heterogeneity and symmetry elements that do not coincide, is a rather intricate task. However it can be solved experimentally.

8.3. Experimental results of detecting the DSW phenomenon in rocks

During determination of elastic-anisotropic properties of the rock samples extracted from the Kola (SD-3) and Ural (SD-4) superdeep boreholes and from the wells at Ukhta oil fields and some others by the acoustopolariscopy method a rather frequent display of the depolarization of shear waves (DSW) effect was observed. Fig. 8.4 gives acoustopolarigrams for six samples of sedimentary and crystalline rocks in which this effect was detected.

The measurements were performed on cubic samples in three mutually perpendicular directions. Accordingly, acoustopolarigrams 1, 2 and 3 (Fig. 5.5) were obtained for the first, second and third sides of one sample. The samples properties, such as density, sampling depth H, quasi-matrix of velocity V_{ij} (see point 5.5), index of LAAA, are presented in Table 8.1.

Sedimentary rock samples 22 and 1724 (Fig. 8.4a, 8.4b) have been taken from a well of "PechorNIPINeft'" oil fields. In the limestone (sample 22) the DSW effect was displayed on side 2. If the acoustopolarigram of side 2 is compared with the diagrams in Fig. 3.2 and 3.3 it may be concluded that the elastic symmetry elements of mineral grains that are in the side plane are randomly oriented relative to each other within 15^o or 75^o. On the other sides of this sample the LAAA display is very strong. In the sandstone (sample 1724) the DSW effect was displayed on side 3, the random orientation of the grain symmetry elements here being about $30\text{-}40^o$.

Samples 182 and 1191 taken from the Ural Superdeep Borehole (Fig. 8.4c, 8.4d) are crystalline diorite (sample 182) and tuff (sample 1191) of volcanic origin. The DSW effect is displayed on the acoustopolarigrams of sides 1 and 2 of sample 182. The angle of random orientation of the grain elastic symmetry elements may be assessed as close to 80^o (see Figs 3.2, 3.3). On sides 3 and 4 of sample 1191 a joint display of the DSW and LAAA effects is observed. The angles of random orientation of elastic symmetry elements in mineral grains may be within $30\text{-}50^o$.

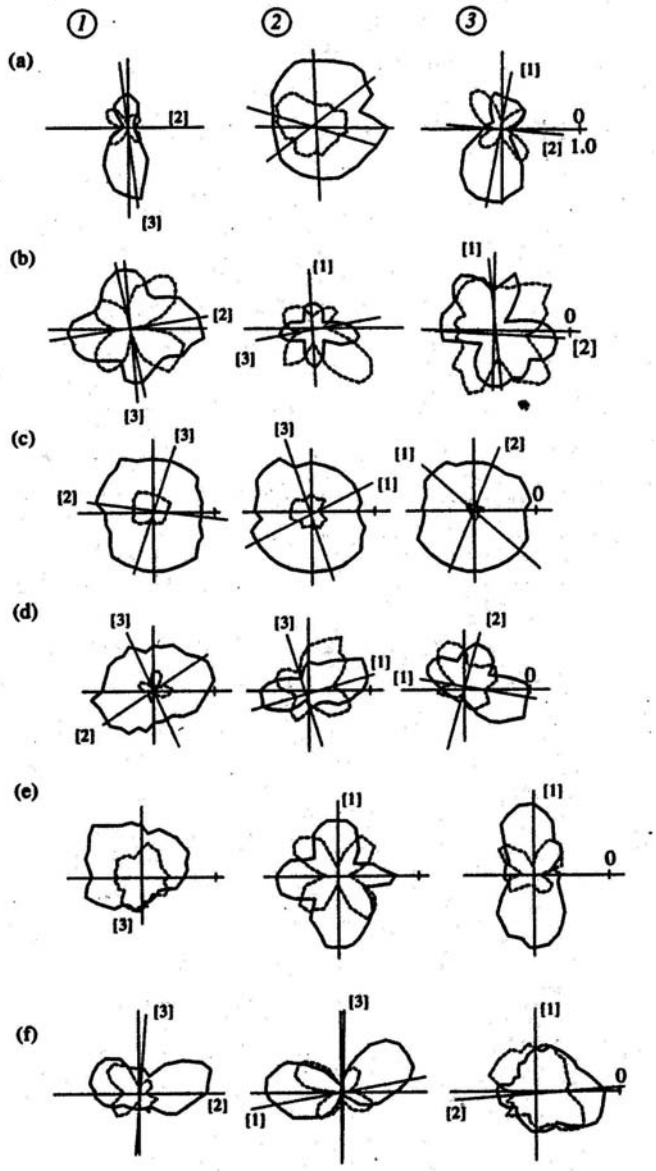

Fig. 8.4. Acoustopolarigrams for sample 22 of brown limestone (a), sample 1724 of sandstone (b), sample 182 of subalkaline quartz diorite (c), sample 1191 of tuff of andesite basalt (d), sample 30020of biotite plagioclase gneiss (e), sample 31587 of garnet-clinopyroxene-hornblende amphibolite (f). 1, 2, 3 are sample sides. VP - solid lines, VC - dotted lines

A comparatively frequent DSW manifestation is observed in metamorphosed Archean rocks along the Kola superdeep borehole section. As an example Fig. 8.4e and 8.4f present acoustopolarigrams of biotite-plagioclase gneiss (sample 30020) and garnet-clinopyroxene-hornblende amphibolite (sample 31587). Judging by the acoustopolarigrams, both samples have schistose structure. However, in the plane of side 1 (sample 30020) and side 3 (sample 31587) a fan pattern of elastic symmetry elements in grains up to mutual angles of 50-70^{o} is observed. On sides 1 and 2 a very strong LAAA manifestation has been detected.

Table 8.1.

Elastic-anisotropic properties of rock samples displaying the DSW effect.

No.	Sampling location	Rock	Sample	Density ρ, g/sm^3	Depth H, m	Velocity matrix V_{ij}, km/s	LAAA index, D
1	Usa deposit	Brown limestone	22	2.57	1234	3.32 2.18 2.20 2.22 3.64 2.26 2.15 2.09 3.52	0.82 0.03 0.61
2	Yarigskoye deposit	Sandstone	1724	2.68	35.1	1.89 1.39 1.38 1.36 2.14 1.42 1.41 1.39 2.03	0.07 0.09 -
3	Ural superdeep borehole SD-4	Subalkaline quartz diorite	182	2.79	806.6	6.01 3.46 3.47 3.50 6.11 3.48 3.48 3.52 6.10	0.07 0.06 0.03
4	- " -	Tuff of andesite basalt	1191	2.90	2963.6	5.40 3.42 2.94 3.31 5.20 2.92 3.05 2.60 4.22	0.20 0.40 0.28
5	Kola superdeep borehole SD-3	Biotite plagioclase gneiss	30020	2.59	8566.4	3.12 1.75 1.75 1.66 3.93 2.05 1.70 1.90 3.71	0.00 0.05 0.59
6	- " -	Garnet clinopyroxene hornblende amphibolite	31587	3.03	8867	4.82 2.77 2.35 2.81 4.08 2.18 - 2.00 2.69	0.47 0.45 0.09

The above assessment for the angles of random orientation of elastic symmetry elements in mineral grains is particularly rough, since it does not include the grain size, the relation between the wave length and wave frequency and other factors. Determination of angles α, for instance, by optical indicatrixes is very complicated due to the difference in mutual orientation of optical and elastic symmetry elements in crystals [Kazakov, 1987]. It is difficult to take this difference into account. It should be also noted that the detected depolarization effect arises precisely due to the random orientation of elastic symmetry elements in the plane perpendicular to the wave propagation. For instance, in Fig 8.4 this effect has been detected only in one direction for the three samples and in Fig. 8.4c and 8.4d - in two directions. If the effect display had been caused by scattering of the shear waves on small- and large-scale heterogeneities, the effect of depolarization would have been observed in all three directions. Earlier the effect of depolarization of volume elastic waves when scattering in a randomly heterogeneous medium has been described by S.I. Alexandrov [1997].

A theoretical analysis, experiments on the model and measurements of elastic anisotropic properties of some rock samples by the acoustopolariscopy method showed that as shear waves propagate through anisotropic media consisting of structural units with differently oriented elements of elastic symmetry, previously unexplored phenomena may be observed.

1. From the analysis of shear waves propagation, for instance, by the acoustopolariscopy method anisotropic heterogeneous media, consisting of

mutually orthogonal by elastic properties layers (grains), can be identified as isotropic.

2. If the elastic symmetry elements in layers or grains constituting an anisotropic medium are mutually randomly oriented in the range of 10-80°, the propagation of linear polarized shear waves in the directions close to the normal to the plane of random orientation is accompanied by their depolarization, i.e. increase in their ellipticity grade. This phenomenon called the effect of depolarization of shear waves (DSW) is most displayed when the angle of random orientation between the elastic symmetry elements in grains (layers) is close to 45°. In the acoustopolarigrams of multicomponent media samples the DSW phenomenon may be discovered in the cases when the A_{VC} amplitudes at crossed polarization vectors in their minima points are markedly higher than those detected at the same points in the acoustopolariscope without the sample. The DSW phenomenon allows one to assess the angle of random orientation of the elastic symmetry elements in grains (layers) in mono-and polymineral rocks.
3. The DSW phenomenon displayed as shear waves propagate through anisotropic media composed of structural units with randomly oriented elastic symmetry elements, unlike the similar effect arising in heterogeneous media, is detected only in one or two directions in a solid body.
4. To our mind, the DSW phenomenon under study can also occur when shear waves propagate through geological media during seismic investigations. An increase in the shear waves ellipticity on the seismic work routes in Western Siberia mentioned in [Rezyapov, 1992; Skavinskiy & Din Yun En, 1992] can be explained by the display of this phenomenon. Further investigation of the phenomena accompanying propagation of shear waves in multicomponent anisotropic media will facilitate the analysis of properties of crystalline rocks as well as metals, ceramics, plastic, concrete, composite material et al.

8.4. Correspondence principle for metamorphosed rocks

The application of the acoustopolariscopy method for investigation of elastic and non-elastic characteristics of minerals and rocks has greatly expanded our knowledge of their structure and properties. Acoustopolarization investigations of the rocks from the Voche-Lambina geodynamic region and the core extracted from various depths of the Kola (SD-3) and Ural (SD-4) superdeeps, Vorotilov and Tyrnyauz deep boreholes etc. showed that in the upper crust anisotropic rocks of orthorhombic and, to a lesser degree, of transverse-isotropic symmetry types prevail [Gorbatsevich, 1995; Rozaev & Gorbatsevich, 1996]. Following Aleksandrov and Prodaivoda [Aleksandrov & Prodaivoda, 2000], in Archean gneisses and amphibolites lower symmetry forms are observed as well. One of common effects reflecting structural features of rocks is the effect of linear acoustic anisotropic absorption (LAAA). This effect is registered by the acoustopolarization method in layered and linearly textured rocks and in rock forming minerals displaying perfect cleavage [Gorbatsevich et al., 1999].

The results of acoustopolarization observations, on the whole, allow one to conclude that elastic properties of crystalline rocks have both determined and statistical components. Their proportion should be determined for every specific rock taken at every specific location. In our opinion, in most cases the elastic symmetry type of metamorphosed crystalline rocks may be not lower than orthorhombic. This consideration is based on the fact that the factor forming the rock elastic anisotropy is

most often the stress tensor, especially if those stresses, let us call them palaeostresses, act during a long (geological) time.

According to the elasticity theory, there is a direct relation between the palaeostress tensor and the type of elastic anisotropy of a rock. This has been corroborated by the observations as well [Robin, 1979; Kozhevnikov, 1982]. For instance, under the action of a uniaxial palaeostress field, with $T_1 > T_2 = T_3$, it may be concluded with certainty that anisotropy of transverse-isotropic type will arise in the rock. Given lithostatic and horizontal tectonic fields, with $T_1 > T_2 > T_3$, the orthorhombic type of elastic symmetry appears in the rock. Heterogeneities, the presence of primary anisotropy will distort the state of the rock total anisotropy.

During metamorphic transformations when anisotropy arises the principle of potential power minimum is realised in the rock. According to this principle in the direction of the greatest component of the palaeostress field T_{max} the least velocity of compression waves V_{min}, is observed, while in the direction of the least component T_{min} the greatest velocity V_{max} is detected [Belikov et al., 1970; Kozhevnikov, 1982; Gorbatsevich, 1995]. For the rock element located in the massif the value of T_{min} is unknown as a rule. Near the earth surface it may be close to zero. At the same time the values of elastic wave velocities in a sample always have the values other than zero. With this, on the whole, the ratios between the palaeostresses and velocities in a metamorphosed rock can be presented in the following way:

$$T_{max} = f_1(V_{max} - V_{min}) + T_{min} \ , \tag{8.1}$$

$$T_{av} = f_2(V_{av} - V_{min}) + T_{min} . \tag{8.2}$$

The value of the third component T_{min} can be determined by the ratio

$$T_{min} = f_3(V_{min} - V_0) , \tag{8.3}$$

where V_{av} is the average velocity, V_0 is the velocity value in the isotropic sample measured to the changes caused by a metamorphic process.

There is a problem of determining the value of V_0 in an altered metamorphosed rock. The value of V_{av} from the expression (6.13) can be taken for the value of V_0. But, on the whole, the velocities of wave propagation in metamorphosed rocks, as a rule, are lower than, for instance, those in volcanic rocks. In Eq. (8.1)-(8.3) f_1, f_2, f_3 reflect some functional dependencies of V_{ii} vs components of the palaeostress field. The proportionality reflected in Eq. (8.1)-(8.3) will extend to the agreement between the rank of the velocity matrix and the rank of the palaeostress field tensor.

Since the stress field in homogeneous bodies is described by the tensor of not higher than the second rank, the quasi-matrix (5.5) can quite adequately reflect the relationship among the velocity values in an anisotropic metamorphosed rock. Thus, the relations between the palaeostresses and velocities in a metamorphosed rock may be considered as corresponding to some correspondence principle. This principle results from the more general superposition principle stated by Pier Curie [1966]: if certain causes initiate the corresponding effects, the symmetry elements of the causes should manifest themselves in the effects induced by them.

As applied to the relation between the stress field type and the elastic symmetry type of the rock, the correspondence principle can be formulated in the following way. In the palaeostress field, in which the three main components are not equal, the

crystalline rock acquires the orthorhombic symmetry type. In the palaeostress field, in which two components are equal and the third one differs from them in value, the rock acquires the transverse-isotropic symmetry type. Rocks that experienced substantial metamorphic transformations with persistent orientation of the palaeostress field components will have the symmetry type not lower than orthorhombic.

In accordance with the stated correspondence principle in metamorphosed rocks the orthorhombic and transverse-isotropic types of elastic symmetry will be most frequent. Rocks penetrated by the Kola superdeep borehole have the orthorhombic and transverse-isotropic types of elastic symmetry, the orthorhombic type being predominant [Gorbatsevich, 1995]. The predominance of the orthorhombic type corroborates the fact that in the geological past of the Pechenga massif tectonic shoves were very active [Orlov & Laverov, 1998].

The principle of correspondence of the palaeostress type with the type of the elastic constants matrix will be broken if some other reasons arise and their influence on the rock will be greater than that of the palaeostresses. For instance, it may be the mechanism of a viscous flow. It should be believed that with depth the component distribution in the stress field will be close to hydrostatic [Gorbatsevich, 1996]. In a heterogeneous rock that experienced several superimposed cycles of the stress state alteration and other influences this correspondence principle will be also violated.

8.5. Assessment of palaeostresses parameters in metamorphosed rock massifs

As indicated above, the transition of a rock to the anisotropic state occurs under the influence of palaeostresses and deformations during structural-metamorphic evolution of metamorphic complexes. Therefore a comparative analysis of elasticity constants $C_{\alpha\beta}$ (6.4), anisotropy factors A_p, B_S and other data allow obtaining information on the rocks stressed state that existed at the most significant stage of the palaeostress activity.

Following Kozhevnikov [Kozhevnikov, 1982], in polymineral rocks under the non-hydrostatic palaeostress field influence minerals will acquire a new orientation that reflects the evolution of the main factors - pressure, temperature and time of their activity. At one and the same period some minerals will experience syntectonic crystallization and acquire a thermodynamically stable orientation. On the whole, in anisotropic rocks the elasticity values of $C_{\alpha\beta}$ will be related to the components of the stress (palaeostress) tensor T_{ij} of the deformation stage ε_{ij}^n by a similarity of generalized Hook's law:

$$T_{ij} = C_{\alpha\beta}\varepsilon_{ij}^n f(t,\Lambda). \qquad (8.4)$$

In this equation t and Λ are the time factor and temperature, whose functional relation to the T_{ij}, $C_{\alpha\beta}$, ε_{ij}^n parameters is still to be established.

However it is known that syntectonic crystallization causes a rigid connection between T_{ij} and $C_{\alpha\beta}$ in amphibolite and some other metamorphic rocks (Kazakov, 1987). If a polymineral rock is formed in the compression stress field, then, as mentioned above, the minimum value of the compression wave velocity (V_{33}) or elasticity constants (C_{33}) correlate with the orientation of the maximum compression

force (T_1). Thus, the maximum compression force (T_1) will be oriented along the normal to schistosity.

The least palaeostress T_3 is oriented along the axis coinciding with linearity and corresponding to the greatest compression wave velocity V_{11} and, accordingly, to C_{11}. The intermediate value of T_2 will be predominantly oriented parallel to schistosity, but along the normal to linearity. The diagram in Fig. 8.5a will correspond to rocks of rhombic symmetry. As mentioned above, in direction 3 the compression wave velocity is minimum.

For the model, Fig. 8.5a, in direction 1 coinciding with the linearity the value of this velocity is maximum and in direction 2 it acquires an intermediate value. In the schistose rock model of pseudohexagonal symmetry the orientation of palaeostresses T_1, $T_2 = T_3$ components can be presented as it is shown in Fig. 8.5b.

The models, Fig. 8.5, allow suggesting the coefficients reflecting the relative values of the stress field components under which elastic properties were formed, a certain orientation of the symmetry elements and anisotropy type arose. For the model, Fig 8.5a, in accordance with generalized Hook's law, the coefficients K_{ij} will be proportional to the relationship among the elasticity constants values C_{11}, C_{22}, C_{33}:

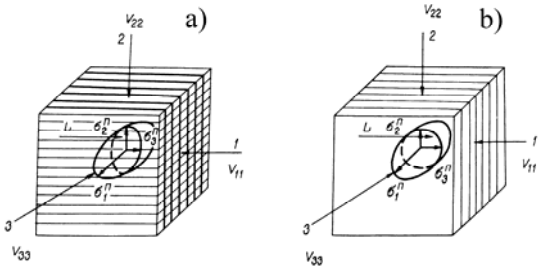

Fig. 8.5. Schematic orientation of components $T_1 = \sigma_1^n$; $T_2 = \sigma_2^n$; $T_3 = \sigma_3^n$ of the compressing stresses field for the rock of orthorhombic (a) and pseudohexagonal (b) symmetries. The arrows show the direction of linearity *L*.

$$K_{13} = T_1/T_3 = C_{11}/C_{33} = (V_{11})^2/(V_{33})^2,$$
$$K_{23} = T_2/T_3 = C_{11}/C_{22} = (V_{11})^2/(V_{22})^2,$$
$$K_{33} = T_3/T_3 = 1. \qquad (8.5)$$

Those coefficients will reflect the relationship among the stress field components for rocks of rhombic symmetry in directions 1, 2, 3. For the model in Fig. 8.5b the coefficients, accordingly, are:

$$K_{12} = K_{13} = T_1/T_2 = C_{11}/C_{33} = (V_{11})^2/(V_{33})^2, \; K_2/K_3 = 1, \qquad (8.6)$$

since here the relationship among the palaeostress components is $T_1 > T_2 = T_3$.

The analysis of the coefficients K_{12}, K_{13}, K_{23} as well as spatial orientation of the greatest, least and average velocities measured in the samples with their preserved spatial orientation in the rock mass will allow one to reconstruct the main characteristics of the palaeostress field.

An example of such reconstruction performed at outcrop 145 of the Voche-Lambina geodynamic region is given in Fig. 8.6 [Voche-Lambina…, 1991]. The procedure of measurements and determinations was the following. First we took samples marking an azimuth and incidence angle of their main surfaces. Then being oriented to layering (schistosity) and linearity, samples in a cubic form were sawn. After that by the acoustopolariscopy method (see point 5.3) the planes of the greatest anisotropy relative to the sample sides were determined.

Using the Wulff net and the data on the azimuth and the angle of side incidence we made the calculations of the azimuth and the incidence angle of the normal to the plane of the greatest anisotropy. In Fig. 8.6 on the outcrop 145 sketch map these

directions are depicted as arrows. The arrow size is proportional to the relative value K_{ij}. The values of the pitch angle for direction T_1 are given alongside the arrows.

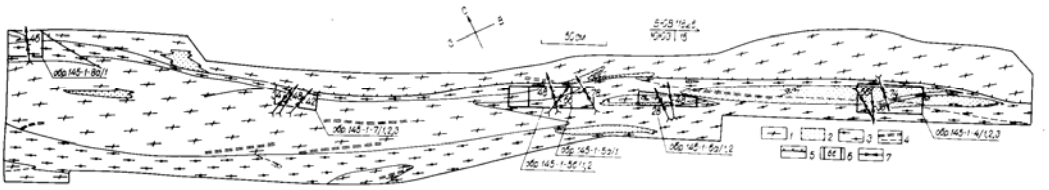

Fig. 8.6. The direction and relative value of the compressing palaeostresses greatest component on the sketch map of outcrop 145 of Voche-Lambina geodynamic region.
1 - plagiogranite, 2 - granodiorite, 3 - oligoclase-microcline granite, 4 - veined occurrences, 5 - ruptures, 6 - sampling locations, 7 - palaeostresses directions (the outcrop sketch map compiled by V.V.Balagansky and L.N.Korolyova).

An overview of the data from Fig. 8.6 shows that at outcrop 145 two isolated directions of the component T_1 action are revealed. Measurements on 8 samples (series 145-1-4, 145-1-5, 145-1-6, 145-1-8) detected one direction with the azimuth in the range of 354-28^o and incidence angles of 28-78^o. The azimuth of the second direction is maintained rather strictly and is 58-67^o with the incidence angles of 30-66^o. The second direction has been detected in the samples of series 145-1-7 and in the sample 145-1-5b/2. From the above data one may conclude that the first and second directions of T_1 reflect the processes that occurred, accordingly, at different deformation stages or metamorphism cycles.

The assessment made for the direction and relative value of palaeostresses, to our mind, is more reliable in terms of their direction. The relative value of palaeostresses is likely to depend not only on the factors reflected in Eq. (8.4). For instance, under the oriented stress hornblende in plagioamphibolite can acquire a strict orientation and thus cause stronger anisotropy than that observed in plagiogranite. Further investigations, including those in experimental mineralogy for individual rocks, will allow establishing scales of correspondence of palaeostress values to the measured elasticity characteristics.

To summarize the outlined aspects for the acoustopolariscopy use in the crystalline rock investigations it should be noted that the most complete summaries for determined properties of the samples from the Kola and Ural superdeep boreholes and Voche-Lambina region have already been published [Gorbatsevich, 1995]. This chapter is mainly devoted to the experimental study of the peculiarities of the new effects display - linear acoustic anisotropic absorption (LAAA) and depolarization of shear waves (DSW). The combination of comparatively strong elastic anisotropy and LAAA occurs rather often, but they can manifest themselves independently of one another. The detected convergence between the orientations of the symmetry elements of elastic anisotropy and LAAA can provide additional information on peculiarities of the rock structure. The other phenomenon - DSW allows one to assess the angle of random orientation of elastic symmetry elements in grains (layers) of mono-and polymineral rocks.

The study of palaeostress parameters is of no less importance. So far not so much has been done in this field. At the same time, acoustopolariscopy enables determining

the spatial orientation of the palaeostress field components in a metamorphosed rock. The observed relations between the values of components and elastic wave velocities allows one to judge the relative values of these components.

In our opinion, of great importance is the principle of correspondence of the palaeostress field parameters with the type of anisotropy transformed by this field of the metamorphosed crystalline rock. According to this principle, in the palaeostress field, where three main components are not equal to each other, a crystalline rock acquires an orthorhombic symmetry type. In the palaeostress field, where two components are equal and the third one differs from them in value, a rock acquires a transverse-isotropic symmetry type. Rocks that experienced substantial metamorphic transformations with persistent orientations of palaeostress field components will possess a symmetry type not lower than orthorhombic.

On the whole, the acoustopolariscopy results obtained for a large number of rocks of various genesis - sedimentary, volcanic, metamorphosed rocks including sandstone, dolomite, diabase, plagiogranite, granodiorite, biotite gneiss, shale, feldspar amphibolite et al. showed that in every sample, even in weakly anisotropic ones, the spatial orientation of symmetry elements can be revealed. Rather often, especially in metamorphosed rocks, the LAAA effect is displayed. Property determination of the samples from the Kola, Ural superdeep boreholes, Voche-Lambina region et al. have clearly showed that without the first stage - acoustopolarization measurements of spatial location of elastic symmetry elements in a sample - anisotropic characteristics of a rock cannot be obtained correctly. As the measurement practice showed, the elastic symmetry elements may not coincide with the elements of visible layering (schistosity) and linearity of the sample. A rock can be highly anisotropic even without visible texture manifestation in the sample.

9. VARIABILITY OF ELASTIC PROPERTIES OF ROCK SAMPLES FROM THE URAL SUPERDEEP BOREHOLE (SD-4)

9.1. Brief description of rocks from the Ural SD-4 section

The Ural Superdeep Borehole (SD-4) has been laid in the western limb of the Tagil megasynclinorium with the object of a comprehensive study of the Palaeozoic section in the Ural typical eugeosynclinal zone [Zagruzina et al., 1989]. In the range down to a depth of about 3 km a monotonous unit of volcanic-clastic rocks of basic and intermediate composition has been cut - the Silurian Immenov Formation. It is composed of coarse tephroide and tuff of pyroxene-plagiophyre basalt and andesite basalt, whose pyroclastic material pertains mainly to plagiophyre andesite. By the isotopic composition of rock forming and ore elements (oxygen, carbon, sulphur and lead) one may propose a homogeneous high temperature deep source of rocks that is typical of basalts [Zagruzina et al., 1989]. This, in its turn, should cause the similarity of physical properties of rocks cut by the borehole.

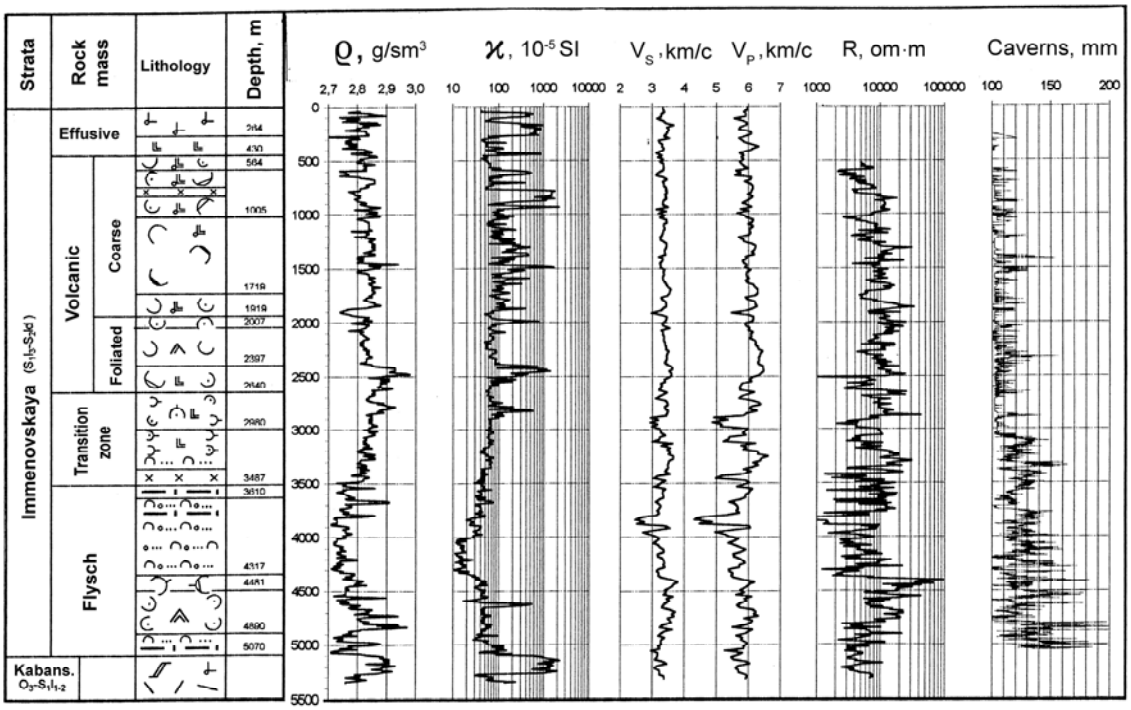

Fig. 9.1. Geological column, density ρ, magnetic susceptibility χ, compression V_P and shear V_S wave velocities, electrical resistance R, dimensions of caverns P in the section of borehole SD-4 [Druzhinin et al., 1999].

Figure 9.1 shows a geological column of rocks. From the surface down to a depth of H = 0.43 *km* basalt and andesite basalt lavas occur. The interval of H = 0.43-1.34 *km* is composed of psephytic andesite-basalt pumice tuff and the interval of H = 1.34-1.92 *km* - psephytic andesite-basalt tuff. In the range of 1.92-3.0 *km* psephytic leucoandesite-basaltic, andesite and basaltic tuffs occur. Below 3.0 *km* tuff sandstone (flysch) and tephroide lie. Accordingly, the unit boundaries are at depths of 430; 1344.6; 1921; 3001 *m*, etc. Inside the unites rock interlayers with quartz carbonaceous veinlets and sulphide penetrated by numerous healed fissures, other textural and structural peculiarities are present.

The aim of the acoustopolarization observations on the Ural SD-4 core samples was revealing rock elastic anisotropy, assessment of its type and degree, orientation of symmetry elements in regard to the borehole axis, comparing them with the stability and location parameters of the borehole. The measurements have been done on 25 cubic samples with the 40 *mm* edge.

The samples have been made of basalt, basalt pillow lava and breccia, andesite basalt porphyrite, andesite basalt, andesite basalt tuff, tuffite etc. (Fig. 9.1, Attachment 2). The samples represent the borehole intervals of 0.3-1.5 *km* and 2.4-3.2 *km*. The adopted indexing of edges and faces is given in Fig. 9.2. Acoustopolarigrams for the samples are given in Figs. 9.3-9.5. The results of the change in density ρ, the velocity of elastic waves located in accordance with the matrix V_{ij} (5.5), LAAA index D and inclination angles of elastic symmetry elements with regard to the sample faces are presented in Attachment 2.

Besides matrix V_{ij} obtained on a cubic sample whose normal to face 3 is oriented along the borehole axis, Attachment 2 presents matrix V_{ij}^{o} in which the velocities have been measured through the sample's additional faces. These faces were arranged parallel and perpendicular to the orientation of the revealed elastic symmetry elements of the medium. The photos of some samples with additional faces are given in Fig. 9.6. When the angles between the revealed symmetry elements and the orientation of faces, Fig. 9.2, were no more than 15-20°, no additional faces were made on the sample.

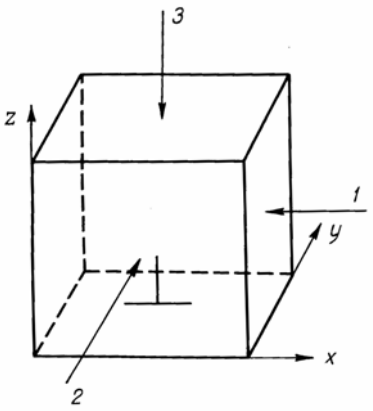

Fig. 9.2. Indexing of cubic samples cut from the SD-4 core. Direction 3 (*Z*) coincides with the core axis. 1, 2 – arbitrary directions.

All matrixes V_{ij}^{o} in Attachment 2 have been re-oriented in such a way that a number of relations (6.1) have been met (followed) if the medium belongs to the orthotropic symmetry type. If the medium is pseudohexagonal, then the matrix is built according to the relations (6.2, 6.3).

9.2. Peculiarities of acoustopolarization diagrams for volcanic rocks

First we consider acoustopolarigrams of the rock samples from the section (Fig. 9.3-9.5). By the acoustopolarigram shapes rocks from SD-4 can be divided in three groups: rocks with weak, marked and strong anisotropy. The VP acoustopolarigrams for the weak anisotropy rocks have a form close to a circle. The VC acoustopolarigrams are small as compared with the VP diagrams. Due to heterogeneity and measurement errors their shape does not often allow distinguishing the A_{VCM} minima and the exact determination of the elastic medium elements direction. By these indications andesite basalts (sample 78), basalts (sample 83), tuffites (samples 105, 152), diorites (sample 182) and tuffs (samples 253, 934, 1119) pertain to weakly anisotropic rocks. They are scattered, within the known data, rather evenly along the borehole section from H = 356.8 m to H = 2643.2 m.

The VP acoustopolarigrams for strongly anisotropic rocks (samples №№ 1138, 1161, 1191, 1223) have the forms close to the theoretically predicted ones providing a joint manifestation of purely elastic effects - anisotropy and non-elastic ones - linear

acoustic anisotropic absorption (LAAA). The VP and VC acoustopolarigrams most often represent four petal rosettes, the size of VC being comparable with that of VP. Clear minima of the amplitudes on the VC lines allow rather precise determination of the spatial orientation of the medium symmetry elements with the error no more than 3^o. The elastic symmetry elements of these rocks form an oblique angle with the orientation to the borehole bottom. All the rocks exhibiting strong anisotropy are fine-psephitic-psammite tuffs. Their appearance and visible structure (for instance, the structure of sample 1223 is characterized as homogeneous) do not allow distinguishing them from the rocks with weak and marked anisotropy. Strongly anisotropic rocks are concentrated in the interval of H = 2867.8-3068 *m*.

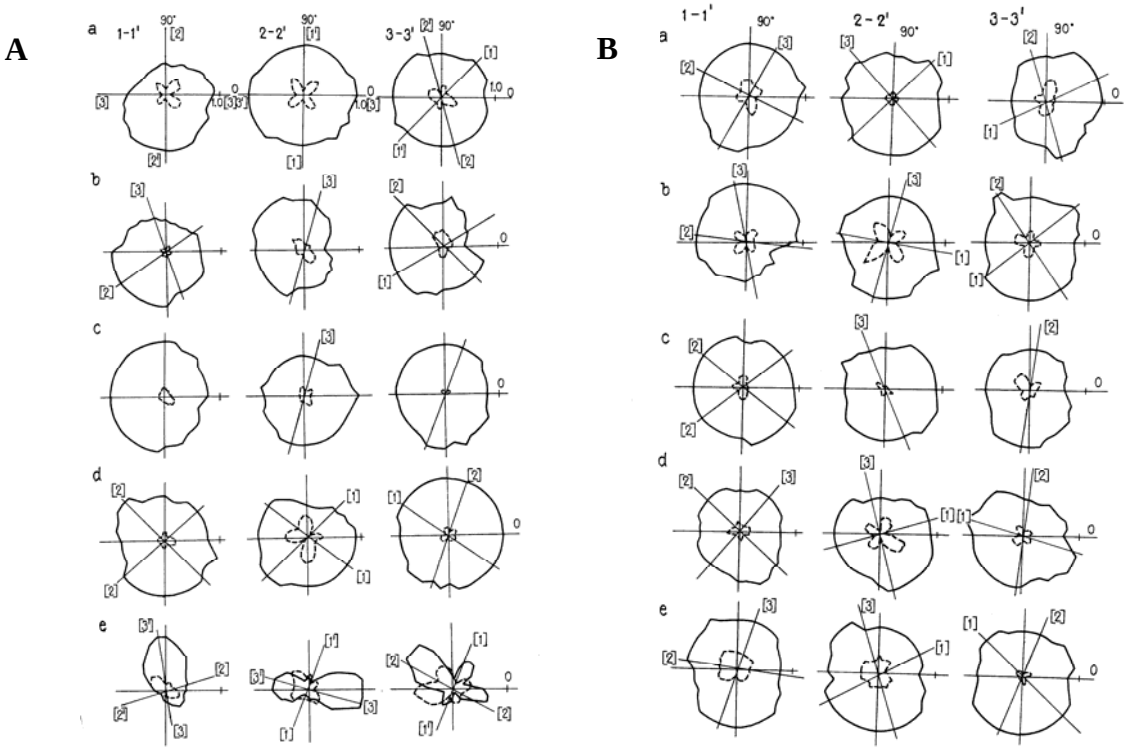

Fig. 9.3. **A** - acoustopolarigrams of samples No. 70, 78, 83, 92, 97 (H = 239-430.1 *m*). **B** - acoustopolarigrams of samples No. 105, 114, 152, 172, 182 (H = 435.9-808.6 *m*).

9.3. Analysis of physical properties, elastic anisotropy and symmetry type of rocks

Analysing the data from Attachment 2 one can see that the rock density varies in the range of ρ = 2.77 g/sm^3 to ρ = 2.93 g/sm^3. This index does not show any regular association with the sampling depth H. The component values of matrix V_{ij} and normalized matrix V_{ij}^o do not always obey the equalities stated in the relations (6.1), (6.2). It means that not all the samples are elastic-homogeneous. By this sign the most heterogeneous are rocks presented by samples №№ 70, 78, 172, I99, 908, 1138.

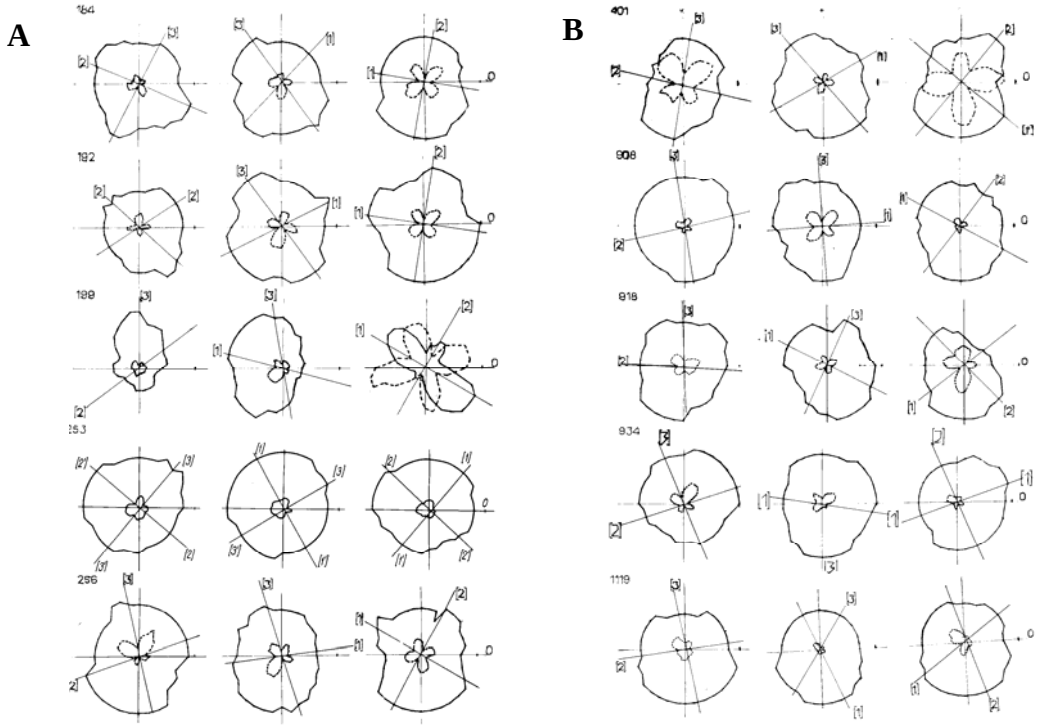

Fig. 9.4. **A** - acoustopolarigrams of samples No. 184, 192, 199, 253, 256 (*H* = 828.9-1128.2 *m*). **B** - acoustopolarigrams of samples No. 401, 908, 918, 934, 1119 (*H* = 1440.4-2843.2 *m*).

One can see from the data presented (Attachment 2) how great is the difference between the values of matrix V_{ij} and V_{ij}^{o} .

For instance, for strongly anisotropic rocks (samples №№ 1138, 1161, 1191 and 1223) the difference between the largest and least velocities V_p, V_s in matrix V_{ij}^{o} is much greater than that in matrix V_{ij}. For V_{ij}^{o} the least values of V_{pmin} = 3.84-3.89 km/sec. They approach the values of shear wave velocities V_s. In matrix V_{ij}^{o} a relationship between the maximum velocities of compression V_{piim} and shear V_{sijm} waves has been found (Fig. 9.7):

$$V_{\text{sijm}} = 0{,}57\ V_{\text{piim}} \tag{9.1}$$

with the factor of mutual correlation r = 0.73.

The most anisotropic rocks have the lowest V_{piim} and V_{sijm}. The index D of the LAAA effect varies in the range of 0.0 to 0.4. It is most conspicuous in strongly anisotropic rocks (samples №№ 1138, 1161, 119I, 1223) and in some rocks with marked anisotropy (samples №№ 97, 199, 401). The samples with marked or high LAAA, as a rule, have been taken near the zones of structural disturbances (H = 430, 924, 1440.4, 2667.8, 3068 *m*). In these zones contacts between the rocks of different types are observed (Fig. 9.1).

On the basis of the data from Attachment 2 we have calculated constants $C_{\alpha\beta}$ by formulas (6.5)-(6.10). The anisotropy factors ε_{1133}, ε_{2233}, γ_{1213}, γ_{1223} Δ_{T} have been determined by formulas similar to (6.11):

$$\varepsilon_{1133} = \frac{V_{11} - V_{33}}{V_{33}}\ , \tag{9.2}$$

$$\varepsilon_{2233} = \frac{V_{22} - V_{33}}{V_{33}} \tag{9.3}$$

where V_{11} is maximum, V_{33} - minimum and V_{22} - medium values of the longitudinal wave velocity in matrix $V_{ij.}$

$$\gamma_{1213} = \frac{V_{12}^c - V_{13}^c}{V_{13}^c} \tag{9.4}$$

$$\gamma_{1223} = \frac{V_{12}^c - V_{23}^c}{V_{23}^c}, \tag{9.5}$$

where $V_{12}^c = (V_{12} + V_{21})/2$, $V_{13}^c = (V_{13} + V_{31})/2$, $V_{23}^c = (V_{23} + V_{32})/2$.

We also introduced the following factor:

$$\Delta_T = \frac{2(\varepsilon_{1133} - \varepsilon_{2233})}{\varepsilon_{1133} + \varepsilon_{2233}}, \tag{9.6}$$

This factor, to our mind, is a criterion that can be used for distinguishing a symmetry type (pseudohexagonal or rhombic). We assume that if $0 < \Delta_T < 0.25$ or $1.75 < \Delta_T < 2.00$, then a rock should be assigned to pseudohexagonal. With Δ_T = 0.25-1.75 by elastic properties a rock should belong to the rhombic symmetry.

The mentioned characteristics including determined symmetry types are given in Attachment 3 and 4. Accordingly, in Attachment 4 rocks of pseudohexagonal symmetry are marked *G* and those of rhombic symmetry - *R*.

In Fig. 9.8 functional relation between the factors ε_{1133}, γ_{1213}, γ_{1223} is given. For the averaging line, Fig. 9.8, the following equation was obtained:

$$\gamma_{1213} = 0.288\ \varepsilon_{1133} \tag{9.7}$$

with the factor of mutual correlation $r = 0.85$,

$$\gamma_{1223} = 0.294\ \varepsilon_{1133} \tag{9.8}$$

with the correlation factor $r = 0.89$.

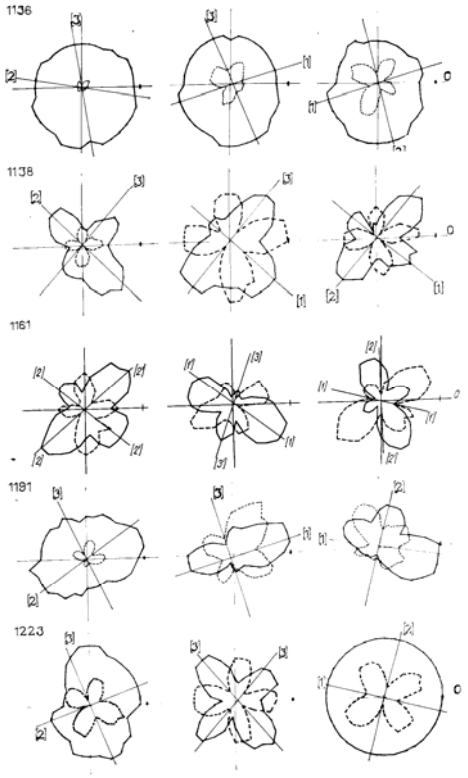

Fig. 9.5. Acoustopolarigrams of samples No. 1136, 1138, 1161, 1191, 1223 (*H* = 2866-3068 *m*).

As follows from the above data, for volcanic rocks elastic anisotropy represented by relationship between the compression wave velocities is closely related with the anisotropy represented by the relations between the shear wave velocities. This is especially true for highly anisotropic rocks in the depth range of 2867.8-3068 *m*. But for tuffs, tuffites and basalts composing the SD-4 units the anisotropy of elastic

properties is much more conspicuous in the compression wave velocities rather than in the shear ones.

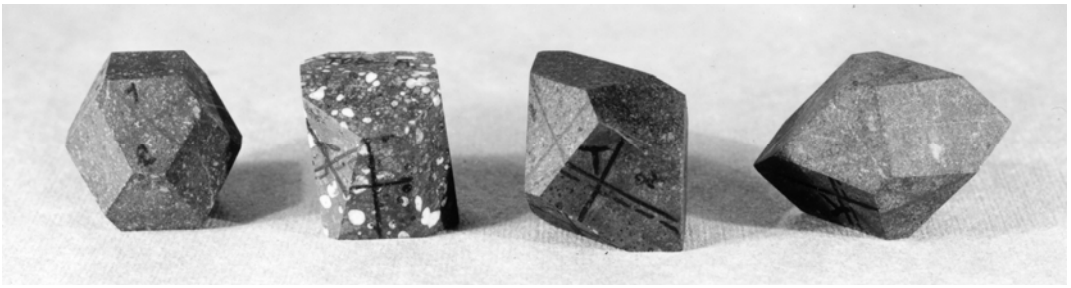

Fig. 9.6. Photo of the samples with additional faces cut from the SD-4 core. From left to right: pyroxene-plagioclase andesite-basalt (sample 92); almond-shaped pyroxene-plagioclase andesite-basalt (sample 401); andesite-basaltic psammitic fine-psephitic tuff (sample 918); fine-psephitic-psammitic tuff (sample 1138).

If we take $\varepsilon_{1133} = 0.05$ (anisotropy factor $V_{p11}/V_{p1} > 5\%$) as the threshold value, then by this sign samples №№ 78, 97, 114, 184, 192, 199, 401, 1131, 1161, 1191, 1223 pertain to anisotropic.

By the factor $\varepsilon_{1133} > 0.15$ the last five samples should be assigned to strongly anisotropic [Gorbatsevich, 1995], have pseudohexagonal symmetry. The symmetry of weakly anisotropic rocks is greatly influenced by the structural heterogeneity. That is why in relation to them the division into rhombic and pseudohexagonal symmetry can be done only approximately. Rocks with marked anisotropy are mainly of rhombic symmetry. These rocks with relatively high values of ε_{1133} belong to the pseudoxehagonal type (samples №№ 97, 192, 401).

9.4. The relation between the parameters of the rock elastic symmetry and the borehole stability

To our mind, the borehole stability is determined by the presence of stresses, anisotropy of elastic properties and the values of angles defining the position of the stress components of the rock elastic symmetry with respect to the borehole direction. From the above data (Attachment 2-4) one can conclude that in the SD-4 vicinity the most complicated stress state will be observed where it intersects highly anisotropic rocks ($H = 2867.8$ *m* and below).

In this case, as noted above, the borehole stability will be greatly decreased if the angle between the normal to the elastic symmetry plane and the borehole axis differs from zero or the right one. According to the observations [Bakhvalov et al., 1988], in this case the borehole axis will deviate from the vertical since during drilling the borehole tends to occupy the position perpendicular to the elastic symmetry plane. To assess the relation between the parameters of elastic symmetry and the borehole stability we used the data from Attachment 2. We calculated the value of the space angle ψ between the perpendicular to the elastic anisotropy plane and the direction to the borehole bottom.

As is known [Korn & Korn, 1968], the angle between the two normals to two planes can be determined by the formula:

$$\Psi = \arccos \frac{A_1 A_2 + B_1 B_2 + C_1 C_2}{\sqrt{A_1^2 + B_1^2 + C_1^2}\sqrt{A_2^2 + B_2^2 + C_2^2}}, \qquad (9.9)$$

where A_1, B_1, C_1, A_2, B_2, C_2, are the factors of the planes equations:

$$A_1x + B_1y, C_1z + D = 0,$$
$$A_2x + B_2y, C_2z + D = 0. \qquad (9.10)$$

If the angle, where directions 1, 2, 3 (*X, Y, Z*) meet, is considered to be the origin of the coordinates, Fig. 9.2, the equation of the normal to the plane *XOY* takes the form

$$Z + D_1 = 0 \qquad (9.11)$$

In this case Eq. (9.9) becomes:

$$\Psi = \arccos \frac{C_2}{\sqrt{A_2^2 + B_2^2 + C_2^2}} \qquad (9.12)$$

The acoustopolarization measurements resulted in determination of the angles β_{n1}, β_{n2} (see Figs. 9.3-9.5 and Attachment 2) between the projections of the elastic symmetry plane and plane *XOY,* accordingly, on the sample sides 1 and 2, Fig. 9.2. In this connection Eq. (9.9) takes the form [Korn & Korn, 1968]:

$$\Psi = \arccos \frac{1}{\sqrt{tg^2\beta_{n1} + tg^2\beta_{n2} + 1}}. \qquad (9.13)$$

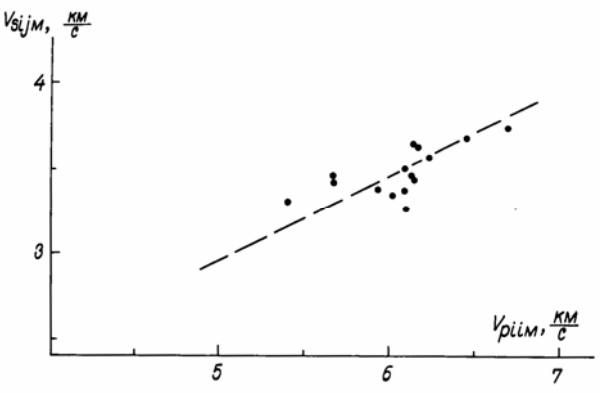

Fig. 9.7. Relation between maximum values of longitudinal V_{piim} and shear V_{sijm}. waves in matrixes V_{ij}.

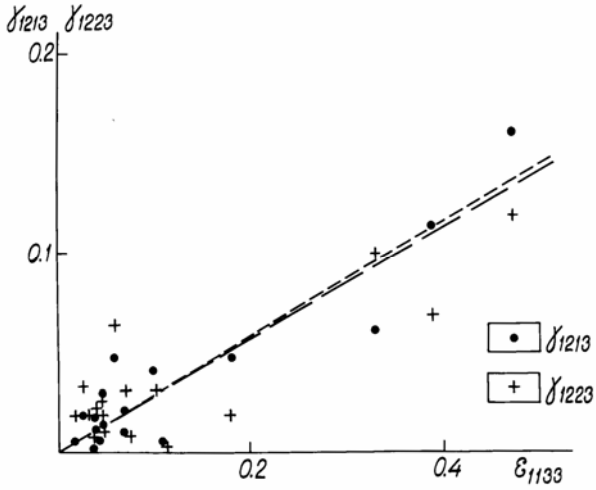

Fig. 9.8. Relation between anisotropy factors ε_{1133} and γ_{1213}, γ_{1223} for the SD-4 rocks.

The calculated angle ψ for the rocks displaying marked and strong anisotropy are given in Attachment 4. Figure 9.9 presents depth-dependent values of anisotropy parameters ε_{1133}, γ_{1213}, linear acoustic anisotropic absorption *D* and space angle ψ. On evidence derived from Yaroslavl Department of KamNIKIGS logging results are given - the borehole real diameter *P* for the interval of 0.3-3.1 *km*. A general overview of the data, Fig. 9.9, shows that in the vicinity of depths *H* = 430, 886, 924, 1440 and 2496 *m*, both by ε_{1133}, γ_{1213} indexes and *D* values, zones with marked anisotropy of elastic and absorbing properties have been found.

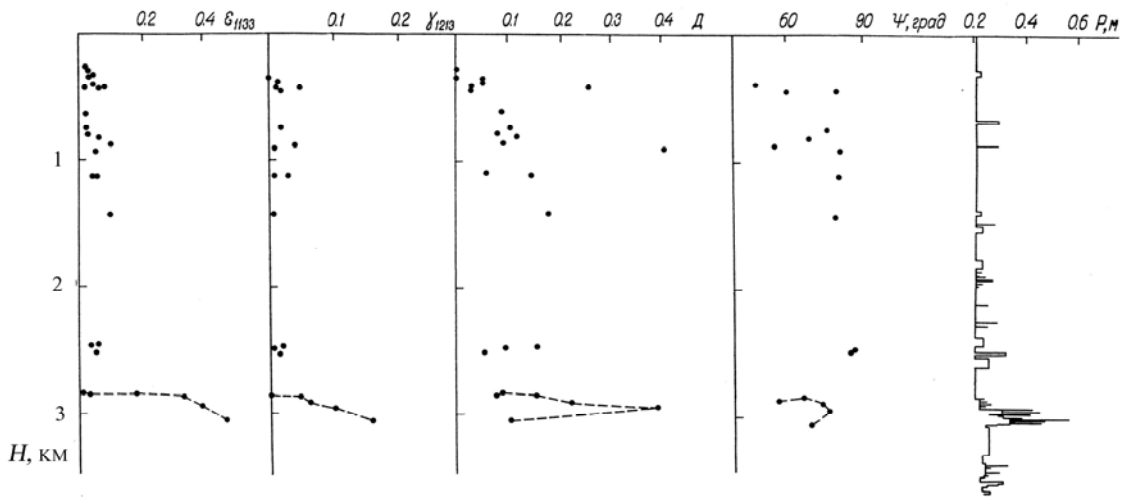

Fig. 9.9. Indexes of elastic anisotropy ε_{1133}, γ_{1213}, linear acoustic anisotropic absorption D, the angle between the perpendicular and the anisotropy plane ψ and the real diameter P of the SD-4 borehole at different depths H.

Down to a depth of 2867 *m* the value of angle ψ ranges from zero to 86°. This suggests the availability of mechanical heterogeneity and nonuniform formation of units I-IV during their melting and accretion.

Starting from a depth of 2867 *m* the results of measurements and determinations show the availability of the zone within which the rock properties greatly differ from those of the overlying rocks. From this depth elastic anisotropy both by compression and shear waves increases virtually linearly. The LAAA index rises as much. By these indexes a zone stands out within which the stress state in the borehole vicinity is heterogeneous due to strong anisotropy of elastic properties. The deviator of the stress tensor will be of substantial value and spatial orientation of the tensor main components will transfer as the variability of the angle ψ = 51-76° shows.

The values of ε_{1133}, γ_{1213}, D and ψ (Fig. 9.9) show a close relation to the value of the diameter P, i.e. to the size of caverns in the borehole. This relation is most conspicuous in indexes ε_{1133} and γ_{1213}. Interestingly, the depth difference between the marks, where the most intense rise in elastic anisotropy by ε_{1133} and γ_{1213} and the most sharp increase in the cavern size P begin, is about 60 *m*. Thus, a prompt assessment of the rock anisotropy will allow prediction of possible cavern and inrush formation.

In conclusion we will set forth the main tenets and implications from the above material. From the outline of rocks from the SD-4 section it follows that the homogeneous deep source which is typical of basalts provided their rather homogeneous chemical composition. Distinctions between the rocks in units I-IV are caused by different crystallization conditions and parameters of the subsequent stress-strain state. The registered rock elastic anisotropy is a result of the prolonged stay under stresses, i.e. most likely palaeostresses [Kozhevnikov, 1982].

The acoustopolariscopy results of SD-4 core allowed one to divide rocks into rather isotropic, rocks with marked and strong anisotropy. Strongly anisotropic rocks occur in the interval of 2867.8-3068 *m* and, probably, deeper. As a rule, they have a pseudohexagonal symmetry. This suggests the availability of a great component of tectonic stress. This component acts along the normal to the symmetry plane determined by the acoustopolariscopy method. It is remarkable that the appearance and visible structure of strongly anisotropic rocks do not allow one to distinguish them from the rocks with weak and marked anisotropy.

In rocks with marked anisotropy the rhombic type of elastic symmetry prevails suggesting much the same influence of geostatic and tectonic stresses. If the anisotropy indexes in rocks with marked anisotropy are higher than the average values then the rock symmetry becomes pseudohexagonal. This allows one to state that at these depths the tectonic component of the stress field begins to dominate over the gravitation one. This predominance is especially great at depths of H = 2867-3068 m. Judging by the value of angle ψ the orientation of the stress tectonic component is close to subhorizontal.

The relations between the matrix V_{ij} values for compression and shear waves for this type of rocks showed that isotropic (weakly anisotropic) rocks have a comparatively low Poisson's ratio – ν = 0.18. During seismic investigations this index can serve as a diagnostic sign for volcanic rocks of this type. The anisotropy expressed by the relations between the compression wave velocities is closely connected with that expressed through shear waves. But for this type of rocks anisotropy of elastic properties is much better expressed in the difference between the compression waves rather than the shear waves. Contrast zones are singled out by the indexes of elastic anisotropy and linear acoustic anisotropic absorption in the SD-4 section (from the data available) in the 430, 886, 924, 1440, 2496 and 3000 m depth vicinity, The presented geological column points to the change or contacts between various rocks within these zones. A high index of LAAA has been fixed for the rocks with the oriented mineralized cracks.

Starting with a depth of H = 2867 m the results of measurements and determinations clearly show the availability of the zone within which the rock properties differ radically from those in the overlying rocks. Within this zone the stress state of the rocks is heterogeneous: the deviator of the stress tensor must be great and the spatial orientation of the tensor's main components must (judging by the value of ψ = 57-76^{o}) transfer in space with depth.

Within the zone of cavern formation a close relation has been found between the indexes of the rock elastic anisotropy and the value of the borehole transverse size P. There is a shift in depth between the initial marks of the most intensive rise in elastic anisotropy and a sharp increase in the sizes (section) of the borehole caverns. Such an increase in the cavern section has been registered 60 m lower than the beginning of the rock anisotropy rise. If a similar shift in depth is fixed in other boreholes, this will allow one to propose a prompt method for forecasting zones of stability loss. To assess the borehole stability exactly the elasticity constants of rocks have been calculated.

The results reported in this work, on the whole, show the efficiency of the acoustopolarization method for determining the availability of elastic anisotropy, spatial arrangement of elastic symmetry elements, calculation of elasticity constants, determination of a symmetry type and calculation of the stability of the borehole drilled in an anisotropic rock mass. It is remarkable that unfavourable zones for the borehole stability, that were preliminary revealed in the SD-4 section through the assessment of the rock elastic anisotropy by shear waves, coincide in depth with the ones determined from the above analysis. This suggests that an express method for an assessment and forecast directly at boreholes can be proposed.

10. ANISOTROPY OF ELASTIC PROPERTIES OF ROCK SAMPLES FROM THE KOLA SUPERDEEP BOREHOLE (SD-3)

10.1. Section lithology

The Kola superdeep borehole (SD-3) has been laid in the north-eastern Baltic shield in the junction area of ore-bearing Precambrian structures that are typical of ancient platforms. It has penetrated all formations of the Proterozoic complexes and a major part of the Archaean complex [Kozlowsky, 1987]. Investigations on the core showed that in the borehole section one can observe metamorphism at prehnite-pumpellyite to amphibolite facies

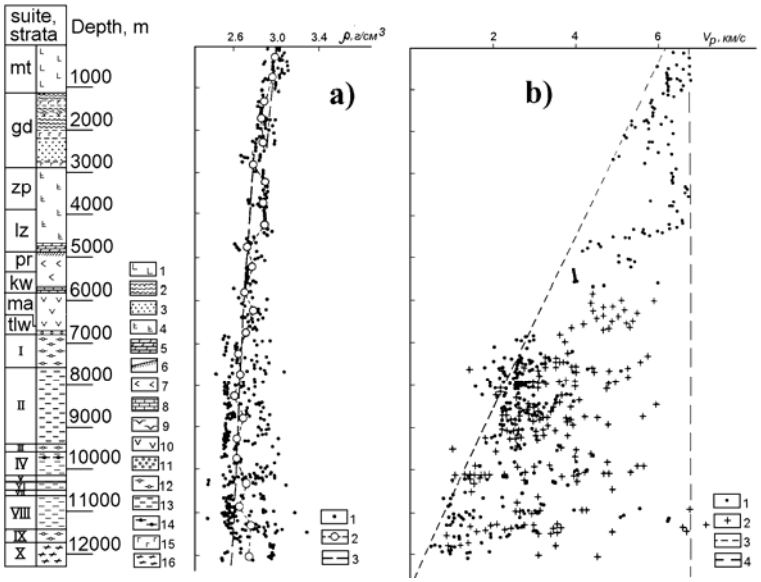

Fig. 10.1. Geological column and core properties in the section of the Kola superdeep borehole (SD-3).
1 - augite metadiabase with interlayers of pyroxene and picrite porphyrite; 2 - metaphyllite, aleurolite with tuff interlayers; 3 - rhythmically layered metasandstone with subordinate aleurolite and phyllite; 4 - actinolized metadiabase; 5 - dolomite, arkose metasandstone; 6 - sericite schist; 7 - diabase; 8 - dolomite, polymict metasandstone; 9 - wehrlite; 10 - diabase porphyrite, schist after them; 11 - metadiabase; 12 - biotite-plagioclase gneiss with high-alumina minerals; 13 - biotite-plagioclase gneiss with amphibole, epidote, sphene; 14 - magnetite-amphibole schist; 15 - gabbro-diabase, 16 - biotite-plagioclase and sphene, biotite-amphibole-plagioclase gneiss, schist.
a - distribution of density values ρ in the section. 1 - unit values measured on separate core samples; 2 - mean interval values; 3 - linear tendency of alteration ρ with depth.
b - scattering of unit values of longitudinal wave propagation velocity V_p, measured on core samples in the air-dry state. 1 -samples of gneiss-granite composition; 2 - amphibole-bearing samples; 3 - boundary line of minimum values; 4 - boundary line of maximum values.

The Proterozoic complex (H = 9-6842 m) is mainly presented by metadiabase, gabbro-diabase, metatuff, serpentine, metaaleurolite, metasandstone, porphyrite and schist, Fig. 10.1.

Metadiabase is composed of monoclinic pyroxene, augite (50-40%) and plagioclase (30-20%). The rest are hornblende, quartz, chlorite, epidote etc. Gabbro-diabase contains plagioclase, (60-20%), monoclinic pyroxene (60-20%), chlorite, saussurite and carbonatite (to 30%). Tuff is mainly composed of volcanic glass fragments, diabase, albite, plagioclase and quartz. Serpentinite contains serpentine,

chlorite (60%), talc (20%), tremolite (10%) etc. Fragments in metaaleurolite and metasandstone are represented mainly by quartz, plagioclase microcline; fragments of amphibole, pyroxene and garnet are scarce. Andesite-dacite porphyrite contains plagioclase, quartz, albite-oligoclase, sericite, chlorite etc. Schists are represented by plagioclase (30-50%), hornblende (50-60%) and, in small quantities, by magnetite and ilmenite.

Among the Archaean rocks (H > 6842 *m*) biotite-plagioclase gneisses, granites, pegmatites, shady migmatites, amphibolites, epidote-biotite schists are most common. Biotite-plagioclase gneisses, granites, pegmatites are composed of biotite (20-30%), sometimes partially substituted by muscovite, quartz (30-40%), plagioclase (about 30%). In pegmatoid rocks biotite is, as a rule, substituted by microcline and muscovite. Varieties enriched in garnet are present. In epidote-biotite schists quartz is displaced by epidote and pyroxene. Compositionally, shady migmatites are close to biotite-plagioclase gneisses. The composition of amphibolites is ordinary: hornblende about 70%, plagioclase 30% and some biotite. The mineral composition of amphibolite schists is close to that of amphibolite.

The Pechenga complex [Orlov & Laverov, 1998] is divided into the Matert (mt - 9-1059 *m*), Zdanov (zd - 1059-2805 *m*), Zapolyarny (zp – 2805-4673 *m*), Luchlompolo (lz - 4673-4884 *m*), Pirttijarvi (pt - 4884-5619 *m*), Kuvernerinjoki (kw - 5619-5717 *m*) Majarvi (ma - 5717-6835 *m*) and Televi (tlw – 6835-6842 *m*) formations (Fig. 10.1).

The Archaean complex is represented by unit I composed of gneisses with high alumina minerals (HAM) (6842-7622 *m*), unit II composed of shady migmatites, gneisses and amphibolites (7622-9456 *m*), unit III composed of two-mica gneisses with fibrolite (9456-9573 *m*), unit IV composed of shady migmatites, gneisses and amphibolites (9573-10144 *m*), unit V composed of two-mica gneisses with fibrolite (10144-10273 *m*), unit VI composed of shady migmatites, gneisses and amphibolites (10278-10448 *m*), unit VII composed of gneisses with HAM (10448-10601 *m*), unit VIII composed of shady migmatites, amphibole gneisses and amphibolites (10601-11411 m), unit IX composed of biotite-plagioclase gneisses with HAM (11411-11708 *m*), unit X composed of biotite- plagioclase gneisses and schists (11708-12261 *m*).

As follows from the above, the SD-3 section is represented by a large variety of rocks of ultrabasic to acid composition, different grade of reworking, metamorphism, structural and textural distinctions. This suggests different conditions of their genesis and possible variations in elastic properties and anisotropy.

10.2. Elastic properties and anisotropy of Proterozoic and Archaean rocks

Attachment 5 presents summary data on determined density ρ, elastic wave velocities arranged in accordance with the normalized matrix V_{ij}^0 (5.5) and index of linear acoustic anisotropic absorption (LAAA) effect D. As a rule, when sawing a sample its sides were oriented along the foliation (schistosity) and linearity. In the notes to the Attachment 5 one can find the cases when the side orientation does not correlate with the elastic symmetry elements of the sample medium. The sample order in Attachment 5 is determined by the depth of their excavation H. Attachment 6 gives calculated constants of elasticity $C_{\alpha\beta}$ (see formulas (6.6)-(6.11) and anisotropy indexes ε_{1133}, ε_{2233}, γ_{1213}, γ_{1223}, Δ_T, (see formulas (9.2)-(9.6)) for the same samples. A type of elastic symmetry was determined by the index Δ_T.

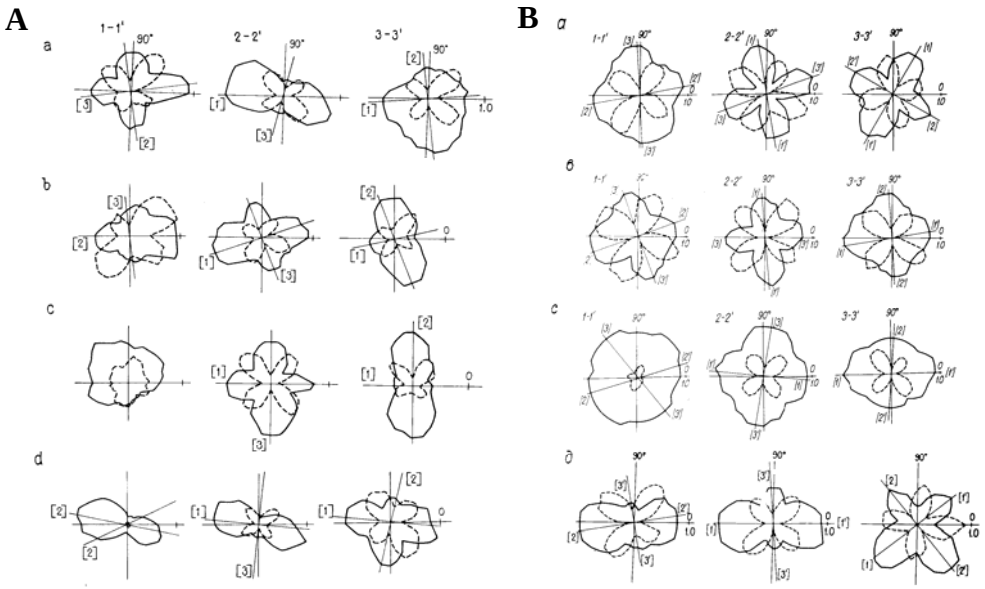

Fig. 10.2. Acoustopolarigrams of SD-3 core samples.
A: a - plagioclase granite with amphibole (sample 24996S); b - epidote-biotite-plagioclase gneiss (sample 28184S); c - biotite-plagioclase gneiss (sample 30020); d - staurolite-andalusite-sillimanite-two-mica gneiss (sample 24256S).
B: a -amphibole-plagioclase schist (sample 19131S); b - amphibole-plagioclase schist with chlorite (sample 21720); c - amphibole-plagioclase schist with chlorite (sample 21722); d - talc-phlogopite-tremolite schist (sample 26716S).

Figures 10.2-10.4 show typical acoustopolarigrams for the samples of biotite-plagioclase gneisses, granites, schists, amphibolites, apogabbro, hornblendite and porphyrite. Judging by the acoustopolarigrams (Fig. 10.2), elastic anisotropy of biotite-plagioclase gneisses and granites is very conspicuous. Acoustopolarigrams of samples 24996S and 28184S point to the symmetry rhombic type, while those of samples 30020, 24256S point to the pseudohexagonal type. In all cases LAAA is manifested along individual directions in the samples. This effect is very strong in staurolite-andalusite-sillimanite-two-mica gneiss (sample 24256S). Using the diagrams, Fig. 2.5, one can see that since the orientation of the largest diameter of the VP diagrams on sides (1-1') and (2-2') is mutual, a plane model (Fig. 2.5, a) is a basis for LAAA manifestation.

Unlike gneisses and granites some schists have acoustopolarigrams without LAAA manifestation (Fig. 10.2) and with a shape close to the classical one (Fig. 1.4). Talc-phlogopite-tremolite schist (sample 26716S) has some distinctions. But a large number of schist samples have acoustopolarigrams that exhibit strong LAAA influence (Fig. 10.3). The model of LAAA manifestation may be of both - plane (samples 26715S, 35924) and linear-plane types (samples 19402S, 27227S). As shown by the acoustopolarigrams, the range of LAAA manifestation in the amphibolite samples is rather wide (Fig. 10.3, 10.4). The amphibolite acoustopolarigrams, as a rule, suggest influence of three factors in various combinations and degree - elastic anisotropy, LAAA and heterogeneities. For instance, the acoustopolarigrams of samples 24947, 35426 were most influenced by the first factor. The acoustopolarigrams of samples 24788S, 27026, 42413-1, 42918-1 show the influence of the first and, to a large extent, the second factors. All the three factors influenced the shape of the acoustopolarigrams for samples 31272 (side 3-3')

and 43553 (side 2-2'). According to the orientation of the largest diameters of the VP diagrams, samples 27026, 31272, 42413-1, 43553 show a plane model of LAAA, while samples 24788S, 42918-1 show a linear model (Fig. 2.5).

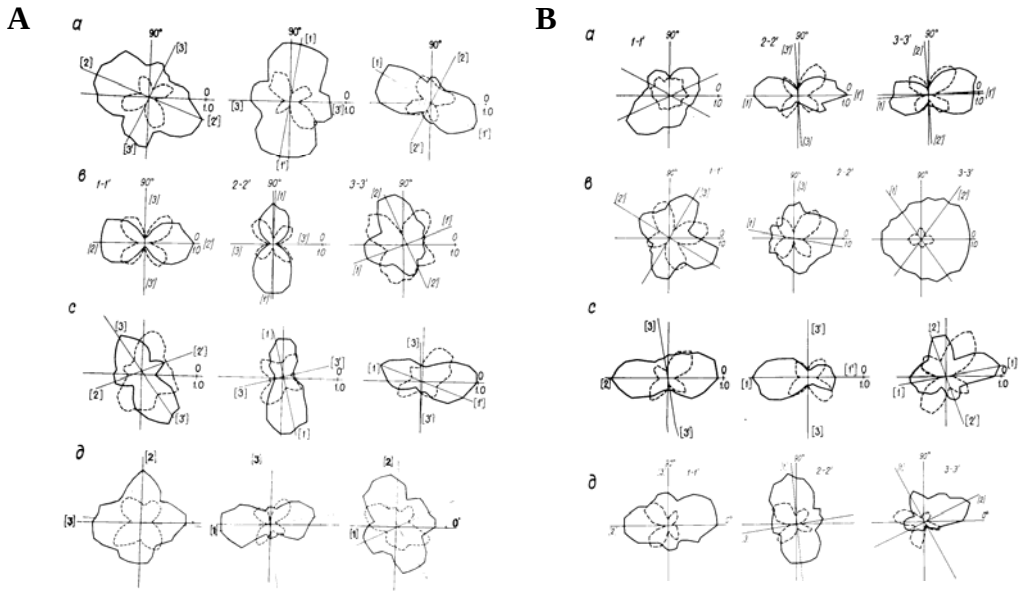

Fig. 10.3. Acoustopolarigrams of SD-3 core samples.
A: a - amphibole-plagioclase schist with biotite (sample 19402S); b - talc-phlogopite-tremolite schist (sample .26715S); c - epidote-biotite-amphibole-plagioclase crystalloschist (sample 27227S); d - apohyperbasic schist (sample .35924).
B: a -clinopyroxene amphibolite (sample 24788S); b - amphibolite with sphene (sample 24947); c - cummingtonite amphibolite (sample 27026); d - epidote-hornblende amphibolite (sample 31272).

Figure 10.4 shows acoustopolarigrams of fine-grained apogabbro, hornblendite, apogabbroic porphyrite samples. All the mentioned samples are also hornblende amphibolites. The acoustopolarigrams for the first three samples suggest strong LAAA and the influence of heterogeneities. Samples 31587, 43579 show a plane model of LAAA, while hornblendite (sample 38846) shows a linear one. Judging by the acoustopolarigrams, elastic anisotropy and LAAA in the porphyrite sample are weak. It is interesting to note that this sample has, besides low values of anisotropy factors, very high compression and shear wave velocities for such depths (H = 11430 m) (Attachment 5).

On the whole, the shapes of VP acoustopolarigrams for the SD-3 section are typical of strongly anisotropic rocks of mainly rhombic symmetry. As a rule, projections of symmetry elements are easily distinguished on all three sides of the sample. The acoustopolarigrams show that the anisotropy of rocks from SD-3 is much higher than that of rocks from SD-4 and from Voche-Lambina deposit area [Gorbatsevich, 1995]. The VP shapes of some acoustopolarigrams for the rocks from SD-3 differ radically from those for the rocks from SD-4 and Voche-Lambina deposit area [Gorbatsevich 1995]. Diagrams for samples 24256S, 26715S, 27227S, 24788S, 27026, 42918-1 in Figs 10.2-10.4 provide examples of this difference. Acoustopolarigrams for samples 21720, 34876, 43579 etc. belong to the same group. All of them are characterized by a very high LAAA manifested on one, or, more often, two or three sample sides. The observed shapes of acoustopolarigrams are like calculated circle diagrams, Fig. 2.2, 2.5.

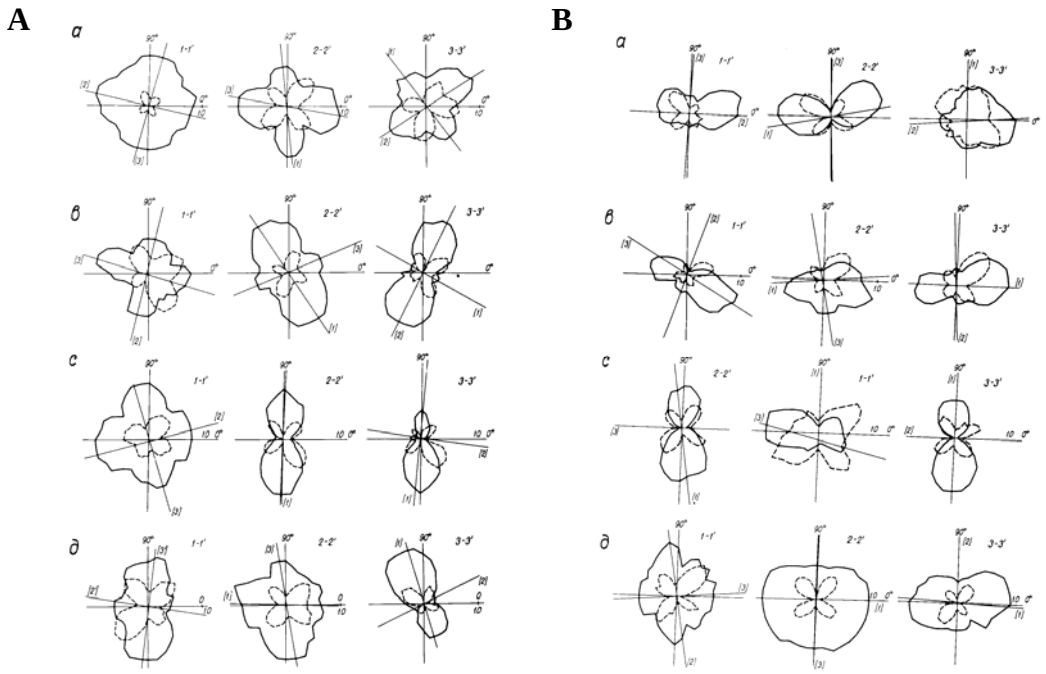

Fig. 10.4. Acoustopolarigrams of SD-3 core samples.
A: a - amphibolite with sphene (sample 35426); b - epidote-biotite hornblende amphibolite (sample 42413-1); c - epidote-biotite hornblende amphibolite (sample 42918-1); d - amphibolite with sphene (sample 43553).
B: a - fine granular apogabbro (sample 31587); b – fine granular apogabbro (sample 43579); c - biotite hornblende amphibolite, hornblendite (sample 38846); d – apogabbroic porphyrite (sample 41487).

An analysis of the data in Attachment 5 shows that in SD-3 rock samples the LAAA effect D varies in the range of all possible values, from D = 0.0 (sample 24947) to D = 0.95 (side 2-2', sample 31587). As shown on the model media (see point 2.4), LAAA is a non-elastic effect that is slightly related to elasticity indexes - compression and shear wave velocities.

The numerical values in Attachment 5 suggest that rocks from SD-3 as well as those taken at the surface or from SD-4 show a close correlation between the maximum velocities of compression V_{piim} and shear V_{sijm} waves in matrixes V_{ij}, Fig. 10.5.

$$V_{\text{sjim}} = 0.56 V_{\text{piim}} \tag{10.1}$$

with the mutual correlation factors r = 0.84.

These relationships to the same extent are true for the three distinguished rock groups: schists, amphibolites and biotite gneisses (granites). On the whole, it is revealed that the largest velocities of compression and shear waves are characteristic of schists, to a lesser extent to amphibolites and still to a lesser extent to biotite gneisses and granites.

An arrangement of the unit values of the factors ε_{1133}, γ_{1223} for the three types of SD-3 rocks is given in Fig. 10.6 in the diagram drawn from the data presented in Attachment 6. A general scattering of the points in the diagram does not allow one to consider anisotropy factors for compression ε_{1133} and shear γ_{1223} waves to be closely related. By the mode of their arrangement two groups of points and, accordingly two lines - I and II, can be distinguished in a qualitative sense. The lines reflect a proportionality of the relationship between the values γ_{1223} and ε_{1133} in these groups.

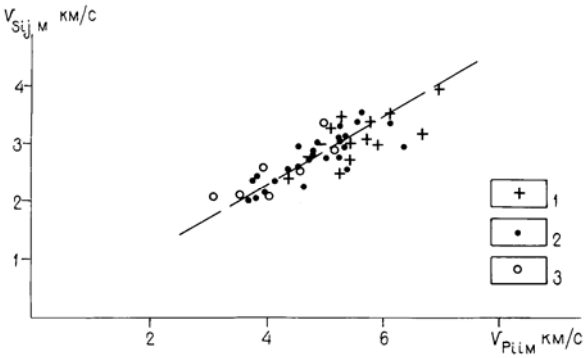

Fig. 10.5. Relation between the maximum values of compression (V_{piim}) and shear (V_{sijm}) wave velocities in the velocity V_{ij} matrixes for rocks from the SD-3 section.

For the first group (line I),

$$\gamma_{1223} \approx 0.8\varepsilon_{1133}. \qquad (10.2)$$

For the second group (line II),

$$\gamma_{1223} \approx 0.31\varepsilon_{1133}. \qquad (10.3)$$

As follows from the relationship (10.2), anisotropy of the shear wave velocities is close to that of the compression waves for the first group of points. Rocks combined in the group of points along line I, have characteristics γ_{1223}, ε_{1133} close to the same characteristics of rocks from the Voche-Lambina deposit area [Gorbatsevich, 1995]. As to the second group of points, here anisotropy of shear wave velocities is much less than that of compression waves. In this case equation (10.3) reflects the relationship close to that observed before for volcanic rocks from the SD-4 section (see point 9.3).

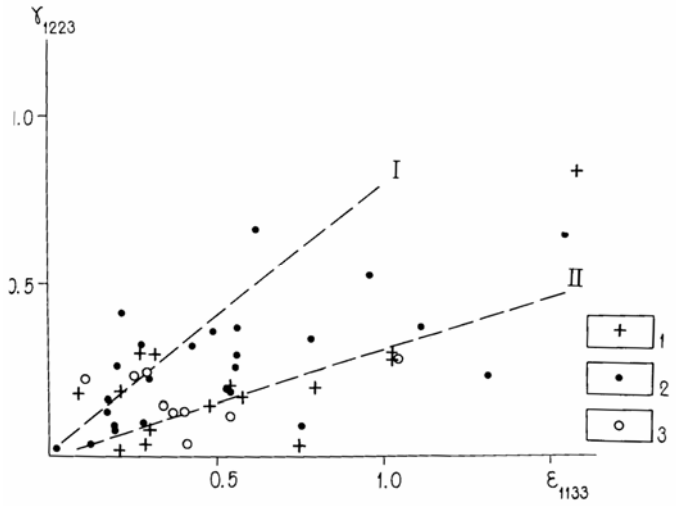

Fig. 10.6. Distribution of unit values of anisotropy factors γ_{1223} and ε_{1133} for rocks from the SD-3 section.
1 - schist, 2 - amphibolite, 3 - biotite gneiss (granite).

It is known that the geological section of the Kola superdeep borehole SD-3 is characterized by alteration of sedimentary and volcanic units [Kozlovsky, 1987]. This is likely to be the reason for the fact that one rock type corresponds to the relation (10.2), while the other one - to the relation (10.3). Accordingly, the type of relationship between the factors γ_{1223} and ε_{1133} can be used for separating volcanic rocks from rocks of other types. But this conclusion is tentative. A final conclusion

may be drawn after detailed petrographical and petrological investigation of the first and second rock groups.

The data from Attachment 6 support the conclusion (drawn before when analysing the acoustopolarigrams) that most of the measured rocks are highly anisotropic and pertain to the rhombic type of symmetry (in Attachment 6 rocks of pseudohexagonal symmetry are marked *G* and those of rhombic symmetry - *R*). Only 10 of 58 samples belong to the pseudohexagonal symmetry type, 6 of them (samples 18994, 21722S, 24221S, 24256S, 25386, 27262) representing a rather interesting variety of the transverse-isotropic or pseudohexagonal type - the compression wave velocity is maximum in the symmetry axis direction and minimum in the plane direction. The system of relations V_{ij} (see Eq. (6.2)) that are true for transverse-isotropic media represents a set of plane-parallel layers (type I) with discriminate properties [Lyakhovsky, Nevsky, 1970; Lyakhovitsky, 1988].

In the SD-3 rocks of type II in the V_{ij} matrix, the following relations are observed (see Eq. (6.3)): $V_{11} = V_{22} < V_{33}$, $V_{12} = V_{21} < V_{13} = V_{31} = V_{23} = V_{32}$. Conventionally, this type (type II) can be conceived of as a bunch of parallel cylindrical rods that are in an isotropic medium different from the rods in elastic properties. The symmetry axis of an endless order will be situated along the rod axes. A model of such medium is given in Fig. 6.3. The origin pattern of type I elastic symmetry in the stress field seems to be quite logic, but the origin of type II symmetry is not quite clear so far. It may be a consequence of some metamorphic [Kozhevnikov, 1982; Robin, 1979, Eliseev, 1959], or metasomatic processes [Vernon, 1980].

10.3. Variability of elastic anisotropy parameters of rocks from the SD-3 section

As shown in chapter 7, the basis for the rock elastic anisotropy is anisotropy of minerals. A rock composed of strongly anisotropic minerals with an identical orientation of crystallophysical axes will be most anisotropic. On the contrary, a polycrystalline rock of a massif structure with differently oriented crystallophysical axes of mineral grains may be moderately anisotropic or lack anisotropy at all. Observations on elastic characteristics of the SD-3 core allowed revealing an effect called the effect of rock disintegration that is directly related to anisotropy of mineral grains. It is manifested during the core release from geostatic stresses in the process of drilling and core recovery [Gorbatsevich & Medvedev; 1986; Gorbatsevich, 2003].

For instance, systematic laboratory

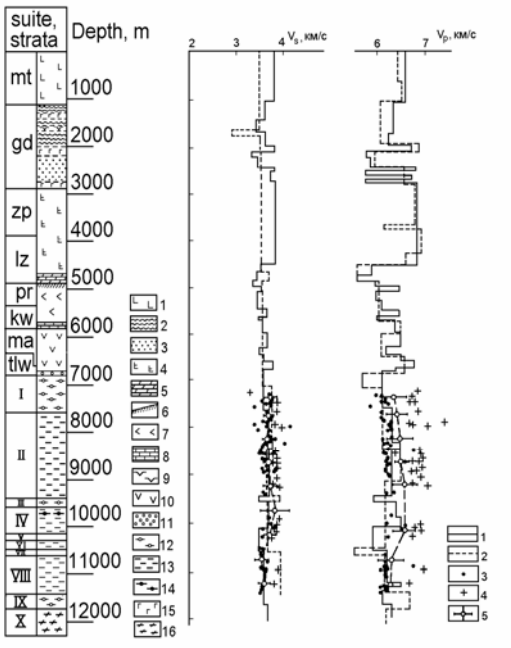

Fig. 10.7. Vertical velocity section along the SD-3 borehole [Sharov, 1997]. For the legend to the geological column see Fig. 10.1.

1 - vertical seismic profiling method (VSP); 2 - acoustic logging method (AL); 3 - calculation method (CM) applied for rocks of gneiss-granite composition; 4 - calculation method for amphibole-bearing rocks; 5 - calculation method, average confidence bounds for intervals.

measurements of compression V_p and shear V_s wave velocities along the core axis showed [Kozlovsky, 1987] that the maximum and minimum values of V_p and V_s tend to decrease with depth. The measurements, Fig. 10.7, showed that there is virtually no difference in the V_p values measured on the core extracted from the near-surface zone and those derived in the borehole by acoustic logging (AL). But the difference between the V_p lab measurements made on the core extracted from the 9-11 *km* depths and those obtained by AL at the same depths is 200% and more, Fig. 10.1b.

In polycrystalline rocks of a massif structure the disintegration effect of rocks during their release from geostatic and other stresses should be most conspicuous [Goryainov, et al. 1992]. Therefore we have measured compression wave velocities V_p in the Archaean granite-gneiss fragments of the SD-3 core. Biotite-plagioclase gneisses, granites and migmatites contain at least three main types of strongly anisotropic minerals: micas (biotite, muscovite etc.), quartz and plagioclase. In Fig. 10.8 are given measured V_p (in air-dry conditions) as a factor of depth H.

As this Figure suggests, the tendency for a decrease of compression wave velocities in the released core is pronounced. One may consider that the core extracted from a depth of H = 11 *km* with the registered value of V_p = 1.2 *km/s* experiences a release from geostatic stresses exceeding σ_z = 300 MPa. Deformations rising under such release in every anisotropic mineral grain cause a break in initially strong intergranular contacts, appearance of microcracks that greatly lengthen an ultrasound propagation way. The disintegration effect observed in the SD-3 core is a manifestation of a more general tectono-caisson effect [Goryainov, et al. 1992]. These effects can help to gain a better insight into geological and geophysical phenomena [Goryainov, 1983]. Their practical use is likely to result in a rise of new unmanned production techniques for extraction of mineral resources from great depths [Gorbatsevich, 2003].

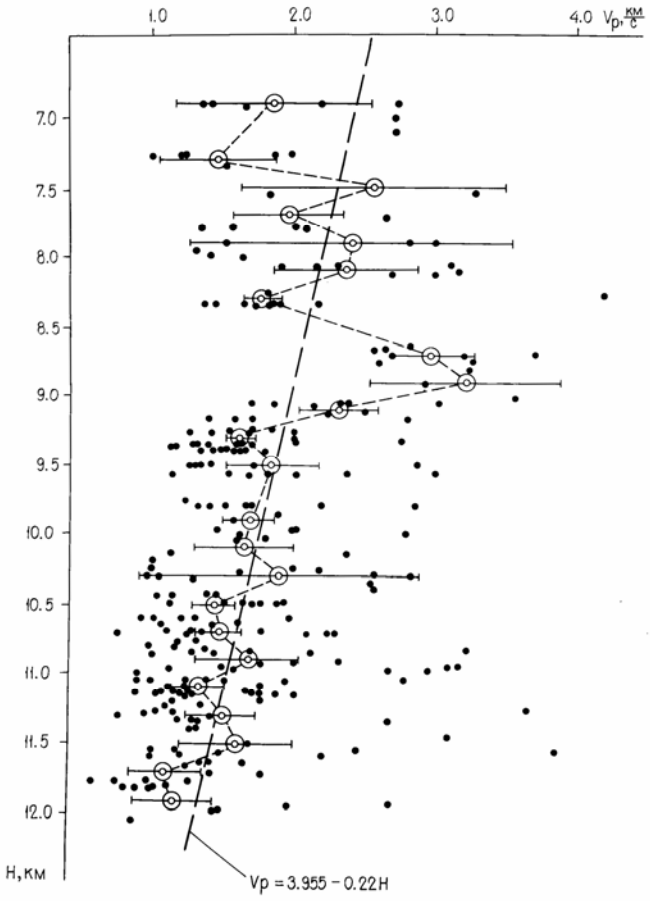

Fig. 10.8. Measured compression wave velocities V_P in the samples from the gneiss-granite complex along the SD-3 section (6905-12050 *m* depth).

As follows from the essence of the disintegration effect, polycrystalline, massif, weakly anisotropic (on the whole) rocks should decompact primarily. The data from Attachment 5 allow observing the variability of the elastic anisotropy parameters B and ε_{1133} (Attachments 5, 6) through the SD-3 section, Fig. 10.9 a, b. The most representative part of the plot shows that

anisotropy of rocks increases rather smoothly from 5 to 8 *km* depths, and then it decreases sharply to a 12 *km* depth. Schists and amphibolites are most strongly anisotropic rocks. By the data from [Gorbatsevich et al., 2002] a dashed line on the plot represents a general envelope of the largest size *P* (diameter) of the caverns in the borehole.

A general review of the plot data allows a conclusion that at 7.0-9.0 *km* depths rocks with strictly oriented structures occur. The proportion of these rocks at depths over 9 *km* decreases dramatically. At these depths the proportion of rocks in which minerals are arranged with mutually incompatible orientation increases. So the core extracted from a depth over 9 *km* will be subjected to disintegration to a greater extent. This is supported by experimental data, Figs. 10.1, 10.8.

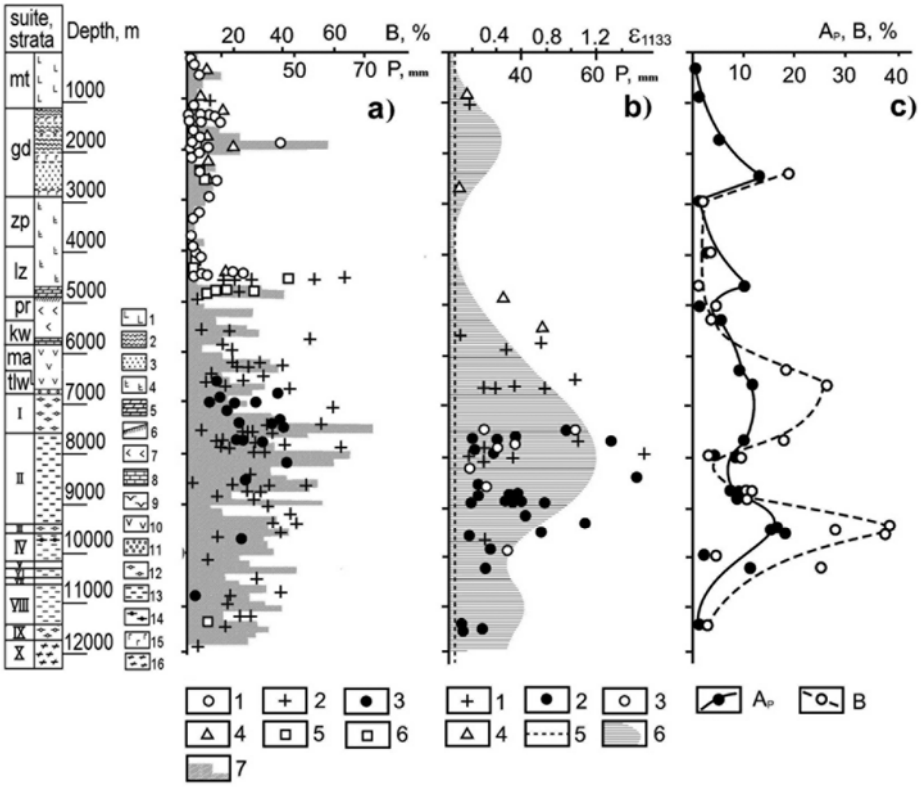

Fig. 10.9. Distribution of unit values of index *B*, factors ε_{1133} and A_P of elastic anisotropy of the rock samples along the SD-3 section [Gorbatsevich et al., 2002]. For the legend to the geological column see Fig. 5.
a - index *B*. 1 - metadiabase, peridotite; 2 - amphibolite, schist; 3 - gneiss, granite, migmatite; 4 - phyllite, tuff; 5 - metasandstone, metaaleurolite; 6 - porphyrite; 7 - average interval cross size of the borehole.
b - factor ε_{1133}. 1 - schist; 2 - amphibolite; 3 - biotite gneiss, granite; 4 - phyllite; 5 - envelope of the cavern greatest size *P*; 6 - boundary line ε_{1133} = 0.05.
The data (a, b) have been obtained on the samples in lab conditions.
c - factor A_P and index *B* (in %). The data (c) have been determined under *in situ* conditions.

Strong elastic anisotropy has been also registered by modelled *in situ* conditions. The alterations of compression (V_p), shear wave velocities (V_s) and density (ρ) were registered in some samples by increasing confining pressure (temperature) up to 600 MPa and up to 600^o C. The experiments were made in a multi-anvil apparatus by Prof. H. Kern at the University of Kiel, Germany [Kern et al., 1997] and in Prof. N.

Christensen's lab at Wisconsin University, USA [Christensen, 1985]. The results of the experiments [Gorbatsevich et al., 2002] are shown in Fig. 10.9c. Greater anisotropy measured on samples in dry air and *in situ* conditions, expressed by the factors A_P, B, ε_{1133}, corresponds to greater cavernosity P of the borehole, Fig. 10.9. This Figure shows that the caverns' largest size $P = 0.6$ *m* is observed at a depth of ~9 *km* where most anisotropic rocks occur.

Thus, with these two examples, one may state that with respect to SD-3 and SD-4, the increased cavernosity of the boreholes drilled in crystalline rocks, as a rule, is related to elastic anisotropy of rocks.

Based on the data from Attachment 5, Fig. 10.10 gives unit values D of the LAAA for the three rock types - schists, amphibolites, biotite-plagioclase gneisses and granites vs depth H. Scattering of points on the plot, on the whole, is similar to the scattering of unit values of the factor ε_{1133} in Fig. 10.9b. As a rule, amphibolites show the greatest D values. The average level of D for all rocks is rather high - $D \approx$ 0.4-0.5. This suggests that when shear waves propagate through such a massif, waves with the polarization vector oriented along the normal to the rock structure will be intensely absorbed.

Let us consider the main results of the investigation into elastic properties and anisotropy of rocks from the SD-3 section. First, the rocks are characterized by very high anisotropy mainly of rhombic symmetry (Attachment 6). For instance, cummingtonite-hornblende amphibolite (sample 28744A) has $\varepsilon_{1133} = 1.55$. Accordingly, in its matrix V_{ij}^o (Attachment 5) the compression wave velocity is 2.54 times larger than that of the shear wave. It is significant that for the side (3-3') $V_{31} =$ 2.05 *km*/*s*, $V_{32} =$ 2.01 *km*/*s*, i.e. the registered shear wave velocities virtually do not differ from those of compression waves. If we consider this sample to be isotropic a priory, then we will obtain a negative Poisson's ratio for side 3-3'. There are rather many such samples in the SD-3 section.

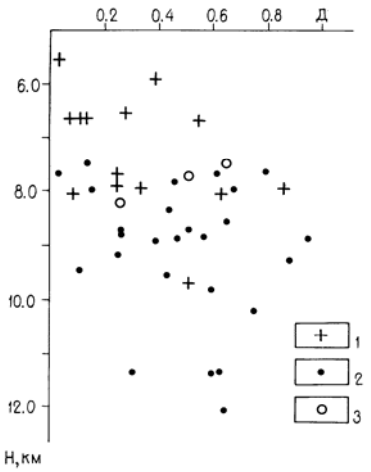

Fig. 10.10. Distribution of unit values *D* - LAAA index for rocks from the SD-3 section in the interval H = 5.5-12 km.
1 – schist, 2 – amphibolite, 3 – biotite gneiss (granites).

Unlike the samples from SD-4, the samples from SD-3, as a rule, have pronounced schistosity and linearity. The orientation of the symmetry elements revealed by acoustopolariscopy mainly coincides with visual orientations of schistosity and linearity. Some disagreement was noticed in migmatized rocks.

During a long geological time and deformation stages including the evolution of the main factors - pressure, temperature etc., rocks from SD-3 as well as those from Voche Lambina deposit area [Gorbatsevich, 1995] experienced repeated reconstruction, recrystallization and acquired a thermodynamically stable form and orientation of crystalline grains (see Fig. 8.6). These conditions are the reason for very strong anisotropy of rocks from SD-3.

The SD-3 core recovered from great depths experiences considerable disintegration caused by its release from appreciable geostatic stresses. This results in the appearance of a large number of intergranular microcracks. The core disintegration is most pronounced in polycrystalline rocks. It causes compression and

shear wave velocities to smoothly decrease, porosity to rise and strength to reduce [Gorbatsevich, 2003]. As in the case with the SD-4 rocks, greater anisotropy of rocks from SD-3 corresponds to greater cavernosity of the borehole. After S.G. Lekhnitsky [1977] in the vicinity of a round hole in a homogeneous at infinity stress field, the shape of isolines for ultimate strains causing release may take a form of a two- or four-petal rosette depending on the syngony type of an anisotropic medium. The SD-3 cross-sections of caverns have the form of an ellipse with sharp angles and the outlines close to a circle [Kozlovsky, 1987]. In this connection the data obtained from SD-3 and SD-4 show that a failure of superdeep boreholes is caused not by heterogeneity of a stress field but by considerable anisotropy of the rock elastic properties.

Rocks from SD-3 are characterized by high LAAA which manifests itself in the form of plane and linear models [Gorbatsevich, 1990] as well as in mixed forms. This effect is most conspicuous in amphibolites. As shear waves propagate in media with a high LAAA, a wave component with the polarization vector directed along the normal to the oriented structural elements is intensely absorbed. In this connection it might be interesting to trace the propagation of seismic waves in a massif composed of amphibolites and to compare the amplitudes of differently polarized transverse waves S_1 and S_2.

10.4. Comparative determined anisotropy parameters of rocks from the SD-3 and SD-4 sections

Complete results of experimental measurements of rock anisotropy for SD-4 and SD-3 are given in Attachments 2-6. With the data on the Voche-Lambina deposit area [Gorbatsevich, 1995] they present more than 3000 units and derived parameters for 104 rock specimens. Due to the data abundance it is expedient to compare them in most common indexes: age of rocks, coupling coefficients K and M between the parameters V_{sijm}, V_{piim}, γ_{1223}, ε_{1133}, a number of isotropic, anisotropic, strongly anisotropic rocks, rocks of rhombic and pseudohexagonal symmetries and a number of linear anisotropy with a small or large index D. These indexes are given in Table 10.1. In the Table, when assessing a degree of anisotropy, rocks have been divided with regard to the below limits (6.12):

Isotropic medium - $0 < \varepsilon_{1133} < 0.05$,

Weakly anisotropic medium - $0.05 < \varepsilon_{1133} < 0.15$,

Strongly anisotropic medium - $\varepsilon_{1133} > 0.15$.

By the LAAA degree rocks have been divided into 3 groups: without manifestation of the effect - $D < 0.1$, with an average degree - $0.1 < D < 0.5$, with a high degree - $D > 0.5$.

Thus, Table 10.1 gives the parameters of rocks of three geological ages: the Silurian, the Proterozoic and the Archaean. Rocks from SD-4 represent metamorphism at greenschist facies, while rocks from the Voche Lambina deposit area (VLDA) and SD-3 - mainly at amphibolite facies. Despite a different age, their coefficients K do not differ greatly. On the contrary, the difference in coefficient M between the Silurian volcanic rocks (SD-4) and, most likely, the Archaean sedimentary rocks is great. As shown in the previous section, on the basis of coefficient M, separating of volcanic rocks from rocks of other types is possible.

Elastic isotropic rocks occur only in the SD-4 section, they account for 56% of the total number. A smaller group (28%) is represented by weakly anisotropic rocks and still a smaller one - by strongly anisotropic rocks. Most samples of Proterozoic

(SD-3) and Archaean (VLDA, SD-3) rocks are included in the group of strongly anisotropic rocks (80-93%). Isotropic rocks are missing among them. Most of weakly anisotropic rocks (20%) are represented by Proterozoic rocks (SD-3), the least amount (7%) - by Archaean rocks (SD-3). Independent of a sampling point and age, rocks of rhombic symmetry dominate, among the SD-4 rocks they account for 60%. Much the same amount is among the rocks from the VLDA and SD-3 (the Proterozoic). Among the SD-3 Archaean rocks their proportion is even higher - 88%. In all places, rocks of pseudohexagonal symmetry account for less than 40% and among the Archaean rocks from SD-3 - only 12%.

The above data reject the commonly encountered in literature [Batugin & Nirenburg, 1972; Nevsky, 1974; Thomsen, 1986] conclusion that weakly anisotropic rocks of transverse-isotropic symmetry dominate at least in the upper Earth crust. The data from Table 10.1 allow the conclusion that the presented rocks (from 55% to 89%) manifest the effect of linear anisotropic absorption of a marked or high degree. Moreover, the amount of rocks with $D > 0.5$ among the SD-3 Archaean rocks is immensely high - 51%.

Table 10.1

Experimentally determined anisotropy parameters of rocks from the SD-4 and SD-3 sections and Voche Lambina deposit area [Gorbatsevich, 1995].

		Ural Borehole (SD-4)	Voche Lambina deposit area	Kola Borehole (SD-3)	
Value of Coupling coefficient between parameters	Age	Immenov formation, Silurian	Archaean	Proterozoic	Archaean
	$V_{sijm} = KV_{piim}$	0.57	0.63	0.56	0.56
	$\gamma_{1223} = M\varepsilon_{1133}$	0.29	0.66	$M_1 = 0.31$	$M_2 = 0.8$
Number of rocks	Total	25	21	15	43
Of these	Isotropic	14(56%)	-	-	-
	Weakly anisotropic	7(28%)	3(14%)	3 (20%)	3 (7%)
	Highly anisotropic	4(16%)	18(86%)	12 (80%)	40 (93%)
	Of pseudohexagonal symmetry	10(40%)	8(38%)	5(33%)	5(12%)
	Of rhombic symmetry-	15(60%)	13(62%)	10(67%)	38(88%)
	With $D > 0.1$	14(56%)	16(59%)	4(57%)	14(38%)
	With $D > 0.5$	-	-	1(13%)	19(51%)

As follows from the above, in the Ural Superdeep section down to a depth of 3.07 *km* mainly isotropic and weakly anisotropic rocks occur, which after their generation underwent rather little change and transformation. The other end of the elastic property spectrum is represented by SD-3 Archaean rocks. During their evolution they

underwent a number of alterations and transformations including stages of progressive and regressive metamorphism, migmatization and other processes. They resulted in dominating of strongly anisotropic rocks of rhombic symmetry and manifestation of high LAAA.

The data from the Table allow the conclusion that the older the rock and the higher metamorphism facies, the larger amount of strongly anisotropic rocks with a high LAAA in the given massif.

CONCLUSION

At present great interest in elastic anisotropy parameters of natural and artificial media is being shown. On the one hand, it is due to the necessity of developing new materials that posses the greatest elasticity and strength in the desired direction. On the other hand, investigations indicate that natural materials, in particular minerals and rocks, have the properties characterized by various symmetry groups, including the lowest ones, and by high degree of anisotropy. Great in volume rock masses, up to the earth crust parts, can be strongly anisotropic. These peculiarities of great geological formations hinder their study by seismic methods.

Presented here the acoustopolariscopy method enables obtaining all the parameters that are necessary for the characteristics of the sample material anisotropy. This method is a combination of dynamic and kinematic methods. To implement the method we have designed acoustopolariscopes and transducers that can radiate and receive purely shear linearly-polarized waves. They allow one to make highly accurate measurements, including those on samples up to 1 *sm*. The latest version of this device permits making measurements automatically with data retention and their processing on the computer. A computer programme allows one to construct acoustopolarigrams, to distinguish symmetry element projections on them and to print out the data.

According to the measurement procedure by acoustopolarization diagrams obtained at crossed polarization vectors one can determine the number, orientation and mutual arrangement of the medium symmetry elements. An analysis of the number and spatial characteristics of these elements permits drawing a conclusion about the medium symmetry type without determining compression and shear wave velocities in the sample.

The shape of the acoustopolarigram obtained at the parallel polarization vectors allows determining the presence and degree of the linear acoustic anisotropic absorption (LAAA) effect and assess heterogeneity of the sample medium. The detection of the LAAA effect implies the presence of the system of parallel heterogeneities in the specimen under study, for instance, the substance layers with different acoustic properties or cracks. The increased amplitudes detected in the sample at crossed polarization vectors at the points lying in the projection lines of the elastic symmetry elements point to the presence of the shear wave depolarization (SWD) effect and, accordingly, to the different orientation of the symmetry elements in the material layers or grains.

At the final stage to calculate a full set of the elasticity constants $C_{\alpha\beta}$, in accordance with the revealed symmetry elements and in additional directions, compression and shear wave velocities are measured. The anisotropy factors obtained from the velocity values allow one to distinguish weakly and highly anisotropic media. The analysis of the relationship among the velocity values measured in the direction of the elastic symmetry elements allows, in addition to the determinations made by the acoustopolarigrams, corroboration of the results for the symmetry type diagnosis.

Theoretical grounds for the acoustopolarization method have been developed only for a simple model of transverse isotropic medium. But, as the measurement practice showed, the mathematical expressions we have suggested are representative of the shear wave propagation in more complicated media up to the rhombic symmetry ones. The acoustopolarigrams for the crystals of quartz, orthoclase, microcline show the feasibility of the obtained experimental results for analysing the

number of the elastic symmetry elements of trigonal, monoclinic, triclinic etc. symmetry media.

Our observations and the existing analogy in the field of optic phenomena allowed suggestion of the theoretical grounds for the LAAA effect and development of its two main models - plane and linear ones. Similarly the origin mechanism of the shear wave depolarization effect in anisotropic heterogeneous media has been revealed.

Interesting new results have been obtained when conducting acoustopolariscopy of rock forming mineral samples. Using analcite, halite, garnet and pyrite samples we have showed that unlike optic methods acoustopolariscopy permits determination of spatial arrangement of the elastic symmetry elements in minerals of cubic syngony. All these sample exhibited a rather weak LAAA effect.

The measurements on the samples of medium syngony (apatite, quartz, nepheline, tourmaline) showed the dependence of some parameters on the frequency of the sounding waves. For instance, elastic properties of apatite samples at the sounding frequency of 2.67 MHz acquire an orthorhombic symmetry type. This mineral samples have not exhibited great LAAA. Nepheline is virtually transverse isotropic medium. In nepheline samples at low frequencies (f_0 = 0.78-1.26 MHz) the LAAA index may reach medium and great values.

The elastic symmetry class of quartz differs from the crystallographic symmetry class determined by its optic properties. This is indicated, for instance, by determination of elasticity parameters of a quartz sample which corroborate the difference in elastic symmetry orientation determined by optic and elastic properties.

Tourmaline samples displayed two effects at the same time - LAAA and SWD. At one frequencies the LAAA linear type is exhibited, at others - the plane type. It should be noted that also in optics tourmaline is noted for a strong manifestation of the pleochroism effect.

The LAAA effect is conspicuous in minerals of low syngony, except for nephrite. The highest values of LAAA have been detected in such minerals as amphibole, microcline and orthoclase. Some minerals exhibit a clear dependence of LAAA manifestation and type on the wave frequency. For instance, in microcline, as well as in orthoclase, at one frequency the greatest absorption occurs on structural elements of one cohesion, at the other frequency - on the elements of another cohesion. A comparatively similar absorption on both elements occurs at f_0 = 1.26 MHz. Accordingly, as the frequency changes, the type of LAAA manifestation changes, too. For instance, when the absorption from one system of structural elements prevails, a plane type will be detected. At the mutual and equal influence of two orthogonal systems of cohesion a linear type will be registered. This observation suggests a different step (stage) in cohesion systems in these silicate minerals.

The obtained V_{ij} values in mineral samples, on the whole, agree with the reference data. But the values of quartz elasticity constants given in the references have been measured along the crystallographic axes and do not reflect the greatest and least elasticity values for this mineral.

A rather large number of samples (25 specimens) of rocks from the Ural Superdeep Borehole (SD-4) have been analysed by the acoustopolariscopy method. Relatively young Silurian volcanic rocks from the borehole that have experienced comparatively few changes are characterized by the green-schist facies of metamorphism. The measurement results allowed subdividing the rocks (andesite basalt, basalt, tuff, and tuffite) into comparatively isotropic (56%), weakly anisotropic (28%) and strongly anisotropic (I6%). Strongly anisotropic rocks occur at a depth of

2867 *m* and below. As a rule, they are of pseudohexagonal symmetry. The axis of elastic symmetry of strongly anisotropic rocks is aligned almost horizontally. Thus, one may assume that substantial horizontal tectonic stresses acted at a depth of 2867 *m* and below. Among weakly anisotropic rocks rhombic symmetry predominates (60%), suggesting about the same influence of geostatic and tectonic stresses.

It is significant that the appearance and visible structure of strongly anisotropic rocks do not allow distinguishing them from isotropic and weakly anisotropic ones. As has been revealed, isotropic (weakly anisotropic) rocks from SD-4 have a rather low Poisson ratio. This index for volcanic rocks of this type can serve as a diagnostic sign during seismic survey. Anisotropy expressed by relations between the compression wave velocities is rather closely connected with that for shear waves. But for the rocks from SD-4 anisotropy of elastic properties is much better registered with shear waves.

The index of linear acoustic anisotropic absorption effect is the highest in strongly anisotropic SD-4 rocks, but on the whole, LAAA is observed in 57% of the samples. Rocks with oriented mineralized cracks show high LAAA. Contrast zones have been distinguished by the indexes of anisotropy and LAAA in the vicinity of 430, 886, 924, I440, 2496 and 3000 *m* depths. The geological column points to interlayers or contacts between different rocks within those zones.

A great increase in elastic anisotropy of SD-4 rocks begins from a depth of 2867 *m*; the zone of intensive cavern formation begins 60 m below this depth. Within this zone the cross dimensions of the borehole become three times larger than its nominal diameter. A close relation between the rock anisotropy and the borehole cross dimension has been found. The discovered correlation provides a basis for developing an efficient method for prediction of stability loss zones in boreholes and workings according to the measurement results for anisotropy parameters.

The second group of rocks is the largest (58 samples). It has been taken from the Kola Superdeep Borehole (SD-3) core. It presents Proterozoic and Archaean rocks that differ in mineral composition: dolomite, phyllite, metasandstone, amphibole-plagioclase schist, amphibole, biotite gneiss, migmatite, apogabbro, apogabbro porphyrite. Acoustopolarization observations showed a total absence of isotropic samples in the group – one can see the symmetry element projections on all three sides of virtually every sample. As a rule, the observations point to the influence of three factors that occur in different combinations and varying degrees: elastic anisotropy, linear anisotropic absorption effect and heterogeneities. The shape of the rock acoustopolarigrams is typical of strongly anisotropic rocks of mainly rhombic symmetry. The VP shape of some acoustopolarigrams is distinctly different from the some diagrams for the SD-4 rocks. They are characterized by a high degree of LAAA at one, three, or more often for two sample sides. The analysis showed that linear, plane or mixed models are observed at a high degree of LAAA. The distribution of LAAA unit values and birefringence factor for all SD-3 rocks showed that the effects of linear anisotropic absorption and elastic anisotropy are exhibited independently of each other. Among the SD-3 rocks 89% of the samples showed the LAAA effect. Of them 51% had $D > 0.5$.

Determinations of the velocity matrix type in the SD-3 samples showed a predominance of rocks with rhombic symmetry both for Proterozoic (67%) and Archaean (88%) rocks. In the same rock groups strongly anisotropic rocks account for 80% and 93% accordingly. Of 58 samples, only 10 have pseudohexagonal symmetry type, 6 of which representing a rather interesting variety – the compression wave velocity was maximum in the symmetry axis direction and minimum in the plane

direction. By convention, this type can be represented as a bundle of parallel cylindric rods that are in an isotropic medium differing in elastic properties from the rods.

As our observations showed, the rock disintegration effect was conspicuous during the SD-3 core recovery from the 6-12 km depths. The essence of the disintegration effect is the following: at relatively great depths polycrystalline rocks under geostatic pressure are in the isostatic state. The contacts between the mineral grains are continuous and strong. During drilling and recovery of the core, the rock releases from geostatic pressure and every mineral grain expands in accordance with its elastic-anisotropic indexes. The strains occurring in every anisotropic mineral grain lead to the damage of initially strong intergranular contacts and to the rise of a great many microcracks. The result of this process is a very low average shear wave velocity registered in the fragments of the SD-3 core recovered from a depth of 12 *km*.

As for the SD-4 rocks, the greater anisotropy of the SD-3 rocks corresponds to the greater cavernosity of the borehole. From the data obtained for SD-3 and SD-4, the following conclusion is quite true: as a rule, the failure in the superdeep boreholes is caused not by heterogeneity of the stress field, but by great anisotropy of the rock elastic properties. Rocks with the strongest anisotropy and most pronounced structure occur in a depth range of 7-9 *km*. In this range the borehole cavernosity is most developed. The indexes of LAAA effect are the greatest at these depths, the maximum ones being registered for the amphibolite samples. One should take into account that as shear waves propagate in the media with high LAAA, the vibration component with the polarization vector directed along the normal to the oriented structural elements is intensively absorbed.

An overall review of the results for acoustopolariscopy of the SD-4, SD-3 and other rocks enables one to conclude that the older are the rocks, the higher is the metamorphism facies and the greater is the relative amount of highly anisotropic rocks exhibiting high LAAA in the massif.

Among other aspects of acoustopolariscopy application for investigation of crystalline rocks we will point out that the study of palaeostresses with this method is a promising direction. Acoustopolariscopy allows determining spatial orientation and relative values of palaeostress field components in a metamorphosed rock. The presented method for the palaeostress study, as well as the palaeomagnetic measurement method, allows compiling, for instance, the palaeogeodynamic map of a region.

We believe that the acoustopolariscopy method will be useful when solving some problems in testing materials, especially when studying and developing new composite, metal-ceramic and other materials of future.

* * *

The main result of the investigation is the discovery of new phenomena: linear acoustic anisotropic absorption and shear wave depolarization in rock forming minerals and crystalline rocks. Elastic symmetry of diopside, quartz, apatite is more complicated than the one revealed in their visual study with electromagnetic oscillations. At the same time, we have still a long way to go toward a comprehensive investigation of elastic properties even of the group of most common rock forming minerals. Our investigation is an initial stage on this way.

The majority of the future applications of the acoustopolarization method, to our mind, is in the field of creation and tests of high-strength anisotropic materials.

REFERENCES

Acoustic polarization measurements of anisotropic properties of rocks (systematic instructions), 1985. Compiled by F. F. Gorbatsevich. Apatity, Kola Branch, USSR Academy of Sciences, p. 32 (in Russian).

Acoustopolarimetry and determining of the rocks elastic symmetry (systematic instructions), 1990. Compiled by F. F. Gorbatsevich, V. V. Balagansky & N. G. Ivanova. Apatity, Kola branch USSR Academy of Sciences, p. 84 (in Russian).

Adamesku, R.A., Geld, P.V. & Mityushov, E.A., 1985. Anisotropy of metal physical properties. M.: Metallurgiya, p. 136 (in Russian).

Aleksandrov, K.S. & Prodaivoda, G.T., 2000. Anisotropy of elastic properties of minerals and rocks. Novosibirsk, SB RAS, p. 354 (in Russian).

Aleksandrov, S.I., 1997. Depolarization of body elastic waves scattered in a randomly heterogeneous medium. Fizika Zemli, No. 9, pp. 81-88 (in Russian).

Alyoshin, N.P., Vadkovsky, N.N. & Medvedev, V.A., 1968. On introduction of shear waves in a controlled article. Defektoskopiya, No. 7, pp. 35-40 (in Russian).

Archean complex in the SG-3 section, 1991. Ed. F.P. Mitrofanov. Apatity, KSC RAS, p. 186 (in Russian).

Bakhvalov, A.I., Ponomaryov, V.N., Smolin, P.P. et al., 1988. Magnetometric investigations of the Kola Superdeep Borehole. Sovetskaya Geologiya, No. 9, pp. 81-87 (in Russian).

Batugin, S.A. & Nirenburg, R.K., 1972. Approximate relationship between elastic constants of rocks and anisotropy parameters. Physical and technical aspects of exploitation of mineral deposits. Vol. 7, No. 1, pp. 7-11 (in Russian).

Belikov, B.P., Aleksandrov, K.S. & Ryzhova, T.V., 1970. Elastic properties of rock forming minerals and rocks. Moscow, Nauka, p. 276 (in Russian).

Bergman, L., 1954. Der ultraschall und seine anwendung in Wisseschaft und Technik. Zurich.

Berry, L.G., Mason, B. & Dietrich, R.V., 1983. Mineralogy. W.H. Freeman and Company. San Francisco.

Bezukhov, N.I., 1968. The foundations of theory of elasticity, plasticity and creeping. Moscow, Vysshaya shkola, p. 512 (in Russian).

Bogdanov, S.V., 1997. Determination of elastic and piezoelectric constants of rhombic crystals by the acoustic method. Akustichesky Zhurnal, Vol. 43, No. 3, pp. 304-309 (in Russian).

Brace, W.F., 1960. Orientation of anisotropic minerals in a stress field. Mem. Geol. Soc. Amer., V.79, No. 9, pp. 9-20.

Brekhovskikh, L.M., 1973. Waves in layered media. Second edition. Moscow, Nauka, p. 343 (in Russian).

Chandra, S. R. & Kenneth, E.H., 1988. Shear-Wave velocity anisotropy in sedimentary rocks: a laboratory study. Geophysics, Vol. 53, No. 6, pp. 800-806.

Chesnokov, E.M., 1977. Seismic anisotropy of the earth's upper mantle. Moscow, Nauka, p. 144 (in Russian).

Christensen, N.I., 1985. Measurements of dynamic properties of rock at elevated temperatures and pressures. In: Measurement of rock properties at elevated pressures and temperatures. In: Pincus, H.J., Hoskins, E.R. (eds.), ASTM STR 869. American Society for Testing and Materials. Philadelphia, pp. 93-107.

Clark, A.V., Mignogna, P.B. & Sanford, R.J., 1983. Acoustoelastic measurements of stress and stress intensity factors around crack tips. Ultrasonics, No. 3, pp. 57-64.

Crampin, S., 1985. Evaluation of anisotropy by shear-wave splitting. Geophysics, Vol. 50, No. 1, pp. 142-152.

Curie, P., 1966. Selected works. Moscow-Leningrad, Nauka, p. 399 (in Russian).
Delitsyn, I.S., 1985. Structure formation in quartz rocks. Moscow, Nauka, p. 190 (in Russian).
Dieulesaint, E. et Royer, D., 1974. Ondes elastiques dans les solides. Application au traitement du signal. Masson et Cie.
Dobrzhinetskaya, L.F., 1978. Structural and metamorphic evolution of the Kola group (Baltic shield). Moscow, Nauka, p. 147 (in Russian).
Druzhinin, V.S., Karetin, Yu.S., Bashta, K.G., Koroteev, V.A. & Kashubin, S.N., 1999. Detailed comparison of surface and borehole data from the Ural superdeep borehole area. Otechestvennaya Geologiya, No. 5, p. 42-48 (in Russian).
D2845-83. Standard method for laboratory determination of pulse velocities and ultrasonic elastic constantsof rocks. ASTM Committee on Standards, USA.
Egorkina, G.V. & Bezgodkov, V.A., 1987. Study of seismic anisotropy of the upper crust. Izv. Akad. Nauk SSSR, Fizika Zemli, No. 4, pp. 28-29 (in Russian).
Eliseev, N.A., 1959. Metamorphism. Leningrad, LGU, p. 415 (in Russian).
Ermolov, I.N., 1981. Theory and practice of ultrasonic control. Moscow, Mashinostroyeniye, p. 240 (in Russian).
Farnell, G.W., 1961. Elastic waves in trigonal crystals. Can. J. Phys., Vol. 39, pp. 65-80.
Fyodorov, F.I., 1965. Theory of elastic waves in crystals. Moscow, Nauka, p. 384 (in Russian).
Geological dictionary, 1973. Vol. 2. Moscow, Nedra, p. 456 (in Russian).
Glozman, A.I., 1972. Piezoceramics. Moscow, Energiya, p. 288 (in Russian).
Goncharenko, A.M., Grum-Grzhimailo, S.V. & Fyodorov, F.I. Light absorption surfaces of crystals of various syngonies. Kristallografiya, 1979, Vol. 9, No. 4, pp. 589-598 (in Russian).
Gorbatsevich, F.F., 1982. Acoustic polarization method for determining elastic anisotropy in rock samples. In: Geophysical and geodynamic investigations in the north-east of the Baltic Shield. Apatity, Kola Branch, USSR Academy of Sciences, pp. 112-124 (in Russian).
Gorbatsevich, F.F., 1986. Acoustic polarization method for the study of anisotropy in rocks. Izv. Akad. Nauk SSSR, Fizika Zemli, No. 11, pp. 74-79 (in Russian).
Gorbatsevich, F.F., 1990. Anisotropic absorption of shear waves in rocks. Izv. Akad. Nauk SSSR, Fizika Zemli, No. 5, pp. 70-79 (in Russian).
Gorbatsevich, F.F., 1995. Acoustic polariscopy of rock samples. Apatity, KSC RAS, p. 204 (in Russian).
Gorbatsevich, F.F., 1996. Non-linearity of stain in hard crystalline rocks. Int. J. Rock Mech. Min. Sci. & Geomech. Abstr. Vol. 33, No. 1, pp.83-91.
Gorbatsevich, F.F., 1998. Depolarization of shear waves in anisotropic heterogeneous media. Izv. RAN, Fizika Zemli, No. 6, pp. 83-90 (in Russian).
Gorbatsevich, F.F., 1999. Acoustic polarization method for determining elastic symmetry and constants of anisotropy in solid media. Ultrasonics, No. 37, pp. 309-319.
Gorbatsevich, F.F. 2003. Decompaction mechanism of deep crystalline rocks under stress relief. Tectonophysics Vol. 370, Issues 1-4, pp. 121-128.
Gorbatsevich, F.F., Abdrakhimov, M.Z. & Belyaev, S.K., 1992. Modeling of linear acoustic anisotropic absorption in solids. Izv. RAN, Defektoskopiya, No. 8, pp. 24-31 (in Russian).

Gorbatsevich, F.F. & Basalayev, A.A., 1993. Experience of determining palaeostresses parameters by acoustic polarization method. Izv. RAN, Fizika Zemli, No. 7, pp. 24-31 (in Russian).
Gorbatsevich, F.F. & Il'chenko, V.L., 1997. On cross effect of elastic symmetry elements and linear anisotropic absorption on propagation of shear waves in an anisotropic solid. Defektoskopiya, No. 5, pp. 27-36 (in Russian).
Gorbatsevich, F.F., Il'chenko, V.L., Golovataya, O.S., Smirnov, Yu.P., Kern, H., Popp, T., Smithson, S., Ay, E. & Christensen, N., 2002. Elastic properties of some rock samples in the section of the Kola Superdeep Borehole determined under surface and in situ conditions. Izvestiya, Physics of the Solid Earth, Vol. 38, No. 7, pp. 576-584.
Gorbatsevich, F.F., Il'chenko, V.L., Kovalevsky, M.V. & Shpachenko, A.K., 1999. Acoustopolariscopy of some rock forming minerals. Zap. VMO, No. 4, pp. 88-92 (in Russian).
Gorbatsevich, F.F. & Medvedev, R.V. 1986. Decompaction mechanism of crystalline rocks under stress release (in Russian). In: Ore geophysical investigations on the Kola Peninsula. Apatity, Acad. Sciences, pp. 83-89 (in Russian).
Goryainov, P.M., 1983. On geodynamically unusual conditions of rock and ore formation in the context of the tectono-caisson effect manifestation. Lithology and mineral resources No. 5, pp. 47-60 (in Russian).
Goryainov, P.M., Davidenko, I.V., Gorbatsevich, F.F. et al., 1992. Theoretical and experimental fundamentals of the tectono-caisson effect (disintegration phenomenon), geodynamic consequences. In: Deep structure and geodynamics of crystalline shields in the USSR European part. Apatity, Acad. Sciences, pp. 136-144 (in Russian).
GOST 21153.0-75, 1975. Sampling and general requirements for the physical tests methods. Moscow, Izd. Standartov, p. 3 (in Russian).
Harder, S. 1988. Analysis of elastic symmetry from velocity measurements with application to dunite and bronzitite. J.G.R., Vol. 94, No. 3, pp. 469-478.
Hess, H.H., 1964. Seismic anisotropy of the uppermost mantle under oceans. Nature., Vol. 203, No. 4945, pp. 629-631.
Hill, R., 1952. The elastic behaviour of a cristalline aggregate. Pros. Phys. Soc., A. 65, No. 5, pp. 349-354.
Kazakov, A.N., 1987. Dynamic analysis of mineral microstructural orientations. Leningrad, Nauka, p. 272 (in Russian).
Kern, H., Liu, B. & Popp, T., 1997. Relationship between anisotropy of P- and S-wave velocities and anisotropy of attenuation in serpentinite and amphibolite. J.G.R., Vol. 102, pp. 3051-3065.
Korn G. & Korn T., 1968. Mathematics handbook. McGraw-Hill Book Company. New York, San Francisco, Toronto, London, Sydney.
Kozhevnikov, V.N., 1982. Formation conditions of structural and metamorphic paragenesises in Precambrian complexes. Moscow, Nauka, p. 184 (in Russian).
Kozlovsky, E.A., 1984. Kola Superdeep Borehole. In: The World of Science No. 3, pp. 38-49.
Kozlovsky, Ye.A., Ed. 1987. The Superdeep well of Kola Peninsula. Springer. Berlin, Heidelberg, New York, Tokio.
Lekhnitsky, S.G., 1977. Elasticity theory for an anisotropic body. Moscow, Nauka, 416 p. (in Russian).
Lyakhovitsky, F.M., 1988. Seismic waves in heterogeneous media. Moscow, Interdepartmental Geophysical Committee attached to the USSR Academy of

Sciences, 161 p. (in Russian).
Lyakhovsky, F.M. & Nevsky, M.V., 1970. Analysis of anisotropy of seismic wave velocities in finely laminated periodic media. Izv. Akad. Nauk SSSR, Fizika Zemli No. 9, pp. 12-21 (in Russian).
Lucas, R. et al., 1961. Mesure an moyen d'ondes ultrasonores polarisees des variations des constants elastique dans les solides souneis a des contraintes. Comptes rendes de l'Academie des sciences, Vol. 252, No. 25, pp. 3937-3939.
Lyamov, V.E., 1983. Polarization effects and anisotropy of interaction between acoustic waves in crystals. Moscow. Moscow State Univ. Publ., p. 224 (in Russian).
MacSkimin, H.J., 1950. Ultrasonic measurements techniques. Journ. Acous. Soc. Amer., July, No. 4, pp. 413-418.
Markov, G.A., 1977. Tectonic stress and rock pressure in the Khibiny massif mines. Leningrad, Nauka, p. 213 (in Russian).
Merkulov, V.M., 1968. Absorption of ultrasonic waves in rocks at 10-160 kHz. Izv. Akad. Nauk SSSR, Fiz. Zemli, No. 6, pp. 24-31 (in Russian).
Musgrave, M.J.P. & Markham, M.F., 1961. Features of the elastic wave surface for a zinc crystal. Proc. Phys. Soc., Vol. 77, No. 2, pp. 335-336.
Nye, Y.F., 1964. Physical properties of crystals. Oxford at the clarendon press.
Nevsky, M.V., 1974. Quasi-anisotropy of seismic waves velocities. Moscow, Nauka, p. 179 (in Russian).
Obolentseva, I.R., 1992. Seismic gyrotropy. In: Investigation of propagation of seismic waves in anisotropic media. Novosibirsk, Nauka, pp. 6-45 (in Russian).
Orlov, V.P. & Laverov, N.P. (eds.), 1998. Kola Superdeep. Scientific results and research experience (in Russian). Moscow, MF "Technoneftegas", 260 p (in Russian).
Patent No. 785737, USSR, MKI G01N 29/04. Transducer of shear ultrasonic waves. - Byull. Izobret., 1980, No. 45 (in Russian).
Patent No. 1281993, USSR, MKI G01N 29/04. Acoustopolariscope for measuring elasticity of solid media samples. - Byull. Izobret., 1987, No. 1 (in Russian).
Patent No. 1434377, USSR, MKI G01V 1/00. A way of seismic prospecting of a geological object. Byull. Izobret., 1988, No. 40 (in Russian).
Petrashen', G.I., 1980. Propagation of waves in anisotropic elastic media. Leningrad, Nauka, p. 280 (in Russian).
Petrophysics. Reference book, 1992. Vol. 1, Moscow, Nedra, p. 392 (in Russian).
Physical properties of minerals and rocks with high thermodynamic parameters. Handbook., 1988. Ed. M. P. Volarovich. Moscow, Nedra, p. 255 (in Russian).
Proctor, T.M., 1971. A passive analizer for ultrasonic shear waves. Journ. Acoust. Soc. Amer., Vol. 50, No. 5, pp. 1379-1381.
Prodaivoda, G.T., 1978. Symmetry principles in petrophysics. Geol. Zhurnal, Vol. 38, No. 4, pp. 61-69 (in Russian).
Prodaivoda, G.T., 1980. Petroacoustical method of rocks structural analysis. Geofiz. Zhurnal, Vol. 2, No. 1, pp. 88-91 (in Russian).
Prodaivoda, G.T., 1991. Theory and procedure of comprehensive investigations on tensor physical characteristics of ordered media. Abstr. of Doctoral Dissert. Moscow, VNIIGEOINFORMSYSTEM, p. 41 (in Russian).
Raitt, R.W., Shor, G.G., Jr., Francis, T.J.G. & Morris, G.B., 1969. Anisotropy of the pacific upper mantle. J.G.R., Vol. 74, No. 12, pp. 3095-3109.
Reference book (cadastre) for physical properties of rocks, 1975. Moscow, Nedra, p. 279 (in Russian).

Rezyapov, G.I., 1992. Experimental study of the reasons for anomalous polarization of the shear waves propagating in the low velocities zone along the vertical. In: Investigation of seismic waves propagation in anisotropic media. Novosibirsk, Nauka, pp. 104-111 (in Russian).
Robin, P.-Y.F., 1979. Theory of metamorphic segregation and related processes. Geochim. & Cosmochim. acta., Vol. 43, No. 10, pp. 1587-1600.
Rozayev, A.E. & Gorbatsevich, F.F., 1996. Elastic and anisotropic properties along the Vorotilov Deep Borehole (VDB) section. Geoecologiya, No. 4, pp. 75-86 (in Russian).
Saxena, S.K., 1973. Thermodynamics of rock-forming crystalline solutions. Springer-Verlag. Heidelberg, New York.
Seleznyov, V.S., Solov'yov, V.M. & Nikitenko, A.B., 1986. Determination of parameters of the crust seismic anisotropy in western Yakutia. Geologiya i Geofizika, No. 8, pp. 90-98 (in Russian).
Sharov, N.V. (ed.), 1997. Seismogeological model of the northern Europe lithosphere. Lapland-Pechenga region Apatity, Acad. Sciences, 226 p. (in Russian).
Shaskol'skaya, M.P., 1976. Crystallography. Moscow, Vysshaya shkola, p. 391 (in Russian).
Shurkliff, W.A., 1962. Polarized light. Harvard University Press.
Silaeva, O.I. & Delitsyn, I.S., 1970. Compression wave velocity in an artificial quartz crystal. Izv. Akad. Nauk SSSR, Fizika Zemli, No. 2, pp. 78-80 (in Russian).
Skavinsky, V.P. & Din Yun En, 1992. On converted reflected PS- and X, Y and Z excitation and three-component (x, y, z) registration. In: Investigation of seismic waves propagation in anisotropic media. Novosibirsk, Nauka, pp. 111-117 (in Russian).
Skuchik, E., 1976. Foundations of acoustics. Moscow, Mir, Vol.1, p. 534, Vol. 2, p. 546 (in Russian).
Smith, G.F.H., 1972. Gemstones. London, Chapman and Hall.
Sobolev, V.S., Khlestakov, V.V. & Kepezhinskas, K.B., 1964. On the use of quartz orientation for the assessment of mineral formation temperature. Doklady AN SSSR, Vol. 154, No. 6, pp. 1355-1358 (in Russian).
Thomsen, L., 1986. Week elastic anisotropy. Geophysics, Vol. 51, No. 10, pp. 1-37.
Tien-When Lo, Karl B.Coyner & Nafi N. Toksoz., 1986. Experimental determination of elastic anisotropy of Berea sandstone, Chicopee shale and Chelmsford granite. Geophysics, Vol. 51, No. 1, pp. 164-171.
Tillman, S.E. & Bennet, H.F., 1973. A sonic method for petrografic analysis. J.G.R., Vol. 78, No. 35, pp. 8463-8469.
Tröger, W.E., 1959. Optische bestimmung der gesteinbildenden minerale. Stuttgart.
Tyulin, V.N., 1976. Introduction to the theory of acoustic radiation and scattering. Moscow, Nauka, p. 254 (in Russian).
Urupov, A.K. & Lapin, S.I., 1972. Seismic waves velocities in anisotropic layered fractured media. Prikladnaya Geofizika, No. 67, pp. 3-16 (in Russian).
Vernon, R.K., 1980. Metamorphic processes. Moscow, Nedra, p. 227 (in Russian).
Voche-Lambina Archean geodynamic region of the Kola Peninsula, 1991. Apatity, KSC RAS. p. 196 (in Russian).
Voigt, W., 1910. Lehrbuch der Kristallphysik. Leipzig, Verl.von B.G. Teubner.
Volkov, A.S. & Grebennik, V.S., 1988. On the use of shear ultrasonic waves with horizontal polarization under defectoscopy of articles. Defektoskopiya, No. 5, pp. 94-95 (in Russian).

Volkova, E.A., 1974. Polarization measurements. Moscow, Izd. Standartov, p. 156 (in Russian).
Zagruzina, I.A., Kaplunov, L.D. & Kirillov, A.S., 1989. Chemical composition of the microinclusion fluid phase in minerals from the Ural superdeep borehole SD-4 // Doklady USSR, Vol. 308, No. 3, pp. 708-711 (in Russian).
Zhevandrov, N.D., 1978. Application of polarized light. Moscow, Nauka, p. 176 (in Russian).

Attachment 1

Unstructions for processing and drawing acoustopolarigrams on a personal computer (PC)

1. Turn on the PC and load the qBASIC program.
2. After loading qBASIC choose the command Open.
3. Out of the file menu choose the file Ud2-12cm if the measurements have been done in the Ud2-12 device. The lines of the computer program in qBASIC will appear for entering amplitudes, calculation and drawing three pairs of acoustopolarigrams (VP and VC) when performing acoustopolariscopy on a cubic sample's sides.
4. To check up the program operation press the key F5. According to the program three acoustopolarigrams should be drawn, the image of the cube with the designation of its axes and sides should be displayed on the screen. Three successive pressing of the key Enter return the program to the editing regime, the program lines appear on the screen.
5. Find the program line starting with 30 DATA and after one interval set all 36 values of A_{1VPM} obtained by VP for side 1-1'.
6. Find the program line 40 DATA, set 36 values of A_{2VPM}.
7. Set 36 values of $A_{1VCM,}$ obtained at crossed polarization vectors, in the line 60 DATA.
8. Set 36 values of A_{2VCM} in the line 70 DATA.
9. Find the program line starting with 1030 DATA and set 36 values of A_{1vpm} obtained for side 2-2'.
10. Set A_{2VPM} in the line 1040 DATA.
11. Set A_{1VCM} in the line 1060 DATA.
12. Set A_{2VCM} in the line 1070 DATA.
13. Perform all the operations in lines 2030, 2040, 2060, 2070 for the data obtained on side 3-3' in the same way as in pp. 5-8.
14. Find line 442 and put the data on the sample between the quotation marks "___".
15. Turn the acoustopolarigram in accordance with the position of the sample on the acoustopolariscope table. For this:
16. find line 312 and put the required angle G = for side 1;
17. find line 1312 and put the required angle G = for side 2;
18. find line 2312 and put the required angle G = for side 3.
19. Check up the drawing correctness for the three pairs of acoustopolarigrams by pressing the key F5.
20. Enter the menu by pressing the key Alt, choose the command Save As, press Enter. In the open window set the name of the new file in which the data will be kept.
21. Leave qBasic, for this purpose press the key Alt, choose the command File out of the menu, then the command Exit, press Enter.

Below is the computer program in qBASIC for entering amplitudes, calculation and drawing three pairs of acoustopolarigrams (VP and VC) when performing acoustopolariscopy on a cubic sample's sides.

```
5 KEY 7, "EDIT "
10 REM PROGRAMM IS FIT FOR CASE - MAXIMUM DECIBEL-MAXIMUM AMPLITUDE
15 PRINT "FOR THE DEVICE UD 2-12"
20 DIM A(100), X(100), B(100), Y(100), P(100), S(100), E(100),
R(100), T(100), U(100), D(100), J(100), L(100)
30 DATA
28,27,28,27,24,23,23,23,24,25,25,26,25,26,26,27,28,29,28,26,23,27,31,
29,28,27,27,28,29,29,29,27,27,26,27,27
40 DATA
25,27,25,23,21,20,20,21,22,24,25,25,25,26,26,27,28,29,29,27,25,27,28,
26,24,24,25,26,27,28,27,26,25,26,26,27
60 DATA
26,23,22,23,26,24,19,22,29,25,23,23,24,27,24,21,19,27,24,23,23,24,26,
26,23,22,21,25,27,22,24,22,22,22,24,24
70 DATA
26,24,25,26,24,20,15,23,28,24,22,21,23,26,20,19,21,25,22,21,21,22,22,
27,22,21,20,23,25,23,23,21,22,21,23,23
90 N = 36
100 FOR I = 1 TO N: READ A(I): NEXT I
105 FOR I = 1 TO N: READ X(I): NEXT I
110 FOR I = 1 TO N: LET P(I) = (A(I) + X(I)) / 2: NEXT I
113 FOR I = 1 TO N: READ B(I): NEXT I
117 FOR I = 1 TO N: READ Y(I): NEXT I
119 FOR I = 1 TO N: LET S(I) = (B(I) + Y(I)) / 2: NEXT I
120 REM FOR I=1 TO 36:Z=10*(I-1): PRINT TAB(1),,"L=";Z;
125 V = P(1)
130 FOR I = 2 TO N
140 IF V > P(I) THEN 160
150 LET V = P(I)
160 NEXT I
162 PRINT TAB(10); , "APMAX="; V;
165 LET Q = S(1)
170 FOR I = 2 TO N
175 IF Q > S(I) THEN 190
180 LET Q = S(I)
190 NEXT I
195 PRINT TAB(40); , "ASMAX="; Q;
200 W = V: IF Q > V THEN W = Q
205 PRINT TAB(25); , "AMAX="; W;
210 REM LPRINT "!---------!------------!-----------!-----------
220 FOR I = 1 TO N
230 P = ABS(A(I) - W): P1 = 1 / (10 ^ (P / 20)): P(I) = P1
240 S = ABS(B(I) - W): S1 = 1 / (10 ^ (S / 20)): S(I) = S1
245 Z = 10 * (I - 1)
250 M = I * 10
255 REM PRINT TAB(1),,"L=";Z; TAB(20),"AOP=";P1; TAB(50),"AOS=";S1
260 REM LPRINT USING "    ###        ##.#        ##.#
270 NEXT I
280 SCREEN 11: CLS : KEY OFF
290 X0 = 105: Y0 = 240: R = 80
300 I = 1
310 A = (I - 2) * 3.141592653# / 18
312 G = 0
314 K = G * 3.141592653# / 180
320 S = SIN(A + K): C = COS(A + K)
340 XA = X0 + R * C * P(I)
350 YA = Y0 - R * S * P(I)
360 XB = X0 + R * C * S(I)
370 YB = Y0 - R * S * S(I)
380 I = 36
382 A = (I - 1) * 3.141592653# / 18
```

```
386 S = SIN(A + K): C = COS(A + K)
390 XC = X0 + R * C * P(I)
400 YC = Y0 - R * S * P(I)
410 XD = X0 + R * C * S(I)
420 YD = Y0 - R * S * S(I)
430 LINE (XA, YA)-(XC, YC), 3
440 LINE (XB, YB)-(XD, YD), 3, , 22211
442 PRINT TAB(2); "Journal No., page, sample No., name of rock,
depth, deposit"
445 LINE (5, 240)-(15, 240), 1: LINE (205, 240)-(215, 240), 1: LINE
(105, 140)-(105, 150), 1: LINE (105, 330)-(105, 340), 1
450 REM S$=INPUT$(1)
470 FOR I = 1 TO 36
480 A = (I - 1) * 3.141592653# / 18
484 K = G * 3.141592653# / 180
490 S = SIN(A + K): C = COS(A + K)
500 X = X0 + R * C * P(I)
510 Y = Y0 - R * S * P(I)
520 IF I > 0 THEN LINE (XA, YA)-(X, Y), 3
530 XA = X: YA = Y
570 NEXT I
575 LINE (205, 240)-(215, 240), 1: LINE (415, 240)-(425, 240), 1:
LINE (315, 140)-(315, 150), 1: LINE (315, 330)-(315, 340), 1
600 FOR I = 1 TO 36
610 A = (I - 1) * 3.141592653# / 18
620 S = SIN(A + K): C = COS(A + K)
630 X = X0 + R * C * S(I)
640 Y = Y0 - R * S * S(I)
650 IF I > 0 THEN LINE (XB, YB)-(X, Y), 2, , 22222
660 XB = X: YB = Y
700 NEXT I
702 LINE (415, 240)-(425, 240), 1: LINE (615, 240)-(625, 240), 1:
LINE (525, 140)-(525, 150), 1: LINE (525, 330)-(525, 340), 1
1030 DATA
36,38,40,44,44,44,43,41,39,40,45,46,48,48,48,47,44,38,40,42,45,46,47,
47,45,43,41,41,45,47,48,49,48,47,45,40
1040 DATA
40,44,44,47,48,47,45,43,40,43,47,48,49,49,48,47,43,38,40,44,46,48,48,
47,45,43,41,42,48,50,50,50,50,48,45,39
1060 DATA
47,46,42,37,31,38,43,46,47,47,46,43,37,30,38,44,46,47,47,46,47,37,31,
38,44,47,48,47,46,42,36,30,39,44,46,47
1070 DATA
47,46,44,37,32,40,44,46,47,47,46,42,36,32,41,46,48,48,48,47,43,36,34,
41,45,47,48,48,46,42,35,32,40,45,47,47
1090 N = 36
1100 FOR I = 1 TO N: READ A(I): NEXT I
1105 FOR I = 1 TO N: READ X(I): NEXT I
1110 FOR I = 1 TO N: LET P(I) = (A(I) + X(I)) / 2: NEXT I
1113 FOR I = 1 TO N: READ B(I): NEXT I
1117 FOR I = 1 TO N: READ Y(I): NEXT I
1119 FOR I = 1 TO N: LET S(I) = (B(I) + Y(I)) / 2: NEXT I
1125 V = P(1)
1130 FOR I = 2 TO N
1140 IF V > P(I) THEN 1160
1150 LET V = P(I)
1160 NEXT I
1165 LET Q = S(1)
1170 FOR I = 2 TO N
1175 IF Q > S(I) THEN 1190
1180 LET Q = S(I)
```

```
1190 NEXT I
1200 W = V: IF Q > V THEN W = Q
1220 FOR I = 1 TO N
1230 P = ABS(A(I) - W): P1 = 1 / (10 ^ (P / 20)): P(I) = P1
1240 S = ABS(B(I) - W): S1 = 1 / (10 ^ (S / 20)): S(I) = S1
1245 Z = 10 * (I - 1)
1250 M = I * 10
1270 NEXT I
1290 X0 = 315: Y0 = 240: R = 80
1300 I = 1
1310 A = (I - 2) * 3.141592653# / 18
1312 G = 0
1314 K = G * 3.141592653# / 180
1320 S = SIN(A + K): C = COS(A + K)
1340 XA = X0 + R * C * P(I)
1350 YA = Y0 - R * S * P(I)
1360 XB = X0 + R * C * S(I)
1370 YB = Y0 - R * S * S(I)
1380 I = 36
1382 A = (I - 1) * 3.141592653# / 18
1386 S = SIN(A + K): C = COS(A + K)
1390 XC = X0 + R * C * P(I)
1400 YC = Y0 - R * S * P(I)
1410 XD = X0 + R * C * S(I)
1420 YD = Y0 - R * S * S(I)
1430 LINE (XA, YA)-(XC, YC), 3
1440 LINE (XB, YB)-(XD, YD), 3, , 22211
1470 FOR I = 1 TO 36
1480 A = (I - 1) * 3.141592653# / 18
1484 K = G * 3.141592653# / 180
1490 S = SIN(A + K): C = COS(A + K)
1500 X = X0 + R * C * P(I)
1510 Y = Y0 - R * S * P(I)
1520 IF I > 0 THEN LINE (XA, YA)-(X, Y), 3
1530 XA = X: YA = Y
1570 NEXT I
1600 FOR I = 1 TO 36
1610 A = (I - 1) * 3.141592653# / 18
1620 S = SIN(A + K): C = COS(A + K)
1630 X = X0 + R * C * S(I)
1640 Y = Y0 - R * S * S(I)
1650 IF I > 0 THEN LINE (XB, YB)-(X, Y), 2, , 22211
1660 XB = X: YB = Y
1700 NEXT I
2030 DATA
40,40,40,40,40,40,40,40,40,40,40,40,40,40,40,40,40,40,40,40,40,40,40,40,
40,40,40,40,40,40,40,40,40,40,40,40
2040 DATA
40,40,40,40,40,40,40,40,40,40,40,40,40,40,40,40,40,40,40,40,40,40,40,40,
40,40,40,40,40,40,40,40,40,40,40,40
2060 DATA
34,34,34,34,34,34,34,34,34,34,34,34,34,34,34,34,34,34,34,34,34,34,34,34,
34,34,34,34,34,34,34,34,34,34,34,34
2070 DATA
34,34,34,34,34,34,34,34,34,34,34,34,34,34,34,34,34,34,34,34,34,34,34,34,
34,34,34,34,34,34,34,34,34,34,34,34
2090 N = 36
2100 FOR I = 1 TO N: READ A(I): NEXT I
2105 FOR I = 1 TO N: READ X(I): NEXT I
2110 FOR I = 1 TO N: LET P(I) = (A(I) + X(I)) / 2: NEXT I
2113 FOR I = 1 TO N: READ B(I): NEXT I
```

```
2117 FOR I = 1 TO N: READ Y(I): NEXT I
2119 FOR I = 1 TO N: LET S(I) = (B(I) + Y(I)) / 2: NEXT I
2125 V = P(1)
2130 FOR I = 2 TO N
2140 IF V > P(I) THEN 2160
2150 LET V = P(I)
2160 NEXT I
2165 LET Q = S(1)
2170 FOR I = 2 TO N
2175 IF Q > S(I) THEN 2190
2180 LET Q = S(I)
2190 NEXT I
2200 W = V: IF Q > V THEN W = Q
2220 FOR I = 1 TO N
2230 P = ABS(A(I) - W): P1 = 1 / (10 ^ (P / 20)): P(I) = P1
2240 S = ABS(B(I) - W): S1 = 1 / (10 ^ (S / 20)): S(I) = S1
2245 Z = 10 * (I - 1)
2250 M = I * 10
2270 NEXT I
2290 X0 = 525: Y0 = 240: R = 80
2300 I = 1
2310 A = (I - 2) * 3.141592653# / 18
2312 G = 0
2314 K = G * 3.141592653# / 180
2320 S = SIN(A + K): C = COS(A + K)
2340 XA = X0 + R * C * P(I)
2350 YA = Y0 - R * S * P(I)
2360 XB = X0 + R * C * S(I)
2370 YB = Y0 - R * S * S(I)
2380 I = 36
2382 A = (I - 1) * 3.141592653# / 18
2386 S = SIN(A + K): C = COS(A + K)
2390 XC = X0 + R * C * P(I)
2400 YC = Y0 - R * S * P(I)
2410 XD = X0 + R * C * S(I)
2420 YD = Y0 - R * S * S(I)
2430 LINE (XA, YA)-(XC, YC), 3
2440 LINE (XB, YB)-(XD, YD), 3, , 22211
2470 FOR I = 1 TO 36
2480 A = (I - 1) * 3.141592653# / 18
2484 K = G * 3.141592653# / 180
2490 S = SIN(A + K): C = COS(A + K)
2500 X = X0 + R * C * P(I)
2510 Y = Y0 - R * S * P(I)
2520 IF I > 0 THEN LINE (XA, YA)-(X, Y), 3
2530 XA = X: YA = Y
2570 NEXT I
2600 FOR I = 1 TO 36
2610 A = (I - 1) * 3.141592653# / 18
2620 S = SIN(A + K): C = COS(A + K)
2630 X = X0 + R * C * S(I)
2640 Y = Y0 - R * S * S(I)
2650 IF I > 0 THEN LINE (XB, YB)-(X, Y), 2, , 22211
2660 XB = X: YB = Y
2700 NEXT I
2705 REM S$ = INPUT$(1)
3010 X = 50: Y = 420' x - not less 50. y – not more 499
3020 SCREEN 11: LINE (X, Y)-(X, Y - 25): LINE (X, Y)-(X + 30, Y)
3030 LINE (X, Y - 25)-(X + 30, Y - 25): LINE (X + 30, Y - 25)-(X +
30, Y)
```

```
3040 LINE (X, Y - 25)-(X + 15, Y - 37.5): LINE (X + 30, Y - 25)-(X +
45, Y - 37.5)
3050 LINE (X + 30, Y)-(X + 45, Y - 12.5)
3060 LINE (X + 12.5, Y - 37.5)-(X + 45, Y - 37.5): LINE (X + 45, Y -
37.5)-(X + 45, Y - 12.5)
3070 LINE (X, Y)-(X + 15, Y - 12.5), , , 22211
3080 LINE (X + 15, Y - 12.5)-(X + 45, Y - 12.5), , , 22211
3090 LINE (X + 15, Y - 12.5)-(X + 15, Y - 37.5), , , 22211
3100 LOCATE 22, 15: PRINT "[3]": LOCATE 15, 1: PRINT "[2']"
3110 LOCATE 15, 27: PRINT "[3]":   LOCATE 9, 41: PRINT "[1]"
3115 LOCATE 9, 67: PRINT "[1]": LOCATE 15, 78: PRINT "[2]"
3117 LOCATE 10, 5: PRINT "1":  LOCATE 10, 31: PRINT "2"
3119 LOCATE 10, 59: PRINT "3"
3120 CIRCLE (X - 14, Y - 270), 14: CIRCLE (X + 194, Y - 270), 14:
CIRCLE (X + 418, Y - 270), 14
3130 LINE (X + 7, Y - 12.5)-(X - 20, Y - 7)
3140 LINE (X + 38, Y - 25)-(X + 60, Y - 25)
3150 LINE (X + 30, Y - 29)-(X + 30, Y - 49)
3160 LOCATE 27, 3: PRINT "[3]": LOCATE 23, 10: PRINT "[1]"
3170 LOCATE 26, 15: PRINT "[2]"
3200 REM LOCATE 1,1:PRINT "INPUT DATA: h1, tDP1, tDS1, tDOP1, tDOS12,
tDOS13"
3210 DATA 10,10,10,20,20,20
3220 READ H1, TDP1, TDS1, TDOP1, TDOS12, TDOS13
3230 V11 = (H1) / (TDOP1 - TDP1)
3240 V12 = (H1) / (TDOS12 - TDS1)
3250 V13 = (H1) / (TDOS13 - TDS1)
3310 DATA 10,10,10,20,20,20
3320 READ H2, TDP2, TDS2, TDOP2, TDOS21, TDOS23
3330 V22 = (H2) / (TDOP2 - TDP2)
3340 V21 = (H2) / (TDOS21 - TDS2)
3350 V23 = (H2) / (TDOS23 - TDS2)
3410 DATA 10,10,10,20,20,20
3420 READ H3, TDP3, TDS3, TDOP3, TDOS31, TDOS32
3430 V33 = (H3) / (TDOP3 - TDP3)
3440 V31 = (H3) / (TDOS31 - TDS3)
3450 V32 = (H3) / (TDOS32 - TDS3)
3580 LOCATE 24, 43: PRINT USING "#.###"; V11
3590 LOCATE 24, 50: PRINT USING "#.###"; V12
3600 LOCATE 24, 57: PRINT USING "#.###"; V13
3610 LOCATE 25, 43: PRINT USING "#.###"; V21
3620 LOCATE 25, 50: PRINT USING "#.###"; V22
3630 LOCATE 25, 57: PRINT USING "#.###"; V23
3640 LOCATE 26, 43: PRINT USING "#.###"; V31
3650 LOCATE 26, 50: PRINT USING "#.###"; V32
3660 LOCATE 26, 57: PRINT USING "#.###"; V33
4180 S$ = INPUT$(1)
4190 CLS
4200 SCREEN 2: SCREEN 0
```

Attachment 2

Density and elasticity indexes of the rock samples from the SG-4 section

Sa-mp-le No.	Rock name	Depth, H, m	Den-sity p, g/sm^3	Velocity matrix, V_{ij}, *km/s*	LAAA degree D	Orientation of symmetry elements, degree		Normalized velocity V_{ij}^0 matrix, *km/s*
						β_{n1}	β_{n2}	
1	2	3	4	5	6	7		8
70	Amygdaloidal oligophyric andesite-basalt	293.3	2.91	5.72 3.54 3.55 3.44 5,68 3.46 3.65 3.54 5.58	0.00 0.00 0.00	0 90 107	88 0 77	5.72 3.54 3.55 3.44 5.68 3.46 3.65 3.54 5.58
78	Rare-amygdaloidal plagioclase andesite-basalt-bipyroxene	356.8	2.84	6.50 3.68 3.78 3.78 6.57 3.77 3.71 3.66 6.24	0.00 0.06 0.02	36 75 117	109 180 39	6.57 3.78 3.77 3.68 6.50 3.78 3.66 3.71 6.24
83	Porphyric plagioclase basalt-bipyroxene	384.8	2.88	6.50 3.56 3.56 3.52 6.32 3.52 3.54 3.54 6.23	0.10 0.00 0.00	–	–	6.50 3.56 3.56 3.52 6.32 3.52 3.54 3.54 6.24
92	Plagioclase andesite-basalt-pyroxene	405.2	2.83	5.89 3.34 3.29 3.34 5.84 3.26 3.35 3.38 5.84	0.05 0.03 0.00	135 43 145	41 142 74	6.08 3.35 3.33 3.38 5.85 3.35 3.29 3.30 5.80
97	Andesite-basaltic tuff with a large number of fractures	430.0	2.84	4.99 3.16 2.92 3.20 5.28 3.01 3.03 3.05 4.98	0.26 0.23 0.39	64 62 15	171 151 100	5.28 3.20 3.01 3.16 4.99 2.92 3.05 3.03 4.98
105	Psephitic-psammitic andesite-basaltic tuffite	435.9	2.93	5.80 3.28 3.22 3.29 5.96 3.31 3.31 3.32 5.90	0.00 0.00 0.03	61 37 108	153 132 26	6.02 3.38 3.31 3.32 5.96 3.26 3.31 3.29 5.79
114	Crystal-clastic psammitic-fine-psephitic andesite-basaltic porphyrite	458.7	2.92	5.25 3.27 3.33 3.27 5.38 3.36 3.33 3.40 5.61	0.03 0.00 0.00	174 172 38	102 74- 126	5.61 3.40 3.30 3.36 5.38 3.27 3.33 3.27 5.25
152	Psammitic andesite-basaltic tuffite	637.0	2.84	5.94 3.21 3.21 3.23 6.03 3.23 3.23 3.25 6.03	0.00 0.09 0.00	38 113 80	143 - 180	6.10 - 3.26 3.23 6.03 3.23 3.28 3.23 5.97
172	Psephitic andesite-basaltic tuff	759.3	2.83	6.06 3.35 3.48 3.40 5.88 3.40 3.44 3.40 5.83	0.06 0.06 0.11	138 17 83	50 105 165	6.22 3.23 5.97 3.47 6.11 3.40 3.35 3.48 6.06

Extension of Attachment 2

1	2	3	4	5	6	7	8
182	Subalkaline quartz diorite with massive ataxic structure	806.6	2.79	6.01 3.46 3.47 3.50 6.11 3.48 3.48 3.52 6.10	0.07 0.06 0,03	173 73 107 29 137 68	6.13 3.46 3.48 3.44 6.12 3.52 3.47 3.49 6.01
184	Subalkaline quartz diorite with massive ataxitic structure	828.9	2.81	5.96 3.47 3.50 3.47 6.12 3.56 3.40 3.43 5.99	0.03 0.00 0.12	158 62 46 127 170 78	6.14 3.45 3,52 3.42 5.90 3.45 3.40 3.47 5.75
192	Fine psephitic andesite-basaltic tuff	886.7	2.81	5.43 3.28 3.34 3.27 5.91 3.39 3.26 3.37 5.85	0.10 0.00 0.00	139 33 26 127 171 80	5.94 3.36 3.26 3.39 5.91 3.27 3.22 3.26 5.40
199	Plagioclase-pyroxene rare-metal andesite-basalt	924.2	2.89	6.03 3.58 3.57 3.43 5.91 3.44 3.50 3.59 6.22	0.19 016 0.41	90 36 166 99 140 60	6.22 3.50 3.59 3.57 6.03 3.58 3.44 3.43 5.91
253	Pyroxene-plagioclase andesite-basaltic tuff	1123.8	2.86	5.84 3.67 3.60 3.65 5.97 3.63 3:63 3.65 5.72	0.06 0.00 0.04	50 140 31 119 48 137	5.97 3.65 3.63 3.67 5.84 3.60 3.65 3.63 5.73
256	Psephitic andesite-basaltic tuff	1128.2	2,91	5.94 3.56 3.58 3.54 6.02 3.59 3.64 3.64 6.22	0.09 0.09 0.15	19 103 7 107 149 61	6.22 3.64 3.64 3.59 6.02 3.54 3.58 3.56 5.94
401	Fragment of pyroxene-plagioclase amygdaloidal andesite-basalt	1440.4	2.77	5.79 3.53 3.64 3.54 5.82 3.63 3.65 3.75 5.98	0.15 0.04 0.18	167 79 28 131 140 50	6.13 3.64 3.52 3.65 6.09 3.57 3.49 3.51 5.51
908	Andesite-basaltic coarse-psephitic tuff with ataxitic structure	2468.2	2.97	6,46 3.62 3.64 3,64 6.58 3.65 3.69 3.72 6.62	0.00 0.10 0.07	19 98 4 93 151 51	6.69 3.69 3.69 3.72 6.62 3.69 3.59 3.58 6.42
918	Psammitic fine-psephitic tuff of andesite basalt	2496.4	2.89	6.23 3.69 3.73 3.66 6.23 3.73 3.78 3.70 6.36	0.0.7 0.03 0.16	178 94 153 65 135 38	6.45 3.67 3.69 3.68 6.33 3.74 3.63 3.74 6.35

End of Attachment 2

1	2	3	4	5	6	7		8
934	Prehnitized coarse-psephitic tuff of andesite-basalt	2530.6	2.90	6.28 3.42 3.51 3.42 6.04 3.42 3.45 3.44 6.33	0.00 0.06 0.02	20 170 113	113 90 19	6.33 3.45 3.44 3.51 6.28 3.42 3.42 3.42 6.04
1119	Psammitic andesite-basaltic tuff	2843.2	2.85	6.49 3.67 3.67 3.66 6.49 3.67 3.67 3.68 6.58	0.00 0.03 0.09	102 11 35	8 84 108	6.58 3.67 3.68 3.67 6.49 3.67 3.67 3.66 6.49
1136	Psammitic andesite-basaltic tuff	2866.0	2.82	6.23 3.54 3.50 3.53 6.49 3.58 3.44 3.49 6.28	0.00 0.04 0.08	109 12 12	171 114 104	6.49 3.58 3.53 3.49 6.28 3.44 3.54 3.50 6.23
1138	Fine-psephitic-psammitic tuff	2867.8	2.84	5.97 3.60 3.51 3.49 5.76 3.57 3.62 3.56 5.91	0.16 0.16 0.20	47 138 140	135 49 48	6.16 3.62 3.43 3.61 6.01 3.64 3.46 3.45 5.21
1161	Fine-psephitic-psammitic tuff of andesite-basalt	2909.0	2.86	5.49 3.03 3.43 3.24 5.08 2.97 3.25 3.00 5.06	0.09 0.23 0.18	142 167 127	49 73 32	5.67 3.42 3.39 3.45 5.66 3.09 3.06 3.07 4.26
1191	Ataxitic psammitic-psephitic andesite-basaltic tuff	2963.6	2.90	5.40 3.42 2.94 3.31 5.20 2.92 3.05 2.60 4.22	0.20 0.40 0.28	35 17 170	116 106 75	5.40 3.34 2.93 3.28 5.04 3.18 2.94 2.97 3.89
1223	Homogenous psammitic tuff	3068.0	2.84	5.48 2.94 3.45 2.84 4.05 3.05 3.42 2.97 5.47	0.11 0.07 0.00	20 49 75	112 129 167	5.66 3.44 2.98 3.49 5.61 3.02 2.84 3.08 3.84

Note. Additional faces were made for samples №№ 105, 152, 172,192, 401, 908, 1138, 1161

Attachment 3

Constants of SD-4 rock samples elasticity

Number of sample	Depth H, m	C_{11}	C_{22}	C_{33}	C_{23}	C_{44}	C_{55}	C_{66}
70	293.3	9.52	9.39	9.07	-	3.56	3.77	3.54
78	356.8	12.3	12.0	11.0	-	3.98	3.92	3.95
83	384.8	12.2	11.5	11.2	-	3.59	13.63	3.61
92	405.2	10.5	9.68	9..52	-	3.13	3.10	3.20
97	430.1	7.9	7.1	7.04	1.99	2.51	2.61	2.87
105	435.9	10.6	10.4	9.82	-	3.14	3.21	3.29
114	458.7	9.19	8.45	8.05	-	3.12	3.21	3.34
152	637.0	10.6	10.3	10.01	-	2.96	3.04	2.96
172	759.3	10.9	10.6	10.4	-	3.35	3.47	3.60
182	806.6	10.5	10.4	10.1	-	3.43	3.37	3.32
184	828.9	10.6	9.78	9.29	-	3.36	3.36	3.32
192	886.7	9.91	9.81	8.19	0.22	3.00	2.95	3.20
199	924.2	11.2	10.5	10.1	-	3.55	3.57	3.61
253	1123.8	10.2	9.8	9.4	-	3.74	3.79	3.83
256	1128.2	11.3	10.6	10.3	-	3.67	3.79	3.80
401	1140.4	10.4	10.3	8.41	-	3.49	3.40	3.68
908	2486.2	13.3	13.0	12.2	-	3.92	3.94	4.08
918	2496.4	12.1	11.6	11.6	-	4.06	3.88	3.92
934	2530.6	11.6	11.4	10.6	-	3.39	3.41	3.51
1119	2843.2	12.3	12.0	12.0	-	3.83	3.85	3.84
1136	2866.0	11.9	11.1	10.9	-	3.39	3.52	3.52
1138	2867.8	10.8	10.3	7.71	1.82	3.37	3.37	3.71
1161	2909.0	9.19	9.16	5.19	-	2.71	2.88	3.37
1191	2963.6	8.46	7.37	4.39		2.74	2.50	3.18
1223	3068.0	9.10	8.94	4.19	-	2.64	2.40	3.41

Notes: 1. Values $C_{\alpha\beta}$ are given in 10^{10} Pa.

2. Names of rocks see in Attachment 2.

Attachment 4

Characteristics of SD-4 rock samples elasticity

Number of sample	Depth, H, m	ε_{1133}	ε_{2233}	Δ_T	γ_{1213}	γ_{1223}	Type of elasticity	Angle Ψ, degree.
70	293.3	0.025	0.018	0.33	-0.032	-0.003	R	-
78	356.8	0.053	0.042	0.24	0.000	-0.004	G	-
83	384.8	0.043	0.014	1.00	-0.003	-0.003	R	-
92	405.2	0.048	0.009	1.39	0.016	0.0119	R	49
97	430.1	0.06	0.002	1.87	0.047	0.064	G	60
105	435.9	0.04	0.029	0.30	0.012	0.022	R	-
114	458.7	0.069	0.025	0.94	0.019	0.032	R	80
152	637.0	0.022	0.01	0.74	0.012	0.00	R	-
172	759.3	0.026	0.0082	1.05	0.018	0.035	R	76
182	806.6	0.020	0.018	0.084	-	-0.025	G	-
184	828.9	0.068	0,026	0.89	-	-0.007	R	69
192	886.7	0.10	0.094	0.062	0.04	0.033	G	56
199	924.2	0.052	0.020	0.88	0.06	0.008	R	81
253	1123.8	0.044	0.021	0.70	0.006	0.012	R	-
256	1128.2	0.047	0.014	1.11	0.029	0.018	R	80
401	1440.4	0.113	0.11	0.073	0.0038	0.029	G	79
908	2486.2	0.042	0.031	0.30	0.017	0.019	R	86
918	2496.4	0.021	0.002	1.71	0.0141	0.0177	R	86
934	2530.6	0.048	0.040	0.189	0.0144	0.172	G	-
1119	2843.2	0.014	0.00	2.00	-	0.0014	G	-
1136	2866.0	0.042	0.008	1.36	0.00	0.018	R	66
1138	2867.8	0.182	0.154	0.170	0.049	0.019	G	57
1161	2909.0	0.331	0.329	0.006	0.061	0.103	G	74
1191	2963.6	0.338	0.296	0.27	0.113	0.071	R	76
1223	3068.0	0.474	0.46	0.029	0.160	0.120	G	70

Note: Names of rock see in Attachment 2.

Attachment 5

Density and elasticity indexes of the samples from the SG-3 section

Sample No	Rock name	Depth *H*, *m*	Density ρ, g/cm^3	Velocity matrix V_{ij} *km/s*	LAAA effect *D*	Birefringence index *B*
1	2	3	4	5	6	7
D	Dolomite	Surface	2.84	6.14 3.54 3.42 3.56 6.11 3.59 3.58 3.54 5.83	-	0.034 0.001 0.011
T-26-2	Melanocratic biotite-plagioclase gneiss	Surface	2.80	5.05 3.34 2.68 3.17 4.95 2.63 2.83 2.65 4.02	-	0.219 0.186 0.066
2264B	Fyllite	835.8	2.98	6.72 3.25 3.20 3.20 6.06 3.19 3.33 3.16 5.79	-	0.016 0.003 0.052
2187S	Schist after agglomerate tuff	1013.6	2.88	6.47 3.13 3.39 3.17 5.59 3.11 3.29 3.11 5.39	-	0.078 0.019 0.056
10026	Thin interstratification of fyllite with aleurolite	2633.1	2.88	6.05 3.40 3.14 3.41 5.66 3.22 3.19 3.20 5.49	-	0.079 0.057 0.003
18334	Arkose sandstone with magnetite	4853.6	2.77	3.26 2.32 2.03 2.28 3.16 1.96 2.07 2.05 2.24	- - -	0.133 0.15 0.01
18994	Albitophyre	5490.0	2.84	4.42 3.04 2.94 2.54 1.71 1.43 - - 2.53	- - -	0.033
19131S	Amphibole-plagioclase schist	5558.2	2.93	5.09 3.29 3.00 3.24 4.83 2.82 3.00 2.69 4.67	0.04 0.01 0.03	0.09 0.138 0.108
19385	Amphibole-plagioclase schist	5776.0	2.90	5.74 2.76 2.62 2.81 3.73 2.15 3.53 2.25 3.30	- - -	0.052 0.266 0.442
19402S	Amphibole-plagioclase schist with biotite	5893.0	2.96	4.99 3.06 2.83 2.93 4.22 2.60 2.58 - 3.38	0.13 0.14 0.39	0.08 0.12 -

Extension of Attachment 5

1	2	3	4	5	6	7
20915S	Amphibole-plagioclase schist with chlorite	6517.8	2.93	5.26 2.46 2.22 2.44 3.42 1.86 2.26 1.97 2.59	0.16 0.28 0.08	0.10 0.27 0.14
21720	Amphibole-plagioclase schist with chlorite	6637.7	2.94	6.13 3.58 3.43 3.41 5.17 3.36 3.17 2.95 4.44	0.02 0.02 0.08	0.04 0.02 0.07
21720	Amphibole-plagioclase schist with chlorite	6637.7	2.94	4.71 2.89 2.63 2.68 3.80 2.59 2.69 2.57 3.65	0.17 0.55 0.51	0.094 0.034 0.046
21720S	Amphibole-plagioclase schist with chlorite	6637.7	2.97	5.89 2.91 2.82 2.95 3.74 2.43 2.77 2.46 3.29	0.02 0.12 0.04	0.031 0.193 0.118
21720S	Amphibole-plagioclase schist with chlorite	6637.95	2.94	6.66 3.13 3.02 3.15 4.28 2.67 3.13 2.68 4.23	0.03 0.13 0.03	0.036 0.164 0.154
24212	Apodiabasic blastoamigdaloidal amphibolite (A-12)	7467.5	3.13	5.27 2.81 2.22 2.65 3.17 1.70 2.21 1.85 2.68	0.06 0.03 0.14	0.234 0.436 0.177
24221S	Biotite-plagioclase gneiss	7469.8	2.69	4.05 2.13 1.88 2.12 2.10 1.80 2.04 1.51 2.00	- - -	0.124 0.163 0.300
24256S	Staurolite-andalusite-sillimanite-two-mica gneiss	7475.7	2.74	4.54 2.49 2.49 2.57 3.50 2.16 2.23 1.94 3.49	0.65 0.61 0.14	0.000 0.173 0.139
44580A	Mesocratic amphibolite	7643.4-7651.4	2.99	4.90 3.04 2.73 3.03 3.71 2.36 2.65 2.43 3.13	0.16 0.62 0.42	0.107 0.248 0.087
44579	Clinopyroxene-hornblende amphibolite, crystalloschist (A-4)	7651.4	2.97	4.68 2.23 2.01 2.17 3.68 1.54 1.94 1.86 2.30	0. 17 0.04 0.25	0.103 0.340 0.042
24788S	Clinopyroxene amphibolite	7659.2	3.04	6.40 2.88 3.21 2.94 4.86 2.58 3.14 2.61 4.54	0.17 0.73 0.79	0.108 0.130 0.184
24804	Amphibolite	7660.6	3.02	3.85 2.08 1.87 1.97 2.78 1.68 1.77 1.58 1.66	- - -	0.106 0.158 0.113
24947*	Amphibolite with sphene	7484.6	3.01	5.27 3.05 2.97 3.06 4.83 2.97 - 2.73 4.38	0.03 0.02 0.00	0.026 0.058 -

Extension of Attachment 5

1	2	3	4	5	6	7
24996S	Plagioclase granite with amphibole	7695.5	2.65	5.21 2.72 2.54 2.84 4.33 2.48 2.55 2.52 3.36	0.09 0.51 0.03	0.068 0.135 0.012
25386	Migmatite	7779.4	2.64	3.54 2.07 1.68 2.53 1.93 2.04 2.06 2.50 -	- - -	0.208 - -
23469*	Apodiabasic blasto-amygdaloidal amphibolite	7822.0	3.06	3.67 2.97 0.42 3.45 5.26 2.89 3.05 2.76 4.71	0.42 0.30 0.46	0.210 0.176 0.010
26480	Phlogopite-anthofyllite-actinolite schist (A-11)	7894.4	2.94	4.37 2.40 2.23 - 3.66 2.31 2.69 - 3.42	0.75 0.23 0.02	0.073 - -
26715S	Talc-phlogopite-tremolite schist	7930.9	2.95	5.73 3.40 2.57 3.35 4.10 1.76 - 1.80 2.22	0.82 0.86 0.13	0.278 0.571 -
26716S*	Talc-phlogopite-tremolite schist	7931.3	2.80	5.25 3.45 - 3.39 5.13 2.86 3.02 2.89 4.32	0.29 0.34 0.01	0.169 0.042 -
26746**	Apodiabasic cummingtonite-hornblende-amphibolite (A-3)	7944.6	2.92	4.40 2.50 2.54 2.53 3.36 2.33 2.48 2.15 3.20	0.15 0.09 0.04	0.026 0.082 0.142
27026S	Cummingtonite amphibolite	7959.1	2.89	5.38 3.13 2.39 3.06 4.66 2.24 2.15 2.12 4.41	0.49 0.68 0.16	0.268 0.310 0.014
27227S*	Epidote-biotite-amphibole-plagioclase crystalloschist	8017.0	2.99	5.39 2.84 2.48 2.61 4.64 2.01 2.37 2.18 4.21	0.31 0.63 0.56	0.135 0.259 0.084
27262**	Phlogopite-anthofyllite-actinolite schist (A-11)	8022.4	3.12	5.19 2.72 2.65 2.78 3.42 2.18 2.68 2.33 3.37	0.05 0.08 0.02	0.026 0.241 0.139
28184S	Epidote-biotite-plagioclase gneiss	8234.0	2.67	3.99 2.58 2.25 2.53 3.72 2.13 2.29 2.28 3.40	0.17 0.14 0.26	0.136 0.172 0.390
28744A	Apodiabasic cummingtonite-hornblende amphibolite (A3)	8359.4	2.91	5.63 3.35 2.09 3.36 4.58 2.04 2.05 2.01 2.21	0.44 0.38 0.42	0.463 0.488 0.020
29686*	Amphibolite with sphene	8538.0	3.00	4.54 2.59 1.99 3.69 1.76 2.16 2.15 3.56 -	0.19 0.28 0.65	0.262 - 0.005

Extension of Attachment 5

1	2	3	4	5	6	7
30137	Epidote-biotite-plagioclase gneiss	8589.5	2.67	3.23 1.79 1.56 1.65 2.77 1.80 1.56 1.91 2.49	- 	0.137 0.187 0.200
31122	Magnetite-ilmenite-hornblende amphibolite, apogabbro (A-8)	8727.5	3.05	5.31 2.93 2.75 2.86 3.98 2.44 2.62 2.41 3.43	0.06 0.47 0.51	0.063 0.158 0.083
31268	Amphibolite with sphene	8760.9	3.06	6.18 3.27 3.31 3.38 5.82 3.36 3.44 3.37 4.89	- - -	0.012 0.006 0.021
31260	Epidote-hornblende amphibolite (A-5)	8759.9	3.00	4.75 2.73 2.30 2.72 3.63 2.10 2.13 1.84 3.02	0.10 0.26 0.13	0.170 0.257 0.146
31272	Epidote-hornblende amphibolite (A-5)	8761.4	3.02	5.30 3.38 2.56 3.20 4.85 2.40 2.50 2.43 3.53	0.24 0.26 0.21	0.276 0.285 0.028
31537A**	Amphibolite with sphene	8856.0	3.05	3.73 1.84 2.19 2.14 2.76 1.52 1.99 1.50 2.51	0.18 0.95 0.20	0.173 0.338 0.280
31568	Epidote-hornblende amphibolite (A-5)	8862.8	2.98	3.79 2.41 2.17 2.31 3.04 1.85 2.05 1.92 2.42	0.31 0.57 0.23	0.104 0.221 0.065
31587	Garnet-clinopyroxene-hornblende amphibolite, fine-grained apogabbro (A-9a)	8867.0	3.03	4.82 2.77 2.35 2.81 4.08 2.18 - 2.00 2.69	0.47 0.45 0.09	0.164 0.252 -
31863	Amphibolite with sphene	8939.6	2.98	5.32 3.02 3.04 3.03 4.61 2.78 3.11 2.82 4.46	- - -	0.007 0.086 0.098
31868	Amphibolite with sphene	8940	3.06	5.06 2.89 2.54 2.77 3.51 2.29 2.65 2.26 3.29	0.06 0.39 0.18	0.128 0.189 0.158
34191A	Garnet-clinopyroxene-hornblende amphibolite, fine-grained apogabbro (A-9a)	9169.8	3.01	4.82 2.87 2.40 - 3.83 1.66 2.39 1.78 2.96	0.06 0.25 0.24	0.178 - 0.158
34876	Biotite-hornblende amphibolite, hornblendite (A-6)	9268.3	3.12	4.44 2.42 1.82 2.38 2.86 1.74 1.80 1.75 2.10	0.48 0.88 0.87	0.283 0.310 0.028
35426*	Amphibolite with sphene	9451	3.08	3.98 2.05 2.38 2.25 3.65 1.76 2.33 1.90 3.38	0.04 0.11 0.07	0.148 0.244 0.203

End of Attachment 5

1	2	3	4	5	6	7
35679	Biotite-hornblende amphibolite, hornblendite (A-6)	9534.3	3.12	5.40 2.53 2.19 2.49 3.56 2.49 3.08 1.98 3.08	0.43 0.23 0.15	0.144 0.000 0.434
35924**	Phlogopite-anthophyllite-actinolite amphibolite, apoultrabasic schist (A-11)	9672	3.02	4.92 3.01 2.30 2.89 4.55 2.18 2.43 2.36 3.76	0.51 0.01 0.13	0.267 0.280 0.029
42413-1*	Epidote-biotite-hornblende amphibolite, most ancient (A-1)	9813.1	2.96	5.42 3.14 3.18 3.04 4.78 2.79 2.90 2.60 4.03	0.23 0.10 0.59	0.01-3 0.086 0.109
36398	Granite-migmatite after epidote-biotite – plagioclase gneiss	9865.0	2.63	3.10 2.02 1.63 2.07 2.64 - 1.64 1.49 2.09	- - -	0.213 - 0.096
42918-1	Epidote-biotite-hornblende amphibolite, most ancient (A-1)	10209.3	2.91	4.76 2.85 2.71 - 3.84 2.28 2.54 2.35 3.65	0.04 0.74 0.73	0.05 - 0.078

Note: No* - direction of symmetry elements is not parallel to the sample edges

No** - one of directions of the symmetry elements is not parallel to the sample edges

Attachment 6

Constants and characteristics of SD-3 rock samples elasticity

Number of sample	C_{11}	C_{22}	C_{33}	C_{44}	C_{55}	C_{66}	ε_{1133}	ε_{2233}	γ_{1213}	γ_{1223}	Δ_T	Type of elasticity
1	2	3	4	5	6	7	8	9	10	11	12	13
D	10.	10.	9.6	3.6	3.48	3.58	0.0	0.04	0.01	-	0.10	G
T-26-2	7.1	6.8	4.5	1.9	2.12	2.97	0.2	0.23	0.18	0.23	0.10	G
2264B	13.	10.	9.9	3.0	3.18	3.10	0.1	0.04	-	0.01	1.10	R
2187C	12.	9.0	8.2	2.7	3.21	2.86	0.2	0.03	-	0.01	1.37	R
10026	10.	9.2	8.6	2.9	2.88	3.33	0.1	0.03	0.07	0.06	1.07	R
18334	2.9	2.7	1.3	0.5	1.16	1.46	0.4	0.41	0.12	0.15	0.10	G
18994	5.5	1.8	1.8	0.7	2.45	2.62	0.7	0.00	0.03	0.94	1.98	G
19131	7.5	6.8	6.3	2.2	2.64	3.11	0.0	0.03	0.08	0.19	0.89	R
19385	9.5	4.0	3.1	1.4	1.92	2.25	0.7	0.13	0.78	0.03	1.40	R
19402S	7.3	5.2	3.3	2.0	2.17	2.66	0.4	0.25	0.10	0.15	0.63	R
20915	8.1	3.4	1.9	1.0	1.50	1.76	1.0	0.32	0.08	0.28	1.05	R
21720	11.	7.8	5.7	2.9	3.20	3.58	0.3	0.16	0.06	0.10	0.79	R
21720’	10.	4.1	3.2	1.7	2.32	2.55	0.7	0.13	0.04	0.07	1.42	R
21720	6.5	4.2	3.9	1.9	2.08	2.27	0.2	0.04	0.04	0.19	1.50	R
21722	13.	5.3	5.2	2.1	2.78	2.90	0.5	0.01	0.01	0.17	1.92	G
24212	8.6	3.1	2.2	0.9	1.54	2.33	0.9	0.18	0.23	0.53	1.36	R
24221	4.4	1.1	1.0	0.7	1.03	1.21	1.0	0.05	0.08	0.28	1.81	G
24256	5.6	3.3	3.3	1.1	1.53	1.75	0.3	0.00	0.02	0.23	1.96	G
44580	7.1	4.1	2.9	1.6	2.16	2.75	0.5	0.18	0.13	0.29	1.01	R
44579	6.5	4.0	1.5	0.8	1.16	1.44	1.0	0.60	0.11	0.29	0.53	R
24788	12.	7.1	6.2	2.0	3.06	2.57	0.4	0.07	-	0.12	1.41	R
24804	4.4	2.3	0.8	0.8	1.00	1.24	1.3	0.67	0.11	0.24	0.65	R
24947	8.3	7.0	5.7	2.4	2.65	2.82	0.2	0.10	0.03	0.07	0.66	R
24996	7.1	4.9	2.9	1.6	1.71	2.05	0.5	0.28	0.09	0.11	0.62	R
25386	3.3	1.6	1.6	1.0	0.90	1.13	0.4	0.01	0.11	0.03	1.89	G
23469	9.9	8.4	6.7	2.4	2.77	3.88	0.2	0.11	0.18	0.26	0.57	R
26480	5.6	3,9	3.4	1.5	1.78	1.69	0.2	0.07	-	0.03	1.19	R
26715	9.6	4.9	1.4	0.9	1.95	3.36	1.5	0.85	0.15	0.84	0.60	R
26716	7.7	7.3	5.2	2.3	2.55	3.27	0.2	0.18	0.13	0.19	0.14	G
26746	5.6	3.3	2.9	1.4	1.84	1.85	0.3	0.05	0.00	0.12	1.53	R
27026	8.3	6.2	5.6	1.3	1.49	2.77	0.2	0.05	0.36	0.42	1.18	R
27227	8.6	6.4	5.3	1.3	1.76	2.22	0.2	0.10	0.11	0.29	0.93	R
27262	8.4	3.6	3.5	1.5	2.21	2.31	0.5	0.01	0.03	0.21	1.89	G
28184	4.2	3.6	3.0	1.3	1.38	1.74	0.1	0.09	0.12	0.16	0.59	R
28744	9.2	6.1	1.4	1.1	1.25	3.28	1.5	1.07	0.62	0.65	0.36	R
29686	6.18	4.0	3.8	1.1	1.29	2.02	0.1	0.03	0.24	0.32	1.53	R
30137	2.7	2.0	1.6	0.9	0.65	0.79	0.2	0.11	0.10	-	0.90	R
31122	8.5	4.7	3.5	1.7	2.18	2.53	0.5	0.16	0.07	0.19	1.09	R
31268	11.	10.	7.6	3.4	3.48	3.38	0.2	0.06	-0.16	-0.12	0.36	R
31260	6.77	3.9	2.7	1.1	1.47	2.23	0.5	0.20	0.22	0.38	0.96	R
31272	8.4	7.1	3.7	1.7	1.93	3.27	0.5	0.37	0.30	0.36	0.29	R

End of Attachment 6

1	2	3	4	5	6	7	8	9	10	11	12	13
31537A	4.24	2.32	1.92	0.69	1.33	1.21	0.48	0.099	-0.048	0.318	1.32	R
31568	4.28	2.75	1.74	1.06	1.33	1.66	0.57	0.25	0.118	0.255	0.75	R
31587	7.04	5.04	2.19	1.32	1.67	2.36	0.79	0.52	0.187	0.335	0.42	R
31863	8.43	6.33	5.93	2.34	2.82	2.73	0.193	0.034	-0.016	0.079	1.41	R
31868	7.83	3.77	3.31	1.58	2.06	2.28	0.54	0.27	0.08	0.197	1.56	R
34191A	6.99	4.41	2.64	0.89	1.73	2.48	0.63	0.294	0.196	0.67	0.73	R
34876	6.15	2.55	1.38	0.95	1.02	1.80	1.11	0.36	0.33	0.38	1.02	R
35426	4.88	4.10	3.52	1.27	2.11	1.42	0.75	0.156	-0.089	0.082	1.31	R
35679	9.10	3.95	2.96	1.56	2.17	1.97	0.177	0.079	-0.049	0.120	0.76	R
35924	7.31	6.25	4.27	1.56	1.69	2.63	0.308	0.210	0.252	0.299	0.38	R
42413-1	8.69	6.76	4.81	2.15	2.74	2.83	0.35	0.186	0.016	0.148	0.60	R
36398	2.53	1.83	1.15	0.58	0.70	1.10	0.48	0.263	0.247	0.376	0.60	R
42918-1	6.59	4.29	3.88	1.56	2.00	3.18	0.304	0.052	0.059	0.23	1.42	R
43553	4.36	3.99	3.54	1.16	1.23	1.74	0.11	0.061	0.186	0.222	0.56	R
43579	5.21	3.85	3.16	1.32	1.62	1.61	0.285	0.104	-0.004	0.099	0.93	R
41487-4	14.6	13.3	11.6	4.18	4.19	4.43	0.120	0.070	0.029	0.032	0.52	R
44340-2	6.40	6.29	6.10	2.58	2.43	2.65	0.024	0.016	0.046	0.14	0.44	R

Notes: 1. Values $C_{\alpha\beta}$ are given in 10^{10} Pa.

2. Names of samples see in Attachment 5.

CONTENTS